N.N. Zubov State Oceanographic Institute

On the rights of the manuscript

Shulga Tatiana Yakovlevna

MODELING OF WATER DYNAMICS AND SUBSTANCE TRANSFER IN THE SEA OF AZOV

Scientific specialty 1.6.17. Oceanology

Thesis for the degree of Doctor of Physical and Mathematical Sciences

Translation from Russian

Scientific consultants:

Evgeny Alexandrovich Zakharchuk,
Doctor of Geographical Sciences, Professor

Vyacheslav Vladimirovich Suslin
Candidate of Physical and Mathematical Sciences

Sevastopol – 2024

Contents

INTRODUCTION

Relevance of the research topic. The interest in mathematical modeling of the movements of natural stratified media is determined by the problems of geophysics, oceanology, atmospheric physics, environmental protection and study, operation of complex hydraulic structures, including offshore oil production complexes, and other urgent tasks of science and technology. In some cases, the initial understanding of the studied range of physical phenomena related to the wave dynamics of real marine environments can be obtained on the basis of models of fluid mechanics and analytical methods of their study. In this regard, the improvement of numerical models of fluid mechanics, especially predictive ones, is due not only to practical needs, but also to the large theoretical content of the problems that arise.

The Azov-Black Sea basin, located in the south-west of Russia, belongs to one of the most studied marine areas. Regular expeditionary and onshore hydrometeorological observations in the Sea of Azov are provided by a complex of hydrological (60) and hydrochemical (20) coastal stations and posts, the data of which (for the period 1891–2014) are systematized in oceanographic data banks. A complete solution to the urgent scientific problem of timely prevention of natural and man-made impacts in the coastal areas of the Sea of Azov should be based on the joint use of monitoring data and numerical modeling results. The increasing need for accurate forecasts of extreme hydrological phenomena in marine areas requires the development of methods for mathematical modeling of fluid mechanics and the development of modern forecasting models. The use of mathematical models for numerical forecasting of extreme hydrological phenomena, operational assessment of the speed of currents, the extent of the spread of impurities in the sea, including pollutants, will avoid expensive field measurements and reduce damage from natural disasters.

The presence of extensive and extended shallow water areas, small slopes of the bottom and coast, a complex configuration of the coastline, and the active influence of wind create favorable conditions for the development of significant level fluctuations in the Sea of Azov, accompanied by intense currents. Extreme weather conditions (for example, the storm events of 2014, 2013, 2007, 1969, 1944 and 1914, which caused

catastrophic hydrological phenomena) cause significant damage to the sea coast, surges penetrate far beyond the coastline, flooding vast expanses of land. Significant changes in hydrological, morphological, hydrochemical and ecological processes occur in the coastal zone due to overburden phenomena. Industrial activities on the offshore shelf, including those related to mining, also require the development of effective methods for predicting extreme hydrological phenomena. The production load on the rather actively exploited water area of the Sea of Azov causes the manifestation of acute environmental problems. Under these conditions, knowledge of the hydrochemical regime of the sea and its changes, which largely determine the ecological situation, is of great value. Special attention should be paid to the study of the circulation of the waters of the Sea of Azov, which provides information on the spatial structure of currents necessary for the safe construction and operation of offshore platforms, bridges, laying underwater structures and pipelines in coastal areas. The relevance of numerical experiments is enhanced by the fact that with the help of modeling, it is possible not only to study the influence of natural factors on the circulation of marine waters, but also to test various hypotheses related to human economic activity.

New knowledge about the processes occurring in the marine environment is relevant in scientific and applied aspects and requires the use of modern three-dimensional numerical hydrodynamic models that take into account real atmospheric influences, bottom relief, and the complex configuration of the coastline. New experimental and technical capabilities, interpretation of the data of modern observations obtained by sounding the sea surface from space, and their theoretical understanding make it necessary to improve and supplement existing mathematical models of marine hydrodynamics. All of the above determines the relevance of the research presented in the dissertation work.

The goals and objectives of the thesis. The main purpose of the work presented in the dissertation is to draw conclusions about the influence of dangerous hydrodynamic and atmospheric conditions that lead to the emergence and intensification of natural phenomena that can cause serious damage to the ecosystem of the studied reservoir with vast areas of shallow water. Solving this scientific problem will make it possible to obtain

a forecast of the key parameters of the marine environment in order to assess extreme impacts on the most important components of marine environmental and technological systems in real time. The results of such an analysis will allow us to draw conclusions about the current ecological state and possible risks associated with anthropogenic load, taking into account the regional climatic conditions of the Azov-Black Sea region.

To achieve these goals, the following tasks were formulated and solved:

– mathematical models were developed, implemented in the form of program codes complementing the three-dimensional hydrodynamic model, to obtain operational forecasts of water dynamics and pollution evolution in the Sea of Azov;

– mathematical models of atmospheric disturbances have been developed to study the effect of their individual parameters on the emerging stationary and non-stationary movements in the sea;

– the hydrodynamic model has been modified in order to use model scenarios of atmospheric disturbances and/or atmospheric reanalysis data as boundary meteorological conditions;

– the analysis of free liquid fluctuations in the Sea of Azov, resulting from the cessation of long-period atmospheric exposure, was performed; the hypothesis of the role of the resonant mechanism in the occurrence of extremely high amplitudes of overburden vibrations, seiches and the resulting currents was tested;

– the hypothesis of the occurrence of level fluctuations with maximum amplitudes in the Sea of Azov generated by a moving inhomogeneous baric front with resonant parameters has been tested;

– the hydrodynamic model has been supplemented with mathematical procedures for the assimilation of satellite sensing data in order to predict the spread of pollutants in the marine environment;

– an analysis of the results of modeling the evolution of optically active passive suspension has been performed in order to predict the extent of pollution in the sea area and estimate the total content of suspension in the Sea of Azov for the period 2013-2014.;

– a method has been developed and used to restore the salinity of the Sea of Azov using regression models linking remote sensing data and *in situ* climate observations;

– the results of modeling historical storms were compared with the observed data on sea level and the extent of flooding areas;

– the size of flooding/drainage areas was predicted with overburden winds and predictive wind on high-resolution bathymetry;

– the influence of the intensity and alternation of the directions of the acting wind on the extremes of run-off and run-up, and the speed of currents in the Sea of Azov has been revealed;

– conclusions have been obtained on the effect of seawater incurrents through the Kerch Strait on extreme deviations in the level and velocity of currents in the Sea of Azov caused by the action of moving anticyclones in the ice seasons of 1948-2017.

The theoretical significance of the work. The approach described in the dissertation to the study of dynamic processes in the Sea of Azov, taking into account geometric and evolutionary variations of meteorological parameters, allows us to identify patterns in the formation of a three-dimensional structure of currents, to determine the conditions for violation of the stability of stationary currents. The proposed method of conducting numerical experiments when setting various physical boundary and initial conditions makes it possible to establish priority parameters of external disturbances that determine the dynamics of waters in such a shallow closed basin as the Sea of Azov.

The discovered experimental features of the evolution of optically active suspension in seawater and analytical estimates show that vortex atmospheric disturbances contribute to the propagation of the substance in the near-surface layer of the sea, decreasing with depth. The fundamental point is the presence of a consistent, constantly changing system of water inhomogeneities, which explains such non-trivial physical effects as the high rate of propagation of substances in the marine environment.

The practical significance of the results obtained. The applicant obtained conclusions about extreme current velocities at various sea horizons, extreme sea level amplitudes, and the extent of flooding/drainage areas based on the results of numerical experiments during hazardous events, which can be used as recommendations on possible risks for coastal areas.

The methods proposed in the dissertation work for labeling the total content of optically active suspension using the sea brightness coefficient allow us to build an algorithm for assimilation of initial data when solving the transfer-diffusion equations. This, in turn, makes it possible to restore satellite data gaps, which increases the adequacy of the assessment of the bio-optical state of the waters of the Sea of Azov. At the same time, the amount of lost data due to non-standard atmospheric conditions and illumination from the shore is significantly reduced.

The methodology developed in the dissertation for restoring salinity based on remote sensing data will make it possible to reduce the cost of work on assessing salinity by direct methods, fill in gaps in the hydrochemical study of the Sea of Azov in the past years, as well as expand understanding of the processes of circulation of water masses, on which the development of biological resources and coastal infrastructure of the Sea of Azov depends. Comparison of real and satellite data made it possible to build regression dependencies between the obtained values in order to further use only satellite images to assess the salinity of the Azov Sea water. This mainly concerns those sections

of the reservoir and the time when field research was not carried out in the Azov.

The main advantage of the author's algorithms for calculating the characteristics of the three-dimensional structure of currents, the values of run-offs and run-offs, the extent of flooding/drainage areas, and the extent of pollution is the high accuracy of the calculation results. Therefore, these numerical algorithms can be used to build spreadsheets of data, spatial maps, as well as to solve inverse problems.

Research methods. The thesis used theoretical, experimental research methods and numerical modeling methods. Computer codes are written in the following languages: Fortran, embedded programming languages MathCad, MatLab, OriginLab.

The following analytical methods were used: methods of integro-differential and matrix calculus, optimal spatial interpolation method, linear regression method, Kalman filter. Statistical, cluster and correlation analysis were used among the statistical methods.

Standard methods of calculation and localization of extremes were used in programs and algorithms for calculating the scale and evolution of a polluting substance. Proprietary algorithms for assimilation of remote sensing data were created, based

on a sequential recursive algorithm based on the theory of optimal Kalman filtering. A simplified model was used to calculate the covariance matrices of forecast errors. The optimal spatial interpolation method was used to recalculate the parameters of optically active suspension, temperature, salinity from the data space to the regular grid of the basin.

Measurements of the brightness coefficient with continuous wavelength scanning were used to study the bio-optical state of seawater. To build maps of the distribution of salinity, optically active suspension and bio-optical parameters, the results of data processing of the Level II optical scanner MODIS were used.

The amplitude-phase characteristics of the seiche at the frequencies of energy-carrying maxima were estimated using Fourier analysis. Validation of simulation results based on *in situ* observation data was performed using classical statistical methods for the analysis of standard errors and deviations.

Reliability and validity of the main results. The validity of the results obtained follows from the use of modern and historical data from contact and remote observations; the mathematical apparatus of fluid mechanics based on solving a system of primitive equations of ocean hydrodynamics; and from comparing the solutions obtained with natural data known in the literature and direct measurement data. A good agreement between the results of numerical calculations and reliable experimental data also indicates the validity of the results obtained.

Practical significance of the results of the work. The practical significance of the research results follows from the need to build adequate predictive models of catastrophic hydrological phenomena that ensure the advanced development of this strategically important region. The use of advanced mathematical models for predictive calculations makes it possible to provide early warning of the possible consequences of extreme natural phenomena in the formation of operational and long-term forecasts.

New estimates clarifying modern ideas about the dynamics of wind currents, overburden processes, and the level of anthropogenic load will allow us to obtain scientifically based recommendations on their basis to support the equilibrium of the ecosystem of the studied water area and the use of the resources of the Sea of Azov. The results of the study of the hydrometeorological and hydrological regimes of the Sea of Azov in the conditions of modern climatic changes are relevant for the environmental services of the region.

Approbation of the work. The main results of the dissertation were discussed at theoretical seminars of the Marine Hydrophysical Institute, the Nizhny Novgorod State Technical University named after R.E. Alekseev, and were also presented at All-Russian and international scientific conferences:

X International Scientific and Practical Conference "Intellectual and Applied Research in the modern world" (St. Petersburg, 2015);

International Scientific and Practical Conference "Marine Research and Education (MARESEDU)" (Moscow, 2015);

The All-Russian Conference on Applied Oceanography dedicated to the 90th anniversary of the outstanding Russian scientist Academician A.S. Sargsyan (Moscow, 2016);

the International Scientific Conference in memory of Corresponding Member of the Russian Academy of Sciences D.G. Matishov "Environment and Man. Modern problems of genetics, breeding and biotechnology: materials" (Rostov-on-Don, 2016);

Scientific Conference "World Ocean: Models, data and Operational Oceanology" (Sevastopol, 2016);

International Conference EMECS 11 – Sea Coasts XXVI (St. Petersburg, 2016);

In the international conference "Water Resources: study and management (limnological school of practice)" (Petrozavodsk, 2016, 2020);

III All-Russian Conference "Ecology. Economy. Computer science. System Analysis and modeling of Economic and Environmental Systems (SAMES)" (Rostov-on-Don, 2015-2017);

XIV and XV All-Russian Scientific and Technical Conferences "Modern methods and means of oceanological research" (MSOI-2015, 2017) (Moscow, 2015, 2017);

International Scientific Conference "Ecology in the XXI century: new approaches, models, methods and means" (Rostov-on-Don, 2017 d.);

IX, X, XI, XII All-Russian conference "Actual problems of ecology" (2017, 2019, 2021, 2023) (St. Petersburg, 2017, 2019, 2021, 2023)

International Seminar on Remote Sensing of the Coastal Zone (Kaliningrad, 2017);

I International Environmental Forum in Crimea "Crimea - socio-economic region. The Space of noospheric development" (Sevastopol, 2017);

II–III All-Russian Scientific Conference "Thermophysics and Biological Hydrodynamics" (Yalta, 2017, 2018);

The Third and Fourth International School of Young Scientists, the A.Y. Ishlinsky Institute of Problems of Mechanics of the Russian Academy of Sciences and the Lomonosov Moscow State University (Moscow, 2017, 2018);

Director General of the European Union Earth Science City EGU-2019 (Vienna, Austria, 2019);

The Fourth International Ocean Color Survey (IOCS) (Busan, South Korea, 2019);

The second symposium on operational satellite oceanography, a virtual meeting. 2021;

"Oceans from Space" V Scuola Grande di San Marco Symposium (Venice (Italy), 2022);

Mediterranean Geosciences Union (MedGU-2022), (Stambul (Türkiye), 2023)

The 9th Russian Conference on Applied Oceanography "Seas and Oceans in a Changing Climate" (Moscow, 2022);

XIV– XXIX International Symposia "Optics of the atmosphere and ocean. Atmospheric Physics" (Tomsk, 2018-2023);

International Scientific Conference "Freshwater Ecosystems – modern challenges" (Irkutsk, 2018);

XXI International Conference "Modern Problems of Remote Sensing of the Earth" (Moscow, 2023).

All-Russian scientific conferences "Seas of Russia: methods, tools and research results" (Sevastopol, 2017-2023).

The work was carried out in accordance with the plans of scientific research and applied topics of state assignments of the Federal State Budgetary Educational Institution of the Moscow State University of the Russian Academy of Sciences:

"Complex interdisciplinary studies of oceanological processes determining the functioning and evolution of ecosystems of the Black and Azov Seas based on modern methods of monitoring the state of the marine environment and grid technologies" (cipher "Fundamental Oceanology").

"Complex interdisciplinary studies of oceanological processes determining the functioning and evolution of ecosystems of the coastal zones of the Black and Azov Seas" (cipher "Coastal research")

The dissertation includes the results of research supported by the RFBR (project No. 17-05-00113-a "Photosynthetically active radiation at the bottom of the sea shelf according to satellite data").

Publications and personal contributions of the author. The main provisions of the dissertation have been published in 47 (forty seven) papers, including 28 articles in journals included in the list of the Higher Attestation Commission and included in the world citation indexes Scopus and/or Web of Science; 14 articles in peer-reviewed periodical scientific journals and proceedings of international conferences, 1 co-authored monograph, 2 collective monographs, 1 atlas in collaboration, 1 certificate of registration of the database.

The main scientific results of the dissertation are sufficiently fully reflected:

In works published in peer-reviewed scientific publications (from the list of the Higher Attestation Commission), as well as in scientific publications indexed by Scopus and/or Web of Science databases:

1. Ivanov, V. A. Investigation of the influence of wind action upon the currents and propagation of impurities in the Azov Sea / V. A. Ivanov, V. V. Fomin, L. V. Cherkesov, **T. Ya. Shulga** // Physical Oceanography. – 2010. – Vol. 20, no. 3. – P. 170–183. – DOI:10.1007/s11110-010-9076-0.
2. Ivanov, V. A. Analysis of the influence of water exchange through the Kerch Strait on the surge processes and currents in the Azov Sea / V. A. Ivanov, L. V. Cherkesov,

T. Ya. Shulga // Physical Oceanography. – 2010. – Vol. 20, no. 4. – P. 239–250. – DOI:10.1007/s11110-010-9081-3.

3. . Ivanov, V. A. Extreme deviations of the sea level and the velocities of currents induced by constant winds in the Azov Sea / V. A. Ivanov, L. V. Cherkesov, **T. Ya. Shul'ga** // Physical Oceanography. – 2011. – Vol. 21, no. 2. – P. 98–105. – DOI:10.1007/s11110-011-9107-5.
4. Ivanov, V. A. Investigation of effects of spatially and temporally variable wind on currents, surges, and admixture spread in the Sea of Azov / V. A. Ivanov, L. V. Cherkesov, **T. Ya. Shul'ga** // Russian Meteorology and Hydrology. – 2012. – Vol. 37, no. 8. – P. 553–559. – DOI:10.3103/S1068373912080079.
5. Ivanov, V. A. Dynamic processes and their influence on the transformation of the passive admixture in the sea of Azov / V. A. Ivanov, L. V. Cherkesov, **T. Ya. Shul'ga** // Oceanology. – 2014. – Vol. 54, no. 4. – P. 426–434. – DOI:10.1134/S0001437014030023.
6. Ivanov, V. A. Studies of free fluctuations of the Sea of Azov level arising after the termination of prolonged wind effect / V. A. Ivanov, L. V. Cherkesov, **T. Ya. Shul'ga** // Physical Oceanography. – 2015. – no. 2. – P. 15–25. – DOI:10.22449/1573-160X-2015-2-14-23.
7. Cherkesov, L. V. Investigation of the effect of the baric formation parameters on free and forced oscillations of the level and currents in the Sea of Azov / L. V. Cherkesov, **T. Ya. Shulga** // Physical Oceanography. – 2016. – no. 4. – P. 12–24. – DOI:10.22449/1573-160X-2016-4-12-24.
8. Demyshev, S. G. Aanalysis of effects of constant wind on the velocity of currents and seiche oscillations in the Azov Sea level / S. G. Demyshev, L. V. Cherkesov, **T. Ya. Shul'ga** // Russian Meteorology and Hydrology. – 2017. – Vol. 42, no. 6. – P. 388–393. – DOI:10.3103/S1068373917060048.
9. Cherkesov, L. V. Numerical study of storm surge processes and currents of the Sea of Azov during a period of extreme winds / L. V. Cherkesov, **T. Ya. Shul'ga**, N. N. Dyakov, R. R. Stanichnaya // Physical Oceanography. – 2017. – Iss. 5. – P. 3–18. – DOI:10.22449/1573-160X-2017-5-3-18.

10. **Shul'ga, T. Ya.** Numerical research of the pollution surface and deep-sea evolution in the Sea of Azov using satellite observation data / **T. Ya. Shul'ga,** V. V. Suslin, R. R. Stanichnaya // Physical Oceanography. – 2017. – Iss 6. – P. 36–46. – DOI:10.22449/1573-160X-2017-6-36-46.
11. Ivanov, V. A. Numerical analysis of surge phenomena, currents, and pollution transport in the Sea of Azov / V. A. Ivanov, **T. Ya. Shul'ga** // Doklady Earth Sciences. – 2018. – Vol. 479, part 2. – P. 543-546. – DOI:10.1134/S1028334X18040256.
12. Matishov, G. G. Studies of particulate matter distribution by Aqua MODIS data and simulation results / G. G. Matishov, **T. Y. Shul'ga,** S. M. Khartiyev, A. R. Ioshpa // Doklady Earth Sciences. – 2018. – Vol. 481, no. 1. – P. 967–971. – https://doi.org/10.1134/S1028334X18070267.
13. Cherkesov, L. V. Numerical analysis of the effect of active wind speed and direction on circulation of Sea of Azov water with and without allowance for the water exchange through the Kerch Strait / L. V. Cherkesov, **T. Ya. Shul'ga** // Oceanology. – 2018. – Vol. 58, no. 1. – P. 19–27. –DOI:10.1134/S0001437018010022.
14. **Shul'ga, T. Ya.** Investigation of the evolution of the suspended solids in the Sea of Azov based on the assimilation of satellite data in a hydrodynamic model / **T. Ya. Shul'ga,** V. V. Suslin // Fundamental and Applied Hydrophysics. – 2018. – Vol. 11, iss. 3. – P. 73–80. – DOI:10.7868/S2073667318030097.
15. Ivanov, V. A. The influence of atmospheric fronts on free and forced oscillations of the water level in the Sea of Azov / V. A. Ivanov, **T. Ya. Shul'ga** // Doklady Earth Sciences. – 2019. – Vol. 486, no. 2. – P. 737–740.
16. **Shul'ga, T. Ya.** Research of the relations between the seasonal variability of salinity and bio-optical features in the Sea of Azov using the satellite data in the visible spectrum range / **T. Ya. Shul'ga,** V. V. Suslin, D. M. Shukalo, A. V. Ingerov // Fundamental and Applied Hydrophysics. – 2020. – Vol. 13, № 2. – С. 68–75. – DOI:10.7868/S2073667320020082.
17. **Shul'ga. T.Y.** Numerical Analysis of the Velocities of Currents Forming in the Kerch Strait at the Motion of Domains of Higher Atmospheric Pressure / T. Y. Shul'ga,

A. E. Shchodro, A. V. Kholoptsev // Water Resources. – 2021. – Vol. 48(3). – P. 378–386. – DOI:10.1134/S0097807821030131.

18. **Shul'ga, T. Ya.** Data recovery of the Sea of Azov salinity fields using regression analysis between *in situ* data and regional satellite products / **T. Ya. Shul'ga,** V. V. Suslin, D. M. Shukalo // Fundamental and Applied Hydrophysics. – 2022. – Vol. 15, no. 3. – C. 114–124. – DOI:10.59887/fpg/bkug-hzez-xx59.
19. **Shul'ga, T. Ya.** Analysis of the distribution of pollution in the Sea of Azov by the results of numerical simulation and data of satellite observations / **T. Ya. Shul'ga** // Journal of Physics: Conf. Series. – 2017. – Vol. 899, Iss. 092013.
20. Ivanov, V. A. Impact of atmospheric front parameters on free and forced oscillations of level and current in the Sea of Azov / V. A. Ivanov, **T. Ya. Shul'ga** // Journal of Applied Mechanics and Technical Physics. – 2018. – Vol. 59, no. 5. – P. 912–921. – DOI:10.1134/S002189441805019X.
21. Ivanov, V. A. Computer simulation of dynamic processes in the Sea of Azov / V. A. Ivanov, L. V. Cherkesov, **T. Ya. Shul'ga** // Ecological Safety of Coastal and Shelf Zones of Sea. – 2011. – no. 25-2. – P. 294–304.
22. Ivanov, V. A. Numerical analysis of currents, surge phenomena, and evolution of pollutants caused by the action of unsteady wind in the Sea of Azov / V. A. Ivanov, L. V. Cherkesov, **T. Ya. Shul'ga** // Ecological Safety of Coastal and Shelf Zones of Sea. – 2014. – no. 28. – P. 375–386.
23. Ivanov, V. A. The study of the spatial structure of free oscillations in the Sea of Azov by mathematical modeling / V. A. Ivanov, L. V. Cherkesov, **T. Ya. Shul'ga** // Ecological Safety of Coastal and Shelf Zones of Sea. – 2014. – no. 28. – P. 453–461.
24. Cherkesov, L. V. Simulation and early warning of natural and technogenic influences in coastal areas in the Sea of Azov / L. V. Cherkesov, **T. Ya. Shul'ga** // Russian Journal of Hydrometeorology and ecology. – 2016. – no. 45. – P. 100–112.
25. Cherkesov, L. V. Study of the transformation of pollution caused by cyclones passing over the Sea of Azov / L. V. Cherkesov, **T. Ya. Shul'ga** // Proceedings of the Karelian Scientific Center of RAS. – 2016. – no. 8. – P. 108–115.

26. **Shul'ga, T. Ya.** Evolution of the pollution in the Sea of Azov by satellite data and simulation results / **T. Ya. Shul'ga** // Vestnik Udmurtskogo Universiteta: Matematika, Mekhanika, Komp'yuternye Nauki. – 2017. – Vol. 27, iss. 3. – P. 450–459. – DOI: 10.20537/vm170312.

Chapter in the monograph

27. **Shul'ga, T. Ya.** Numerical Analysis and Prediction of the Consequences of Natural and Technological Impacts in Coastal Areas of the Azov Sea / T. Ya. Shul'ga, S. M. Khartiev, A. R. Ioshpa // Physical and Mathematical Modeling of Earth and Environment Processes, Springer Geology. – 2018. – P. 317–326.

Results of intellectual activity

28. «Thermohaline electronic atlas of the Sea of Azov» : database [Electronic resource] / **T. Ya. Shul'ga,** D. M. Shukalo ; FSBIS FRC MHI. Electron. dan. Moscow, 2023. State registration number № 2023621161.

Articles in peer-reviewed periodical scientific journals and collections of scientific papers

29. Cherkesov, L. V. Investigation of the dependence of the impurity evolution on the initial distribution of its concentration and cyclone parameters / L. V. Cherkesov, **T. Ya. Shul'ga** // Physical Oceanography. – 2012. – no. 5. – P. 24–33.

30. **Shul'ga, T. Ya.** Influence of intensity of driving wind fields on dynamic processes and transformation of passive admixture in the presence of stationary currents in the Sea of Azov / T. Ya. Shul'ga // Physical Oceanography. – 2013. – no. 4. – P. 3–16.

31. **Shul'ga, T. Ya.** Analysis of the distribution of pollution in the Sea of Azov by the results of numerical simulation and data of satellite observations / **T. Ya. Shul'ga** // Journal of Physics: Conf. Series. – 2017. – Vol. 899, Iss. 092013.

32. **Shulga, T.Ya.** Remote sensing and modeling of the evolution of suspended matter in the Sea of Azov / T. Ya. Shul'ga, V. V. Suslin // Proceedings of SPIE – The International Society for Optical Engineering. – 2018. – Vol. 10833, № 108334G.
33. Kholoptsev, A.V. The Influence of Anticyclonic Movement Over the Sea of Azov on Variations of Maximum Instantaneous Current Speed in the Kerch Strait During 1948-2017 Ice Seasons / A. V. Kholoptsev, **T. Ya. Shul'ga**, O. Ye. Shchodro, S. A. Podporin // Physical and Mathematical Modeling of Earth and Environment Processes (2018) / Springer Proceedings in Earth and Environmental Sciences. – 2019. – P. 1–14.
34. **Shulga, T. Ya.** Assimilation modeling and MODIS color scanner data to obtain continuous information about the thermohaline structure in the Sea of Azov / T. Ya. Shul'ga, V. V. Suslin // Proceedings of SPIE - The International Society for Optical Engineering. – 2020. – Vol. 11560, № 115603J.
35. Shukalo, D. M. Long-term and seasonal anomalies of the Sea of the Azov thermohaline structure for 1913–2018 / D. M. Shukalo, **T. Ya. Shul'ga** // Journal of Physics Conference Series. – 2021. – 2057(1): 012133.
36. **Shulga, T.Ya.** Results of salinity recovery in the Sea of Azov according to *in situ* data and regional biooptical parameters / T. Ya. Shul'ga, V. V. Suslin // Proc. SPIE 12341, 28th International Symposium on Atmospheric and Ocean Optics: Atmospheric Physics. – 2022. – Vol. 12341, № 1234149.
37. **Shulga, T.Ya.** The *in situ* and satellite data blended for reconstruction of the surface salinity of the Sea of Azov / T. Ya. Shul'ga, V. V. Suslin // International Journal of Remote Sensing. – 2023. – P. 1–25.
38. Shukalo, D.M. Analysis of the monthly average salinity of the surface layer of the Sea of Azov, obtained by remote sensing and *in situ* measurement methods / D. M. Shukalo, **T. Ya. Shul'ga**, V. V. Suslin // Proceedings Volume 12780, 29th International Symposium on Atmospheric and Ocean Optics: Atmospheric Physics. – 2023. – 127804A.
39. **Shulga, T.Ya.** Analysis of seasonal anomalies of recovered salinity in the Sea of Azov in 2000–2018 by climatology / T. Ya. Shul'ga, V. V. Suslin // Proceedings Volume

12780, 29th International Symposium on Atmospheric and Ocean Optics: Atmospheric Physics. – 2023. – 127803X.

40. Cherkesov, L. V. Numerical analysis of the effect of moving the pressure fields on the currents free and forced oscillations of level in the Azov Sea / L. V. Cherkesov, **T. Ya. Shul'ga** // Environmental Bulletin of the scientific centers of the Black Sea Economic Cooperation. – 2016. – no. 2. – P. 99–110.
41. Cherkesov, L. V. Numerical analysis of the influence of parameters of atmospheric fronts to the free and forced oscillations level and incurrentss into the Azov Sea / L. V. Cherkesov, **T. Ya. Shul'ga** // Proceedings of N.N. Zubov State Oceanographic Institute. – M. : SOIN, 2017. – iss. 218. – P. 120–136.
42. Cherkesov, L. V. Study of stationary currents for dynamic processes and admixtures of pollution in the sea of Azov / L. V. Cherkesov, **T. Ya. Shul'ga** // Bulletin of the South Ural State University. Series: Computational Mathematics and Software Engineering. – 2017. – vol. 6, no. 1. – P. 56–72. (in Russian). – DOI:10.14529/cmse170104.
43. **Shulga, T.Ya.** Analysis of the distribution of pollution in the Sea of Azov by satellite data and simulation results / T. Ya. Shul'ga, V. V. Suslin // Proceedings of the IX Russian Conference "Modern problems of optics of natural waters" (ONW'2017). – SPb., 2017. – P. 156–160.
44. **Shulga, T.Ya.** Analysis results of numerical simulation and data of satellite monitoring of evolution of pollution in the Sea of Azov for the period from 2013 to 2014 / T. Ya. Shul'ga // Ecology. Economy. Informatics. System analysis and mathematical modeling of ecological and economic systems. – 2017. – Vol. 1, no. 2. – P. 123–133.

Atlas

45. Ivanov, V. A. Atlas of overburden processes, waves and currents caused by atmospheric disturbances in the Sea of Azov / V. A. Ivanov, L. V. Cherkesov, **T. Ya. Shul'ga**. – Sevastopol: MHI NANU, 2012. – 96 p.

Chapters in collective monographs

46. Ivanov, V. A. Features of circulation in the Strait, taking into account the influence of the Azov and Black Seas / V. A. Ivanov, V. V. Fomin, L. V. Cherkesov, **T. Ya. Shulga** // Modeling of water dynamics in the Kerch Strait and strait zones. – Sevastopol: ECOSI-Hydrophysics, 2010. – P. 182–197.
47. Cherkesov, L. V. Waves, currents, overburden processes and pollution transformation in the Sea of Azov / L. V. Cherkesov, **T. Ya. Shul'ga**. – Sevastopol: MHI RAS, 2017. – 228 p.

When performing the dissertation work, the author owns:

– at the stages of setting and formulating tasks, formulating theoretical conclusions, the author took a parity part in co-authorship with Doctor of Physical and Mathematical Sciences, Professor, corresponding member of NASU L.V. Cherkesov and Doctor of Physical and Mathematical Sciences, Professor, academician of NASU and RAS V.A. Ivanov;

– creation of hydrodynamic and numerical models describing scenarios of possible regional meteorological conditions under the guidance of L.V. Cherkesov and V.A. Ivanov;

– selection of methods and tools for conducting numerical experiments using atmospheric reanalysis data, development of techniques;

– direct contribution to the processing and analysis of remote sensing data;

– development of methods and creation of software products for processing and analyzing experimental data in calculating parameters characterizing the evolution of a passive impurity;

– analysis and interpretation of research results led by L.V. Cherkesov and V.A. Ivanov.

The results presented in the dissertation were obtained in the course of many years of research, in which the author was directly involved, and during numerical experiments, the scientific planning of which was carried out by the author. In joint research

on the evolution of optically active passive suspension based on the assimilation of MODIS-Aqua/Terra scanner data into a hydrodynamic model, the author presents the problem statement, as well as the idea, methods and implementation of integrated data processing. In the studies of run-up phenomena and currents, the idea of experiments and the method of analysis were proposed by V.A. Ivanov. The author's contribution consisted in obtaining the results of numerical calculations, in data processing, in the development and implementation of software tools and calculation methods, in numerical modeling, in discussion and analysis of the results.

Main scientific results. The following results of the dissertation work, obtained personally by the applicant, have fundamental scientific novelty and were obtained for the first time:

1) mathematical models have been created and tested, designed in the form of program codes that complement the computing complex of the three-dimensional nonlinear sigma-coordinate hydrodynamic model Princeton Ocean Model, which allow:

– take into account possible meteorological scenarios described in the proposed mathematical models to set boundary conditions on the free surface when integrating the equations of motion and drawing conclusions about the influence of atmospheric disturbance parameters on dynamic processes in the Sea of Azov [Investigation of the influence..., 2010, p. 62; Ivanov, Cherkesov, Shulga, 2011, p. 194; Ivanov, Cherkesov, Shulga, 2012, p. 61; Numerical analysis ..., 2014, p. 61; Cherkesov, Shulga, Study of transformation ..., 2016, p. 59; Cherkesov, Shulga, Modeling ... , 2016, p. 207];

– use the developed mathematical models to determine the areas and volumes of polluting substances in the sea and the time for complete purification of sea water, depending on the parameters of the operating wind [Investigation of the influence..., 2010, p. 62, 182; Ivanov, Cherkesov, Shulga, 2012, p. 61, 62; Ivanov, Cherkesov, Shulga, 2014, p. 192; Cherkesov, Shulga, Study of transformation..., 2016, p. 189; Shulga, Suslin, Stanichnaya, 2017, p. 65; Ivanov, Shulga, 2018, p. 63, 201; Shul'ga, Khartiev, Ioshpa, 2018, p. 218];

– use the proposed mathematical models and remote sensing data to set the initial conditions for the content of optically active suspended matter in seawater when

integrating the transport-diffusion equations and drawing conclusions about the evolution of pollution [Investigation of the influence..., 2010, p. 62; Shulga, Suslin, Stanichnaya, 2017, p. 66; Shulga, 2017, p. 203; Studies … 2018, p. 65];

– take into account the various conditions of fluid passage at the entrance to the Kerch Strait, in the form of appropriate mathematical procedures when integrating the equations of motion [Ivanov, Cherkesov, Shulga, 2010, p. 73, 76; Cherkesov, Shulga, 2018, p. 72; Shul'ga, Shchodro, Kholoptsev, 2021, p. 91];

– carry out risk forecasts for the extent of areas of flooding/drying of the sea coast using the proposed mathematical procedures [Cherkesov, Shulga, Impact Study ..., 2017, p. 172];

– perform operational assimilation of remote sensing data onto a regular grid of the basin under study based on the proposed procedures and algorithms [Shulga, Suslin, Stanichnaya, 2017, p. 209].

2) the modeling results were verified with observational data on the course of sea level and the extent of flooded areas during numerical experiments reproducing historical storms that caused catastrophic floods in the Don Delta and Taganrog Bay on March 23–24, 2013 and September 24, 2014 [Numerical study ..., 2017, p. 145, 148]. Based on comparison with field measurement data, it is shown that deviations from the calculated values do not exceed 8 – 14% [Numerical study..., 2017, p. 159]. This result is confirmed by comparing sea level measurements with calculation data using the POM hydrodynamic model for other forecast scenarios [Ivanov, Cherkesov, Shulga, Computer..., 2011, p. 160],

3) for the first time, the influence of the resonance mechanism in the occurrence of waves with maximum amplitudes generated by an inhomogeneous pressure front moving over the sea was tested numerically [Cherkesov, Shulga, 2016, p. 59, 60]. Free vibrations of fluid in the Sea of Azov, occurring after the cessation of long-lasting wind, have been studied [Study ... , 2014, p. 106; Ivanov, Cherkesov, Shulga, 2015, p. 100, 101; Demyshev, Cherkesov, Shulga, 2017, p. 102, 106, 119]. A simple mathematical model has been proposed that simulates the movement of pressure depression, allowing the model to be run with various parameters [Demyshev, Cherkesov, Shulga, 2017, p.

60]. As a result, for the first time it was possible to determine the value of the speed of movement of the front in the direction of the greatest acceleration of the Sea of Azov, at which extreme deviations in the level and speed of currents are achieved [Ivanov, Shulga, 2019, p. 118]. A spectral analysis of free and forced sea level fluctuations at coastal stations of the Azov Sea was performed. The amplitude-phase characteristics of free oscillations at frequencies of energy-carrying maxima were obtained and assessed using Fourier analysis for simulated time series of sea surface level deviations,

4) a new technique for joint use of numerical modeling results and remote sensing data is proposed [Studies … 2018, p. 216]. A mechanism is proposed, based on developed and tested assimilation procedures, complementing the three-dimensional nonlinear hydrodynamic model POM, implementing a one-time and regular assimilation of available satellite data [Shulga, Suslin, Stanichnaya, 2017, p. 212, 216; Shulga, Suslin, 2018, p. 210]. Using the model modified in this way, the numerical forecast of the content of a polluting substance, marked with the value of the content of optically active suspended matter, was improved to solve the problem of the transfer of polluting substances in the sea [Shulga, Suslin, 2018, p. 218]. The algorithm was tested on measurement data from the MODIS optical scanner; for the first time, estimates of the content of substances in the Sea of Azov for 2013–2014 were obtained;

5) a new method for restoring the salinity of the Sea of Azov using remote sensing data is proposed. The method is based on the creation of semiparametric regression models that relate the values of bio-optical parameters obtained from satellite images of the surface of a reservoir with *in situ* measurements. The method has been tested and verified using *in situ* climate observation data and MODIS optical scanner measurement data for 2000–2018. In particular:

– in order to create regression models and verify modeling results, a climate data set of *in situ* observations for 1913 – 2018. was regionally and vertically divided into subregions, for each of which climatic averages for temperature and salinity were found [Research ... , 2020, p. 226, 227];
– For the first time, analytical expressions for seasonal regressions for four biooptical parameters were obtained [Shulga, Suslin, Shukalo, 2022, p. 235];

– an effective bio-optical parameter was identified from the point of view of the best correlation with observed climate averages, and a statistical analysis of errors between model and climate data for the period from 2000 to 2018 was performed. which made it possible to establish statistically significant regression coefficients [Shulga, Suslin, Shukalo, 2022, p. 244];
– new sets of data on temperature and salinity, basic bio-optical parameters were obtained based on remote sensing data and modeling “Thermohaline Electronic Atlas of the Sea of Azov” [Shulga, Shukalo, 2023, p. 229].

Provisions for defense:

1) the main reason for the occurrence of prevailing surge fluctuations in the Sea of Azov is the atmospheric impact, the nature of which determines the magnitude and position of extreme sea level deviations on its coast. Great variability of currents is a consequence of unstable wind conditions, shallowness of the sea and its small area;

2) an additional factor leading to sharp changes in the direction and speed of currents in the open part of the Azov Sea and maximum level deviations on its coast is the manifestation of seiche-like oscillations that occur after the cessation of a steady wind, and also when the pressure front with resonant parameters moves;

3) the formation of extreme surges at the entrance to the Kerch Strait and an increase in the speed of currents in the strait necessitate the setting of conditions for the free passage of waves on the liquid boundary when modeling situations associated with the movement of cyclones/anticyclones over the Sea of Azov;

4) the length of the boundaries of penetration/removal of sea water from the coastline, caused by surge processes in the Sea of Azov, calculated using the proposed approach, was the basis for creating reference information in the form of data sets and prognostic maps of flooding/drying of the coast of the Sea of Azov depending on stationary /non-stationary meteorological conditions;

5) integration of the results of mathematical modeling and remote sensing data, implemented in the proposed method for assimilation of satellite information into a three-dimensional hydrodynamic model, makes it possible to fill in the gaps in satellite data

and determines long-term forecasts of the highest and total content of optically active suspended matter in the Sea of Azov;

6) systematization of accumulated information on temperature, salinity, basic bio-optical indicators of sea water using remote sensing and *in situ* observations was carried out within the framework of the created database “Thermohaline Electronic Atlas of the Azov Sea”. Complementing the observational database are simulated salinity data obtained using the proposed seasonal regression models.

The structure and scope of the dissertation. The dissertation consists of an introduction, seven chapters, a conclusion, and a list of references. The total volume of the dissertation is 282 pages, including 68 figures and 43 tables.

Thanks. The author expresses deep gratitude to his scientific supervisors – Doctor of Physical and Mathematical Sciences, Professor, Corresponding Member of the National Academy of Sciences L.V. Cherkesov and Doctor of Physical and Mathematical Sciences, Professor, Academician of the Russian Academy of Sciences V.A. Ivanov, Doctor of Physical and Mathematical Sciences V.V. Fomin – for consultations during numerical modeling, head of the Department of Dynamics of Oceanic Processes Candidate of Physical and Mathematical Sciences V.V. Suslin – for assistance in the preparation of satellite observation data arrays, Head of the Department of Remote Research Methods, Candidate of Physical and Mathematical Sciences S.V. Stanichny – for his help in preparing atmospheric reanalysis data sets, and the entire staff of the Department of Shelf Hydrophysics of the Moscow State University of the Russian Academy of Sciences – for moral support, advisory assistance and critical comments made during the discussion of the results obtained. The author expresses special gratitude to the Doctor of Physical and Mathematical Sciences V.V. Knysh, Doctor of Physical and Mathematical Sciences, Professor A.A. Kurkin for his help and great attention to the work at all its stages. I would also like to mention all the co-authors of the works, whose cooperation was very useful and interesting.

Chapter 1.
MODERN AND HISTORICAL RESEARCH OF NATURAL AND TECHNOGENIC IMPACTS IN THE SEA OF AZOV: RESULTS OF OBSERVATIONS AND MODELING

1.1. Studies of waves, currents, surges and surges in the Sea of Azov based on the results of modeling and data from expeditionary and coastal observations

The shallow, partially limited, intracontinental Sea of Azov is a body of water with an area of ~39 thousand km^2 and a volume at an average long-term level of ~320 km^3 with an average depth of ~ 7 m [Hydrometeorology … , 1991]. It occupies an intermediate position between marine and freshwater reservoirs (based on the physico-chemical characteristics and biological features according to N. M. Knipovich [Knipovich, 1926; Knipovich, 1938]. The transport, industrial and recreational potential, as well as the geographical location of the Sea of Azov, necessitated its study. The first works analyzing the state of the aquatic environment and biological resources date back to the middle of the 19th century (for example, in the reports of the famous researcher of the south seas of Russia N.Y. Danilevsky [Research on the condition …, 1871]. In the period 1890–1891, I.B. Spindler and F.F. Wrangel organized expeditionary work in the open part of the Black and Azov Seas [Wrangel, 1875; Spindler, Wrangel, 1899]. In 1922-1928, the Azov-Black Sea scientific and fishing expedition was conducted under the leadership of N.M. Knipovich. The results of the research, containing primary data and a description of measurement methods, are reflected in the reports published by N.M. Knipovich in 1926, 1932, 1938. [Knipovich, 1926; Knipovich, 1938] and in the hydrological handbook of the Sea of Azov, published in 1937 under the editorship of N.M. Knipovich and G.R. Bergman [Knipovich, Bergman, 1937]. In the same period of 1928-1932, regular expeditionary research was carried out by employees of the Azov-Black Sea Scientific Research Institute of Fisheries and Oceanography (Azcherniro). In the post-war period (since 1946), the materials of the expedition research conducted

by AZCHERNIRO were published in marine hydrometeorological yearbooks. They systematize the data of biological, hydrological and hydrochemical studies, including measurements of the concentration of phosphates, nitrogen, silicon, and oxygen dissolved in seawater. Since 1961, the arrays of expeditionary observations in the Sea of Azov have been produced by the Hydrometeorological Observatory of the Black and Azov Seas, which coordinated all expeditionary work in the Sea of Azov.

The basis for the regular collection of data on the state of the marine environment in the standard hydrological sections of the Sea of Azov and the network of hydrometeorological stations was the creation in 1936 of the USSR Hydrometeorological Service. The information obtained during the expedition and coastal observations served as an information base for the creation of a number of atlases and reference manuals published by the State Oceanographic Institute [Belov, Filippov, 1978; Belov, Filippov, 1980; Bronfman, 1964]. By the end of the 1980s, the daily hydrometeorological information was provided by data from coastal stations marked in the Figure

Figure 1.1.1, *a*. Since 1958, regular expeditions have been carried out to collect oceanographic and biological data at the stations shown in Figure 1.1.1, *b*. The accumulated and systematized materials of expeditionary hydrological and hydrochemical observations are reflected in numerous publications of reference literature [Hydrometeorological … , 1962; Hydrometeorological conditions … , 1986; Hydrometeorology … , 1991].

Modern oceanographic information on the state and spatiotemporal changes in the hydrological, hydrochemical and biological regimes of the Black and Azov Seas was provided through the collection of observation data from the complex Black Sea expeditions conducted in 2000–2002. During these expeditions, the hydrophysical, hydrochemical and biological processes of the northeastern sector of the Black Sea basin were studied at scientific research vessel Aquanaut [The Azov Sea … , 2003].

Information on the state of the Sea of Azov and its coastal ecosystem was collected by the Southern Scientific Center of the Russian Academy of Sciences (SSC RAS) during

marine expeditions on research vessels (SRV) “Professor Panov” and “Deneb" in 2003–2008. The materials of hydrological surveys (planktonic, benthic) in the entire water area of the Sea of Azov were obtained from these vessels as a result of 48 marine expeditions with a total number of oceanographic stations of more than 3.500 (hydrological and hydrochemical). Based on their own long-term research, maps of bathymetry and bottom sediments of the Sea of Azov were built [Patterns … , 2006; Modern … , 2015; Intrasecual fluctuations … , 2008; Matishov G. G., Matishov D. G., 2013].

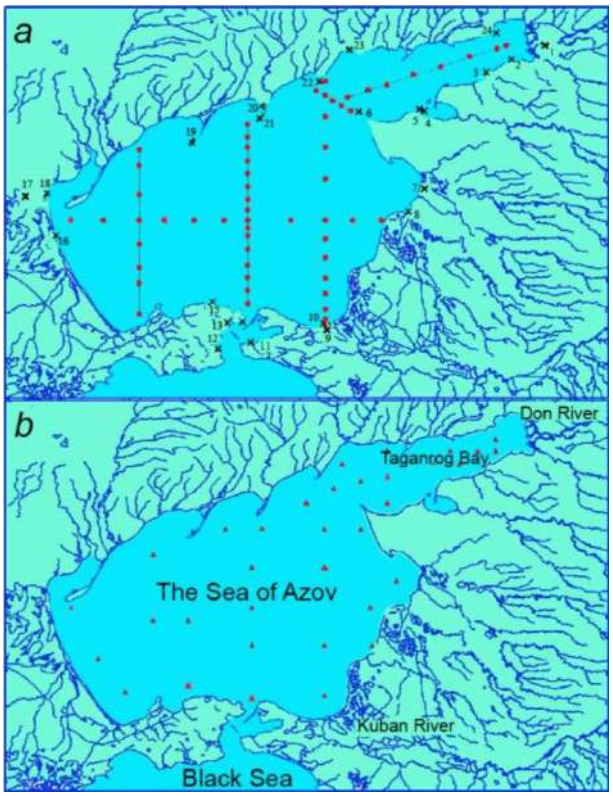

Figure 1.1.1 – The scheme of hydrological sections and locations of stations of coastal observations of the Hydrometeorological Service of the USSR (*а*): 1 – Azov; 2 – Ochakovskaya spit; 3 – Margaritovo; 4 – Yeysk port; 5 – Yeysk; 6 –Dolzhanskaya; 7 – Yasenskaya ferry; 8 – Primorsko-Akhtarsk; 9 – Temryuk; 10 – Temryuk; 11 – Taman; 12 – Cherished; 13 – Kerch; 14 – Dangerous; 15 – Mysovoye; 16 – Strelkovoye; 17 – Chongarsky Bridge; 18 – Genichesk; 19 – Obitochnaya spit; 20 – Berdyansk; 21 – Berdyanskaya spit; 22 – Belosarayskaya spit; 23 – Mariupol; 24 – Taganrog; station layout Azov-Black Sea Scientific Research Institute of Marine Fisheries and Oceanography (*б*) [Climatic Atlas of the Sea of Azov, 2006]

The continuation of the collection of operational information on the state of the marine environment and ecosystem of the Sea of Azov was the conduct of marine expeditions of the UNC RAS to the NIS "Professor Panov" and "Deneb" in 2006-2007. (10 expeditions have been completed, and measurement results from more than 1,500 oceanographic stations have been processed). Visualization of the obtained expedition data was carried out using classical methods of lithogeomorphological interpolation (map of bottom sediments) using methods of geoinformation technologies based on data processing using the licensed ArcGIS 9.2 software package (integrated indicators of environmental indices). The data of the expeditionary research formed the basis for the publications of the SSC RAS [Patterns …, 2006; Ecological mapping …, 2008; Intrasecual fluctuations …, 2008; Matishov G. G., Matishov D. G., 2013; Modern …, 2015]. Currently, the Bank of oceanographic information of the Sea of Azov includes about 76 thousand hydrological stations completed during the period 1891 – 2014. Based on the data of expedition observations since 1914, the accumulated practical material on the Black and Azov Seas is summarized in a number of manuals and atlases published by the Federal State Budgetary Institution GOIN [Hydrometeorological conditions … , 2009; Oceanographic atlas … , 2009; Atlas of the ice … , 2016].

The scientific results of the expeditionary research conducted by the SSC RAS and the Institute of Arid Zones of the SSC RAS in the Black, Azov and Caspian Seas are presented in the works of academician G.G. Matishov, Yu.I. Ingebeikin, S.V. Berdnikov [Ingebeikin, 2011; Matishov, Ingebeikin, 2009; Matishov, Chikin, 2012; Матишов, Gargopa, Chikin, 2012; Matishov, Ingebeikin, Savitsky, 2013; The ice regime …, 2014]. In [Ingebeikin and Matishov, 2012], a detailed description of the coastal trapped waves detected on the northeastern shelf of the Black Sea is given, which can play a significant role in changes in surface temperature and salinity of water, as well as sea currents. Based on the results of joint research by the Murmansk Marine Biological Institute, the UNC RAS and the Ocean Climate Laboratory of the National Oceanographic Data Center of NOAA (USA), the Climatic Atlas of the Sea of Azov 2006 was published (Climatic Atlas of the Sea of Azov 2006). He formed the basis of a database of oceanographic data on the temperature and salinity of seawater collected by specialists of various marine research

organizations in the Sea of Azov and the adjacent part of the Black Sea for the period 1913-2004. The climatic atlas of the Sea of Azov, which includes over 14 thousand marine and coastal stations [Climatic Atlas of the Sea of Azov, 2006], became the main source of digital data for constructing climatic maps of the Sea of Azov and was continued in a new version of the database presented in the Climatic Atlas of the Sea of Azov 2008 [Climatic Atlas of the Sea of Azov, 2008] according to observations at coastal posts for the period 1891-2006.

Based on long-term observations, conclusions have been drawn about the nature of fluctuations in the Sea of Azov level. Seasonal and uplift changes in the Sea of Azov level occur most often in autumn and spring with prevailing easterly, northeasterly, westerly and southwesterly winds coinciding with the direction of the greatest extent of the sea [Hydrometeorology …, 1991]. Table 1.1.1 shows the extreme characteristics of level fluctuations according to the data of the coastal network of hydrometeorological stations [Hydrometeorological ..., 1962]. As can be seen from the data given in Table 1.1.1, level rises of more than 2 m relative to zero marks are possible at the stations of Genichesk, Taganrog and Temryuk. In turn, the level drops by more than 2.5 m take place at the stations of Taganrog and Yeysk.

The maximum oscillation range at most stations exceeds 3 m, at Taganrog station – 6 m. Since overburden level changes have the appearance of a seiche with one nodal line passing approximately through the center of the sea, the smallest oscillation amplitudes are observed near the nodal line at Berdyansk station, the largest – in remote locations at Genichesk, Yeysk, Taganrog stations.

The currents in the Sea of Azov mainly depend on the wind. The high variability of currents is a consequence of the instability of the wind regime, the shallow waters of the sea and its relatively small area. The prevailing winds in the cold season are the winds of the north-east and east directions, and in the warm season – the winds of the south-west and west directions. If this wind continues for a long time and a surge of water occurs near the Arabatskaya Strelka spit, two different systems of currents form in the sea area (Figure 1.1.2). With weak and variable winds, the water circulation is disrupted

and the currents become chaotic. In the Kerch Strait, the current is usually directed from the Sea of Azov to the Black Sea and less often vice versa.

Table 1.1.1 – Observed values of the Sea of Azov level fluctuations (cm)

Points	Observation period (years)	Maximum level	Minimum level	The magnitude of the level fluctuations
Berdyansk, port	1923–2001	84	–112	196
Genichesk, a port point	1878–2001	225	–187	412
Yeysk, port	1915–1998	151	–287	438
Mariupol, port	1923–2001	128	–121	249
Primorsko-Akhtarsk, a port point	1916–1998	188	–175	363
Taganrog, port	1882–1998	251	–358	609
Temryuk, port	1910–1998	316	–84	400

The prevailing current velocity in the Sea of Azov (Table 1.1.2) is 0.1–0.2 m/s, the maximum is 0.5–0.8 m/s. During the period of strong and prolonged winds, the current velocity reaches 0.9 m/s.

Table 1.1.2 – Observed values of the surface currents of the Sea of Azov at different wind directions (m/s)

Wind speed, m/s	Wind direction							
	N	N-E	E	S-E	S	S-W	W	N-W
5–10	0,1	0,2	0,2	0,1	0,1	0,2	0,2	0,1
10–15	0,3	0,5	0,4	0,3	0,3	0,4	0,4	0,4
15–20	0,7	0,9	0,9	0,6	0,6	0,8	0,8	0,6

In the narrow places of the Kerch Strait, with gale-force winds (Table 1.1.3), the currents velocity increases to 1.4 m/s.

Table 1.1.3 – The highest values of the observed current velocity in various sections of the Kerch Strait (m/s)

Region	Current	
	Azov	The Black Sea
Yenikalsky knee	1,2	1,4
Pavlovsky knee	1,2	1,0

At the same time, the frequency of the Azov and Black Sea currents is 62% and 38%, respectively [Belov, Filippov, 1978; Hydrometeorological … , 1962; The lot of the Sea of Azov]. When the speed of the north-easterly wind is the same over the entire sea or it is greater in the northern part of the sea than in the southern, a counterclockwise circulation is observed in the western part of the sea. If the speed of the north-easterly wind in the southern region of the sea is greater than in the northern one, then in the northern part the circulation is directed clockwise (Figure 1.1.2) [Cherkesov, Shul'ga, 2017]. During the initial period of the moderate north-easterly wind, the direction of the currents coincides with the direction of the wind in the entire sea area.

As follows from Figure 1.1.2, there is a counterclockwise circulation of waters in the central part of the sea. If the speed of the southwesterly wind in the northern part of the sea is higher than in the southern part, then in its central part the water circulation occurs clockwise.

The need to obtain operational forecasts of extreme level increases due to the limited number of coastal hydrometeorological stations and observations on them has led to the use of numerical modeling as an essential research tool. Currently, hydrodynamic three-dimensional nonlinear numerical models are used in numerical calculations, which more accurately reproduce the circulation of waters in marine basins. Basically, these studies relate to the Black Sea basin, known from the works [Marchuk, Sargsyan, 1988; Dashkevich, Berdnikov, 2008; Demyshev, Knysh, Korotaev, 2002; Stanev, 2005; Oguz, Malanotte-Rizzoli, 1996; Korotenko, Dietrich, Bowman, 2003; Zalesny, Gusev, Moshonkin, 2013; Marchuk, Moshkalyov, 2014].

The dynamic structure of estuaries, bays and lakes located along the coast of the Black and Azov Seas, in particular the largest bay of Sivash, has been less studied.

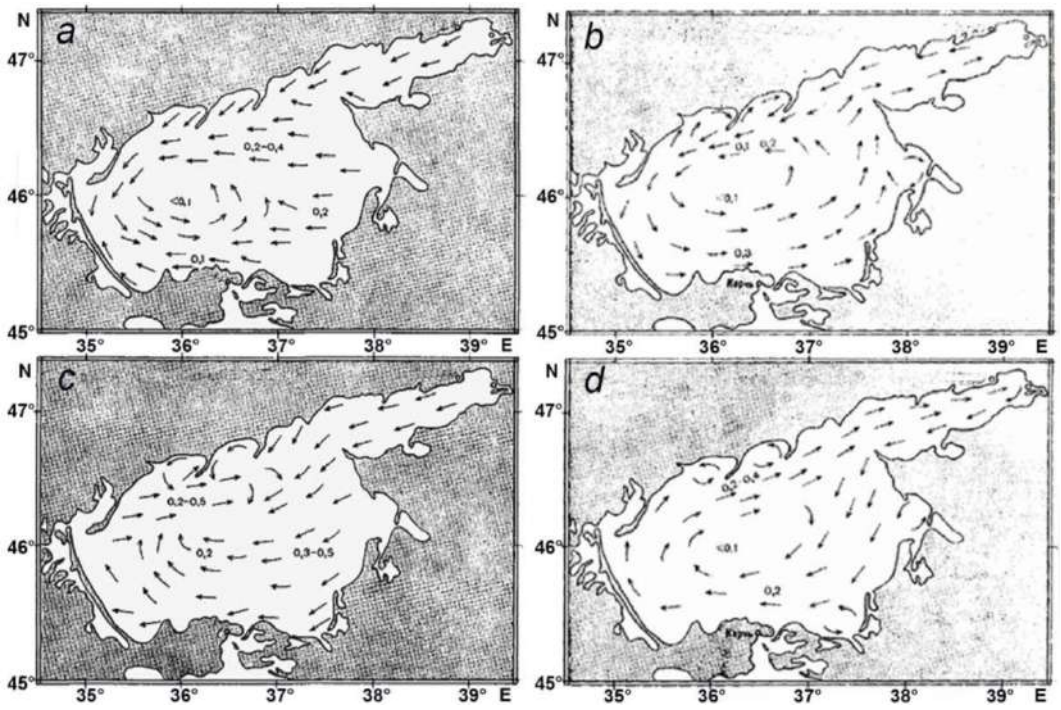

Figure 1.1.2 – Diagram of surface currents (m/s) in the Sea of Azov according to observations with moderate north-easterly (*a*), south-westerly (*b*), easterly (*c*) and westerly (*d*) winds [Lot of the Sea of Azov]

Quite a large number of works are devoted to experimental and theoretical studies of physical processes in the Sea of Azov. Thus, the seasonal fluctuations in sea level according to long-term observations are analyzed in the works [Ovsienko, 1972; Ovsienko, 1973; Altman, 1975; Altman, 1976; Scriptunov, 1978; Abuzyarov, 1981; Features of water … , 1998; Mikhailova, Shapiro, Yushchenko, 1999; Regime … , 2013]. The prognostic direction, based on the determination of empirical dependencies between fluctuations in the Sea of Azov level and meteorological factors, has been developed in the works [Karakash, 1939; Aksenov, 1955; Hydrodynamics … , 1970; Sheremetevskaya, 1977; Calculation of the transfer … , 1999]. In these works, based on the materials of the expeditions, the features of the hydrometeorological regime of the Sea of Azov and the anthropogenic load on it were revealed. The results of the

analysis using statistical methods of short-term forecasts of non-periodic fluctuations in the Sea of Azov level are presented in the works [German, 1970; German, 1971]. In these studies, based on the results of observations and empirical calculation methods, special attention is paid to the problem of water exchange between the Black and Azov Seas. In [Bronfman, 1964], one of the few publications analyzing the issues of circulation of waters and currents of the Sea of Azov, based on empirical materials, the features of water circulation in the Taganrog Bay during surges and overcurrentss are presented. Most of the published results of the analysis of dynamic processes in the Sea of Azov are based on numerical modeling data performed using existing numerical models, which can be divided into two classes: two-dimensional linear and three-dimensional nonlinear models based on shallow water equations [Volzinger, Pyaskovsky, 1968; Volzinger, 1985, Volzinger, Klevanny, Pelinovsky, 1989, Didenkulova, Kurkin, Pelinovsky, 2007; Shamin, 2008; Averbukh, Tyugin, Kurkin, Kurkina, 2011].

A number of works are devoted to the analysis of the results of modeling dynamic processes in the Sea of Azov [Filippov, 1970; Filippov, 1975; Belov, Filippov, 1978; Belov, Filippov, 1980]. Here, for the first time, on the basis of linear two-dimensional models, the main characteristics of wind currents, run-up processes for typical stationary wind fields are studied. Simulation of the circulation of unsteady motions based on two-dimensional linear equations of the theory of long waves for a homogeneous liquid was carried out in the works [Ovsienko, 1972].

Recent publications on circulation modeling include works in which two-dimensional linear shallow water models were also used. In [Konovalov, Manyluk, Cherkesov, 2000], the generation of long-wave disturbances caused by the passage of cyclones over the Sea of Azov is analyzed using two-dimensional shallow water equations. In [Matishov, Matishov, Ingebeikin, 2008; Matishov, Matishov, Savitsky, Ingebeikin, 2008; Matishov, Ingebeikin, Savitsky, 2013], free fluctuations of the Sea of Azov level are investigated within the framework of the theory of long waves based on the results of two-dimensional modeling. Based on mathematical modeling and observational data, the mechanism of formation of short-term floods and extreme currents, often observed in certain areas of the coast of the Sea of Azov and sometimes

leading to human casualties and material damage, is analyzed [Cherkesov, Shulga, 2017; Study of stationary currents … , 2017]. In [Ingebeikin, 2011], coastal areas were identified in which a similar mechanism for the formation of floods and extreme currents can operate.

Based on the finite element method in [Bukatov, Zavyalov, Solomakha, 2006], the problem of run-up oscillations in the Sea of Azov under the influence of constant wind was solved in a linear approximation. A number of works [Fomin, 2002; Fomin, Cherkesov, 2006] are devoted to the study of stationary currents in the Sea of Azov using a three-dimensional nonlinear model of current dynamics. In these works, the study of waves and currents in the Sea of Azov under the action of a stationary and spatially homogeneous wind was carried out using a three-dimensional nonlinear sigma coordinate model.

The numerical studies carried out in the works are distinguished from modern publications on circulation modeling [Shabas, Chikin, 2001; Chikin, 2001; Chikin, Shabas, Sidiropulo, 2008; Chikin, A two-layer mathematical model ..., 2009; Chikin, Mathematical model ..., 2009; Chikin, Biryukov, 2010], in which three-dimensional nonlinear shallow water models were used to study stationary movements and transport of impurities. In these studies, a scheme of surface and bottom currents was obtained and the most characteristic features of circulation were revealed depending on the direction and speed of the wind. Using a two-layer mathematical model and based on the materials of daily hydrometeorological observations at the coastal base of the Southern Scientific Center of the Russian Academy of Sciences in the period from March 20 to March 26, 2013, the reconstruction of the picture of abnormal flooding of the Don Delta was carried out [Modeling of extreme …, 2014].

On three-dimensional modeling of currents in the Sea of Azov and the Kerch Strait, there are known works based on the analysis of results obtained using a two-layer model of hydrodynamics using uniform rectangular grids using shallow water equations for the upper layer and three-dimensional equations of motion of a viscous incompressible liquid in the lower layer [Matishov, Chikin, 2012; Matishov, Chikin, 2012; Matishov, 2015]. Using this model, in the absence of background stationary currents, currents

patterns were obtained in various wind situations, and the influence of the presence or absence of a dam along the Tuzlin Spit on currents in the central part of the Kerch Strait was studied. Based on the results of modeling and based on the materials of daily hydrometeorological observations at the coastal base of the Southern Scientific Center of the Russian Academy of Sciences, the reconstruction of the picture of anomalous phenomena in the Kerch Strait was carried out [Matishov, Berdnikov, 2015].

The works [Ivanov, Cherkesov, Shulga, 2012; Ivanov, Cherkesov, Shulga, 2014] are devoted to the study of overburden phenomena and currents of the Sea of Azov without taking into account the Kerch Strait, in which the features of the formation of level fields are revealed using a three-dimensional hydrodynamic σ-coordinate POM model adapted to the area of the Sea of Azov [Fomin, 2002] seas and currents generated by various wind fields.

The ecological state of marine basins and their biological productivity are directly related to the entry of polluting organic and inorganic substances into the marine environment. There are a number of studies on the evolution of impurities in the Sea of Azov [Calculation of the transfer … , 1999; Shabas, Chikin, 2001]. The generator of the motion of the aquatic environment in these studies is either a constant or averaged wind at certain time intervals. The latest results of research on oceanological processes in the Sea of Azov are presented in the cycle of works by G.G. Matishov [Modern dangerous exogenous processes …, 2015]. The paper presents the patterns of long-term changes in the oceanological regime due to climatic influences and anthropogenic factors. The changes in the bioproductivity of the Sea of Azov have been studied, and a hydroecological assessment of the maximum permissible transformations of river currents has been given.

Summing up, we can say that every year interest in the problem of forecasting the ecological state of the Sea of Azov is growing. Most of the existing approaches to the processing of measurement data make it possible to analyze the state of the Sea of Azov only using unidirectional data characterizing the current state of the marine environment. To obtain forecasts and simulate processes that cannot be directly observed, it is advisable to conduct numerical experiments using modern hydrodynamic models.

And perhaps most importantly, the numerical simulation results interpolate between the rare ocean observations obtained from ships, drifters and satellites.

Numerical models in general, models can be divided into two groups: physical (mechanistic) and simulation models. The first are simplified models that give an idea of the physical mechanisms that affect the marine environment. Simulation models are used to calculate the circulation of pools with a realistic seabed. With their help, it is possible to calculate and predict currents in the sea, the algebraic approximations of differential equations used in them allow us to take into account the influence of viscosity and nonlinear dynamics of currents. Models of this type require adaptation – parameter settings for modeling in real marine reservoirs with their own unique hydrodynamic and geographical features.

In addition, joint modeling of currents and waves is currently of great theoretical and practical interest. Due to the close connection of these processes, it becomes necessary to build joint models that take into account the mechanisms of interaction between them. In the numerical implementation of such models, complexity arises due to the incommensurability of the spatial and temporal scales of currents and wind waves, which significantly complicates modeling within the framework of a unified system of Navier-Stokes equations. An alternative approach is to use an adapted simulation model in conjunction with additional simplified software modules that meet the regional characteristics of the studied basin and solve auxiliary tasks (transfer and distribution of suspended solids, assimilation of satellite and *in situ* observations). The latter can be implemented with the same or similar spatial-temporal resolution as the currents model. This makes it possible to carry out joint calculations with an acceptable cost of computing resources.

1.2. Three-dimensional hydrodynamic model

The numerical study of water circulation in a basin with the specified bottom topography and extensive shallow areas is based on the application of a modern, well-known three-dimensional sigma-coordinate hydrodynamic model POM, the code

of which is publicly available (*http://www.ccpo.odu.edu/POMWEB*). The POM model proposed in [Blumberg, Mellor, 1987] is a model of ocean circulation that implements the solution of a system of primitive equations of hydrodynamics written in the approximations of incompressibility, hydrostatics and Boussinesq. For an incompressible stratified fluid in the Boussinesq approximation, the equations of motion in the Cartesian coordinate system, taking into account the rotation of the Earth with angular velocity Ω, viscosity and diffusion, have the form [Kamenkovich, 1973; Monin, 1978; Miropolsky, 1981; Goldstein, Gorodtsov, 2000]:

$$\mathbf{u}_t + (\mathbf{u}\nabla)\mathbf{u} = -\nabla P + \vartheta\nabla\mathbf{u} + Sg - 2\,\Omega \times \mathbf{u}, \tag{1.2.1}$$

$$S_t + (\mathbf{u}\nabla)\mathrm{S} = k\Delta\mathrm{S}, \tag{1.2.2}$$

$$\mathrm{div}\,\mathbf{u} = 0, \tag{1.2.3}$$

here $\mathbf{u} = (u, v, w)$ – is the velocityis the velocity; u, v, w – are the velocity projections along the x, y, z axes, respectively, S – is the impurity concentration, P is the pressure related to the unit density, $\Omega = \Omega\mathbf{e}_z$ – is the angular velocity of the Earth's rotation where Ω – is the angular velocity of the Earth's rotation taking into account the annual rotation around the Sun, $\Omega \times \mathbf{u} = \Omega\,(-\mathbf{e}_x v + \mathbf{e}_y u)$, $\mathbf{e} = (\mathbf{e}_x, \mathbf{e}_y, \mathbf{e}_z)$ – are the guiding orthes of the Cartesian coordinate system, g is the acceleration of gravity, ϑ and k are the coefficients of kinematic viscosity and diffusion, respectively.

In this model, a computational splitting scheme is used to integrate the barotropic (external) and baroclinic (internal) modes at the corresponding time steps in order to reduce the calculation time. Based on the assumption of hydrostatic equilibrium, the nonlinear equations of motion of a homogeneous viscous incompressible fluid in the approximation of the theory of shallow water in Cartesian coordinates are expressed as follows [Blumberg, Mellor, 1987]:

$$\nabla \cdot \mathbf{U} + \frac{\partial w}{\partial z} = 0, \tag{1.2.4}$$

$$\frac{\partial u}{\partial t} + \mathbf{U} \cdot \nabla u + w\frac{\partial u}{\partial z} - fv = -\frac{1}{\rho_0}\frac{\partial P}{\partial x} + \frac{\partial}{\partial z}\left(K_M \frac{\partial u}{\partial z} \right) + A_x, \tag{1.2.5}$$

$$\frac{\partial v}{\partial t} + \mathbf{U} \cdot \nabla v + w\frac{\partial v}{\partial z} + fu = -\frac{1}{\rho_0}\frac{\partial P}{\partial y} + \frac{\partial}{\partial z}\left(K_M \frac{\partial u}{\partial z} \right) + A_y, \tag{1.2.6}$$

$$\frac{\partial P}{\partial z} + g\rho = 0. \tag{1.2.7}$$

In these equations, z is the vertical coordinate in depth; the x axis is directed to the east; y – to the north; $\zeta = \zeta(x, y, t)$ – deviation of the sea level from its undisturbed state; t – time; $\mathbf{U} = (u, v)$ – horizontal velocity vector; $\nabla = \left\{ \frac{\partial}{\partial x}, \frac{\partial}{\partial y} \right\}$ – vector differential horizontal operator; ρ – water density; $\rho_0 = \frac{1}{\zeta + H}\int_{-H}^{\zeta} \rho dz$ – average water density by depth; $f = 2\Omega\sin\phi$ is the Coriolis parameter, ϕ – latitude; $P(x, y, z, t)$ – pressure at depth z based on vertical integration (1.2.7): $P(x, y, z, t) = P_{\text{atm}} + g\rho_0(\zeta - z)$, $P_{\text{atm}} = 1013{,}25$ gPa – standard atmospheric pressure at 0°C at latitude 45°; K_M – the coefficient of vertical turbulent viscosity, which was parameterized using the Mellor-Yamada differential model [Mellor, Yamada, 1982].

The terms A_x и A_y in equations (1.2.5) and (1.2.6) determine the horizontal viscosity:

$$\begin{aligned} A_x &= \frac{\partial}{\partial x}\left(2A_M \frac{\partial u}{\partial x} \right) + \frac{\partial}{\partial y}\left(A_M \left(\frac{\partial v}{\partial x} + \frac{\partial u}{\partial y} \right) \right), \\ A_y &= \frac{\partial}{\partial y}\left(2A_M \frac{\partial v}{\partial y} \right) + \frac{\partial}{\partial x}\left(A_M \left(\frac{\partial v}{\partial x} + \frac{\partial u}{\partial y} \right) \right), \end{aligned} \tag{1.2.8}$$

where $A_M(x, y, z, t)$ – is the coefficient of turbulent viscosity (≥ 10 м^2/с), depending on the horizontal velocity gradients, calculated using the Smagorinsky formula [Smagorinsky J., 1963]:

$$A_M = \alpha \Delta x \Delta y \sqrt{\left(\frac{\partial u}{\partial x}\right)^2 + \left(\frac{\partial v}{\partial y}\right)^2 + \frac{1}{2}\left(\frac{\partial v}{\partial x} + \frac{\partial u}{\partial y}\right)^2}\,. \qquad (1.2.9)$$

Here Δx, Δy – are the size of the model grid in the direction of the x and y axes, respectively, and α is some horizontal mixing constant, taking values from 0.10 to 0.20. When calibrating the model for the Sea of Azov, the value α = 0,10 was used. Using the Smagorinsky formula allows for modeling to adjust to changes in the resolution of the model grid and the values of velocity gradients. For example, the use of a more precise lattice size reduces the need for calculating horizontal diffusion, because, as mentioned in [Blumberg, Mellor, 1987], horizontal advection followed by vertical mixing effectively acts as horizontal diffusion.

To solve the problem of turbulent closure, the POM model uses the Mellor-Yamada closure scheme level 2.5, which is a simplified version of the more general turbulent closure model of level 4. This parameterization, based on Kolmogorov's theory of small-scale locally homogeneous turbulence (details on the development and assumptions in [Mellor, Yamada, 1974; Mellor, Yamada, 1982], is based on the equation of turbulent kinetic energy, the right part of which includes the terms, depending on vertical wind gradients and potential temperature. The closure scheme is based on the solution of two additional partial differential equations (1.2.10) and (1.2.11) to determine the kinetic energy of turbulence $q^2/2$ and the turbulence macro scale l:

$$\frac{dq^2}{dt} = \frac{\partial}{\partial x}\left(K_V \frac{\partial q^2}{\partial x}\right) + \frac{\partial}{\partial y}\left(K_V \frac{\partial q^2}{\partial y}\right) + \frac{\partial}{\partial z}\left(K_M \frac{\partial q^2}{\partial z}\right) + \\ + 2\left[A_V\left(\left(\frac{\partial u}{\partial z}\right)^2 + \left(\frac{\partial v}{\partial z}\right)^2\right) + K_V \frac{g}{\rho_0} - \frac{q^3}{B_1 l}\right], \qquad (1.2.10)$$

$$\frac{dq^2l}{dt} = \frac{\partial}{\partial x}\left(K_V \frac{\partial q^2 l}{\partial x}\right) + \frac{\partial}{\partial y}\left(K_V \frac{\partial q^2 l}{\partial y}\right) + \frac{\partial}{\partial z}\left(K_M \frac{\partial q^2 l}{\partial z}\right) + \\ + lE_1 A_V \left(\left(\frac{\partial u}{\partial z}\right)^2 + \left(\frac{\partial v}{\partial z}\right)^2\right) + K_V \frac{E_1 g}{\rho_0} - \frac{q^3}{B_1}\left(1 + E_2 \frac{l}{kL}\right). \quad (1.2.11)$$

Here k = 0,4 – is the Pocket constant; $L^{-1} = (\zeta - z)^{-1} + (H - z)^{-1}$ – is the scale of the distance to a solid surface; $1+ E_2(l/kL)$ – is the function of proximity to the side wall of the pool; $E_1 = 1.8$; $E_2 = 1.33$. Calculation of the coefficients of vertical kinematic viscosity and turbulent diffusion (K_V, A_V и K_M) in accordance with the semi-empirical model [Mellor, Yamada, 1982] are defined as functions of the kinetic energy of turbulence $q^2/2$ and the turbulence macro scale l:

$$K_V = qLS_K, \quad A_V = qLS_A, \quad K_M = qLS_M. \quad (1.2.12)$$

Here S_K, S_A and S_M – stability functions are analytically derived from closure hypotheses generalized by Mellor and Yamada [Mellor, Yamada, 1982]:

$$S_K = \frac{A_2(1-6A_1/B_1)}{1-3A_2G_H(B_2+6A_1)}, \quad (1.2.13)$$

$$S_A = \frac{B_1^{-1/3} - 3A_1A_2G_H[(B_2-3A_2)(1-6A_1/B_1) - 3C_1(B_2+6A_1)]}{[1-3A_2G_H(B_2+6A_1)](1-9A_1A_2G_H)}, \quad (1.2.14)$$

$$S_M = 0.20, \quad (1.2.15)$$

$$G_H = \left(\frac{l}{q}\right)^2 \frac{g}{\rho_0}\left(\frac{\partial \rho}{\partial z} - \frac{1}{c_s^2}\frac{\partial P}{\partial z}\right), \quad (1.2.16)$$

where G_H – the Richardson number; five constants in the expressions (1.2.13), (1.2.14) are estimated from neutral homogeneous and close to surface turbulence data $A_1 = 0.92$; $A_2 = 0.74$; $B_1 = 16.6$; $B_2 = 10.1$; $C_1 = 0.08$; c_s^2 in the formula (1.2.16) is the speed of sound squared. The stability functions are limited to infinity, since G_H is approaching a value of 0.0288 – greater than expected in nature. In the model, the vertical pressure gradient

is calculated from the hydrostatic ratio, but here the density is assumed to be constant, consistent with the definition of pressure $\partial P/\partial z = -\rho_o g$.

The boundary conditions on the free surface $\zeta = \zeta(x, y, t)$:

$$w|_{z=\zeta} = \frac{\partial \zeta}{\partial t} + u\frac{\partial \zeta}{\partial x} + v\frac{\partial \zeta}{\partial y},\ K_M\left(\frac{\partial u}{\partial z}, \frac{\partial v}{\partial z}\right)\Big|_{z=\zeta} = (\tau_{0x}, \tau_{0y}),\ q^2|_{z=\zeta} = B_1^{\frac{2}{3}}\mathbf{U}_0^2,\ l|_{z=\zeta} = 0, \quad (1.2.17)$$

where $\mathbf{U}_0 = \{u_0, v_0\}$ – velocity in the near-surface layer of the sea; $\tau_{0x} = \rho_a C_a^i W_x|\mathbf{W}|$ and $\tau_{0y} = \rho_a C_a^i W_y|\mathbf{W}|$ – projections of tangential wind stresses $\mathbf{W} = \{W_x, W_y\}$ – the vector of the driving wind velocity at an altitude of 10 m above sea level [Blumberg, Mellor, 1987]; ρ_a – air density in standard atmospheric conditions; $C_a{}^i$ ($i = 1, \ldots, 4$) – the coefficient of surface friction, depending on the wind speed, which can be calculated based on a number of empirical formulas proposed by various authors [Large, Pond, 1981; Pond, 1981; Hsu, 1986].

The boundary conditions at the bottom $z = H(x, y)$ satisfy the equality of zero of the normal component of velocity, and the bottom shear stresses are related to velocity by a quadratic dependence [Blumberg, Mellor, 1987]:

$$\left(w + u\frac{\partial H}{\partial x} + v\frac{\partial H}{\partial y}\right)\Big|_{z=-H} = 0, K_M\left(\frac{\partial u}{\partial z}, \frac{\partial v}{\partial z}\right)\Big|_{z=-H} = (\tau_{1x}, \tau_{1y}), q^2|_{z=-H} = B_1^{\frac{2}{3}}\mathbf{U}_b^2, l|_{z=-H} = 0, \quad (1.2.18)$$

where $\mathbf{U}_b = \{u_b, v_b\}$ – the currents velocity at the point closest to the bottom of the model grid of the basin; $\tau_{1x} = \rho_0 c_b u_b|\mathbf{U}_b|$; $\tau_{1y} = \rho_0 c_b v_b|\mathbf{U}_b|$ – parameterization of the friction stress on the bottom; c_b – the coefficient of bottom friction, defined as the maximum between the value calculated in accordance with the standard logarithmic dependence and the value equal to 0.0025 [Blumberg, Mellor, 1987];

$$c_b = \max\left[k^2(\ln\frac{H + z_b}{z_0})^{-2};\ 0{,}0025\right], \quad (1.2.19)$$

where z_b – the first point of the pool grid closest to the bottom; z_0 = 00.003 m is a roughness parameter characterizing the hydrodynamic properties of the underlying bottom surface. The values of z_0 in (1.2.19) are determined using Grant-Madsen theory [Grant, Madsen, 1979], describing the mechanism of the influence of waves on currents in the bottom boundary layer. At the initial moment of time t = 0, there is no fluid movement, the free surface is horizontal:

$$u(x, y, z, t) = v(x, y, z, t) = w(x, y, z, t) = \zeta(x, y, z, t) = 0. \quad (1.2.20)$$

To solve the problem of impurity transfer and dispersion, the system of equations of fluid motion (1.2.4) – (1.2.7) is supplemented by a three-dimensional equation of transfer and diffusion (1.2.21). The impurity concentration is given by the function $C = C(x, y, z, t)$, depending on coordinates and time. Assuming that an admixture of neutral buoyancy consists of particles of the same type, the evolution equation has the form [Blumberg, Mellor, 1987; Yang, Hamrick, 2003]:

$$\frac{dC}{dt} = \frac{\partial}{\partial x}\left(A_H \frac{\partial C}{\partial x}\right) + \frac{\partial}{\partial y}\left(A_H \frac{\partial C}{\partial y}\right) + \frac{\partial}{\partial z}\left(K_H \frac{\partial C}{\partial z}\right). \quad (1.2.21)$$

Here A_H – coefficient of horizontal turbulent diffusion; K_H – the coefficient of vertical turbulent diffusion. The boundary conditions for the equations of motion (1.2.17), (1.2.22) are supplemented by conditions for the absence of an impurity currents: the condition is fulfilled on the free surface $\left(K_H \frac{\partial C}{\partial \mathbf{n}}\right)\Big|_{z=\zeta} = 0$; in the bottom layer – $\left(K_H \frac{\partial C}{\partial \mathbf{n}}\right)\Big|_{z=\zeta} = 0$, on the lateral boundaries – $\left(A_H \frac{\partial C}{\partial \mathbf{n}}\right)\Big|_S = 0$.

The POM model is designed to perform calculations in shallow marine basins with complex coastal topography, requiring the use of coordinates unevenly distributed

in depth (sigma coordinates). In this model, a dimensionless coordinate is used as a vertical variable σ ∈ [0, 1]:

$$\sigma = \frac{z-\zeta(x,y,t)}{H(x,y)+\zeta(x,y,t)}. \quad (1.2.22)$$

Here $H = H(x, y)$ – the depth of the sea is at rest. In the initial equations (1.2.4) – (1.2.7), boundary conditions (1.2.17), (1.2.22) and initial conditions (1.2.24), the transition from the z coordinate to the σ coordinate is carried out [Blumberg, Mellor, 1987]. When switching to a new system, the equations of ocean hydrodynamics using the Boussinesq and hydrostatics approximations are rewritten as follows:

$$\frac{\partial\zeta}{\partial t}+\frac{\partial(Du)}{\partial x}+\frac{\partial(Dv)}{\partial y}+\frac{\partial W}{\partial\sigma}=0, \quad (1.2.23)$$

$$\frac{\partial(Du)}{\partial t}+\mathrm{A}u-fvD+gD\frac{\partial\zeta}{\partial x}+\frac{D}{\rho_0}\frac{\partial P}{\partial x}=\frac{\partial}{\partial\sigma}\left(\frac{K_M}{D}\frac{\partial u}{\partial\sigma}\right)+DF_x, \quad (1.2.24)$$

$$\frac{\partial(Dv)}{\partial t}+\mathrm{A}v+fuD+gD\frac{\partial\zeta}{\partial y}+\frac{D}{\rho_0}\frac{\partial P}{\partial y}=\frac{\partial}{\partial\sigma}\left(\frac{K_M}{D}\frac{\partial v}{\partial\sigma}\right)+DF_y, \quad (1.2.25)$$

$$\frac{\partial P}{\partial z}+g\rho=0. \quad (1.2.26)$$

Here W – the Lagrangian velocity of the liquid on the σ-layer; w – the Eulerian velocity of a liquid; $D = H + \zeta$ – the dynamic depth of the sea at the point (x, y), allowing to rewrite (1.2.22) as $D\sigma = z - \zeta$; A – the transfer operator, which is part of the total derivative

of the velocity component in (1.2.23) and (1.2.24), is disclosed as follows: $\mathrm{A}\Psi = \frac{\partial(uD\Psi)}{\partial x} + \frac{\partial(uD\Psi)}{\partial y} + \frac{\partial(W\Psi)}{\partial \sigma}$. The terms F_x, F_y, parametrizing horizontal turbulent viscosity and diffusion, have the form

$$\begin{aligned} DF_X &= \frac{\partial}{\partial x}\left(2A_M D\frac{\partial u}{\partial x}\right) + \frac{\partial}{\partial y}\left[A_M D\left(\frac{\partial u}{\partial y} + \frac{\partial v}{\partial x}\right)\right], \\ DF_Y &= \frac{\partial}{\partial x}\left[A_M D\left(\frac{\partial v}{\partial x} + \frac{\partial u}{\partial y}\right)\right] + \frac{\partial}{\partial y}\left(2A_M D\frac{\partial v}{\partial y}\right) \end{aligned}. \qquad (1.2.27)$$

The system of equations (1.3.4) – (1.3.7) is solved under the following boundary conditions along the vertical coordinate:

$$\omega\big|_{\sigma=0} = 0, \qquad \frac{K_M}{D}\left(\frac{\partial u}{\partial \sigma}, \frac{\partial v}{\partial \sigma}\right) = \frac{1}{\rho}\left(\tau_{0x}, \tau_{0y}\right), \qquad (1.2.28)$$

$$\omega\big|_{\sigma=-1} = 0, \qquad \frac{K_M}{D}\left(\frac{\partial u}{\partial \sigma}, \frac{\partial v}{\partial \sigma}\right) = \frac{1}{\rho}\left(\tau_{1x}, \tau_{1y}\right). \qquad (1.2.29)$$

To increase the speed of numerical calculations, the transformed equations (1.2.23) – (1.2.25) are presented in the form of two systems. The first system of equations describes the barotropic component of the solution (depth–averaged horizontal components of the currents velocity and level), the second – deviations of the horizontal velocity components from the corresponding averaged components and vertical velocity. Therefore, the horizontal velocity **U** is represented as the sum, independent of depth, of the components of the $\bar{\mathbf{U}}$ (barotropic component) and **U**' (baroclinic component):

$$\mathbf{U} = \bar{\bar{\mathbf{U}}}(x, y, t) + \mathbf{U}'(x, y, \sigma, t). \qquad (1.22.30)$$

The transfer operator (A) is approximated using the TVD scheme (Total Variation Diminishing) [Pietrzak, 1998; Yang, Hamrick, 2003], (linear combination of directed difference scheme and Lax-Wendroff scheme), the spatial discretization of the equations is performed on a *C*-grid.

The integration of the obtained systems of equations is performed using difference schemes, where two-dimensional vertically integrated equations of motion (i.e. barotropic mode) are solved using a short time step (Δt_A) to describe fast-moving barotropic waves, and three-dimensional momentum equations (i.e. baroclinic mode) are solved using a longer time step (Δt). This splitting method is common to many models of the ocean with a free surface, since it is more efficient than solving three–dimensional equations with a short time step required by the Friedrichs-Levy (CFL) Courant stability condition [Courant, Friedrichs, Lewy, 1967]. For the barotropic and baroclinic modes, the computational stability conditions have the form

$$\Delta t_A = \frac{1}{c_t}\left(\frac{1}{\Delta x^2} + \frac{1}{\Delta y^2}\right)^{-1/2}, \tag{1.2.31}$$

$$\Delta t \le \frac{1}{c_T}\left(\frac{1}{\Delta x^2} + \frac{1}{\Delta y^2}\right)^{-1/2}, \tag{1.2.32}$$

where $C_t = 2(gH_{\max})^{1/2} + U_{1\max}$; $C_T = 2C + U_{2\max}$ $U_{1\max}$ and $U_{2\max}$ – maximum velocities and maximum advective transfer velocities;Δx and Δy – are the grid steps in the direction of the x and y; $H_{\max}$ – is the maximum depth of the basin; C – is the maximum internal velocity of the gravitational wave, usually of the order of 2 m/s. Additional information on the sensitivity of the POM model to time steps is given in [Ezer, Arango, Shchepetkin, 2002], where the recommended ratio between internal and external time steps $\Delta t/\Delta t_A$ is about 20 – 80.

1.3. Adaptation of the hydrodynamic POM model to the Azov Sea basin

In order to apply the described hydrodynamic model to the shallow basin, which is the Sea of Azov, we had to carry out some work on its adaptation. First of all, this is due to the consideration of the actual bathymetry of the Azov basin. The depth array of the Sea of Azov, taken from navigation maps and set in the standard geographical coordinate system, is transferred to the model area inside the calculation block of the model by spatial interpolation. The Kerch Strait is narrow, so we considered two types of bottom relief (Figure 1.3.1). The first model basin of the Sea of Azov is closed, with a border at the entrance to the Kerch Strait (Figure 1.3.1, right). The second one includes the Sea of Azov and the Kerch Strait with a liquid border at the nasty entrance to the strait.

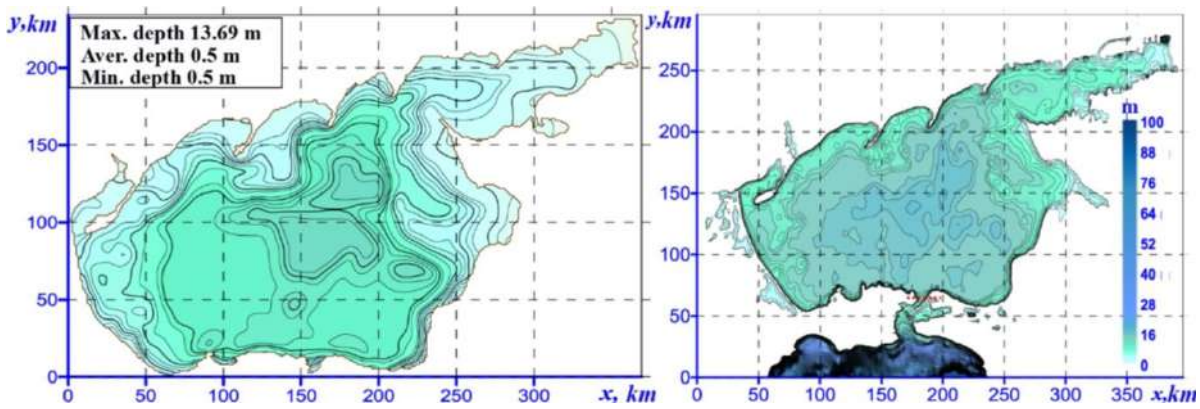

Figure 1.3.1 – The used bathymetric grid of the Sea of Azov (m): on the left – without taking into account the currents of water through the Kerch Strait; on the right – with the condition of free passage of liquid through the Kerch Strait

In one of the variants of the model grid, the liquid boundary runs along 45.25°N (the red line in Figure 1.3.1, on the left). In the other, the border runs along the Black Sea at a section of 44.81° N ($60 \le x \le 240$ km, $y = 0$) (the x axis in Figure 1.3.1, on the left). The simulation is performed without taking into account the incurrents and outcurrents of river waters from the Azov basin. In this case, at the boundaries of the basin,

the condition of the absence of a liquid currents perpendicular to the lateral boundaries ($\partial \mathbf{U_n}/\partial \mathbf{n} = 0$), is fulfilled, and the tangential stresses are zero ($\mathbf{U_\tau} = 0$), were $\mathbf{n}$ and $\boldsymbol{\tau}$ – are vectors indicating normal and tangential directions [Cherkesov, Ivanov, Khartiev, 1992; Blumberg, Mellor, 1987].

The bathymetric grids described above (Figure 1.3.1) are based on diagrams with polyphonic projections. The transformation of geographical coordinates (latitude and longitude) into grid coordinates (x and y) and vice versa is performed using precise polyconic projection formulas, but these formulas are complex and calculations based on them, even with the help of a computer, take a lot of time. Coordinate transformation formulas with sufficient accuracy (~500 m) can be obtained by simply decomposing the geographical coordinate by the grid coordinate, and vice versa [Schwab, Sellers, 1980].

For the Azov basin, which has a small length, the calculation of the steps of a rectangular grid is performed without taking into account the sphericity of the Earth:

$$\Delta x = \Delta_{\text{long}} \cdot (Lon_R - Lon_L)/(m - 1),\ \Delta y = \Delta_{\text{lati}} \cdot (Lat_N - Lat_S)/(n - 1), \qquad (1.3.1)$$

where Δx and Δy – are the resolution in the coordinate system of the model grid with dimensions $N = m \times n$, in which the distance is calculated to the east and north from the origin located at a point with latitude and longitude corresponding to the values in the usual geographical coordinate system: Lon_L = 34°E, Lat_S = 44.50104° N; the value in meters is 1° in longitude Δ_{long} = 80000 and in latitude Δ_{lati} = 112500. For a better fit of the coastline to the x-axis, the bathymetric grid rotates counterclockwise by 51° relative to the central meridian of the bathymetric map. The number of nodes of the calculated grid (N) for the selected model basins shown in Figure 1.3.1 is different, since it depends on the size of the studied area and on the resolution in latitude and longitude. For a basin with a boundary at the entrance to the Kerch Strait (Figure 1.3.1, right), the resolution of the calculated grid is 276 × 176 nodes, for a basin with a boundary at the section in the Black Sea (Figure 1.3.1, left), the grid resolution is 396 × 295 nodes.

The heterogeneous distribution of depths in the Sea of Azov (in its southern part up to 19 m and 0.5 – 4 m in the coastal areas – Taman and Dinsky Bays) necessitates the use of three-dimensional hydrodynamic models with curved coordinate systems. This circumstance led to the choice of the POM model as a numerical calculation tool. Integration in the POM model is performed in Cartesian coordinates, which is consistent with the geometric dimensions of the studied basin. The length of the Sea of Azov in the zonal direction (360 km) makes it possible to neglect the curvature of the Earth (much less than the radius of the Earth, 6.400 km) and consider the undisturbed surface of the reservoir flat. To substantiate this statement, we will evaluate the errors that arise based on a comparison of the length of the arc of the earth's surface (orthodromy, L_{ort}), contracting the extreme points of the Sea of Azov (45°12′30″ – 47°17′30″ N and 33°38′ – 39°18′ E), with a distance between them horizontally (loxodromy, L_{lok}). The calculation of the lengths of the orthodromy arc is performed according to the well–known formulas of spherical trigonometry – the cosine theorem of the sides [Kozhukhov, Zhukhlin, 1987], the length of the loxodromy - according to the Pythagorean theorem:

$$L_{ort} = \arccos(\cos(90° - \varphi_1)\cos(90° - \varphi_2) + \sin(90° - \varphi_1)\sin(90° - \varphi_2)\cos\Delta\lambda), \qquad (1.3.2)$$

$$L_{lok} = (\Delta\varphi^2 - \Delta\lambda^2\cos^2\varphi_{cp})^{1/2}. \qquad (1.3.3)$$

Here φ_1, φ_2 и λ_1, λ_2 – the values of the latitudes and longitudes of the extreme points of the Sea of Azov; $\Delta\varphi = \varphi_2 - \varphi_1$ и $\Delta\lambda = \lambda_2 - \lambda_1$ – the difference in latitude and longitude of these points; $\varphi_{cp} = (\varphi_2 + \varphi_1)/2$ – the value of the average latitude between them. The value of the arc length calculated by the formula (1.2.2), L_{ort} = 376.28 km, the value of the horizontal distance calculated by the formula (1.2.3), L_{lok} = 356.34 km. Thus, the relative error of numerical calculations without taking into account the sphericity of the Earth $\delta = 100\% (L_{ort} - L_{lok})/ L_{ort}$ = 0.02 %.

When adapting the POM model to the Azov basin, a series of numerical experiments were carried out to adjust the optimal values of spatial and temporal integration steps. The result of the study of the sensitivity of the POM model to the ratio

between the time steps (1.2.31) and (1.2.32) allowed us to select their optimal values. The determination of the averaged two–dimensional horizontal components of velocity and sea level (integration of the equations of the barotropic regime) is performed in steps of $\Delta t_A = 18$ s, and in steps of $\Delta t = 3$ min - calculation of deviations from the found average and vertical components of velocity [Ivanov, Cherkesov, Shulga Computer … , 2011]. The basic calculations were carried out on a rectilinear horizontal grid with a spatial resolution of $\Delta x = \Delta y \sim 1$ км and on a vertical grid σ with 11 layers.

The results of numerical experiments on model verification based on comparison with direct measurement data are described in detail in a number of papers [Ivanov, Cherkesov, Shulga, 2010; Numerical research ... , 2017; Cherkesov, Shulga, Waves, currents … , 2017]. They present the results of assessing the impact of changes in the size of steps in spatial ($\Delta x = \Delta y \sim 2$ km) and temporal coordinates (Δt = 6 min). The results of testing the model for various atmospheric conditions: for example, the extreme storm on November 11, 2007, which caused a shipwreck in the Kerch Strait, as well as the effects of moderate wind, are given in [Cherkesov, Shulga, Waves, currents … , 2017]. These studies were performed using data from the reanalysis of the SKIRON/Eta atmospheric model (http://forecast.uoa.gr) [The Regional Weather ..., 1997]. The issue of model verification is described in more detail in chapters 3 and 4. Here are the results of comparing simulation data in conditions of a real non-stationary wind with data from direct level measurements given in the tables of hourly elevation data of the State Meteorological Service for nine stations located near large settlements of the coast of the Sea of Azov.

At the stage of setting the model parameters, the hydrodynamic model was tested taking into account a number of empirical formulas that determine the coefficient of surface friction in boundary conditions (1.2.17). The first coefficient (1.3.4) is based on the well-known ratio [Large, Pond, 1981], according to a later work [Hsu, 1986], the calculation of the coefficient of surface friction C_a^2 an be perform according to the formula (1.3.5). The following coefficients C_a^3 and C_a^4 are calculated according to the most modern representation (1.3.6) [Wu, 1987] and (1.3.7) [Mathematical modeling … , 2011].

$$10^3 \mathrm{C}_a^1 = \begin{cases} 1.14; & |\mathbf{W}| \leq 10\ m/s, \\ 0.49 + 0.065|\mathbf{W}|; & |\mathbf{W}| > 10\ m/s, \end{cases} \quad (1.3.4)$$

$$\mathrm{C}_a^2 = k^2\left(14.56 - 2\ln(W_0)\right)^{-2}, \quad (1.3.5)$$

were $W_0 = |\mathbf{W}|/W_1$; W_1 = 1 m/s,

$$10^3 \mathrm{C}_a^3 = \begin{cases} 1.2; & |\mathbf{W}| \leq 7.5\ m/s, \\ 0.8 + 0.065|\mathbf{W}|; & |\mathbf{W}| > 7.5\ m/s, \end{cases} \quad (1.3.6)$$

$$10^3 C_a = \begin{cases} 2.5; & |\mathbf{W}| > 22\ m/s, \\ 0.49 + 0.065|\mathbf{W}|; & 8 \leq |\mathbf{W}| \leq 22\ m/s, \\ 1.2; & 4 \leq |\mathbf{W}| \leq 8\ m/s, \\ 1.1; & 1 \leq |\mathbf{W}| \leq 4\ m/s. \end{cases} \quad (1.3.7)$$

Figure 1.3.2 shows graphs of the dependence of the coefficients of surface friction on the magnitude of the wind speed, varying in the range from 0 to 30 m/s, calculated using formulas (1.3.4) – (1.3.7). Despite the fact that the bounded smooth function (1.3.4) with bounded derivatives is more preferable for use in numerical calculations, at low wind speeds (0 – 7 m/s) the corresponding value of the coefficient of friction will be underestimated.

For a moderate wind speed of 7 – 10 m/s, the values of C_a^i (i = 1, ... ,4) differ little ($C_a^3 > C_a^4 > C_a^1$), however, at the right boundary of this interval (10 m/s) there is a sharp overestimation of the coefficient of friction, calculated also by the formula (1.3.5). At a wind speed of 10 – 22 m/s, the inequality $C_a^2 > C_a^3 > C_a^1 = C_a^4$. is satisfied between the values of the friction coefficients. For strong winds with speeds of more than 22 m/s, the values of the friction coefficients C_a^2, C_a^3 and C_a^4 are comparable, and the value obtained by the formula (1.3.4) is underestimated. Thus, when setting the boundary conditions, the most optimal choice will be the value of C_a^2 (1.3.7) provided that the current wind speed exceeds 5 m/s. Calculations related to changes in wind speed over the entire range of 0 – 30 m/s for the Azov Sea basin were performed using formulas

(1.3.4) and (1.3.7) [Ivanov, Cherkesov, Shulga, 2014, Cherkesov, Shulga, Waves, currents … , 2017, Cherkesov, Shulga, 2018].

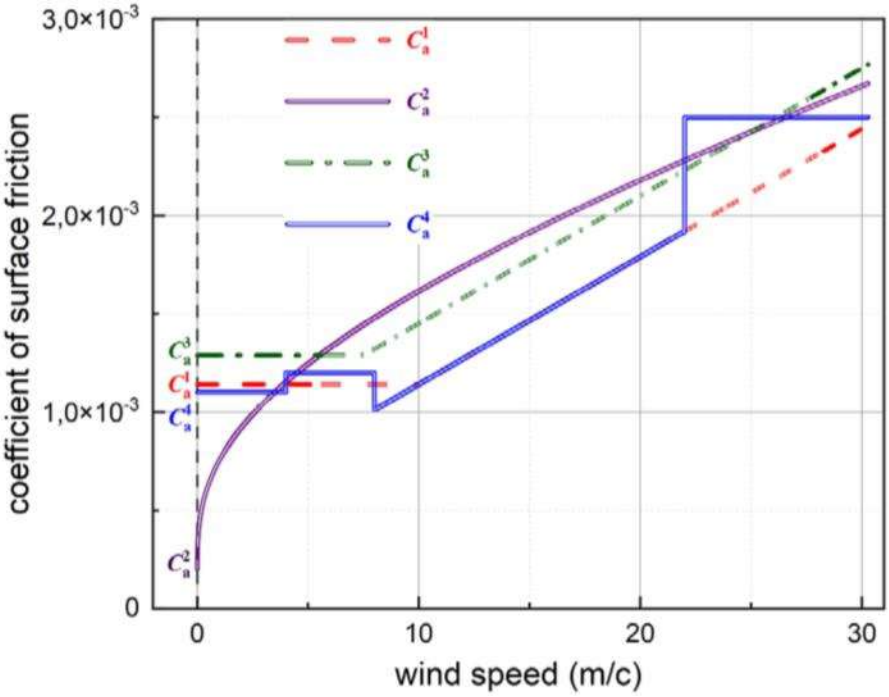

Figure 1.3.2 – Dependence of the coefficient of surface friction on wind speed

The study of the evolution of a contaminant in the Azov Sea basin requires adjusting the hydrodynamic POM model to the features of this marine basin. First of all, in the block for calculating the transport-diffusion equations (1.2.21), based on the analysis of the results given in [Altman, Lagutin, Tolmazin, 1966; Pukhtyar, Osipov, 1981; Sudolsky, 1991; Tolmazin, Schneidman, Atsikhovskaya, 1969], the following were selected for the Sea of Azov The values of the turbulent diffusion coefficients are: A_H = 10 m^2/s, K_H = 10^{-4} m^2/s. In numerous works, the features of turbulence for shallow sea areas and its differences from Richardson Obukhov's law of "four thirds" are studied in detail. Thus, for the Kerch Strait and the coastal areas of the Black and Azov Seas (up to 2 km and 6–12 km from the shore [Tolmazin, Schneidman, Atsikhovskaya, 1969]) empirical dependences of the coefficients of turbulent exchange A_H [Altman, Lagutin, Tolmazin, 1966] and horizontal turbulent

diffusion K_H [Pukhtyar, Osipov, 1981] on the average currents velocity with a clearly defined linear relationship between A_H and K_H [Polupanov, Zhugailo, 2017].

1.4. Conclusions to Chapter 1

Based on long-term observations, conclusions have been drawn about the nature of fluctuations in the Sea of Azov level, determined by the presence of overburden and seiches fluctuations. The greatest run-up and surge changes in sea level occur with prevailing easterly, northeasterly, westerly and southwesterly winds coinciding with the direction of the greatest extent of the sea. The high variability of currents, which significantly depend on the current wind, is a consequence of the instability of the wind regime, the shallow waters of the sea and its relatively small area.

Forecasting of overburden processes, which often lead to the destruction of coastal infrastructure, coastal flooding, drainage of ports and shipping channels, and loss of life is an important problem of the hydrological regime of the Sea of Azov. The solution to this problem is based primarily on the analysis of the latest scientific results of expedition observations conducted by the UNC RAS, the Institute of Arid Zones of the UNC RAS, the Murmansk Marine Biological Institute and the Ocean Climate Laboratory of the National NOAA Center (USA). The modern bank of oceanographic information of the Sea of Azov, which includes ~76 thousand hydrological stations for the period 1891-2014, is summarized in manuals and atlases published by the Federal State Budgetary Institution GOIN. At the same time, the need to obtain operational forecasts determines the use of numerical modeling based on the use of modern hydrodynamic systems.

The geometric characteristics of shallow-water basins have determined the requirements for mathematical models that use a curved coordinate system. The numerical study of water circulation in the Azov Sea basin is based on the application of the well-known, modern, three-dimensional sigma-coordinate hydrodynamic model POM, the code of which is publicly available.

The author's adaptation of the POM model consisted of:

- in setting up two bathymetric grids that take into account the features of the natural basin of the Sea of Azov, adjustable depending on the modeling conditions: without taking into account the currents of water through the Kerch Strait and with the condition of free passage of liquid through the Kerch Strait;
- in setting up the space-time steps of the model for various configurations of computational grids;
- in setting the parameters necessary for calculating the coefficients of turbulent viscosity and diffusion;
- in setting the parameters necessary for calculating the coefficients of surface friction.

Chapter 2.
SCENARIOS OF ATMOSPHERIC DISTURBANCES AND INITIAL IMPURITY CONCENTRATION FIELDS FOR STUDYING FLUID MOVEMENTS AND POLLUTION EVOLUTION IN THE SEA OF AZOV

2.1.1. Scenarios of atmospheric disturbances generating fluid movements in the Sea of Azov

The analysis of published meteorological data [Hydrometeorological ..., 1962; Hydrometeorological conditions ..., 1986] made it possible to identify characteristic weather types for the Azov Sea region [Ivanov, Cherkesov, Shulga, 2011]. The anticyclonic type of weather occurs during the warm period (April − October) and is characterized by winds with a speed of more than 8 m/s, when the Sea of Azov turns out to be in the rear of the anticyclone, shifting from west to east. At this time, easterly and northeasterly winds prevail. A weak cyclonic type of weather [The Lot of the Sea of Azov] occurs when weak atmospheric fronts or the peripheries of individual cyclones pass over the Sea of Azov. Its average repeatability is 12% in the cold period and 22% in the warm period. This type of weather is characterized by weak and moderate winds of variable directions, clouds of the middle and lower tiers; sometimes light precipitation falls. The cyclonic type of weather occurs when Mediterranean cyclones or cyclones develop over the Black and Azov Seas on well-defined atmospheric fronts north of the 50° N parallel. Its repeatability in winter and summer does not exceed 15%. This type of weather is characterized by winds with a speed of 6 – 14 m/s, initially from the east, and then from the south and west. Westerly winds are usually gusty and squally.

The occurrence of stationary and non–stationary movements in the shallow sea basin - the Sea of Azov is due to the nature and intensity of atmospheric disturbances. To study the influence of wind direction and speed, as well as the magnitude and differences of atmospheric pressure on the movement of liquid in the sea, the simplest scenarios of atmospheric disturbances have been developed, realizing possible meteorological situations. These situations are further used as boundary meteorological

conditions in numerical modeling, the analysis of the results of which is described in chapters 3–6. The hydrodynamic model of POM is supplemented by the author's procedures implementing the considered meteorological conditions.

Five hypothetical cases of atmospheric disturbances are proposed: (1) quasi-stationary wind; (2) non-stationary wind, which is the result of a superposition of a constant and non-stationary component; (3) idealized cyclones and anticyclones passing along different trajectories and speeds over the Sea of Azov; (4) an inhomogeneous baric field with a sharp pressure drop at the boundary; (5) SKIRON regional atmospheric reanalysis data fields obtained with the assimilation of meteorological observations (http://forecast.uoa.gr) [The Regional Weather ... , 1997]. The first two scenarios are considered at a constant value of the standard atmospheric pressure.

2.1.1.1. In the first case, the atmospheric disturbance scenario reproduces a quasi-stationary and spatially homogeneous wind in the presence of constant atmospheric pressure ($P = P_{atm}$ = 1013,25 gPa). This case is considered when conducting numerical experiments to evaluate stationary and surge phenomena in the Sea of Azov. The velocity of the idealized quasi-stationary wind varies according to the following scenario. Starting from the moment of time $t = t_0 = 0$, when there is no movement of the liquid, and the free surface is horizontal, a uniform wind of a given (constant) direction begins to act on the water surface. Its speed increases with time ($0 < t \leq 3$ ч) according to a linear law. After 3 h, the wind speed at each point of the water area reaches its maximum, predetermined value $|\mathbf{W}|_{st}$, and then does not change during a given long time interval ΔT (h) [Features of circulation … , 2010; Cherkesov, Shulga, Waves, currents … , 2017]. After a period of time ΔT, the duration of which exceeds 6 h, the wind speed decreases to zero in the next 3 h (Figure 2.1.1.1).

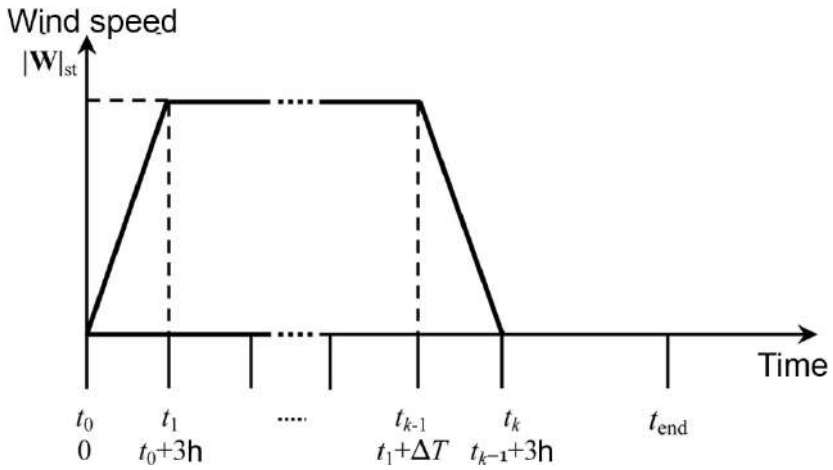

Figure 2.1.1.1 – Change in the velocity modulus of an idealized quasi-stationary wind over time

The change over time of the velocity components of the idealized quasi-stationary wind $\mathbf{W_{st}}(t) = \{W_x(t),\ W_y(t)\}$, the graph of the velocity modulus of which is shown in Figure 2.1.1.1, is performed according to the following law:

$$\begin{Bmatrix} W_x(t) \\ W_y(t) \end{Bmatrix}_j = \begin{pmatrix} at, & 0 \le t < t_1 \\ at_1, & t_1 \le t < t_{2j} \\ at_1 - a(t - t_{2j}), & t_{2j} \le t < t_{3j} \\ 0, & t_{3j} \le t < t_{4j} \end{pmatrix} \begin{pmatrix} \cos\Psi \\ \sin\Psi \end{pmatrix}. \qquad (2.1.1.1)$$

Here $at_1 = |\mathbf{W}|_{\mathbf{st}}^{l}$; $l = 1, 2,\ldots,4$ – corresponds to the set value of the wind speed ($|\mathbf{W}|_{\mathbf{st}}^{1} = 5$, $|\mathbf{W}|_{\mathbf{st}}^{2} = 10$, $|\mathbf{W}|_{\mathbf{st}}^{3} = 15$ and $|\mathbf{W}|_{\mathbf{st}}^{4} = 20$ м/с); $t_1 = 3$ ч; $t_{2j} = t_1 + \Delta T_j$; $t_{3j} = t_1 + t_{2j}$; $t_{4j} = t_{\text{end}}$; $j = 1, 2,\ldots$; $t = t_{\text{end}}$ – the completion time of the simulation is selected according to the formulation of the research task; Ψ – the angle formed by the direction of the wind with the meridian of the place. This angle is counted from the north clockwise: the North direction will correspond to 0° (360°), North-East – 45°, East – 90°, South – 180°, West – 270°.

2.1.1.2. A theoretical description of a hypothetical unsteady wind is proposed to describe situations that begin with sudden gusts of wind and occur in the field

of background stationary wind. The simplest case of the mathematical description of the non-stationary component is the assignment of a term simulating a gust of wind, defined as the sudden appearance of a homogeneous in space and variable in time wind $\mathbf{W}_{var}(\mathbf{r}, t)$. The variable wind $\mathbf{W}_{var}$ begins to affect the sea surface after a period of time counted from the initial $t = t_0 + \Delta t$. Its duration is usually determined by the time required to establish stationary currents in the sea ($\Delta t = t_{st}$). The direction of the gusts of the non-stationary wind $\mathbf{W}_{var}(\mathbf{r}, t)$ is a given angle with the direction of the quasi-stationary wind $\mathbf{W}_{st}$, and its speed changes every 3 h. So, from the beginning of the action of the unsteady wind ($t = t_{st}$) its velocity increases linearly and after 3 h reaches its highest value $|\mathbf{W}|_{var}$ at each point of the sea area. Further, the speed does not change for 3 h, and the next 3 h decreases linearly to zero. The total exposure time of the unsteady wind over the sea area is – 9 h.

Thus, the speed of the driving wind $\mathbf{W}(\mathbf{r}, t)$, which varies with time, is set as the result of the vector sum of the stationary and non-stationary components:

$$\mathbf{W}(\mathbf{r}, t) = \begin{cases} \mathbf{W}_{st}; & t_0 \le t \le t_{end} \\ \mathbf{W}_{st} + \mathbf{W}_{var}; & t_{st} \le t \le t_{end} \end{cases}, \qquad (2.1.1.2)$$

were $\mathbf{W}_{st}$ – the velocity vector of the quasi-stationary wind, the components of which are calculated based on the expression (2.1.1.1). A more detailed description of this case of atmospheric disturbance is presented in [Features of circulation … , 2010; Cherkesov, Shulga, Waves, currents … , 2017].

2.1.1.3. A vortex atmospheric formation reproducing the passage of hypothetical cyclones and anticyclones over the Sea of Azov is considered as a more complex non-stationary effect on the sea surface. The idealized scenario describing such phenomena takes into account the velocity $\mathbf{W}_c(\mathbf{r}, t)$ and pressure $P(\mathbf{r}, t)$, which change over time and in space, as well as the geometric and evolutionary parameters of atmospheric vortex formations: the radius of the base, the direction and speed of movement, the pressure drop between the center of the cyclone and the periphery. The system of equations (2.1.1.3) – (2.1.1.5) reflecting the change in velocity and pressure

in atmospheric formations passing over the water area of the Sea of Azov also determines their spatial and temporal scales.

Considering the radius of the atmospheric vortex formation equal to R_c, we write down the atmospheric pressure $P(\mathbf{r}, t)$, depending on the coordinates ($\mathbf{r} = (x, y)$) and time (t), in the form [Grigorkina, Fuchs, 1986]

$$P(\mathbf{r},t)=\begin{cases} P_{\text{atm}}, & r > R_c;\ t_0 \le t \le t_{\text{end}} \\ -P_0\cos^2\left(\dfrac{\pi r}{2R_c}\right)+P_{\text{atm}}, & r \le R_c;\ t_{\text{c}} \le t \le t_{\text{end}} \end{cases}, \qquad (2.1.1.3)$$

were P_{atm} – background value of atmospheric pressure; P_0 – maximum deviation from P_{atm} in atmospheric disturbance; r – the distance from the center of the moving cyclone to the point with coordinates (x, y); t_{c} – the time of the beginning of the impact of non-stationary baric formation (as a rule, from the moment of the establishment of background stationary currents in the basin).

In a stationary cyclone, the wind velocity vector is calculated by multiplying the modulus of the geocyclostrophic velocity vector $W_g = -f_r/2 + \sqrt{(f_r/2)^2} + (P_a)_r r/\rho_a$, by an empirical coefficient $\mu = 0{,}7$, considering at the same time that the wind direction deviates from tangents to isobars by an angle of $\gamma = 20^{\circ}$ (the angle of the beam) counterclockwise, according to [Grigorkina R.G., Fuchs V.R., 1986]. Provided that the atmospheric vortex formation moves at a constant velocity $\mathbf{c}$, we obtain the following expression for the velocity vector of the driving wind $\mathbf{W}(\mathbf{r}, t)$ [Influence of the Kerch Strait …, 2009] in the general case, when the movement begins ($t_{\text{c}} = t_{\text{st}}$) in the field o f stationary currents caused by the background wind $\mathbf{W}_{\text{st}}$ in (2.1.1.1):

$$\mathbf{W}(\mathbf{r},t)=\begin{cases} \mathbf{W}_{\text{st}}; & r > R_c;\ t_0 \le t \le t_{\text{end}} \\ \mathbf{W}_{\text{st}} + \mathbf{W}_{\text{c}}(\mathbf{r},t); & r \le R_c;\ t_{\text{c}} \le t \le t_{\text{end}} \end{cases}, \qquad (2.1.1.4)$$

$$\mathbf{W}_{\text{c}}(\mathbf{r},t) = \mu W_g \mathrm{T}(90^{\circ}+\gamma)\frac{\mathbf{r}}{r} + \mathbf{c}, \qquad (2.1.1.5)$$

were $(P_a)_r$ – the radial gradient of atmospheric pressure; the vector r is directed from the center of the cyclone to the point at which its velocity is calculated $\mathbf{W_c}(\mathbf{r}, t)$; T(α) – the matrix of rotation by angle α; $t = t_{end}$ – the completion time of the simulation, which is set according to the formulation of the research task. When considering the motion of atmospheric vortex formation in the absence of background stationary currentss, we assume $\mathbf{W}_{st} = 0$ in formula (2.1.1.4) and $t_c = t_0$ in (2.1.1.3) and (2.1.1.4) [Cherkesov, Shulga, Study of the transformation ..., 2016].

2.1.1.4. The motion of an inhomogeneous baric field with a sharp pressure drop at the boundary is considered as a possible scenario of atmospheric disturbance. The time of its movement ($t = t_f$) over the water area is set equal to half of the period of the highest mode of free oscillations capable of causing the greatest rise in the Sea of Azov level. At the stage from the beginning of the movement of an inhomogeneous baric formation ($0 \le t \le t_f$) the water area of the Sea of Azov is divided into two parts: the area Θ, over which the pressure is constant and equal to the normal atmospheric pressure Patm, and its complement Θ' to the entire water area (Ω = Θ U Θ '), over which the inhomogeneous baric field moves. The sizes and positions of the regions Θ and Θ' in the water area change over time and are limited by the linear dimensions of the Azov Sea basin ($0 \le x \le x_{max}$ = 350 km, $0 \le y \le y_{max}$ = 250 km) [Cherkesov, Shulga, 2016]. Thus, the function modeling the pressure in the atmospheric front depends on the coordinates and time $P(\mathbf{r}, t)$ is given by two different analytical expressions for the regions Θ and Θ':

$$P(\mathbf{r},t) = \begin{cases} P_{atm}; & \mathbf{r} \in \Omega, t_0 \le t \le t_{st}; \quad \mathbf{r} \in \Omega \setminus \Theta', t_{st} \le t \le t_{end} \\ P_{atm} + b(t - t_{st}); & \mathbf{r} \in \Theta'; \ t_{st} \le t \le t_f \end{cases}. \qquad (2.1.1.6)$$

Here, the coefficient b is selected so that the function $P(\mathbf{r}, t)$ has a single jump with an amplitude equal to the surface pressure gradient along the front line ($b(t_f - t_{st}) = \Delta P_f$). At the same time, ΔP_f is calculated according to the wind velocity value known in this experiment based on the formula $|\mathbf{W}_{st}| = 0.7\sqrt{(4.8/sin\varphi)^2(\Delta P_f^2 + \alpha^2 \Delta\theta_f^2) + 64}$,

proposed in [Masterskih, 1980]. Here $\Delta\theta_f$ – is the air temperature drop in the front zone at a distance of 50 km; α is the transition coefficient; φ is the geographical latitude; t_f is the time interval during which the front passes the distance between the extreme points of the Sea of Azov. The time of passage of the atmospheric front is determined based on observational data and the results of analytical calculations [Demyshev, Cherkesov, Shulga, 2017; Cherkesov, Shulga, 2016]. Thus, in the works [Hydrometeorological ... , 1962; Hydrometeorological conditions ... , 1986], seiches with periods of 6 – 7 and 23 h were noted in the Sea of Azov. The theoretical values of the periods of free oscillations obtained by the Merian formula, taking into account the Rayleigh correction, are also used [German, 1971].

2.1.1.5. The most difficult, but the closest to real wind conditions, is the method of setting the non-stationary components of wind and atmospheric pressure based on the use of data from the SKIRON regional atmospheric reanalysis. The specified atmospheric SKIRON model was created and developed at the University of Athens by the Atmospheric Modeling and Weather Forecasting Group. It is based on the mesoscale numerical atmospheric Eta model, originally developed at the University of Belgrade. The main development of the model was provided by NCEP (National Centers for Environmental Prediction). The results of the SKIRON model prediction were obtained by the Marine Hydrophysical Institute of the Russian Academy of Sciences as a full participant in the MFSTEP (Mediterranean Forecasting System Towards Environmental Predictions) project. This version of the model is a 72-h forecast of meteorological parameters for the Azov-Black Sea and Mediterranean basins. Data output for the first 48 h is carried out after 2 h, then the values are output after 6 h. The parameters are calculated on a grid with a step of 0.1° in latitude and longitude. The model provides 16 different parameters, including data on the speed of the driving wind. The SKIRON model data are interpolated onto the calculated grid of the Azov Sea basin with the specified horizontal resolution [Cherkesov, Shulga Numerical analysis ..., 2017].

In this case, the vector of the driving wind velocity $\mathbf{W}(\mathbf{r}, t)$ and the atmospheric pressure value $P(\mathbf{r}, t)$ in each node of the computational grid domain of the model region are given as

$$\mathbf{W}(\mathbf{r},t)=\begin{cases}\mathbf{W}_{\text{st}}; & t_0 \le t \le t_{\text{end}} \\ \mathbf{W}_{\text{st}} + \mu_l \mathbf{W}_{\text{SKIRON}}(\mathbf{r},t); & t_{\text{SKIRON}} \le t \le t_{\text{end}}\end{cases}, \qquad (2.1.1.7)$$
$$P(\mathbf{r},t)=\begin{cases}P_{\text{atm}}; & t_0 \le t \le t_{\text{end}} \\ P_{\text{SKIRON}}(\mathbf{r},t); & t_{\text{SKIRON}} \le t \le t_{\text{end}}\end{cases}.$$

Here μ_l (l = 1, 2, 3) – a coefficient that sets the intensity of predictive wind fields, and allows us to draw conclusions about the degree of influence of the non-stationary component of the wind obtained from the data of the atmospheric SKIRON/Eta model. The values of this coefficient (μ_1 = ½; μ_2 = 1 и μ_3 = 2) are selected in such a way as to investigate the effect of wind fields of twice greater and lower intensity in relation to the original data ($\mathbf{W}_{\text{SKIRON}}$ при μ_2 = 1) [Ivanov, Cherkesov, Shulga, 2012]. The time of the beginning of the action of the $\mathbf{W}_{\text{SKIRON}}$ wind can be both the moment when the movement of the liquid in the sea is established (in this case, we assume $t_{\text{SKIRON}} = t_{\text{st}}$), and the moment when the simulation begins (in this case, we assume $t_{\text{SKIRON}} = t_0$).

2.1.2. Setting the initial impurity concentration fields used for numerical investigation of the evolution of pollutants in the Sea of Azov

The next step in setting up the POM model for numerical investigation of the evolution of pollutants is the correct setting of the initial field of its concentration and the place of release in the waters of the Sea of Azov. Three scenarios have been proposed in the work, specifying the position of the initial impurity field with a concentration of $C^0 = C(x, y, z, t_0)$ in the surface layer of the sea. These scenarios are further used as initial conditions for numerical modeling of the evolution of pollution in the Sea of Azov, the analysis of the results of which is described in chapters 4 – 6,

and the hydrodynamic POM model is supplemented by author's procedures implementing the conditions under consideration.

The first two scenarios describe pollution at the initial moment of time in the form of a hypothetical area bounded by a straight circular cylinder of a given radius and a depth equal to the thickness of the near-surface layer of the sea. The position of the pollution emission center is selected in the area of gas fields and/or near large industrial cities. The initial moment of pollution entering the marine environment is selected depending on the conditions of numerical experiments. In the third case, remote sensing data obtained from MODIS-Aqua/Terra satellites, available on the OceanColor WEB resource, are used as initial values of the impurity concentration http://oceancolor.gsfc.nasa.gov [Moderate-resolution imaging ... , 2014]). In this case, the initial time of receipt of the optically active passive suspension into the marine environment corresponds to the actual data obtained from a satellite flying every 24 h over the Sea of Azov.

The POM model has been supplemented with author's software blocks for calculating the geometric and temporal parameters of the evolution of a passive impurity, which allow analyzing the stages of its transformation. The following parameters of the impurity transformation were chosen: its dispersion time (t_d), the coefficient of the maximum area of its propagation at various horizons (K_{max}) and the corresponding time point (t_{max}) [Investigation of the influence … , 2010]. In this case, the relative size of the maximum contamination area is determined by the ratio $K_{max} = S_{max}/S_0$, were S_0 – is the area of the initial contamination area in the surface layer; S_{max} – is its largest value on the horizon under consideration during the transformation of the impurity. The condition for complete dispersion of pollution is the value of its concentration, not exceeding $2{,}5 \cdot 10^{-2}$ from the initial one throughout the entire sea area ($C_d = 2{,}5 \cdot 10^{-2}$). We also introduce the value N_{max}, equal to the ratio of the maximum volume V_{max}, limited by the surface with concentrations of impurity C_d at time $t = t_{max}$, to the volume of initial contaminationV_0, calculated as the product of the area S_0 by the thickness of the layer z_1 [Ivanov, Cherkesov, Shulga, 2012].

The spatial position of the coordinates of the place of probable pollution release was chosen based on an assessment of the state of the ecosystem of the Sea of Azov [Krukier, 1991; Drozdov, 2010; Complex satellite monitoring ... , 2011; Matishov, Engebeikin, Savitsky, 2013; Matishov, Matishov, 2013; Modern ..., 2015]. These include areas located in the areas of the Vostochno-Kazantipskoye gas field; above the deepest (central) part of the sea; in the Taganrog Bay.

2.1.2.1. The simplest scenario determining the position and boundaries of the initial pollution area in the Sea of Azov is implemented using a dimensionless indicator depending on coordinates and time [Ivanov, Shulga, 2018]. The area occupied by pollution is marked with a concentration value equal to one ($C^0 = 1$), and zero outside it ($C^0 = 0$). In this case, at the time of pollution release ($t = t_{0p}$) the impurity distribution over the water area of the Sea of Azov is set by the ratio

$$C_1^0\left(x,\, y,\, z,\, t_{0\,p}\right) = \begin{cases} 1, & r \le R_p,\ 0 \ge z \ge -z_1, \\ 0, & r > R_p,\ z < 0;\ r \le R,\ \ z < -z_1 \end{cases}, \qquad (2.1.2.1)$$

were z_1 – vertical step in the surface layer of the sea, equal to the depth of the upper calculated σ-layer; R_p – the radius of the contamination area, the value of which is selected according to the experimental conditions; (x_0, y_0) – pollution center; $r = \sqrt{(x - x_0)^2 + (y - y_0)^2}$ – the distance from this center to the point where the current concentration value is calculated [Ivanov, Cherkesov, Shulga, 2012].

2.1.2.2. A more realistic case is when the initial area of contamination with a concentration decreasing from the center of the emission is specified. In this case, in the surface layer at time $t = t_{0p}$ the gradient of the initial concentration is set in the direction from the center of the pollution release. Assuming that the concentration changes from a maximum value equal to one (at the center of the emission) to zero (at the boundary of the region) according to a linear law, the model of the impurity distribution over the sea area at the initial time ($t = t_{0p}$) it has the form

$$C_2^0(x,\ y,\ z,\ 0)=\begin{cases} C_{\max}(R-r_1)/R, & r_1 \le R,\ 0 \ge z \ge -h_1, \\ 0, & r_1 > R,\ z < 0;\ r_1 \le R,\ z < -h_1 \end{cases}, \qquad (2.1.2.2)$$

were $C_{\max}$ – the maximum concentration value in the center of the contamination area.

As a rule, the propagation of pollutants entering the sea at the initial moment of time (t_{0p} = t_0 = 0), as well as at the highest value of the current wind speed, is investigated. For example, when studying the evolution of pollution in seawater in a number of numerical experiments, the time of the beginning of admixture entry into the sea is chosen to be$t_{0p} = t_{st} = 48$ h, the values of $C_{\max} = 1$, $C_{\max} = 2$; $C_{\max} = 3$, and the change in the concentration field from the maximum value (in the center emission) to zero (at the boundary of the region) according to the linear law [Cherkesov, Shulga, 2012].

2.1.2.3. The most effective method of studying the evolution of pollution in the Sea of Azov is a joint analysis of the results of hydrodynamic modeling and satellite optical images that provide more complete information about the directions of transport, sizes and concentrations of pollution areas. New subroutines of the POM model have been created that allow reproducing the processes of transport and diffusion of pollutants using the assimilation of satellite observation data as initial values of the concentration of optically active passive suspension. For this study, observational data for 2013-2014 from the Aqua and Terra satellites (with a MODIS scanner on board) were used. The data source of the second level (L2) of the MODIS device is the Ocean Color WEB resource, which is publicly available on the network (Figure 2.1.2.1).

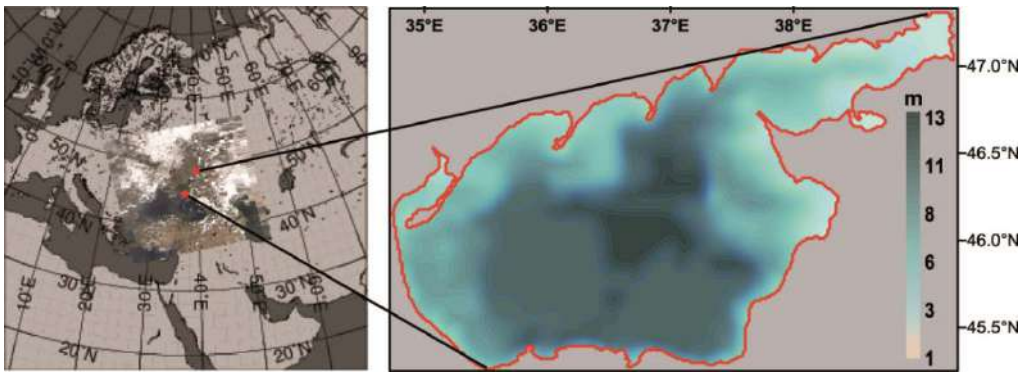

Figure 2.1.2.1 – Location of the studied basin of the Sea of Azov (real color image from the OceanColor WEB site, left) and its bathymetry (right)

Based on these data, biotic indices are calculated to determine the presence of pollutants in the upper layer of the Sea of Azov. The first parameter (the dimensionless *index*34 coefficient) is the ratio of the sea brightness coefficients (remote sensing reflectance $R_{rs}(\lambda)$) at the wavelength λ with the central wavelengths of the two spectral channels:

$$index34 = R_{rs}(531)F_o(531)/\,R_{rs}(488)F_o(488), \qquad (2.1.2.3)$$

were $R_{rs}(\lambda)$ – the brightness coefficients of the sea with the central wavelengths of the spectral channels are 531 and 488 nm, respectively; $F_o(\lambda)$ – solar constants [Studies of particulate ... , 2018; Shul'ga, Suslin, 2018; Studies … 2018].

The physical essence of this parameter is that it characterizes the total absorption of all optically active substances contained in the upper layer of seawater. For oceanic waters, this statement is justified in Section 4.1. Analytical Basis of Band-Ratio Models of [The SeaWiFS ... , 1995]. In the application to seas with a high content of dissolved organic matter relative to the open ocean, this statement is justified in the works [Estimation of variability ... , 2002; Application ..., 2014]. For seas strongly influenced by river runoff, this index characterizes the concentration of the colored component of dissolved organic matter [Estimation of variability ... , 2002; Bio-optical characteristics ..., 2011]. The solar constants Fo for the spectral channels under consideration can be found, for example, in [Suslin, Churilova, 2016].

The second parameter is the backscattering coefficient of light by suspended particles at a wavelength of 555 nm ($b_{bp}(555)$, $м^{-1}$), which allows us to observe the features of light scattering in the upper layer of water. Basically, it can be a suspension of biological origin (for example, coccolithophorid blooms) and inanimate suspension (for example, mineral suspension associated with river outcurrentss or its rise from the bottom as a result of strong wind). Following the work [A simple approach ... , 2011], the calculation of $b_{bp}(555)$ is carried out according to the formula:

$$b_{bp}(555) = [6{,}76L_{WN}(555) + 0{,}03(L_{WN}(555))^3 + 3{,}4L_{WN}(555)(I_{510})^{3{,}8} - 0{,}84]10^{-3}, \quad (2.1.2.4)$$

were $I_{510} = L_{WN}(455)/L_{WN}(510)$ [Shulga, Suslin, Stanichnaya, 2017].

Further, the processed satellite images are analyzed for the presence of a pair (images with an interval of 30 min from the same date), the found pairs are combined into one image, including data from both of these images. For example, for assimilation, the model uses the distribution of the backscattering coefficient (b_{bp}(555)) in the upper layer of the sea, obtained as a result of concatenation of two consecutive images on June 23, 2013 at 9:35 and 11:50 (Figure 1.2.2.2) [Shulga, Suslin, Stanichnaya, 2017; Shul'ga, 2017, Shulga, Suslin, 2018].

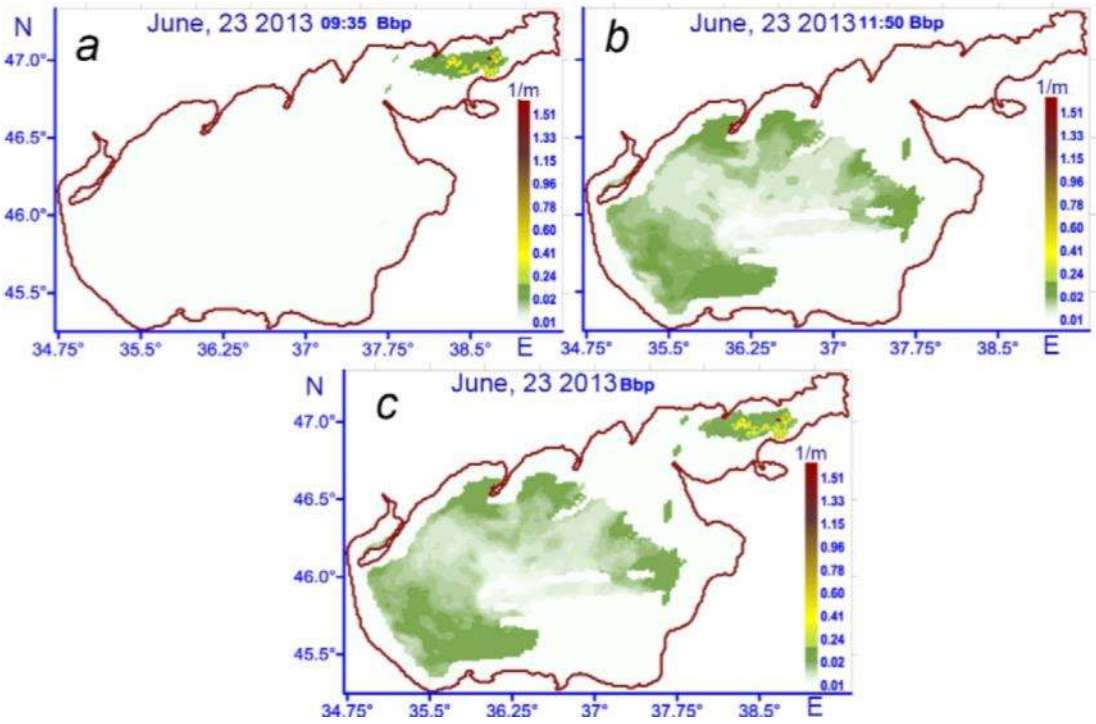

Figure 2.1.2.2. Data on the distribution of the b_{bp}(555) parameter in the near–surface layer of the Sea of Azov (June 23, 2013): (*a*) – at 9:35; (*b*) – at 11:50; (*c*) – processed data [Shulga, Suslin, Stanichnaya, 2017].

Maps of the distribution of these biotic indices over the water area of the Sea of Azov are interpolated onto the calculated grid of the basin with the necessary horizontal resolution and used to set initial conditions, as well as to perform the assimilation procedure during modeling. The calculation of transport and diffusion of passive suspension is carried out using additional procedures of the three-dimensional POM model when setting the initial values of the suspension concentration $C^0 = C(x, y, z, t_{0p})$.

Its horizontal distribution corresponds to a two-dimensional field of satellite data, and the vertical distribution is determined by the corresponding thickness of the sigma level in depth, reaching values of no more than 1 m in the deep part of the sea. In this case, at a given initial time ($t = t_{0p}$) the distribution of the impurity over the water area of the Sea of Azov is set by one of the ratios

$$C^0_{index}\left(\mathbf{r}, z, t_{0\,p}\right)=\begin{cases} index34;\ \mathbf{r}\in\Theta;\ 0\ge z\ge -z_1, \\ 0, \qquad \mathbf{r}\in\Theta';\qquad z<-z_1, \end{cases}, \tag{2.1.2.5}$$

$$C^0_{bbp}\left(\mathbf{r}, z, t_{0\,p}\right)=\begin{cases} b_{bp}(555), \text{м}^{-1};\ \mathbf{r}\in\Theta;\ 0\ge z\ge -z_1, \\ 0, \qquad \mathbf{r}\in\Theta';\qquad z<-z_1, \end{cases}, \tag{2.1.2.6}$$

were Θ – the area of the Azov Sea covered by pollution, based on data on the distribution of biotic indices *index*34 и $b_{bp}(555)$; Θ' – its addition to the entire sea area (Ω = Θ U Θ' and Θ ∩ Θ' = Ø).

The resolution of remote time data is due to the satellite's passage over the area of the Sea of Azov, which are registered here daily in the interval 9:00 – 14:00 local time. The smallest time step between satellite images is ~24 h [Shulga, Suslin, Stanichnaya, 2017]. The moment of time ($t = t_{0p}$), at which the initial distribution is assimilated, given by formulas (1.3.2.5) or (1.3.2.6), corresponds to the date and local time of the specified satellite image. At the same time, the start of the simulation is planned 6 days in advance before the start of the assimilation procedure ($t = t_{0p}$) for the formation of a field of currents in the sea generated by the active wind of the SKIRON model.

2.2. Conclusions to Chapter 2

In order to conduct numerical experiments on the study of fluid currentss and movements in the Sea of Azov and the evolution of pollution, the POM model was supplemented with blocks of author's procedures that provide the assignment of possible

scenarios of atmospheric disturbances and the position and concentration of the area of initial intake of the contaminant into the Sea of Azov.

Author's mathematical procedures that complement the POM model.:

– in the construction and implementation of equations of theoretical scenarios simulating atmospheric disturbances over the Sea of Azov from the simplest to the closest to real prognostic data: (1) quasi-stationary wind; (2) sharp, unsteady gusts of wind in the background stationary wind field; (3) Atmospheric vortex formations (moving cyclones and anticyclones); (4) the movement of atmospheric fronts; (5) real prognostic meteorological conditions according to the data of the SKIRON regional atmospheric reanalysis (http://forecast.uoa.gr).

– in the construction and implementation of theoretical scenarios that determine the position and value of the initial concentration of pollutants in the Sea of Azov: (1) in the form of an indicator that takes zero values outside the area occupied by pollution; (2) taking into account the gradient of pollution concentration depending on the distance to the source; (3) according to bio-optical indices calculated from observations from MODIS-Aqua/Terra satellites used to predict environmental risks under various atmospheric conditions;

– in setting the parameters necessary for setting atmospheric fields, and initial data on the position of pollution sources, geometric and temporal parameters characterizing the evolution of a passive impurity in the process of its transformation.

Chapter 3.
REPRODUCTION OF WATER EXCHANGE THROUGH THE KERCH STRAIT AND ANALYSIS OF ITS INFLUENCE ON CURRENTS AND SURGE PHENOMENA PROCESSES IN THE SEA OF AZOV

The Kerch Strait, connecting the Black and Azov Seas, is an important shipping lane and a fishing area of the Azov-Black Sea basin. Occupying a border position at the intersection of land and sea transport routes, the Kerch Strait is involved in active economic activity, which is the cause of both environmental and political problems. Unstable weather in the Kerch Strait, characterized by regular strong gusts of wind and storms, poses a great danger to all surface structures. It was precisely because of the stormy weather conditions in 1944. The 4.452 m long bridge, which had existed for less than four months, was destroyed. A storm on October 11, 2007 led to a serious environmental disaster on the Crimean coast due to the flooding of ships and an oil spill. An additional anthropogenic factor affecting hydrodynamic processes was the construction of a dam that began (currently stopped) in October 2003, as a result of which the width of the strait between about. Tuzla and the Taman Peninsula decreased from almost 4 km to 300 m [Faschuk, Ovsienko, Petrenko, 2007].

The relevance of research related to the reproduction of the circulation of the waters of the Sea of Azov, provided that the Kerch Strait is blocked, is due to the transport crossing under construction in this area between the Kerch and Taman peninsulas through Tuzla Island and Tuzla Spit. It is a combination of bulk earthworks and structures located in parallel axes for railway and automobile communication. Supports for road and railway bridges are based on more than 5.500 piles, which has led to a narrowing of the waterway. Therefore, it is of practical interest to study the relationship between currents, level deviations in the Kerch Strait, formed under the influence of wind in significant directions, and extreme characteristics of run-up oscillations and currents in the Sea of Azov.

Figure 3.1 – Map of the Sea of Azov with the location of the spit, straits and large settlements along its coast

The relevance of the study is due to the need to predict the extreme values of overburden fluctuations in the level and currents in the basin of the Sea of Azov, which is relatively small in size relative to the Black Sea, and their influence on currents arising in the Kerch Strait. In this chapter, the processes of water exchange through the Kerch Strait under the influence of various atmospheric disturbances are studied, the value of the velocity of currents from the Sea of Azov to the Black Sea arising from the movement of areas of increased atmospheric pressure from the northern points is estimated, the possibility of using a simplified model of the basin of the Sea of Azov with a solid boundary at the entrance to the strait is analyzed.

3.1. Numerical analysis of the effect of water exchange with the Black Sea on stationary movements in the Sea of Azov

The hydrological regime of the Kerch Strait is due to its shallow waters and water exchange resulting from the movement of water due to the difference in levels in the northern (Azov) and southern (Black Sea) parts, as well as the action of wind, whose influence on the water level in the strait is on average 5 – 6, and in storms 10 – 15 times stronger than the impact of the river stock [Altman, 1991; Faschuk, Ovsienko, Petrenko, 2007]. Based on published data from long-term observations [Hydrometeorological ... , 1962; Hydrometeorology ... , 1991] it can be noted that currents from the Sea of Azov are observed more often with northern winds, and currents from the Black Sea are less common with southern ones. At the same time, in the narrow areas, the currents velocity reaches 154 cm/s [Black Sea, 2003].

The Kerch Strait is quite shallow, the depth at the entrance to the strait from the Sea of Azov is 10.5 m, at the exit to the Black Sea is 18 m. In most of the water area, the depths do not exceed 5.5 m, and in the Kerch-Yenikalsky Canal, dug by Russia in 1874, they are 9 – 10 m. The length of the Kerch Strait is 43 km in a straight line and 48 km along the fairway. The maximum width is 42 km, the minimum is 3.7 km (in the area of the port of Crimea, the port of Kavkaz). It is of interest to conduct a study of the effect of accounting for water exchange on currents and level deviations in the Sea of Azov. Throughout the history of instrumental observations (since 1936), waves with a height of 0.7 – 1 m and less prevail in the strait throughout the year [Hydrometeorological ..., 1962; Hydrometeorology ..., 1991; Matishov, Chikin, 2012; Extreme flooding ..., 2014; The extreme flood ..., 2014; Climatic Atlas of the Sea of Azov, 2006].

With northerly winds in the Kerch Strait, there is a currents from the Sea of Azov with maximum current velocities up to 70 cm/s. With southerly winds, the Black Sea stream is observed in the strait with maximum speeds up to 80 cm/s. The frequency of the Azov currents is 58% on average per year, and the Black Sea currents are 42% of cases. Over the past 50 years, waves of maximum height (2 m) in the northern part of the Kerch Strait have been observed with winds of the northern quarter. The frequency

of winds of the southern quarter in the northeastern part of the sea is 12%, their speed does not exceed 15 – 17 m/s [Cherkesov, Shulga, 2018].

Conclusions about the peculiarities of the formation of stationary currents and fields of the Sea of Azov level, taking into account water exchange with the Black Sea, are made on the basis of a series of numerical experiments using a bathymetric grid that includes the Sea of Azov, the Kerch Strait and the adjacent part of the Black Sea. This area is shown in Figures 1.3.1 (right) and 3.1.1. The open zonal boundary (Ξ) corresponds to a section of the Black Sea basin at 44.81°N. (Figure 3.1.1, *a*).

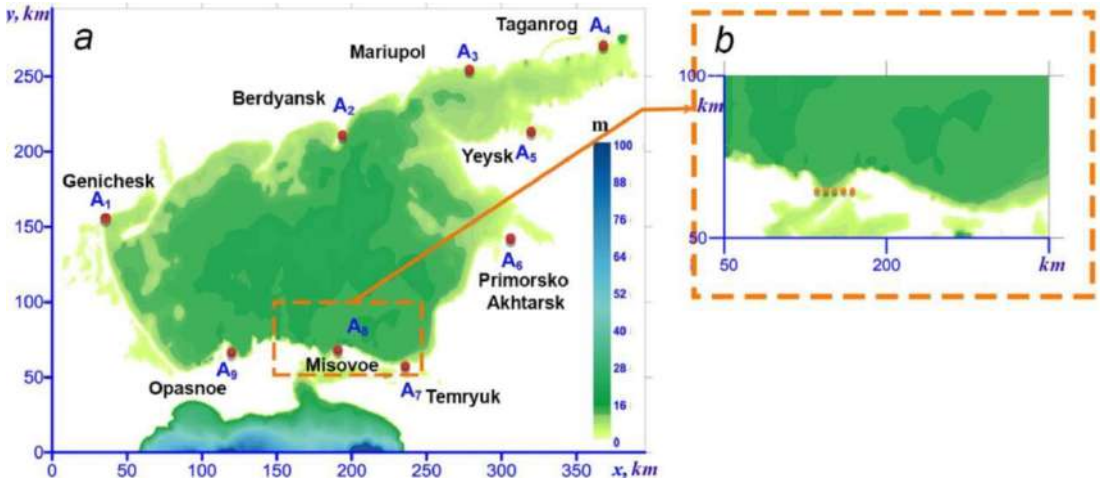

Figure 3.1.1 – The position of stations along the coast of the Sea of Azov: A_1 – Genichesk, A_2 – Berdyansk, A_3 – Mariupol, A_4 – Taganrog, A_5 – Yeysk, A_6 – Primorsko Akhtarsk, A_7 – Temryuk, A_8 – Opasnoe, A_9 – Mysovoe (*a*); section on the section along 39.33° N, through which the water currents rate and points in the strait are calculated (red dots, P_1 – P_5), considered for the analysis of the currents velocity (*b*)

In all grid nodes located on this boundary ($60 \le x \le 240$ км, $y = 0$), the condition of free exit of waves from the calculated area is fulfilled:

$$\left.\frac{\partial v}{\partial y}\right|_{\Xi} = 0, \qquad (3.1.1)$$

where the *y*-axis is normal to the liquid boundary. When solving the problem without taking into account the strait, an enclosed basin is considered, in which along 39.33° N ($177 \le x \le 192$ km, $y = 62$ km) there is a vertical side wall (dotted red line in Figures 3.1.1, *b* and 1.3.1, on the right). To calculate the water exchange through the Kerch Strait, at each time step, the total currents rate of water passing through the section located at the section $177 \le x \le 192$ km, $y = 62$ km is calculated (Figure 3.1.1, *b*) [Ivanov, Cherkesov, Shulga, 2010].

In this case, the volume of the leaked liquid during the time $0 \le t \le t_n$ is determined by the expression

$$G(t) = S\sum_{i=1}^{n} \overline{\mathbf{U}(t_i)}t_i, \qquad (3.1.2)$$

were $\overline{\mathbf{U}(t_i)}$ – the average velocity of currents in the cross-section of the strait at the i^{th} time step; S – is the cross-sectional area.

In a stationary problem, wind and water currents should be set as two independent external factors, but, according to [Altman, 1991], currents is proportional to the projection of wind speed (average daily) on the "axis" of the strait, and the wind effect on the strait level exceeds its stock changes. In order to test this hypothesis, we conducted a comparative analysis of the simulation results according to the scenarios of the computational domain consisting of the Sea of Azov and the Kerch Strait, and an area with simplified geometry – with a boundary at the entrance to the strait (Figure 1.3.1). The dependences of the velocities of surface and deep currents, extremes of run-off and run-up on the direction and speed of constant wind, taking into account and without taking into account water exchange through the strait, are investigated.

Modeling of fluid motion in the Sea of Azov, arising under the action of a stationary wind homogeneous in space, was performed using the idealized wind model $\mathbf{W}_{\mathbf{st}}$ (2.1.1.1). Numerical experiments were implemented for stationary winds of different speeds

($|\mathbf{W}|_{st}^1$ = 5, $|\mathbf{W}|_{st}^2$ = 10, $|\mathbf{W}|_{st}^3$ = 15 and $|\mathbf{W}|_{st}^4$ = 20 m/s) of the west (W), north (N) and South (S). The results obtained are compared with calculations carried out when modeling steady-state movements in the Sea of Azov without taking into account water exchange through the Kerch Strait.

As a result of the action of a wind uniform in space and time over a long period of time ($\Delta T \geq 6$ ч) steady movements occur in the marine basin. The study of the basic patterns of these movements allows us to establish the general nature of the circulation of waters in the basin. In this case, the obtained stationary solution can be used as initial data in a non-stationary problem. In order to determine the time required for the formation of steady-state fluid movements in the Sea of Azov, the program code is implemented in the form of a subroutine of the used hydrodynamic model POM (subsection 2.1.2). In the new calculation module, a procedure is performed to determine the approximation to the steady-state regime by estimating the relative changes in the average value of the total energy $\bar{E}_T(t)$, which is found as the sum of the space-averaged values of kinetic and potential energy $\bar{E}_K(t)$ and $\bar{E}_P(t)$. At each time step, the estimate of the change in $E_T(t)$ is determined based on the ratio

$$\delta\bar{E}_T^j = |\bar{E}_T^{j+1} - \bar{E}_T^j|/\bar{E}_T^j, \tag{3.1.3}$$

were $\bar{E}_T^j = \bar{E}_K^j + \bar{E}_P^j$; i – time step number. We believe that the stationary mode is achieved when the inequality $\delta\bar{E}_T^j \leq 10^{-2}$ is fulfilled. The condition for entering the stationary mode is also determined by the fact that between two adjacent time intervals $[t_i, t_{i+1}]$ there are no noticeable changes in the amplitudes of sea level deviation and current velocity (changes do not exceed 5%). The fulfillment of these conditions makes it possible to determine the time of establishing the movement of the liquid $t = t_{st}$.

Using the procedure described above, the time required to establish a liquid in the Sea of Azov as a result of prolonged wind action with a speed and direction characteristic of this region has been numerically investigated. Based on the analysis of the data provided in meteorological reference books, it is possible to note the greatest recurrence during almost the entire year of winds in the north-eastern and eastern directions

at a speed of 5 – 15 m/s [Hydrometeorological ..., 1962; Hydrometeorology ..., 1991; Climatic Atlas of the Sea of Azov, 2006]. In different seasons, the winds of the north and north-west directions have the greatest continuous duration (up to 2.5 days). At the same time, the north-easterly and easterly winds reach the highest speed. Thus, the maximum recorded speed of the north wind (40 m/s) took place in Kerch in September 1956. The wind force during one of the most destructive storms of recent years on November 11, 2007 reached 27 – 32 m/s in Kerch, and the wave height in the area of the port of Kavkaz was 4 m [Faschuk, 2009].

Based on the analysis of the wind regime according to long–term observations, we have modeled the steady-state regime of currents in the Sea of Azov using constant wind fields with a velocity modulus of 5, 10, 15 and 20 m/s ($|\mathbf{W}|_{st}^1 - |\mathbf{W}|_{st}^4$) for each of the three selected directions – western, northern and southern. Based on the analysis of the simulation results, it was found that the time (t_{st}) for the level fields and currents to reach a steady state depends on the wind speed. At high values of wind speed, the liquid setting time increases. Numerical analysis has shown that, under the influence of, for example, a quasi-stationary easterly wind, the duration of formation of steady movements in the sea for the studied velocities is: 37 ($|\mathbf{W}|_{st}^1$); 42 ($|\mathbf{W}|_{st}^2$); 45 ($|\mathbf{W}|_{st}^3$) and 48 h ($|\mathbf{W}|_{st}^4$). A more detailed description is presented in the works [Features of circulation ... , 2010; Atlas ... , 2012; Cherkesov, Shulga Waves, currents … , 2017].

Figure 3.1.2 shows the model level fields generated by a constant wind acting at a speed of 15 m/s in the three directions under consideration. Analysis of the simulation results indicates that under the influence of quasi-stationary wind (2.1.1.1), there is a gradual increase in the level at the windward shores (overburden) and a decrease at the leeward (overburden) (Figure 3.1.2) [Shulga, 2013]. In steady motion ($t = t_{st}$), the level field corresponds to a single-node seisha. The zero amplitude curve (dashed line) is oriented almost perpendicular to the direction of the current wind and crosses the central part of the sea in the zonal (Figure 3.1.2, *b*, *c*) and meridional (Figure 2.1.2, *a*) directions.

Table 3.1.1 shows the maximum level deviations at the coastal stations of the Sea of Azov, depending on the direction and speed of the wind, taking into account and

excluding water exchange through the strait. From the analysis of the data given in Table 3.1.1, it follows that at each station the most significant overburden processes are observed in most cases with high-speed winds and taking into account the exchange with the Black Sea. With the winds of the considered directions, the Taganrog Bay is exposed to the strongest effects of overburden processes. Here, the maximum sea level deviations (up to 1 m) occur with winds from different directions.

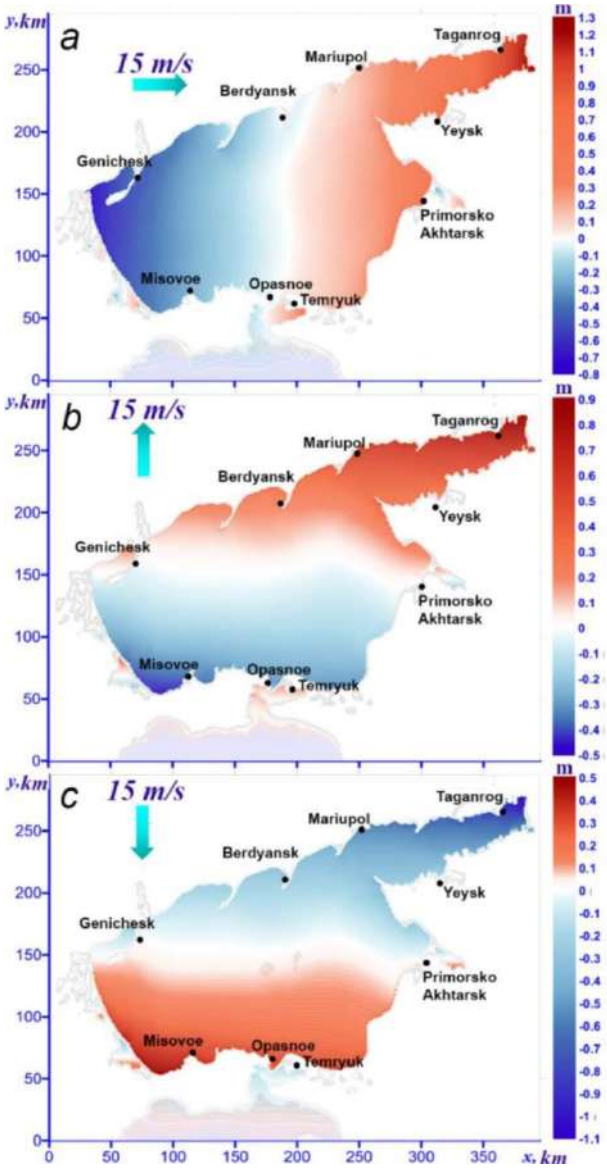

Figure 3.1.2 – Fields of the Sea of Azov level (m) in steady state with western (*a*), southern (*b*) and northern (*c*) wind directions [Ivanov, Cherkesov, Shulga, 2010; Shulga, 2013]

The action of a stationary wind in one direction, at a higher speed (10 and 15 m/s) leads to an increase in level deviations up to 60%. A comparison of the values $|\zeta_{max}|$ obtained for winds of the same direction and velocity when solving the problem with and without taking into account the strait shows that taking into account water exchange leads to an increase in extreme values of the level. Thus, at a wind speed of 10 m/s, the greatest differences in absolute maxima at the stations are: 43% (west wind), 45% (south), 46% (north); at a wind speed of 15 m/s, 44% (west wind), 43% (south), 45% (north). It significantly affects the greatest deviations in the level and direction of the stationary wind. It should be noted that at the stations under consideration, the largest rises and decreases in the level take place at a certain wind direction of the same speed [Ivanov, Cherkesov, Shulga, 2011; Shulga, 2013].

The calculation results shown in Table 3.1.1 show that with a westerly wind, maximum surges are observed at Taganrog (138 cm), Yeysk (96 cm), Primorsko-Akhtarsk (73 cm) stations, and maximum surges at Genichesk station (112 cm). With a southerly wind, the highest level rises take place at Berdyansk (46 cm) and Mariupol (79 cm) stations, the maximum level drops are at Temryuk (59 cm), Dangerous (56 cm), Mysovoye (58 cm) stations. The north wind causes the greatest surges at Temryuk (55 cm), Dangerous (53 cm), Mysovoye (53 cm) stations, the greatest surges at Berdyansk (47 cm), Mariupol (82 cm) and Taganrog (140 cm) stations. Thus, for the Genichesk station, the maximum surges will develop with a southerly wind, and the greatest surges will develop with western and northern wind directions. In the Berdyansk region, the highest level rises are observed with a southerly wind, the maximum level drops with a northerly wind. The north wind is the most dangerous from the point of view of run-offs for Mariupol, Taganrog and Yeysk stations, the maximum surges here are caused by winds from the south and west directions.

At the Primorsk-Akhtarsk station, the largest overcurrentss occur with a northerly wind, the wind from the west causes maximum level rises. At Temryuk station, the maximum surges develop with a northerly wind, and the greatest surges develop with a southerly wind. In the area of the Dangerous station, maximum level rises are observed with a northerly wind, the largest level drops are noted here with winds from the south

and west directions. At the station, the Cape occurrence of the largest run–ups occurs with a north wind and run-offs with south and west winds.

Table 3.1.1 – Maximum sea level deviations (cm) under the influence of wind of three speeds and directions, excluding and taking into account water exchange through the strait (*)

Coastal stations	Wind speed and direction								
	5 m/s			10 m/s			15 m/s		
	E	S	N	E	S	N	E	S	N
Henichesk	–7	–0	0	–29	–1	1	–69	–4	4
	–7*	–1*	1*	–42*	0*	0*	–112*	–2*	1*
Berdyansk	0*	–3*	3*	–2*	11*	–12*	–4*	28*	–26*
	1*	–4*	4*	–4*	17*	–18*	–5*	46*	–47*
Mariupol	2	–5	6	6	24	–25	14	57	–60
	4*	–6*	8*	27*	21*	–32*	25*	79*	–82*
Taganrog	10	–8	8	44	32	–34	100	80	–82
	11*	–11*	9*	57*	44*	–48*	138*	108*	–140*
Yeysk	6	–4	4	22	14	–14	52	36	–29
	7*	–6*	5*	38*	16*	–16*	96*	41*	–37*
Primorsko Akhtarsk	5	–1	1	21	3	–4	49	–12	8
	5*	–1*	2*	29*	–8*	8*	73*	–20*	14*
Temryuk	1	3	–3	7	–14	13	20	–33	31
	2*	5*	–7*	5*	–22*	22*	15*	–59*	55*
Opasnoe	–1	3	–3	–3	–12	11	–5	–29	28
	–1*	5*	–6*	–4*	–21*	20*	–9*	–56*	53*
Mysovoe	–3	3	–3	–13	–15	15	–30	–35	36
	–4*	4*	–5*	–18*	–22*	21*	–45*	–58*	53*

* The results of the simulation performed taking into account the water exchange through the Kerch Strait

A comparison of the two values of $|\zeta_{max}|$ found under different conditions in the strait and the same wind exposure indicates similar calculation results. At the same time, the deviations of the obtained values for the three studied directions of constant wind with a speed of 5, 10 and 15 m/s are 13, 19, 24% (west wind); 17, 6, 25% (south); 18, 19, 23% (north). Note that the wind direction also affects the maximum deviations. Thus, under the influence of a stationary wind with a speed of 15 m/s, the highest values $|\zeta_{max}|$, which are reached with a westerly wind (162 cm), exceed the lowest (115 cm) caused by a southerly wind by 29%.

Figures 3.1.3 and 3.1.4 show the velocity of currents caused by the action of constant wind in various directions at a speed of 15 m/s at horizons 1 and 10 m at time $t = t_{st}$. The distributions are obtained by linear interpolation of numerical simulation results from σ-coordinate surfaces on the z = const plane. As the analysis of the above fields shows, steady-state currentss are characterized by pronounced vortex formations. Their positions and configurations are determined by the direction of the wind. At the same time, the most intense currents take place in the deep part of the sea. With a westerly wind (Figure 3.1.3, *a*), two systems of cycles arise in the Sea of Azov, which are oriented in the zonal direction. In a quasi–stationary state, the main structural element of the movement is the current encircling the coastal area of the sea with a width of 50-60 km and characterized by a direction to the northwest. At a distance of 20 – 35 km from the coast, the core of the highest velocities (stream stream) is traced, reaching 60-80 cm/s in the surface layer of the sea [Numerical analysis ... , 2014].

At the boundary between the cycles, the direction of the liquid currents is oriented opposite to the acting wind. A pair of vortices of opposite signs is forming in the Taganrog Bay. With a northerly wind, two cycles of opposite signs are generated in the central part of the sea (Figure 3.1.3, *c*). The larger (cyclonic) one adjoins the western shore and contains a small vortex formation. A smaller but more powerful circulation (anticyclonic) is located in the eastern part of the sea.

Between these two cycles there is a narrow band of water mass transfer oriented opposite to the wind. The south wind causes currents, the fields of which are a mirror

image of the fields of currents arising from the north wind (the same configuration of vortex formations is traced, but they have the opposite sign) (Figure 3.1.3, *b*).

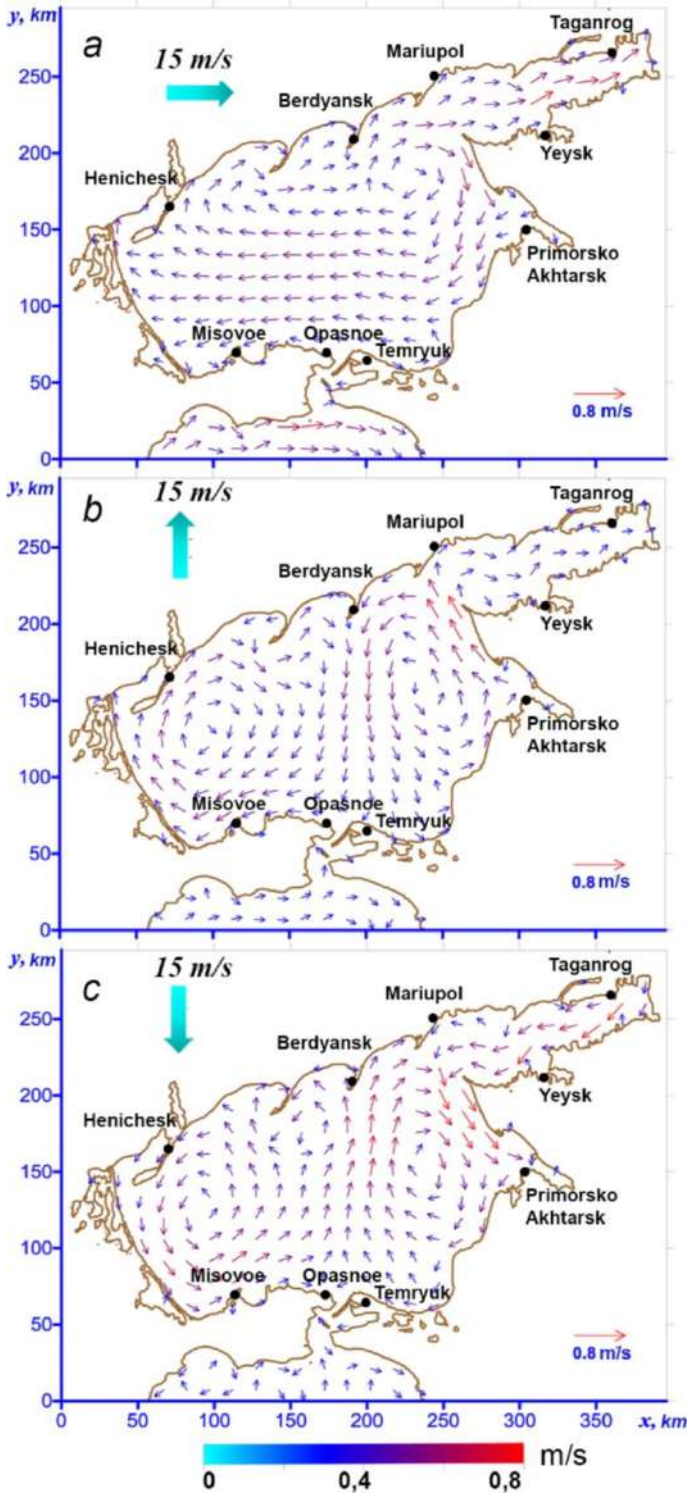

Figure 3.1.3 – Velocity fields of stationary surface currents (m/s) in the Sea of Azov with west (*a*), south (*b*) and north (*c*) winds

At a depth of 10 m (Figure 3.1.4) in the central part of the water area, currents are observed that deviate by 135° or more from the direction of the current wind.

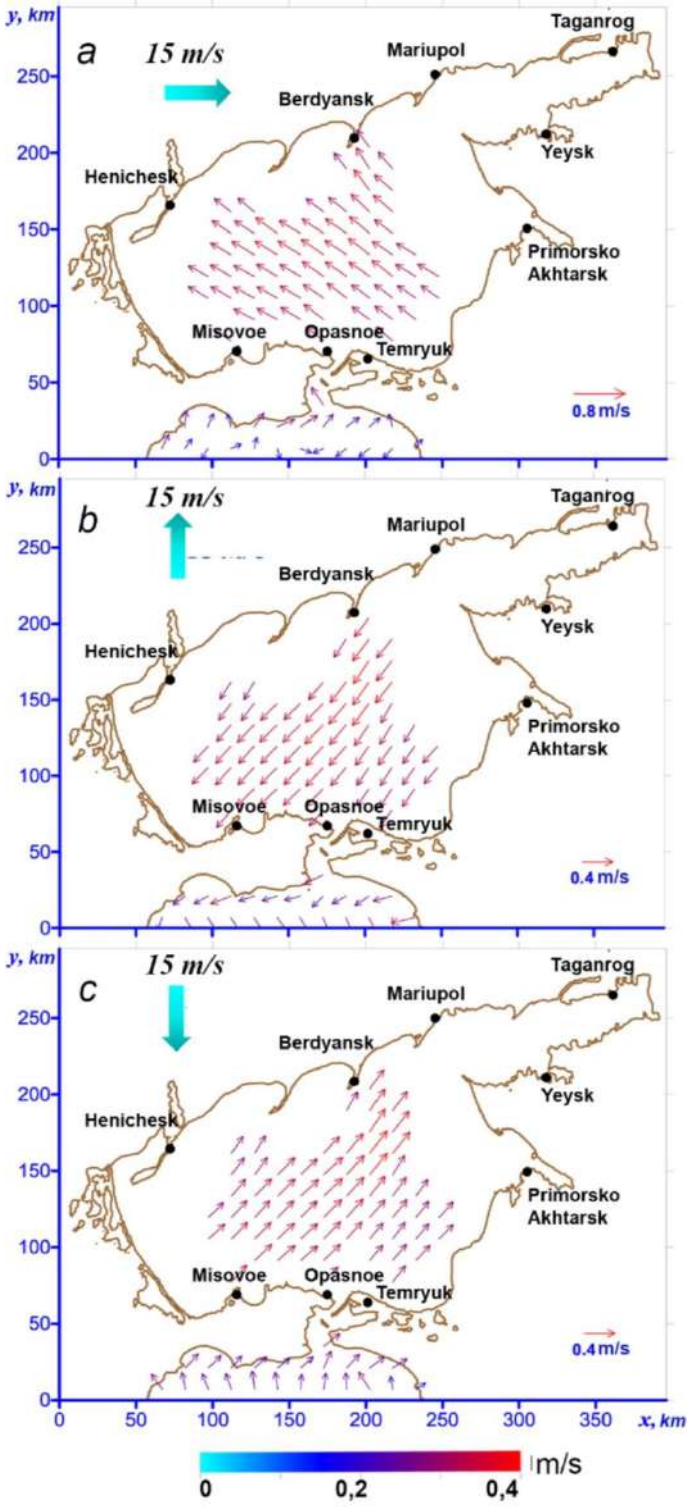

Figure 3.1.4 – Velocity fields of stationary currents (m/s) in the Sea of Azov at a depth of 10 m with west (*a*), south (*b*) and north (*c*) winds

As follows from the analysis of Figures 3.1.3 and 3.1.4, due to the formation of countercurrentss, the currents in the strait in the surface and bottom layers are directed oppositely. Note that in the bottom layer, under the influence of western and northern winds (Figure 3.1.4, *a*, *c*), the currents in the Kerch Strait are directed from the Black Sea to the Sea of Azov, in the surface layer (Figure 3.1.3, *a*, *c*) in the opposite direction. With a southerly wind (Figure 3.1.4, *b*), currents at a depth of 10 m are directed from the Sea of Azov to the Black Sea.

In the Taganrog Bay (Figure 3.1.3), with intense westerly, northwesterly and southwesterly winds, the main direction of currents is easterly. The structure of currents in the bay is preserved during the action of wind fields in all considered directions. It is known [Hydrometeorology ... , 1991] that in the central part of the sea, from March to November, the western and southwestern currents are most often repeated, more intense than the currents of other directions. In the Taganrog Bay, western currents are most often repeated, while the velocities and repeatability of currents in other directions are much lower [Numerical analysis ... , 2014].

Table 3.1.2 shows data on the maximum velocities of stationary currents at different horizons, depending on the speed and direction of the wind, taking into account and without taking into account the currents through the strait. From the analysis of these data, it follows that the values of the velocities of steady currents found during modeling taking into account the strait are greater for the same wind speeds and directions than without taking it into account. At the same time, taking into account water exchange at the considered horizons leads to a relative difference in the values of the current velocity modules not exceeding 45%.

The study of the integral exchange of water through the Kerch Strait in steady state was carried out based on the analysis of the results of numerical experiments, in which the values of the function $G(t)$ were calculated at each time step according to the formula (3.1.2). Positive values of this function correspond to the currents of water into the Sea of Azov, negative values indicate that the currents through the strait changes direction to the opposite. From the analysis of the time dependencies of the integral currents rates (m^3) of water through the strait during the calculation period (t = 200 h), it follows

that the greatest currents of water through the strait occurs with a southerly wind, the lowest with a northerly wind. The currents rate increases to a maximum from the initial moment of time to $t = 20$ h.

Table 3.1.2 – The maximum velocities of stationary currents (cm/s) caused by constant wind of three speeds and directions on different horizons of the Sea of Azov, excluding and taking into account (*) water exchange with the Black Sea

Horizon, m	Wind speed and direction								
	5 m/s			10 m/s			15 m/s		
	E	S	N	E	S	N	E	S	N
1	11	11	11	40	39	41	62	69	58
	14*	17*	14*	44*	46*	42*	87*	99*	85*
3	6	8	8	23	28	28	48	57	47
	11*	14*	12*	28*	38*	35*	52*	59*	58*
5	4	7	7	14	21	22	28	44	43
	9*	12*	11*	24*	35*	31*	46*	52*	46*
10	4	6	6	13	16	16	23	27	27
	6*	8*	7*	17*	24*	21*	32*	42*	35*

The highest speeds of currents caused by the action of wind of the same speed are observed in the southerly direction of the wind, the lowest in the north. So, the maximum speeds of surface currents calculated taking into account the strait at a wind speed of 15 m/s are 0.87 (W); 1.22 (S) and 0.99 m/s (N). The relative difference between the highest and lowest values of the presented speeds is 30%. A similar ratio of the values of the current velocities can be traced on other horizons under the action of a constant wind with a speed of 5 and 10 m/s.

* The results of modeling performed taking into account water exchange through the Kerch Strait

Obviously, in a steady motion, the water currents through the Kerch Strait must be zero, otherwise the task cannot be considered established due to the rise or fall of the Sea of Azov level as a whole due to the currents of water through the Kerch Strait. This is possible due to the difference in the average level of the Sea of Azov and in the vicinity of the Kerch Strait, as well as due to the variability of currents in depth or the presence of opposite barotropic currents in the strait. At the same time, the currents cannot be large due to the shallow waters and narrowness of the Kerch Strait in the area of the Sea of Azov. Thus, stationary movements caused by constant wind, taking into account or without taking into account the Kerch Strait, should be practically the same, and, therefore, simulation of circulation in the Sea of Azov can be carried out without taking into account water exchange through the strait. Thus, the southerly wind acting along the Kerch Strait causes currents whose speeds exceed (by 12 – 30%) the speeds of currents caused by a westerly or northerly wind.These results are presented in more detail in our papers [Shulga, 2013; Cherkesov, Shulga, 2018].

From the analysis of the time dependence of the integral water currents through the strait during the calculation period (200 h), it follows that the largest volume of leaked water occurs with a south-easterly wind, the smallest – with a north-westerly wind: 53.6 (SE), 26.4 (NW), 12.7 m^3 (SW) [Cherkesov, Shulga, 2018]. These results are consistent with observational data on the average annual incurrents of Black Sea waters through the Kerch Strait, and the currents of Azov Sea waters into the Black Sea.

The average annual currents rate through the Kerch Strait for the periods 1927 – 1940, 1948 – 1970 was 50.6 km^3/year for the Azov stream, 32.7 km^3/year for the Black Sea, in general – 17.9 km^3/year [Hydrometeorology ... , 1991], which is consistent with the currents rate obtained on the basis of the water balance for the Sea of Azov based on velocity measurements currents [Altman, 1976]. According to these data (for the period from 1963 to 1974 over 400 definitions of water currents rates were obtained, measured in different seasons and under different synoptic situations) the average currents rates are 77 km^3/year for the Azov and 51 km^3/year for the Black Sea currents, with the predominance of the Azov currents of 26 km^3/year. The magnitude of these costs and the cross-sectional area in the northern narrowness of the Kerch Strait (29.400 m^2)

corresponds to an average currents velocity of 1.7 cm/s. In cases of storm winds, the currents rate calculated from the measured currents velocities [Altman, 1976] reaches 315 km^3/year. At the same time, the currents velocity averaged over the cross-sectional area exceeds 30 cm/s, which is consistent with the found currents rates and average values of currents velocities (Table 3.1.2).

3.2. The effect of anticyclones passing over the Sea of Azov on the maximum currents velocities in the Kerch Strait during the ice seasons 2015 – 2017

An unexpected increase in the speed of the current in any narrow strait poses a significant danger to ships passing through it, and in the months related to the ice season, also for the hydraulic structures located here. The reason leading to an increase in the currents velocity, with a relatively high repeatability, is the rapid change in atmospheric pressure and wind speed caused by the movement of anticyclones in the sea area. As a result of the appearance of anticyclones at the entrance to the strait, there is an increase in the level of water activity and the spread of non-anemobaric wave [Kurkin, 2005; Tengt, Wu, 1994]. This phenomenon affects the change in the currents velocity in the strait the more noticeably the greater the average rate of increase in the average daily values of atmospheric pressure at its entrance. The conjugation of surface distribution also has a significant effect on a not so common phenomenon [Shallow water distribution ... , 2011; Chang, Biol, 2007].

The maximum value of the modulus of the instantaneous currents velocity arising from these processes is achieved at the strait alignment, where its cross-sectional area is minimal. The narrowest point of the Kerch Strait is located between Cape Pavlovsky and the northern tip of the Tuzla spit, where the strait narrows to 3.5 km [Geology of the USSSR ... , 1981; Hydrometeorology ..., 1991]. As follows from [Matishov and Chikin, 2012], the cross–sectional area of the Kerch Strait on its northern alignment (port of Crimea – port of Kavkaz) is 26 km^2, and on the alignment of Tuzla Island (Cape Ak-Burun – Tuzla Island) – 12 km^2. Consequently, estimates of the maximum speed of the Azov current for the section of the fairway of the Kerch Strait corresponding to the

alignment of Tuzla Island are necessary for the development of recommendations for the construction of special structures for the ice protection of bridge supports. This assessment was performed for situations arising from the movement of anticyclones over the Sea of Azov from the northern points in the months related to the ice season.

The strengthening of the Azov current during the ice seasons leads to an increase in the number of ice formations delivered by it per unit of time to the northern part of the strait from the Sea of Azov. Due to the peculiarities of the relief of the bottom of the Kerch Strait in the area where the bridge is located, the removal of ice from the Sea of Azov into the Black Sea by the Azov current is carried out mainly along the fairway (between the bridge supports). The larger the modulus of the velocity vector of ice carried away by the Azov current, the stronger the mechanical effects that this ice is able to exert on ships following the strait and on bridge supports [Hydrometeorology ..., 1991; Hydrometeorological conditions ..., 2009; Atlas of the Ice ..., 2016; Oceanographic Atlas ..., 2009].

Numerous weather stations in Russia and Ukraine are located on the coast of the Sea of Azov, where routine observations of changes in the main meteorological elements, including atmospheric pressure, are carried out [Dubinin, Pospelov, 2014]. During the ice seasons of 1955 – 2014 in the Kerch Strait, including on the Tuzla Island, expeditions from the GOIN occasionally monitored changes in the average currents velocity. It was found that the measured values of the average speed of the Azov current in the specified section of the fairway were 0.14 – 0.18 m/s. In the section of the strait corresponding to its northern narrowness (on the route of the ferry crossing Port of Crimea – Port of Kavkaz), its higher values were also recorded – 0.7–0.83 m/s [Atlas of the Ice ..., 2016]. Observations of changes in the maximum currents velocity at the alignment of Tuzla Island was not carried out during such periods, although it is quite obvious that these maximum values cannot exceed the specified average values. Nevertheless, the assessment of the maximum speed of the Azov current, due to the movement of real anticyclones from the northern points in the months related to the ice season, has not previously been carried out for certain sections of the fairway of the Kerch Strait, which does not allow for adequate consideration of these speeds when developing measures

aimed at improving the safety of navigation in the strait and the operation of the existing bridge.

One of the most versatile tools for testing hypotheses and implementing forecasts about the currents velocity in the Kerch Strait is the use of mathematical modeling results based on the application of the hydrodynamic POM model [Blumberg, Mellor, 1987], additions to which are described in Section 1. Based on the analysis of the simulation results, we have shown the importance of the resonant mechanism in the occurrence of extremely high amplitudes of overburden vibrations and seiches generated by anticyclones moving over the water surface from the northern points at a speed equal to the velocity of propagation of a free long wave in it [Cherkesov, Ivanov, Khartiev, 1992]. The influence of the parameters of idealized anticyclones on the velocity and structure of the resulting currents, run-up oscillations and seiches have been studied in a number of our works. They showed that the currents velocity field in the Kerch Strait is most significantly influenced by anticyclones moving over the Sea of Azov from the northern points.

Synoptic maps based on the results of NCEP/NCAR reanalysis were used to identify anticyclones that moved over the Sea of Azov to the northern entrance to the Kerch Strait (ftp.cdc.noaa.gov/Datasets/ncep.reanalisis.dailyavgs/levelsea/), which contains data for the period from 01/01/1948 to 12/31/2017. The information presented in it on the average daily values of atmospheric pressure, reduced to sea level, is equivalent and corresponds to the nodes of the coordinate grid in increments of 2.5°. Among them there are nodes located between the meridians of 15° and 45° E, as well as the parallels of 40° and 80° N. (the Azov-Black Sea region and the Kerch Strait are also located there). Conclusions about the possibility of using this reanalysis as factual material for solving the problems under consideration are based on its comparison with information obtained during routine observations of changes in the same characteristic in the points of Dangerous, Mysovoye and Taman for the period 01/01/1972–03/31/1988.

Based on the NCEP/NCAR reanalysis, the maximum values of the average rate of increase in atmospheric pressure were determined for the entire studied period: in December 2015 (1870 Pa) and February 2017 (1650 Pa). Figure 3.2.1 shows the

distributions of the average daily values of the sea-level-adjusted surface atmospheric pressure according to NCEP/NCAR data, which correspond to the dates 5 – 7 February, 2017.

As can be seen from Figure 3.2.1, *a*, on 05/02/2017, an extensive area of elevated atmospheric pressure was located above the Sea of Azov (the average daily pressure here was ~ 1012 gPa). The area of high atmospheric pressure, which is part of the Arctic Anticyclone, was located over Scandinavia, the regions of the Northwestern Federal District of Russia and the Barents Sea. An unrelated subtropical anticyclone was located over Turkey and the Caucasus. As follows from Figure 3.2.1, *b*, on 06/02/2017, an invasion of Arctic air occurred, which led to the formation of a submeridional band of increased atmospheric pressure connecting the segment of the Arctic anticyclone with the Subtropical anticyclone. The penetration of Arctic air into the regions of the European territory of Russia located in temperate latitudes led to the fact that atmospheric pressure over the Sea of Azov began to rise on 06/12/2015, approaching the level of 1015 gPa.

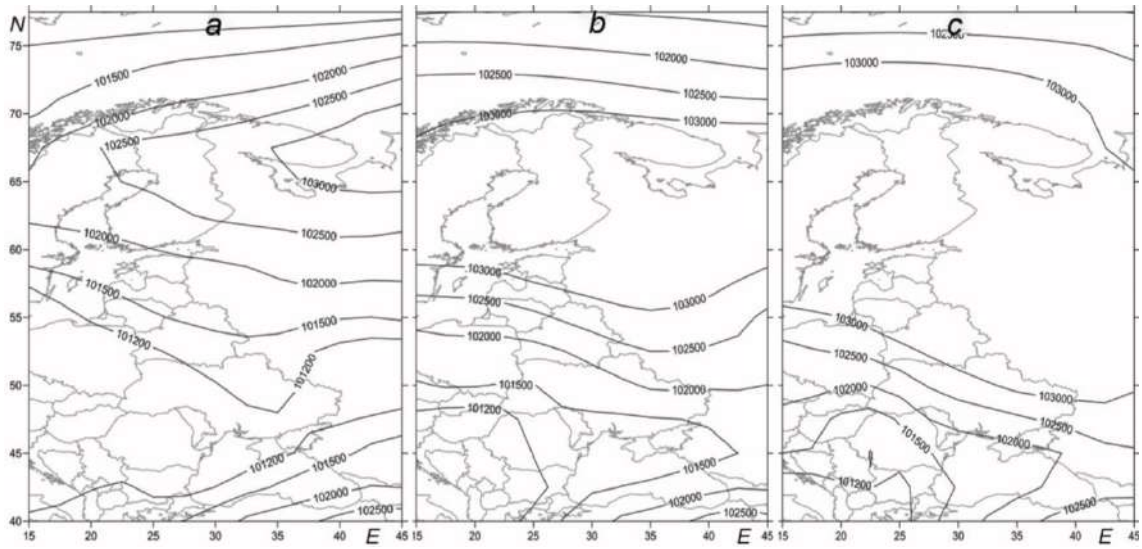

Figure 3.2.1 – Distributions of the average daily values of the surface atmospheric pressure adjusted to sea level over Eastern Europe: 02/5/2017 (*a*); 02/6/2017 (*b*); 02/7/2017 (*c*) [Shul'ga, Shchodro, Kholoptsev, 2021]

From Figure 3.2.1, it can be seen that on 07/02/2017 the invasion of Arctic air continued, which led to a significant expansion of the considered band of increased

atmospheric pressure. At the same time, the atmospheric pressure over the Sea of Azov increased by almost 9 gPa. Comparing Figures 3.2.1, *b* and 3.2.1, *c*, we note that the isobars depicted on them shifted over its water area from the northeast towards the northern entrance to the Kerch Strait on the day in question. Consequently, the anticyclone in question is capable of causing significant changes in the currents velocity in the strait and an increase in the speed of the Azov current. From Figure 3.2.1, it can be seen: in the process under consideration, the atmospheric pressure over the Sea of Azov was significantly higher than over the Black Sea area adjacent to the southern entrance to the Kerch Strait. The latter (due to the law of communicating vessels) also could not but cause an increase in the speed of the Azov current. The peculiarities of the change in the distribution of atmospheric pressure over the Azov region, which appeared on 07/02/2017, are typical for other cases of increased atmospheric pressure that occurred during the movement of anticyclones over the Sea of Azov from the northern points in the ice seasons 2015 – 2017.

Hydrodynamic modeling of situations arising during the detected sharp increases in atmospheric pressure was performed using meteorological fields obtained from the SKIRON model data for 2015 and 2017. The time course of maximum atmospheric pressure values in the Sea of Azov, based on the analysis of meteorological information according to the SKIRON model, is shown in Figure 3.2.2.

The space-averaged atmospheric pressure at each time is determined by the formula

$$\overline{P}(t) = \frac{1}{N}\sum_{k=1}^{N} P_{\mathrm{SKIRON}_k}(t), \qquad (3.2.1)$$

were N – the number of nodes of the model grid of the Azov Sea basin used in this experiment; $P_{\mathrm{SKIRON}k}(t)$ – the value of the current atmospheric pressure value in its kth node.

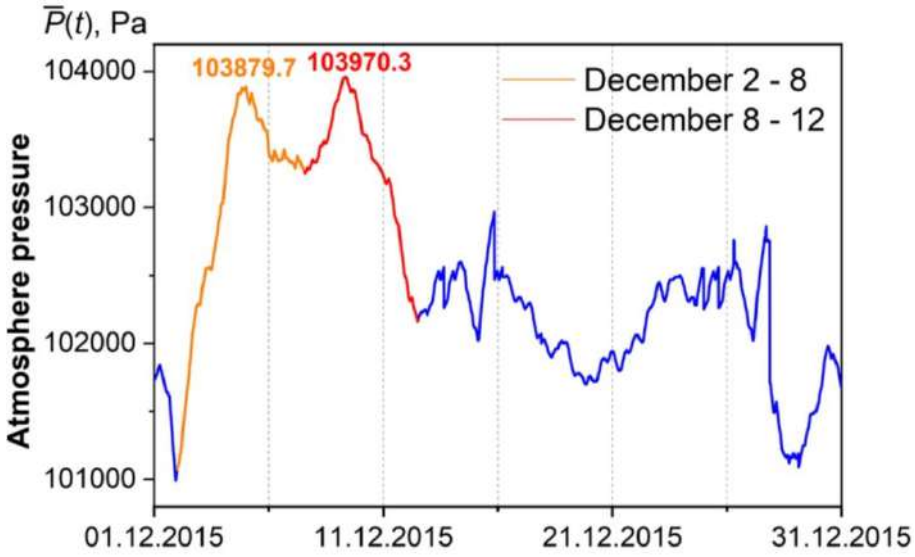

Figure 3.2.2 – Atmospheric pressure, according to the SKIRON/Eta model, averaged over the water area of the Sea of Azov, in December 2015. Vertical dotted lines are drawn with a discreteness of 5 days

As follows from the analysis of the curves marked in red in Figure 3.2.2, atmospheric pressure rise situations were accompanied by a significant increase in atmospheric pressure. It can be seen that the atmospheric pressure in the first decade of December 2015 varied from a minimum (1009.9 gPa) to a maximum (1038.9 gPa) value. The rate of pressure increase during this period was 9.5 gPa/day.

Spatial maps of the driving wind field and atmospheric pressure according to the SKIRON model, corresponding to the time of occurrence of atmospheric pressure increases on February 5 – 7, 2017, are shown in Figure 3.2.3. It is noticeable that in the situations under consideration, significant spatial heterogeneity of wind fields over the sea was observed both in speed and direction. The above maps of surface atmospheric pressure distributions are consistent with the average daily data presented in Figure 3.2.1. The passage of the anticyclone on 6.02.2017 (Figure 3.2.3, *b*) at the northern entrance to the Kerch Strait causes a change in wind direction from northeast to southwest. Figure 3.2.3, *b* shows the movement towards the Black Sea of an extensive baric formation with a high (up to 15 m/s) wind speed, the direction of which changed during the day to the opposite.

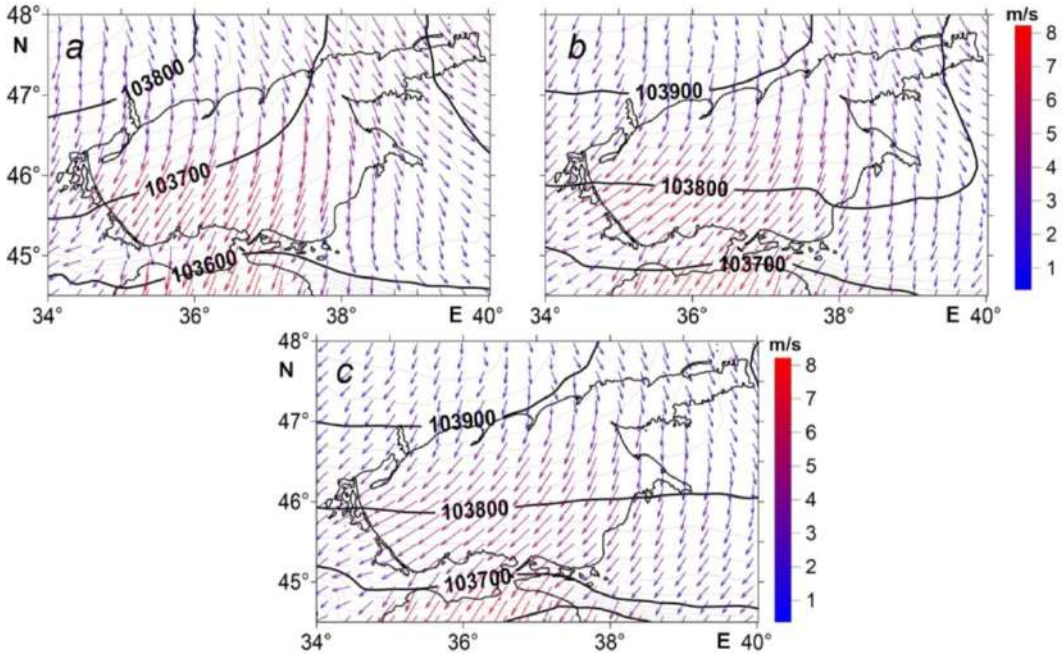

Figure 3.2.3 – Fields of driving wind and surface atmospheric pressure over the Sea of Azov: 05/02/2017 (*a*); 06/02/2017 (*b*); 07/02/2017 (*c*) [Shul'ga, Shchodro, Kholoptsev, 2021]

Analysis of the simulation results (POM) of situations arising during the detected sharp increases in atmospheric pressure in December 2015 and February 2017 ($0 \le t \le 744$ and $0 \le t \le 672$ h) allowed us to estimate the values of the maximum speed of the Azov current at various points of the northern entrance to the Kerch Strait. The simulation data allow us to obtain the values of the current velocity both on the sea surface and at depths of 3, 5 and 10 m at time points that differ by 3 min in the nodes of the calculated grid with a horizontal resolution of 1 km. Calculations have shown that the movement of the anticyclone over the region leads to a change in the distribution of wind speed and atmospheric pressure, at which a significant increase in the level of the Sea of Azov occurs at the northern entrance to the Kerch Strait, due to overcurrentsing water.

The values of the maximum ($|\mathbf{U}|_{\max}$) and vertically averaged $|\bar{\mathbf{U}}|_{(z)}$ velocity of the Azov current according to the data of two experiments conducted for the specified date ranges are presented in Table 3.2.1. Estimates of the currents velocity are given

in points $P_1 – P_5$ shown in Figure 3.2.1, equidistant located at the northern entrance to the Kerch Strait, at latitude 39.33° N (point P_3 is exactly on the fairway).

It follows from Table 3.2.1 that the highest values of the currents velocity are reached in the center of the strait (point P_3). Here, the absolute maximum of this indicator on the surface is 85 cm/s, and the average depth is 64 cm/s (12/06/2015). Calculations have shown that in each episode under consideration, the values of the instantaneous velocity of the Azov Current at various points of the northern entrance to the Kerch Strait fall on the same day. On the same date, the absolute maximum value of the average rate of increase in atmospheric pressure (1870 Pa) for the studied period also falls.

Table 3.2.1 – Maximum velocity values (cm/s) of the Azov current in the surface layer of the sea and averaged vertically at points at the entrance to the Kerch Strait during the movement of anticyclones from the northern points, revealed in December 2015 and February 2017 [The Influence ... , 2018]

Points	December 1 – 31, 2015		February 1 – 28, 2017	
	$\lvert\mathbf{U}\rvert_{\max}$	$\lvert\bar{\mathbf{U}}\rvert_{[z]}$	$\lvert\mathbf{U}\rvert_{\max}$	$\lvert\bar{\mathbf{U}}\rvert_{[z]}$
P_1	37	45	35	50
P_2	41	48	37	44
P_3	64	85	56	76
P_4	47	54	45	48
P_5	50	53	53	61

Based on the data given in Table 3.2.1, we note that the maximum current velocity reaches the highest value not only in the center of the strait, but also in its eastern part (point P_5): 50 (06/12/2015) and 53 cm/s (02/24/2017). The lowest maximum current velocities take place at the point located at the western border of the strait (point P_1): 37 (06/12/2015) and 35 cm/s (02/24/2017). Similar relations take place for the averaged values of the currents velocity. Thus, currents with velocities arise in the central part of the strait, the average and maximum values of which are 1.5 – 1.7 times higher than the corresponding velocity values on its western border. The simulation results make

it possible to determine the excess of the maximum current velocity relative to its monthly average value during the passage of an anticyclone over the Sea of Azov. An analysis of the results presented in Table 3.2.1 shows that the peak values of current velocities exceed the monthly average values by 30 (for December 2015) and 21 cm/s (for February 2017).

The simulation results allow us to draw conclusions about the maximum level of the Sea of Azov at points located at the northern entrance to the Kerch Strait ($P_1 - P_5$). These values are given in Table 3.2.2 at the time when the maximum of the Azov current is reached. As follows from the analysis of the data presented in Table 3.2.2, the highest values of the Sea of Azov level (52 and 48 cm) relative to the average level of the Black Sea on the dates corresponding to the highest values of the maxima of the Azov current (06/12/2015 and 02/24/2017), in both cases, fall on point P_1, located in the western part of the northern entrance to the Kerch strait [Shul'ga, Shchodro, Kholoptsev, 2021].

Table 3.2.2 – Maximum values of the Sea of Azov level (cm) at the points of the northern entrance to the Kerch Strait at the time of reaching the maximum of the Azov current

Date	P_1	P_2	P_3	P_4	P_5
06/12/15 in 22:00	52	33	43	28	47
24/02/17 in 15:45	48	31	37	25	46

3.3. Conclusions to Chapter 3

The results of numerical modeling using the POM model adapted to the Sea of Azov showed the dependence of extreme values of level deviations, the velocity of surface and deep stationary currents on the direction and velocity of the constant wind causing them, as well as taking into account water exchange through the Kerch Strait.

It has been established that the south wind, taking into account the water exchange through the strait, causes currents whose maximum speeds are 30% higher than the speeds of steady movements caused by the west and north winds. Accounting for water exchange through the strait leads to significantly higher values of the velocity of steady currents only at wind speeds of 10 and 15 m/s (increase to 53% compared with the action of wind in the same direction at a speed of 5 m/s). The simulation results made it possible to determine the effect of water exchange with the Black Sea on an increase in the maximum deviations of the Sea of Azov level. In particular, it is shown that at a wind speed of 10 m/s, the maximum values of surges and current velocities, taking into account the strait, are 36 and 42% higher, respectively, than without taking into account the strait. At the same time, the highest current velocities are caused by a southerly wind.

Estimates of the impact of vortex atmospheric formations, taking into account the free passage of liquid through the Kerch Strait, allow us to draw conclusions about an increase in the maxima of run-off and run-off depending on the geometric dimensions of the disturbances. It is shown that a cyclone with a multiple of a large base (for example, the southern cyclone) leads to the appearance of run-offs and run-offs with large amplitudes. Thus, a cyclone with a 2 times larger base causes an increase in the values of run–offs and run-offs by 2.3 times, and having a 4 times larger base – by 3 times. Also, an increase in the size of active atmospheric formations leads to a decrease in the time during which the formation of extreme values of the level occurs.

Vortex atmospheric disturbances of zonal directions (for example, a western cyclone) do not lead to a noticeable change in the values of the run-up and run-up compared with the action of cyclones moving in a meridional direction (for example, a southern cyclone). Accounting for water exchange through the strait causes an increase of no more than 40% in extreme run-offs and surges.

The results of modeling performed using meteorological data from the SKIRON model for situations of a significant increase in atmospheric pressure over the Sea of Azov in December 2015 and February 2017 showed the possibility of reaching the maximum value of the currents velocity at the northern entrance to the Kerch Strait (85 cm/s, 12/06/2015).

The movement of anticyclones over Eastern Europe, passing along the waters of the Sea of Azov from the northern points, can lead to an increase in the surface velocity of the Azov current to a maximum value of 0.54 m/s, and sea level – up to 52 cm. Such a significant and sharp increase in the current can be dangerous both for ships passing between the pillars of the Kerch Bridge, and for these pillars themselves during the ice seasons.

Chapter 4.
FREE FLUCTUATIONS IN THE SEA OF AZOV LEVEL

Fluctuations in the level and currents in the seas and oceans are formed under the influence of various external and internal forces, the diversity of which leads to the formation of multi-scale oceanological processes with periods from several seconds to several decades. An important role in the formation of extreme levels and hydrological processes in the coastal region of the Sea of Azov is played by run-up level fluctuations, which are excited as a result of the Ekman mechanism of generation of wind currents under the influence of the combined effects of tangential wind friction, Earth rotation and friction force. In addition, in the mesoscale and synoptic ranges of spatial and temporal scales, various types of long waves are generated in the basin of the Sea of Azov under the influence of the forces of tangential friction of wind and horizontal atmospheric pressure gradient: inertial-gravitational and gradient-vortex. Very often, the generation and relaxation of long waves occurs at the natural oscillation frequencies of the pool [Appel, 1936; Lamb, 1947; Le Blon, Mysek 1981; Gill, 1986; Rabinovich, 2009; Numerical modeling ... , 2019; Zakharchuk, Tikhonova, Fuks, 2004; Spatiotemporal ... , 2021]. When the velocities of anemobaric formations in the atmosphere are equal to the phase velocities of free long waves, a resonant mechanism of excitation of wave movements in the oceans and seas is realized [Kulikov, Medvedev, 2013; Zakharchuk, Tikhonova, 2011]. In confined and enclosed marine basins, under the influence of the processes of reflection and rotation of the Earth, long waves are modified into standing (seiches) and progressive standing (mixed) wave movements [Rabinovich, 2009; Krylov, 1946; Nekrasov, 1975; Timonov, 1959; Zakharchuk, Sukhachev, Tikhonova, 2020]. Free oscillations, which are wave movements with periods from several h to several days [Monin, 1972; Lotsia of the Sea of Azov; Herman 1970], are constantly observed in the Sea of Azov. At the same time, in areas of narrowing coastal boundaries, the current velocity can reach 1.5 m/s, and the wave height is 0.8 m [Hydrometeorology, 1991; Dotsenko, Ivanov, 2010]. Based on the data of long-term observations, it is known that well-pronounced seiches fluctuations in the level reach

the highest value (55 cm) in the Taganrog Bay. The period of free oscillations that occur after the termination of the overburden wind is equal to one day [Hydrometeorological ... , 1986]. In summer, when good anticyclonic weather is established over the sea, a situation arises when forced fluctuations caused by breezy winds are superimposed on free fluctuations in sea level [Kulikov, Fine, Medvedev, 2015]. In these cases, there is a real threat of extreme currents, flooding of coastal areas of the sea and destruction of coastal structures. The structure of the dominant longitudinal natural oscillations in the Sea of Azov is such that their peaks fall on areas located near large settlements [German, 1971; Modern ..., 2015]. Therefore, it is of interest to study the influence of free oscillations on the formation of extreme amplitudes of fluctuations in the level and currents of the Sea of Azov.

The study of seiches oscillations in the Sea of Azov using mathematical modeling and taking into account the analysis of field observations was carried out in [German, 1971; Modeling long waves … , 2000; Ivanov, Konovalov, Cherkesov, 2003], where the values of periods and structures of the first six modes of free oscillations were found by the finite element method. In a number of works [Matishov, Matishov, Injebeikin, 2008; Matishov, Injebeikin, 2009], the seiche fluctuations of the Sea of Azov level and currents resulting from 1-meter overcurrentss at the open boundary have been studied within the framework of a linear two-dimensional mathematical model. In this chapter, seiches oscillations are investigated within the framework of a three-dimensional hydrodynamic model.

4.1. Investigation of the speed of currents and fluctuations in sea level after the cessation of long-term wind

Atmospheric disturbances are the main source of seiche generation in the Azov-Black Sea region [Belov, 1978; Hydrometeorological ..., 1962; Scientific and Applied ..., 1990]. Under the influence of the wind, which has a stable direction and speed, currents arise and the level rises on one shore and decreases on the other. After the wind ceases, free wave fluctuations of the liquid on the sea surface take place. The analysis of seiche-

like oscillations in the Sea of Azov by mathematical modeling, taking into account the data of field observations, is given in [German, 1970; Matishov, Ingebeikin, 2009]. The author of the work [German, 1970] performed a spectral analysis of the characteristics of periods and structures of higher modes of free oscillations. Seiches fluctuations in the Sea of Azov level and currents resulting from 1 m high overcurrentss on the open border have been studied within the framework of a linear two-dimensional mathematical model [Matishov, Ingebeikin, 2009].

Three-dimensional modeling is of scientific and applied interest, which makes it possible to analyze the physical patterns of free liquid vibrations in the Sea of Azov. Conclusions about the features of such movements are made based on the analysis of the results of a series of numerical experiments conducted on the basis of a modified POM model, which reproduce the fluctuations of the liquid in the pool that occur after the cessation of the action of a steady wind. The action of the wind begins from the initial moment of time ($t = 0$) on the initially undisturbed surface of the sea. Its velocity ($\mathbf{W}_{st}$) is set based on the formula (2.1.1.1) with the modulus $|\mathbf{W}|_{st}^4 = 20$ m/s, and the direction corresponds to the easterly wind. From the moment of establishment of movements in the sea ($t = t_{st} = 48$ h) the wind speed decreases linearly in 3 h to zero, determining the time of occurrence of seiches oscillations ($t_{sei} = 51$ ч).

Figure 4.1.1 shows the sea level contours at various points in time. In the initial period, the surface of the level is a single-node niche. In the steady–state mode (Figure 4.1.1, *a*), there is a decrease in the level along the eastern coast (slopes) and an increase along the western coast (surges). The nodal (dashed) line crosses the central part of the sea, it is oriented perpendicular to the direction of the wind [Ivanov, Cherkesov, Shulga, 2010; Cherkesov, Shulga, The study ... , 2014]. It should be noted that the most intense decreases occur in the east, in the Taganrog Bay, and the greatest increases occur in the western part of the sea. The smallest amplitudes of the level fluctuations take place in its central part. With the cessation of the action of the wind (Figure 4.1.1, *b – e*), there is a significant change over time in the location of the lines of equal level and the nodal line.

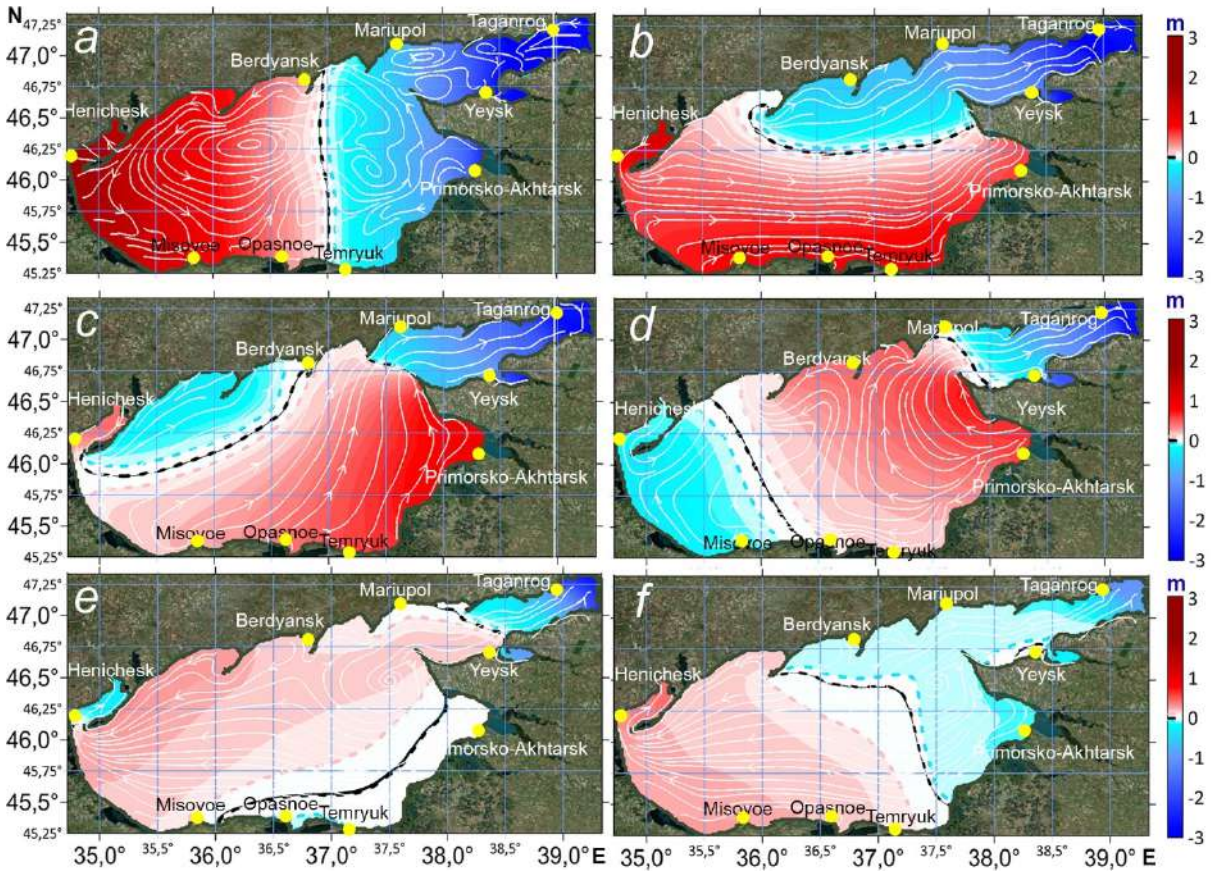

Figure 4.1.1 – Currents and changes in the level (m) of the Sea of Azov at steady motion (*a*), at the moment of cessation of wind action (*b*), after 3 h (*c*), after 6 h (*d*), after 9 h (*e*), after 12 h (*f*). Black dotted line the line of zero amplitudes of sea level is marked [Ivanov, Cherkesov, Shulga, 2015]

At the moment of termination of the wind action (Figure 4.1.1, b), the nodal line has not shifted, and the overtaking and overtaking zones remain in the same areas of the sea as in the steady state. At the same time, the values of the run-off and run-off decrease. From Figure 4.1.1, it can be seen that the nodal line 3 h after the cessation of wind action is deployed relative to the central area of the sea and oriented in the zonal direction. The run-up and run-up zones have also shifted to the west, towards the current wind. In the Taganrog Bay, the cessation of wind action after 3 h has little effect on changes in the level.

After 6 h (Figure 4.1.1, *d*), the nodal line is further moved in an easterly direction. The areas of the run-up and run-down move in the south and north directions, respectively, while their values decrease significantly. Figures 4.1.1, *d* and e show the sea

level isolines 9 and 12 h after the cessation of wind action. It can be seen that the free oscillations at the specified time points have the form of two-node sessions. Changes in the level fluctuations over time at any point of the Sea of Azov represent a superposition of seish of various modes, the formation of which is influenced by many factors. The attenuation of the seiches oscillations to 0.1 cm lasted for 300 h [Ivanov, Cherkesov, Shulga, 2015].

Winds of the same speed, but in different directions (from south-west to north-west) can lead to changes in the areas of maximum values of the run-up. Thus, constant southwesterly and northwesterly winds with a speed of 15 m/s cause the greatest surges at the stations of Taganrog (204 cm) and Primorsko-Akhtarsk (102 cm), respectively. At the same time, under the influence of wind of the considered speeds and directions, the change in the areas of maximum run-off does not occur. In all cases, the highest values of run-offs are achieved at the Genichesk station. The maximum acceleration value (139 cm) occurs with a westerly wind at a speed of 15 m/s. Note also that with winds of the same speed, but in different directions, there may be both surges and overcurrentss in the same coastal area. At the Mariupol station (wind speed 15 m/s), surges (119 and 88 cm) occur with southwesterly and westerly winds and overcurrentss (42 cm) with a northwesterly wind [Impact of atmospheric ..., 2018].

Using the results of numerical modeling, we will analyze changes in the amplitude and periods of seiches oscillations at points along the coast and in the central part of the basin. Table 4.1.1 shows the extremes of seiches oscillations (ζ_k; k = 1, … ,4) in the area of coastal stations of the Sea of Azov and the time of their achievement (t_k). The change in the level of the Sea of Azov near its coast (the height of the run-off and run-off) under the influence of a steady easterly wind $\mathbf{W}_{st}$ at a speed of 20 m/s, the extremes of seiche-like fluctuations in the area of stations on the sea coast that occur after its termination, as well as the time of their achievement tk can be judged from the data in Table 4.1.1. that the greatest overburden is noted at the Genichesk station (2 m), the greatest overburden is at the Yeysk station (-2.44 m). After the complete weakening of the wind action, a monotonous decrease in the level occurs to the lowest value (ζ_1 = – 0,27 m; t = 9,5 h). At the same time, the swing range from a stationary surge is 2.3 m.

At t = 16.5 h, there is an increase in the level to 0.33 m. The span of the second oscillation (0.6 m) is 3.8 times smaller than the first (1.63 m) [Ivanov, Cherkesov, Shulga, 2015].

Table 4.1.1 – Stationary surge phenomena (ζ_{st}, см), caused by the action of a constant easterly wind at a speed of 20 m/s, the time of their achievement (t_k, h) and extremes of seiches oscillations (ζ_k, k = 1,…,4), occurring after the cessation of the wind

Stations	ζ_{st}	ζ_1	t_1	ζ_2	t_2	ζ_3	t_3	ζ_4	t_4
Henichesk	202	–27	9,5	33	16,5	–12	24,7	12	32,7
Berdyansk	25	–57	2,5	46	7,7	–8	17,6	10	25,6
Mariupol	–153	–1	12,3	–20	20,2	17	27,1	2	39,2
Taganrog	–158	–89	24,3	30	31,5	–8	41,3	8	50,4
Yeysk	–244	–6	18,3	21	28,5	–2	38,9	7	55,7
Primorsko-Akhtarsk	–175	92	5,3	–10	13,9	34	21,3	–3	26,7
Temryuk	–18	103	2,7	–14	13,5	25	18,5	–5	28,5
Opasnoe	32	93	1,7	–8	13,0	23	18	–4	27,9
Mysovoe	98	–20	8,7	26	15,4	–6	24,2	3	37,3

The extreme value at the next oscillation (– 0.12 m) takes place after 8.2 h (24.7 h), its span of 0.45 m differs little from the previous one (by 0.15 m). The maximum of the fourth free oscillation ζ_4 = 0.12 m occurs after t_4 = 32.7 h, its span (0.24 m) is half the previous one and 9.6 times less than the first one. Using the data in Table 4.1.1, we will perform an analysis of free oscillations at the station Yeysk, where the greatest acceleration is noted (–2,44 m; $t = t_0$). The cessation of wind action causes an increase in the level (ζ_1 = – 0.06 m; t = 18.3 h). At the same time, the span of the first oscillation is 2.38 m. In the future, the level continues to rise and after 10.2 h reaches the highest value of 0.21 m, the scope of the second oscillation (0.27 m) is 8.8 times less than the first. After another 10.4 h, there is a decrease in the level by 0.23 m (ζ_3 = – 0.02 m;

t = 38.9 h), the swing range differs from the previous one by 0.04 m. The span of the next oscillation (ζ_4 = 0.07 m), which occurs after 16.9 h (t_4 = 55.7 h), is 0.1 m, which is 23.8 times less than the first one. The range of sea level fluctuations $\Delta\zeta_k$ after the cessation of wind action at these two stations is as follows (k is the number of fluctuations) [Demyshev, Cherkesov, Shulga, 2017]:

k	1	2	3	4
$\Delta\zeta_k$, *m*				
Henichesk	2.30	0.60	0.45	0.24
Yeysk	2.38	0.27	0.23	0.10

Figure 4.1.2 shows the fields of currents in the surface layer of the Sea of Azov at various points in time. It can be seen that in steady motion (tst = 48 h), the current velocity vectors are directed along the northeastern part of the coast, and in the Taganrog Bay and the central part of the sea mainly in one direction with the current wind (Figure 4.1.2, *a*). In the central part of the sea, there are two vortex formations of opposite signs with a spatial scale of ~ 100 km. Narrow meandering jets stand out between the vortices.

When the wind speed decreases to zero ($t = t_0$), the vortex formation process continues to develop, and the currents field is a chain of vortices (Figure 4.1.2, *b*). In the future, the currents pattern changes significantly (Figure 4.1.2, *c*). Now, in the entire sea area, the current velocity vectors are directed in the direction opposite to the current wind. It can be seen that the velocities are higher than at tst, and at the same time there is one vortex of disturbances. After 6 and 9 h after the termination of the wind, the currents remain quite intense and are directed in the direction opposite to the stationary wind (Figure 4.1.2, *d*, *e*). At the same time, an anticyclonic vortex begins to form along the northern coast. After 12 h (Figure 4.1.2, *e*), the direction of currents from west to east remains in the Taganrog Bay, an anticyclonic vortex takes place at the entrance to it, in the central and western parts of the sea the currents are directed in the opposite direction (from east to west).

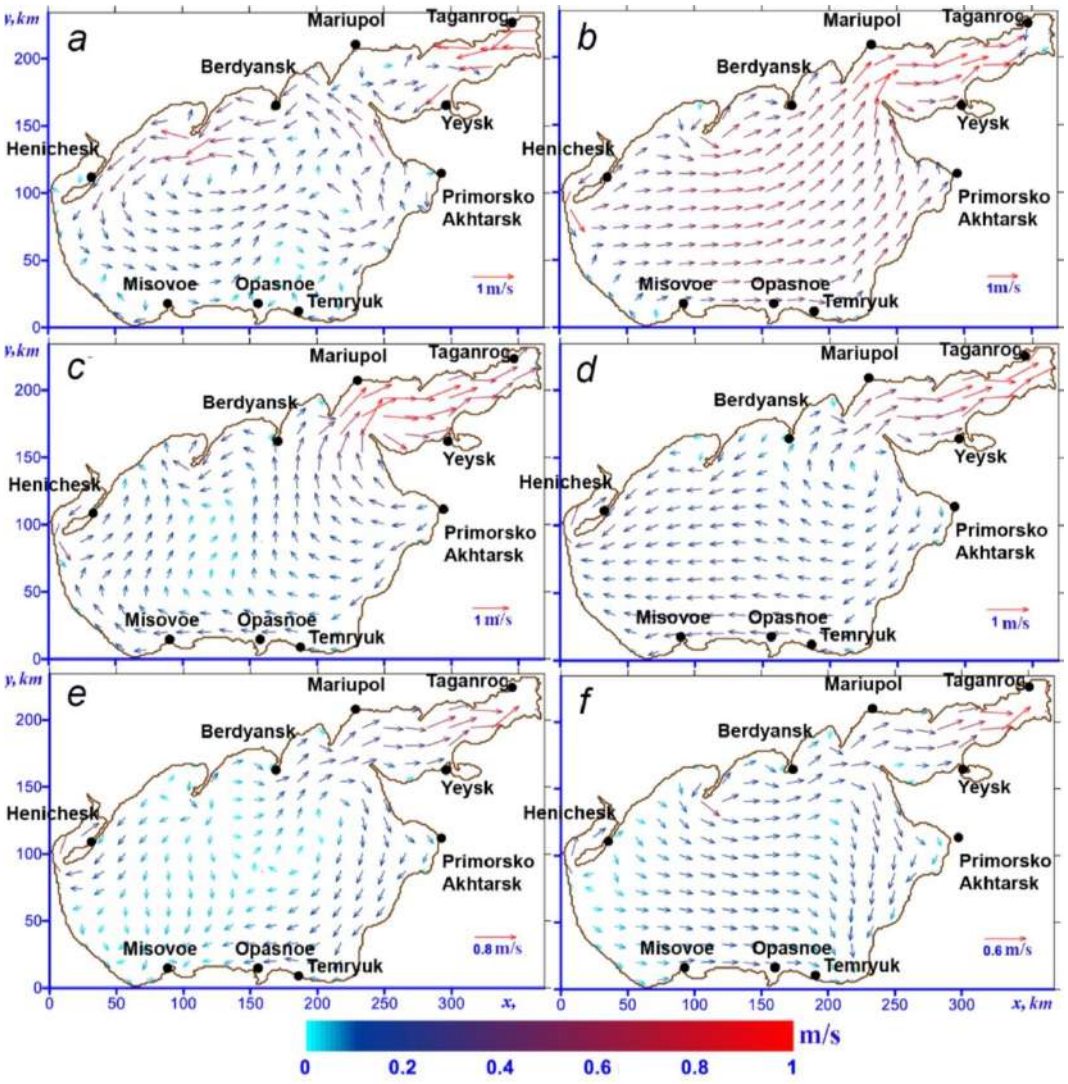

Figure 4.1.2 – Diagrams of the currents of the Sea of Azov at steady motion (*a*), at the moment of wind cessation (*b*), after 3 h (*c*), after 6 h (*d*), after 9 h (e), after 12 h (*f*) [Ivanov, Cherkesov, Shulga, 2015]

The determination of the periods and amplitudes of seiches in the open part of the Sea of Azov was carried out on the basis of the data given in Table 4.1.2. Here are data on the extremes of seiche-like level fluctuations in the deep part of the Sea of Azov that occur after wind attenuation, and their corresponding time points for nine points located in the central part of the Sea of Azov (Figure 4.1.3).

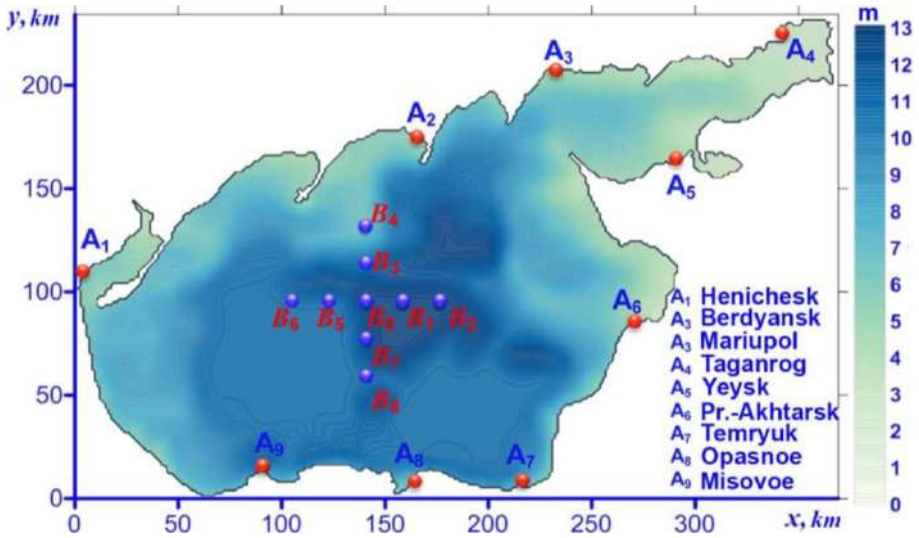

Figure 4.1.3 – The model of the considered computational domain, the position of stations $A_1 – A_9$ on the coast and $B_0 – B_8$ in the central part of the Sea of Azov

From the analysis of the presented data, it follows that the smallest deviation of the level in the steady–state mode of movement (0.04 m) takes place at the amphidromic point B_0 (46,25° N, 36,46° E) – the geometric center of the basin. At points located at a distance of 50 km from the center, the amplitudes of the level are much higher. Thus, the maximum deviations of the level in points B_5 and B_7 are –1.25 and 1 m, respectively, which is 31.3 and 25.3 times more than at the point B_0 ($t = t_{st}$).

As can be seen from the comparison of the highest values of overburden at Genichesk station (2 m, Table 4.1.1) and level rise at point B_7 (1.01 m, Table 4.1.2), overburden at Yeysk station (–2.44 m, Table 4.1.1) and level decrease at point B_5 (–1.25 m, Table 4.1.2), it was found that the change the level under the influence of steady wind in the coastal areas of the sea (stationary surges and overcurrentss) is twice as high as the maximum values of the level deviation in its open part

Analyzing the data given in Table 4.1.2, we note that the maximum sea level rise takes place in point B_7 (1.01 m). After the complete weakening of the wind action, a monotonous decrease in the level occurs to the lowest value ($\zeta_1 = – 0.14$ m; $t_1 = 5.7$ h). At the same time, the swing span is 1.15 m. After 7.6 h, there is an increase in the level ($\zeta_2 = 0.25$ m; $t_2 = 13.3$ h). The span of the second oscillation (0.39 m) is three times

smaller than the first one. An extreme decrease in the next oscillation of $\zeta_3 = -0.02$ m takes place after 7 h, its span of 0.27 m differs from the previous one by 0.12 m. The next extreme increase in the level ($\zeta_4 = 0.07$ m) occurs after 8.5 h with a span of 0.09 m, which is 12.7 times less than the first, it is noted after 28.8 h from the time $t = t_0$.

Table 4.1.2 – Extremes of seiches oscillations occurring after the cessation of wind action in the open part of the Sea of Azov

Coordinates of the points $B_0 - B_8$			ζ_{st}	ζ_1	t_1	ζ_2	t_2	ζ_3	t_3	ζ_4	t_4
	N	E									
B_0	46.25°	36.46°	4	33	7.7	2	14.7	8	20.6	2	29.6
B_1	46.77°	36.46°	–46	59	5.6	–3	15.3	18	22.1	0	30.5
B_2	47.29°	36.46°	5	–37	1.9	43	7.4	–3	17.4	10	23.9
B_3	46.25°	36.21°	48	2	4.3	16	8.8	2	19.4	2	22.3
B_4	46.25°	36.95°	10	53	2.8	1	13.7	15	18.5	0	28.6
B_5	45.20°	36.46°	–125	88	5.3	–10	16.3	30	21.5	–2	27.0
B_6	45.21°	36.46°	10	–52	1.9	45	7.4	–7	17.4	10	24.7
B_7	46.25°	34.97°	101	–14	5.7	25	13.3	–2	20.3	7	28.8
B_8	46.25°	34.97°	11	86	2.5	–8	13.3	22	18.3	–3	28.1

The greatest decrease in sea level among all the considered points occurs at point B_5 (– 1.25 m), after 5.3 h with a span of 2.13 m, the maximum of the first free oscillation is reached ($\zeta_1 = 0.88$ m). After 11 h, the greatest decrease in the level takes place ($\zeta_2 = -0.1$ m; t = 16.3 h) with a swing span (0.98 m) 2.2 times less than the first one. The next extreme of free oscillations is reached after 5.2 h ($\zeta_3 = 0.3$ m), the span of 0.4 m is 2.5 times less than the previous one. A decrease in the level of $\zeta_4 = -0.02$ m occurs after 5.5 h with a swing span of 0.32 m, which is 6.7 times less than the first, it occurs

after 27 h from the time $t = t_0$. The range of free fluctuations of sea level in the deep–water part is 1.2–2 times less than at coastal stations (k is the number of fluctuations):

k	1	2	3	4
$\Delta\zeta_k$, m				
point B_7	1.15	0.39	0.27	0.09
point B_5	2.13	0.98	0.40	0.32

Thus, the extreme values of the magnitude of seiches oscillations in the open part of the sea are comparable to the magnitude of free oscillations in coastal areas and amount to 50-89% of the value of the latter [Demyshev, Cherkesov, Shulga, 2017].

The time to reach the extremes of natural oscillations, given in Tables 4.1.1 and 4.1.2, allows us to compare the first two periods for the coastal and open parts of the sea. The period of the first free oscillation at stations located on the coast is 15–16 h (at Yeysk station – 21 h), the period of the second free oscillation is 13–19 h (at Mysovoye station – 22 h, at Yeysk station – 27 h). At the same time, in the central part of the Sea of Azov, the first seiches oscillation occurs in 13–16.5 h, the second – in 11–17 h. Consequently, with the exception of stations located on the coast with a complex coastline (Figure 4.1.3), the first periods of seiches fluctuations in the central and coastal parts of the sea differ by 2–3 h.

The peculiarities of the heights of the seiche-like oscillations in the central part of the sea are clearly manifested when compared with the heights of the seiche occurring in coastal areas. From the analysis of the data in Tables 4.1.1 and 4.1.2, it follows that the amplitude and magnitude of free oscillations in the points of the open part of the Sea of Azov (Table 4.1.2) are less than at coastal stations. At the same time, the highest values of level deviations in the coastal and central parts of the sea in the stationary mode differ by two times, and the extremes of seiches fluctuations by 1.2 – 2 times. The largest values of the first oscillation ranges for the run-off at art. Yeysk (2.38 m) is 1.2 times smaller than in point B_5 (2.13 m), for the landfills at Genichesk station (2.3 m) they are twice as large as in point B_7 (1.15 m). Thus, the extreme ranges of seiches oscillations

in the open part of the sea are comparable to the ranges of free oscillations in coastal areas and amount to 50 – 89% of the latter.

Table 4.1.3 shows the values of the velocity of surface stationary currents $|\mathbf{U}|_{st}$, cm/s caused by the action of a constant easterly wind at a speed of 20 m/s, as well as the velocity of currents of seiches vibrations $|\mathbf{U}|_k$, k = 1, ...,6 in the central part of the Sea of Azov. The corresponding time points (t_k, h) are also indicated here.

Table 4.1.3 – Maximum velocities of surface stationary currents ($|\mathbf{U}|_{st}$) caused by the action of a constant easterly wind at a speed of 20 m/s, and maximum velocities of currents ($|\mathbf{U}|_k$, k = 1,...,6) arising after the cessation of wind action in the central part of the Sea of Azov

Point	$\|\mathbf{U}\|_{st}$	$\|\mathbf{U}\|_1$	t_1	$\|\mathbf{U}\|_2$	t_2	$\|\mathbf{U}\|_3$	t_3	$\|\mathbf{U}\|_4$	t_4	$\|\mathbf{U}\|_5$	t_5	$\|U\|_6$	t_6
B_0	20.8	66.3	0.6	57.9	2.2	64.2	4.1	3.7	13.8	16.0	20.1	0.2	29.2
B_1	40.1	52.9	4.4	16.7	9.7	5.9	13.4	10.9	16.1	9.0	18.0	1.9	34.3
B_2	47.0	57.1	0.8	7.8	12.0	18.3	20.2	1.4	31.6	2.1	36.4	1.8	37.8
B_3	2.6	84.8	0.8	0.7	8.0	21.0	10.2	0.5	14.2	15.5	17.1	0.1	24.1
B_4	19.0	72.4	0.7	6.5	8.3	18.1	11.0	1.4	14.5	11.5	17.5	3.2	23.3
B_5	13.2	22.5	8.8	6.9	14.0	18.4	7.4	3.4	21.7	10.7	24.1	1.2	35.1
B_6	70.4	69.2	0.8	4.0	10.7	21.4	14.7	2.3	26.8	0.36	31.0	1.1	32.6
B_7	22.8	46.2	0.9	41.1	2.1	43.7	3.9	5.1	8.6	19.5	11.3	3.1	14.4
B_8	24.5	79.2	0.9	5.7	6.1	11.9	17.6	1.4	21.3	11.0	26.3	0.3	33.4

Note. The designations are in Table 4.1.3. Coordinates of pointsB_N (N = 0,…,8) in Table 4.1.2

Points B_0, B_3, B_4, B_7 and B_8 are located in the area of the nodal line of seiche-like oscillations (Figure 4.1.1, *b*), where vertical level fluctuations are close to zero. Let's look at some of them. From the analysis of the data presented in Table 4.1.3, it follows that in B_0, the first extreme velocity value ($|\mathbf{U}|_1$ = 66.3 cm/s) exceeds the stationary velocity

($|\mathbf{U}|_{st}$ = 20.8 cm/s) by 3.2 times. After 13.8 h, the value of the velocity $|\mathbf{U}|_4$ = 3.7 cm/s decreases significantly – 5.6 times compared to $|\mathbf{U}|_{st}$ and 18 times compared to $|\mathbf{U}|_1$. A further decrease in speed to 1 – 2 cm/s occurs after 29.2 h. A similar speed change takes place in point B_3. The velocity of the currents at the beginning of the seiches oscillations (84.8 cm/s) significantly exceeds the velocity at steady motion (2.6 cm/s), while the time during which the intensity of the currents decreases to 1 cm/s is 24.1 h.

At points B_1, B_2, B_5, B_6, located at a distance of 50 and 100 km in the zonal direction from the amphidromic point (B_0), the onset of free fluid movements does not lead to such a sharp change in stationary velocity. Let us consider the change in the velocity of seiches vibrations using the example of point B1, located 50 km east of point B_0. Here the steady-state currents velocity $|\mathbf{U}|_{st}$ = 40.1 cm/s differs little from the first extreme value of the velocity of seiches vibrations $|\mathbf{U}|_1$ = 52.9 cm/s (t_1 = 4.4 h), the excess is 1.3 times. The decrease in speed to 2 cm/s occurs here for 9 – 12 h longer (after 34.3 h) than in the area of the junction line. From the analysis of the values of the current velocity modulus, it follows that high current velocities prevail in the open sea, up to 84.8 cm/s (point B_3). At the same time, the direction of surface currents has a vortex character with a dominant meridional currents motion.

Numerical experiments using a hydrodynamic model have shown that the attenuation of free oscillations in the points of the central part of the sea occurs faster than in coastal areas (the maximum amplitude does not exceed 2 cm). The attenuation time of free liquid oscillations in the coastal area is 92.1 h, which is 23.7 h longer than in the central part of the sea (68.4 h). The periods of the first oscillation in the central and coastal parts of the Sea of Azov are also different. The largest period of seiches fluctuations in the coastal area (st. Yeysk and Taganrog) are 20.6 and 17.0 h, which is 4.1 and 0.8 h more than in the central part of the sea (points B_1 and B_5) – 16.5 and 16.2 h.

Based on the results of modeling free fluid fluctuations in the Sea of Azov that occur after the cessation of wind action, an analysis of the physical patterns of spatial distribution of deviations in the level and velocity of currents is performed. The maximum magnitude of the magnitude of the seiches oscillations in the coastal zone is comparable

to the magnitude of storm surges and surges, while the heights of free oscillations in the open part of the sea are 50 – 89% of the heights of oscillations in the coastal zone.

In the central part of the sea, the maximum velocity of currents (84.8 m/s) with seiches fluctuations is 21% higher than the velocity of stationary currents caused by gale force winds (70.4 m/s). Thus, seiches make a significant contribution to the variability of the currents velocity. Free fluctuations of the level (no more than 2 cm) fade faster (60 h) than the amplitudes of the currents velocities, which do not exceed 2 cm /s and can be traced in the time interval of 60 – 300 h.

The spectra of natural sea level fluctuations at coastal stations A_1 – A_9 and the amplitude-phase characteristics of seish at the frequencies of energy-carrying maxima were estimated using Fourier analysis and are shown in section 4.3 in Figures 4.3.1 – 4.3.2.

4.2. Analysis of the influence of the parameters of baric formations on free and forced fluctuations in the level and current in the Sea of Azov

Changes in atmospheric pressure are a common cause of seiches fluctuations in natural basins [Labzovsky, 1971]. A sharp change in pressure in various parts of the reservoir causes the entire mass of water in it to vibrate. Seiches with a significant amplitude occur during the phenomenon of resonance, when the period of natural oscillations of the basin coincides with the period of the driving force. At the same time, relatively small pressure drops at the ends of the reservoir and the corresponding small level differences cause significant seiches fluctuations. The baric front, moving over the water surface at a speed close to the speed of a free long wave, forms extreme surges and overcurrentss, which turn into large-amplitude seiches after the cessation of atmospheric disturbances. The Taganrog Bay, located in the northeastern part of the Sea of Azov, is an almost rectangular basin with a length of 137 km and a maximum width of 30 km. The single-node longitudinal seiche dominating the Taganrog Bay affects the formation of run-up fluctuations in the level, and this influence can be significant if the periods of natural and forced fluctuations coincide.

The behavior of waves in the field of atmospheric fronts has been studied relatively recently, and practical experience in predicting waves in these conditions is still insufficient [Sirotov, Sidelnikova, 1984; Bykov, Gordin, 2012; Nesterov, 2013]. Currently, the study of the dynamics of the waters of natural marine basins under the influence of mesoscale atmospheric processes is among the most interesting [Efimov, Anisimov, 2011]. The study of seiches vibrations in the Sea of Azov and the analysis of field observations were carried out in [German, 1971].

According to observations in the territories of marine areas that intersect or touch continents, during the transition seasons there are fairly rapid changes in meteorological values in latitude associated with meridional displacements of the trajectories of Atlantic cyclones as they move over Europe [Gulev, Kolinko, Lappo, 1994]. They are frontal zones that move at a speed of 30-35 km/h (8-10 m/s) and travel 600-800 km per day. The width of the frontal surface covering part of the water area of the Sea of Azov is several tens of kilometers. The wind and wave conditions in front of and behind the front differ significantly. In the zones of fronts, especially cold ones, there are significant gradients of air temperature, humidity and other meteorological factors that contribute to a sharp increase in wind to squall [Hydrometeorology ... , 1991].

Within the framework of a three-dimensional model (POM), the development of currents, run-up and seiche-like fluctuations in the Sea of Azov level in the field of exacerbation of the baric gradient in the area separating atmospheric vortices is studied. The hypothesis of the role of the resonant mechanism in the occurrence of extremely high amplitudes of overburden vibrations and seiches generated by a baric field moving over the sea has been tested. The baric formation moves at a velocity equal to the velocity of a free long wave [Labzovsky, 1971], and the period of pressure variability in the front is equal to the period of natural oscillations of the liquid in the basin. In the course of computational experiments, several scenarios of the passage of seasonal atmospheric fronts over the Sea of Azov were reproduced, corresponding to modern data on hydrometeorological conditions in the Azov-Black Sea region, set out in [Hydrometeorological ..., 1962; Hydrometeorological ..., 2009] and shown in Figure 4.2.1.

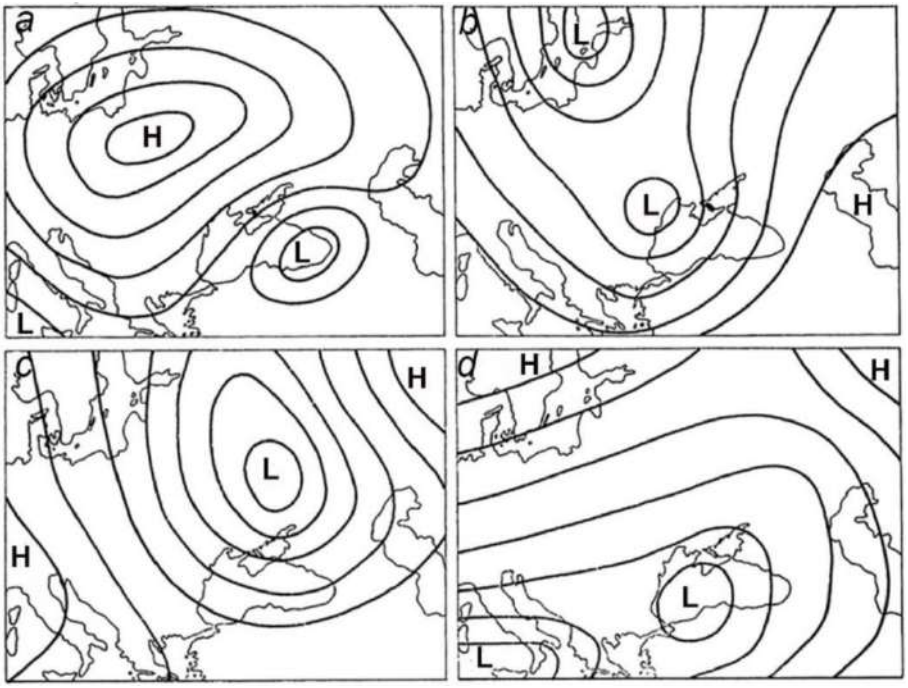

Figure 4.2.1 – Types of baric synoptic processes for the Azov Sea region: anticyclone over the central regions of the European part of Russia (*a*), anticyclone over Asia Minor and Kazakhstan (*b*), anticyclone with a spur over the Balkan Peninsula (*c*), Mediterranean cyclones (*d*) [Ivanov, Shulga, Numerical analysis..., 2018]

The study of the hypothesis of the occurrence of extreme seiches with changes in atmospheric pressure in different parts of the sea is based on the analysis of the results of two series of numerical experiments. The experimental conditions differed in the resonant mechanisms of formation of extreme amplitudes of overburden vibrations and seish of the Sea of Azov. In the first series of experiments, the characteristic of the baric front is the period of action of an inhomogeneous atmospheric pressure field, a multiple of the period of natural oscillations of the basin, in the second series of experiments – a velocity close to the velocity of a free long wave [Cherkesov, Shulga, 2016].

In each experiment, the development of the front occurs in the field of background stationary currentss, and the beginning of its movement corresponds to the time of establishment of fluid motion (t_{st} = 48 h). The steady-state movements in the Sea of Azov are generated by the action of a homogeneous time and space southwesterly wind $\mathbf{W}_{st}$ (2.1.1.1) with a speed of 10 m/s. At this stage ($0 \le t \le t_{st}$), atmospheric pressure

is constant throughout the entire sea area, its value is equal to normal atmospheric pressure at latitude 45 ° and temperature 0° ($P_{атм}$ = 1013.25 gPa).

At the next stage, an inhomogeneous atmospheric field with a sharp pressure drop at the border moves over the water area of the Sea of Azov. The time of its movement ($t = t_f$) over the water area is set equal to half of the period of the highest mode of free oscillations capable of causing the greatest rise in the Sea of Azov level. In addition, t_f is the time interval during which the front passes the distance between the extreme points of the Sea of Azov. Its value is determined based on observational data and the results of analytical calculations. So, in the works [Hydrometeorological ... , 1962; Hydrometeorological conditions ... , 1986] recorded seiches with periods of 6 – 7 and 23 h (T_{observ}). The theoretical values of the periods (T_{Merian}) are obtained using the Merian formula, taking into account the Rayleigh correction [German, 1971]:

$$T_{\text{Мериан}} = \frac{2L}{\sqrt{g\breve{h}}}(1+\varepsilon), \text{ где } \varepsilon = \frac{b}{\pi l}\left(\frac{3}{2} - \ln\frac{\pi b}{l} - C_\varepsilon\right). \qquad (4.2.1)$$

Here C_ε = 0,5772 – Euler's constant; L = 360 km – the length of the sea (along the Genichesk line – Pereboiny); $\breve{h}$ = 10 m – average sea depth; b = 30,6 km – the width of the strait at the entrance to the Taganrog Bay; l = 137 km – the length of the Taganrog Bay. The period of the first mode, calculated by the formula (4.2.1), is equal to T_{Merian} = 24,1 h. Based on a comparison of the values of T_{observ} and T_{Merian}, we believe that the dominant longitudinal natural fluctuations of the first mode of the Sea of Azov level have a period of ~ 24 h. The spatial structure of this mode is such that one of its peaks is located in the Taganrog Bay, and the opposite one is near Genichesk, which necessitates the study of extreme characteristics of overburden phenomena and amplitudes of seiches vibrations.

The regions of constant and variable atmospheric pressure (Θ and Θ') are spaced on both sides of the front line γ, the position of which depends on the current coordinates ($\mathbf{r} = \{x, y\}$) and time (t). The boundary of the front in the form of a spatial curve γ is set using parametric expressions γ*:* $x = x(t)$, $y = y(t)$. The type of parametric equations

determines the configuration of the front lines: straight lines with a certain angle of inclination, curves with a given radius of curvature. The speed and time of movement of disturbing baric fields in the water area of the Sea of Azov is determined by the velocity ($\mathbf{U}_\gamma$) and the time of movement of the front boundary (t_f). For these numerical experiments, these values are set in different ways.

The possible trajectories of the movement of $\gamma(\mathbf{r}, t)$ inhomogeneous baric fields over the Sea of Azov for numerical experiments [Cherkesov, Shulga, 2016] are shown in Figure 4.2.2. The isolines of the baric levels correspond to the time t = 9 h, counted from the beginning of the movement of low-pressure fields. Figure 4.2.2, *a*, *b* shows examples of the propagation of these regions at a speed of $|\mathbf{U}|_\gamma$ = 8 m/s in the direction of the current zonal wind along the Genichesk line – Pereboiny. They differ in the geometry of the dividing lines (γ): in Figure 4.2.2, a is a straight line with an angle of inclination of 135° to the x axis; In Figure 4.2.2, *b* is a curve with a given radius of curvature of 250 km. Detailed maps of these baric fields are presented in [Numerical analysis of the influence ..., 2017]. The movement of the interface of the pressure regions along a diagonal trajectory is shown in Figures 4.2.2, *a* and *d*.

For the first series of numerical experiments, the period of action of atmospheric disturbances ($t = t_f$) is chosen as a multiple of the period of the highest mode of free oscillations of the Sea of Azov ($t = T$). In this case, the modulus of the velocity of the front boundary is obtained based on the formula: $|\mathbf{U}|_\gamma = 2L/T$. For the second series, we set the velocity of movement of the boundary of the atmospheric pressure region equal to the velocity of a free long wave depending on the depth of the sea: $|\mathbf{U}|_\gamma(h) = \sqrt{gh}$ ($\check{h} \le y \le h_{max}$). In this case, the duration of atmospheric disturbances at different speeds of their movement is different and is also determined from the well−known ratio $t_f = L/|\mathbf{U}_\gamma(h)|$. These functions are described in more detail in [Numerical Analysis ..., 2016].

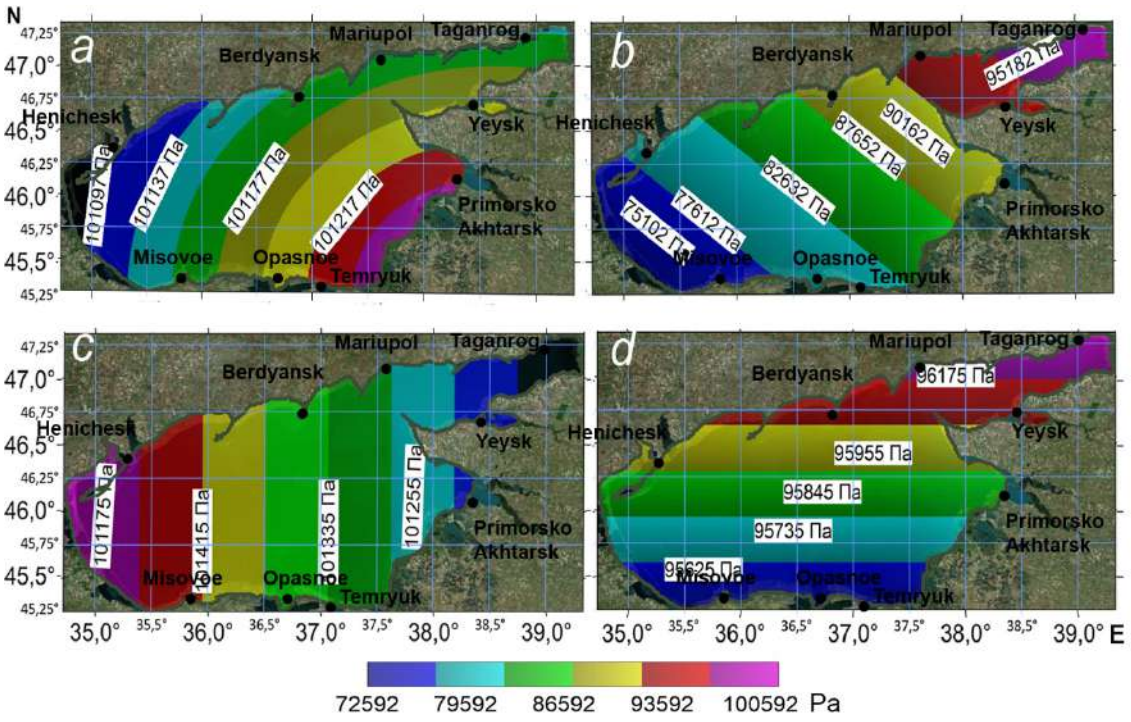

Figure 4.2.2 – Movement of an area of variable atmospheric pressure at a speed of 8 m/s in the direction of Genichesk – Pereboiny with different geometry of its boundaries: straight lines at an angle of 135° and 90° to the *x* axis (*a*) and (*c*); curves with specified radii of curvature (*b*) and (*d*)

In the first experiment, conclusions about the possibility of a relationship between the velocity and time of movement of the baric field with maximum wave amplitudes were made for the case when the period of the driving force approaches the period of natural oscillations of the basin. The movement of the interface of the pressure regions is performed along one of the specified trajectories: meridional (Figure 7.2.2, *a*), zonal (Figure 7.2.2, *b*, *d*), diagonal (Figure 7.2.2, *c*). The values of the baric gradient, the width of the frontal zone, as well as their values in the areas of high and low pressures in numerical experiments are accepted based on the analysis of generalized reference hydrometeorological data [Hydrometeorology ... , 1991].

The results of calculations of extreme sea level deviations obtained at constant pressure, as well as during the passage of an inhomogeneous baric front and the action of the same stationary westerly wind with a speed of 10 m/s, are shown in Table 4.2.1. Here are the maximum and minimum values of level deviations at the coastal stations of the Sea of Azov at the time of wind termination (ζ_{st}, ζ_{extr}) and the first successive extremes

of the amplitudes of the seiches oscillations ($\zeta_{1,2}$) with their corresponding time points ($t_{1,2}$). The left part of the table shows the simulation results at constant pressure (P_{atm}), in the right part − when passing through the entire water area of the variable pressure area $P_a(x, y, t)$ at a speed of 8 m/s.

From the analysis of the data given in the left part of Table 4.2.1, it follows that the current wind causes maximum stationary surges at Genichesk station (202 cm), surges at Yeysk station (244 cm), Primorsko−Akhtarsk (175 cm) and Taganrog (158 cm). In comparison with the extremes of the amplitude of the level deviations caused by the passage of the baric field, it can be seen that the greatest differences at these stations are 14%.

The analysis of the amplitudes of seiches vibrations is performed at stations where the greatest overburden phenomena occur based on the data given in Table 4.2.1. At the station Yeysk, where the greatest overburden occurs (− 2.44 m; $t = t_0$), the cessation of wind action causes an increase in the level (ζ_1 = – 0.06 m; t = 18.3 h). At the same time, the span of the first oscillation is 2.38 m. In the future, the level continues to rise and after 10.2 h reaches the highest value of 0.21 m, the scope of the second oscillation (0.27 m) is 8.8 times less than the first.

The passage of the baric front leads to changes in the values of the ranges and periods of free oscillations, which differ significantly at this station (Eisk). Thus, at the moment of termination of the disturbances, a decrease in the level by 2.62 m forms subsequent free oscillations with ranges of 2.55 and 0.32 m. It should be noted that the magnitude of the stationary acceleration at this station is 7% less than the non-stationary one, the differences in the magnitude of the seiches oscillations do not exceed 16%, and their periods by 0.5 h. Since in both cases the same wind was the basis for generating waves and currents, this difference is obviously due to the passage of a baric front with a pressure drop of 100 gPa.

Figure 4.2.3 shows the fields of currents in the surface layer of the Sea of Azov at regular intervals (3 h) from the moment of cessation of all external influences.

Table 4.2.1 – Stationary overcurrentss and surges (ζ_{st}, cm), extremes of amplitudes of forced (ζ_{extr}, cm) and the first two seiches oscillations ($\zeta_{1,2}$, cm) with corresponding time points ($t_{1,2}$, h) at constant atmospheric pressure and after passing the baric front at a speed of 8 m/s

Stations	$P = P_{atm}$					$P = P_a(\mathbf{r}, t)$				
	ζ_{st}	ζ_1	t_1	ζ_2	T_2	ζ_{extr}	ζ_1	t_1	ζ_2	T_2
Henichesk	202	–27	9.5	33	16.5	215	−28	10.0	39	16.8
Berdyansk	25	–57	2.5	46	7.7	25	−60	2.8	48	7.7
Mariupol	–153	–1	12.3	–20	20.2	−182	−1	12.5	−21	20.6
Taganrog	–158	–89	24.3	30	31.5	−164	−97	24.4	35	31.5
Yeysk	–244	–6	18.3	21	28.5	−262	−7	18.7	25	28.9
Primorsko-Akhtarsk	–175	92	5.3	–10	13.9	−188	95	5.5	−10	13.9
Temryuk	–18	103	2.7	–14	13.5	−18	107	3.1	−14	13.6
Opasnoe	32	93	1.7	–8	13.0	37	93	2.2	−9	13.1
Mysovoe	98	–20	8.7	26	15.4	106	−22	8.7	30	15.6

Figure 4.2.3 shows that the position of the maximum current velocities is shifted towards the Taganrog Bay. The positions of the zero values of the current velocity are widely scattered throughout the water area. At the same time, the boundaries of the baric disturbances over the water area correspond to the same direction of movement of the currents opposite in the direction.

An evidence-based assessment of the hypothesis put forward about the formation of high surges, which then cause large-amplitude seiches, will be carried out based on the analysis of the results of the second series of numerical experiments in which the baric front moves over the water surface at a speed close to the speed of a free long wave. The movement of atmospheric pressure fields over the water area is calculated on the

basis of a known dispersion relation and is a function depending on the depth of the natural basin ($|\mathbf{U}|_\gamma(h) = \sqrt{gh}$).

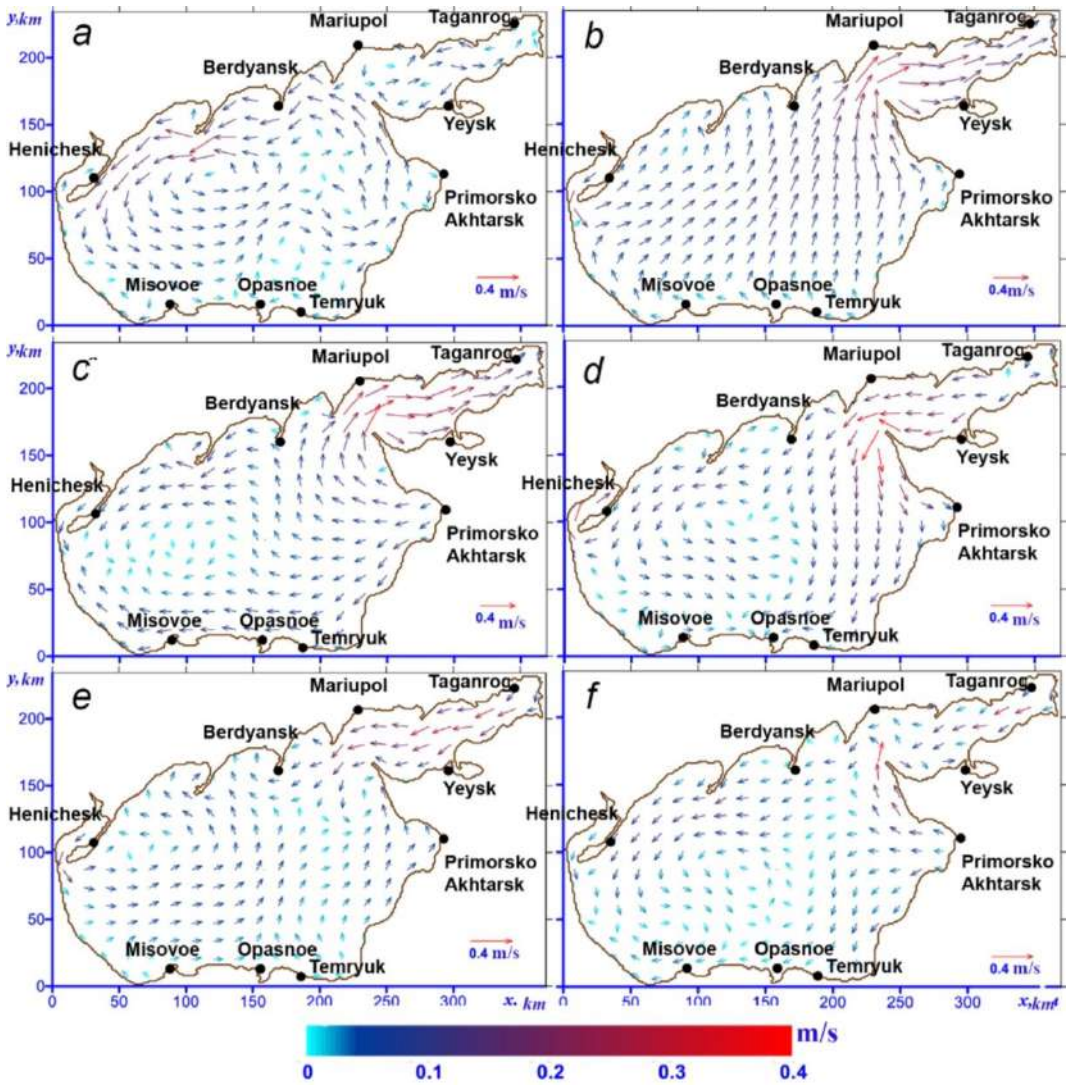

Figure 4.2.3 – Fields of currents of the Sea of Azov at steady motion caused by an easterly wind at a speed of 10 m/s (a), at the moment of cessation of atmospheric influences (*b*) and after 3 h (*c*), 6 h (*d*), 9 h (*e*), 12 h (*e*) [Ivanov, Shulga, Numerical analysis..., 2018]

Table 4.2.2 shows the dependence of the maximum amplitudes of fluctuations in the Sea of Azov level on the velocity of movement of the boundary of the baric disturbance in the meridional direction in the field of a constant westerly wind with a speed of 10 m/s. The speed of the free long wave varies depending on the selected values of the sea depth (7 − 14 m).

Table 4.2.2 – Dependence of extreme wave characteristics on the velocity of movement of baric atmospheric fields $|\mathbf{U}|_\gamma(h)$ over the Sea of Azov [Ivanov, Shulga, 2019]

$\|\mathbf{U}\|_\gamma(h)$, m/s	ζ_{max}, m	ζ_{min}, m	$\|\mathbf{U}\|_{max}$, m/s
8.3	0.56	0.40	0.26
8.9	0.66	0.46	0.27
9.4	0.74	0.52	0.3
9.9	0.70	0.50	0.28
10.4	0.68	0.48	0.24
10.9	0.64	0.41	0.23
11.3	0.58	0.40	0.22
11.7	0.58	0.40	0.21

A comparison of these results presented in Table 4.2.2 with the results of calculations performed at a constant atmospheric pressure is given in more detail in [Ivanov, Cherkesov, Shulga, 2015] confirm the hypothesis about the influence of moving baric formations on fluctuations in the level and velocity of the currents of the Sea of Azov. Increases in the amplitude of the level fluctuations and the maximum currents velocity (ζ_{max} = 0.56 m; ζ_{min} = 0.4 m; $|\mathbf{U}|_{max}$ = 26.2 cm/s), compared with the case of a constant pressure value (1013.0 gPa), reach 20, 23 and 14%.

From the analysis of the data presented in Table 4.2.2, it follows that the speed of movement of baric disturbances affects the maximum speed of currents and sea level deviations. The highest values of these values are achieved at the front velocity $|\mathbf{U}|_\gamma$ = 9.4 m/s, corresponding to the sea depth H = 9 m. The passage time of this baric formation from the extreme western to the extreme eastern border of the Sea of Azov is 10 h and 40 minutes. Note that a front moving longer, for example, at a speed of 8.3 m/s (12.8 h), has less effect on the parameters of wave movements. According to the results of the experiment, we investigate the change in the level of the free surface at the moment of establishing the movement of the liquid, the passage of atmospheric disturbance of the

entire sea area and at regular intervals (3 h) from the moment of cessation of all external influences.

Figure 4.2.4 shows the results of a numerical experiment − the passage of a baric disturbance over the Sea of Azov from west to east in the field of a constant wind blowing at a speed of 10 m/s in the same direction. At the same time, the movement of the interface of air masses with a drop in atmospheric pressure occurs at a free wavelength velocity of 8.29 m/s, corresponding to an average sea depth of 7 m. The passage time of the atmospheric disturbance is chosen to be equal to half of the free oscillation period ($t_f = T/2 = 12$ ч).

In steady motion (see Figure 4.2.4, *a*), the dynamics of the water is determined by the nodal line passing through the center of the basin and the maximum amplitude values in the western and eastern parts of the basin. With the development of the free oscillation process, the generation of vortex disturbances increases, the nodal line asymmetrically rotates counterclockwise, located along the x axis (Figure 4.2.4, *b*) and diagonally to it (see Figure 7.2.4, *c*) 3 h after the cessation of wind action (Figure 4.2.4, *c*), free oscillations represent a two-node seiche with a central nodal line repeating its configuration in the initial time period $t = t_{st}$ (Figure 4.2.4, *a*). The two shorter nodal lines are symmetrical and represent semicircles whose diameters are perpendicular to the direction of the atmospheric front.

The lowest intensity of free level fluctuations is observed in the central region of the basin. 6 h after the cessation of wind action (Figure 4.2.4, *d*), the two-node sei system moves in an easterly direction, with the greatest level deviations taking place in opposite corners of the basin. Further development of the free oscillation process (Figure 4.2.4, *e*, *f*) leads to the fact that small nodal lines are combined into one line running diagonally across the basin and dividing it into areas of increasing and decreasing levels [Ivanov, Shulga, 2019]. At the same time, it was found that disturbances moving at a speed close to the speed of a free long wave cause the generation of waves with amplitudes greater than with the same wind and constant atmospheric pressure [Demyshev, Cherkesov, Shulga, 2017].

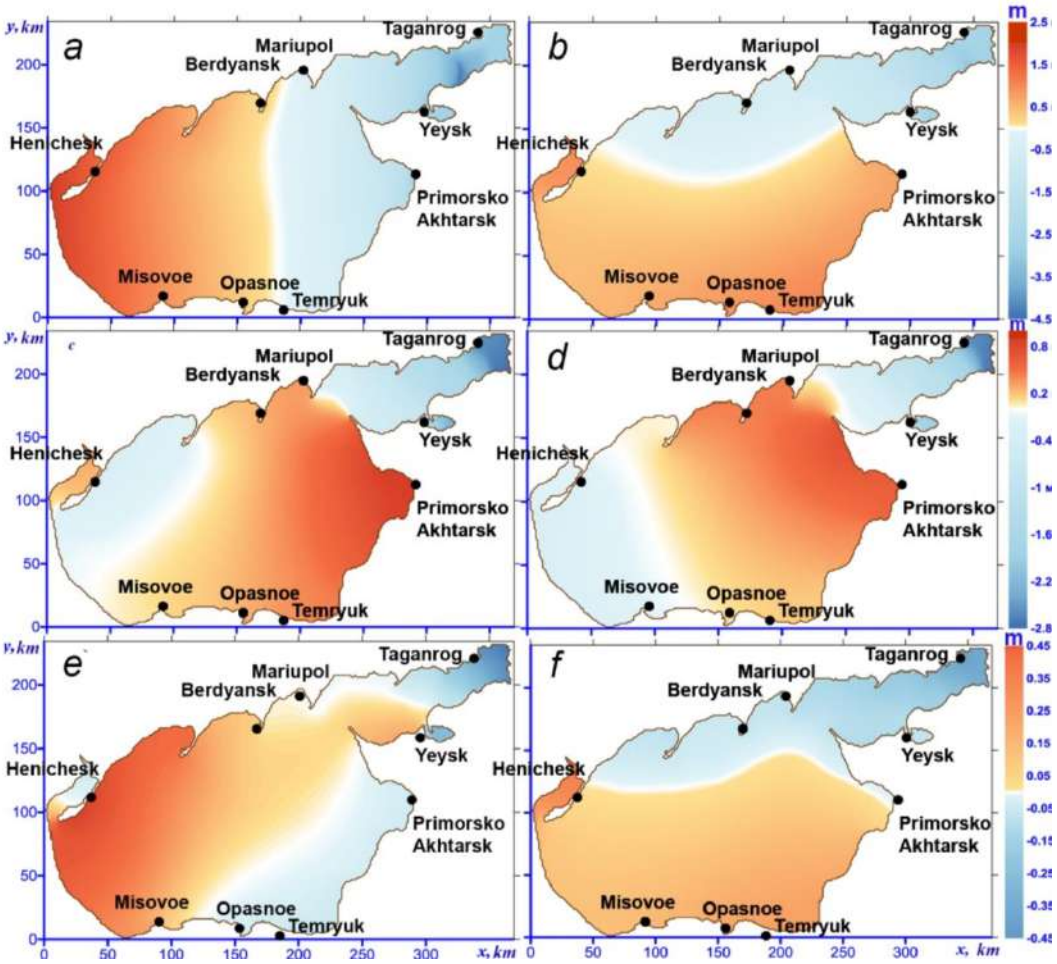

Figure 4.2.4 – Changes in the level (m): with steady motion caused by an easterly wind at a speed of 10 m/s (*a*), at the moment of cessation of atmospheric effects (*b*) and after 3 h (*c*), 6 h (*d*), 9 h (*e*), 12 h (*f*)

4.3. Spectral analysis of free and forced fluctuations of the Sea of Azov level

Spectral analysis allows us to examine in detail the structure of vibrations, find out the nature of individual peaks in the spectrum of level fluctuations and understand which frequencies account for the largest amount of wave energy. To calculate the spectra using the MatLab R2013b application, the Welch method based on the fast Fourier transform was applied. The spectra were calculated for the model series obtained by running the POM model under different input meteorological conditions. The first meteorological scenario reproduces the conditions for the occurrence of seiche-like fluctuations of liquid

in the sea caused by the cessation of long-term wind [Ivanov, Cherkesov, Shulga, 2015]. The second one reproduces meteorological conditions that cause seiches fluctuations in the sea associated with the passage of a baric front over the waters of the Sea of Azov with resonant parameters (front velocity of 10 m/s) [Demyshev, Cherkesov, Shulga, 2017].

Figure 4.3.1 shows the spectra of sea level fluctuations at nine stations located in various areas of the Sea of Azov: Taganrog – at the top of the Taganrog Bay, Primorsko-Akhtarsk, Yeysk – on the east coast, Genichesk – on the west coast, Berdyansk, Mariupol – on the north coast, Temryuk, Dangerous – on the south coast, Mysovoye – in the Kerch Strait (stations on the map, shown in Figure 3.1.1).

The dominant longitudinal fluctuations of the liquid in the Sea of Azov of the lower modes are such that their peaks fall on areas located near large settlements [German, 1971; Modern ..., 2015]. As follows from Figure 4.3.1, fluctuations with a period of ~27.3 h can be traced in all points of the coast and are a longitudinal single-node seiche. The nodal lines run along the Primorsko-Akhtarsk – Berdyansk, Genichesk-Yeysk, Genichesk – Primorsko-Akhtarsk lines, which is confirmed by the absence of spectral density peaks for the 24 h component at Berdyansk, Yeysk and Primorsko-Akhtarsk stations. Waves with periods of 11.4 – 15.2 h in the form of small peaks in Mariupol, Berdyansk, Dangerous and Taganrog are transverse single–node seiches (Mariupol – Yeysk). Fluctuations with periods of 6.8 – 8 h are observed in all points except Genichesk, which is explained by the presence of a nodal line of these fluctuations. Also, in all points, there are overtonal fluctuations with periods of 2.8–4 h, and periods of 1.2–2 h.

The periods of oscillations that occur after the passage of a front with resonant parameters are longer than in the case of constant atmospheric pressure. Spectral density values are higher at most stations, especially at high frequencies.

The amplitude-phase characteristics of free oscillations at the frequencies of energy-carrying maxima were estimated using Fourier analysis for simulated time series of sea surface level deviations (Figure 4.3.2). They were found using the standard fast Fourier transform procedure implemented in the MatLab R2013b application.

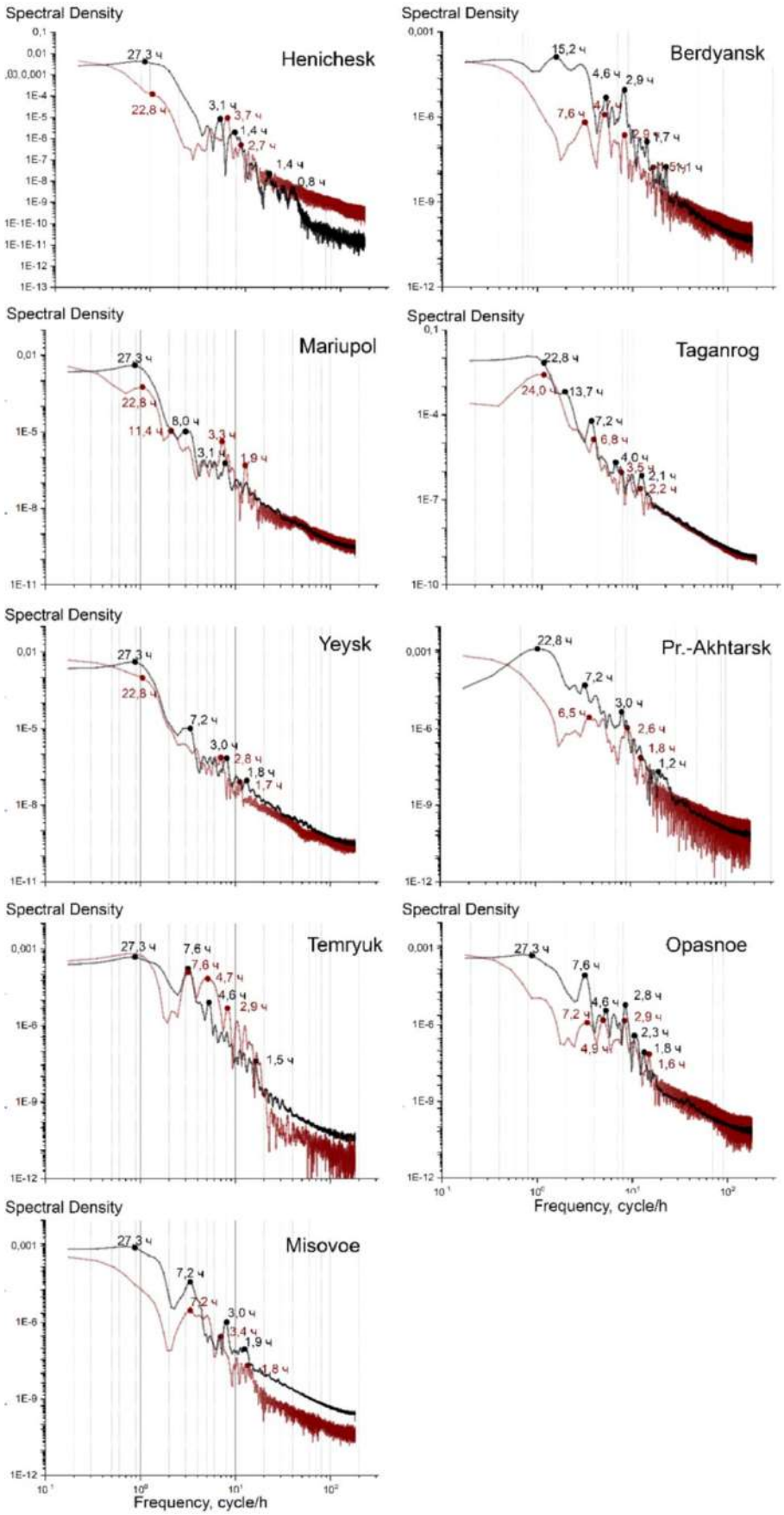

Figure 4.3.1 – Spectra of fluctuations in the Sea of Azov level at stations A_1 – A_9. Black shows the spectra of seiches vibrations that occur after the cessation of wind action, red – after the passage of the baric front

The results presented in Fig. 4.3.2 indicate that at the selected energy-carrying frequencies, due to the significant influence of the Earth's rotation, nodal lines in standing waves contract into nodal points, and free level fluctuations are modified into mixed (progressively standing) waves [Krylov, 1946; Timonov, 1959; Nekrasov, 1975; Zakharchuk, Sukhachev, Tikhonova, 2020], with pronounced amphidromic systems and antinodes.

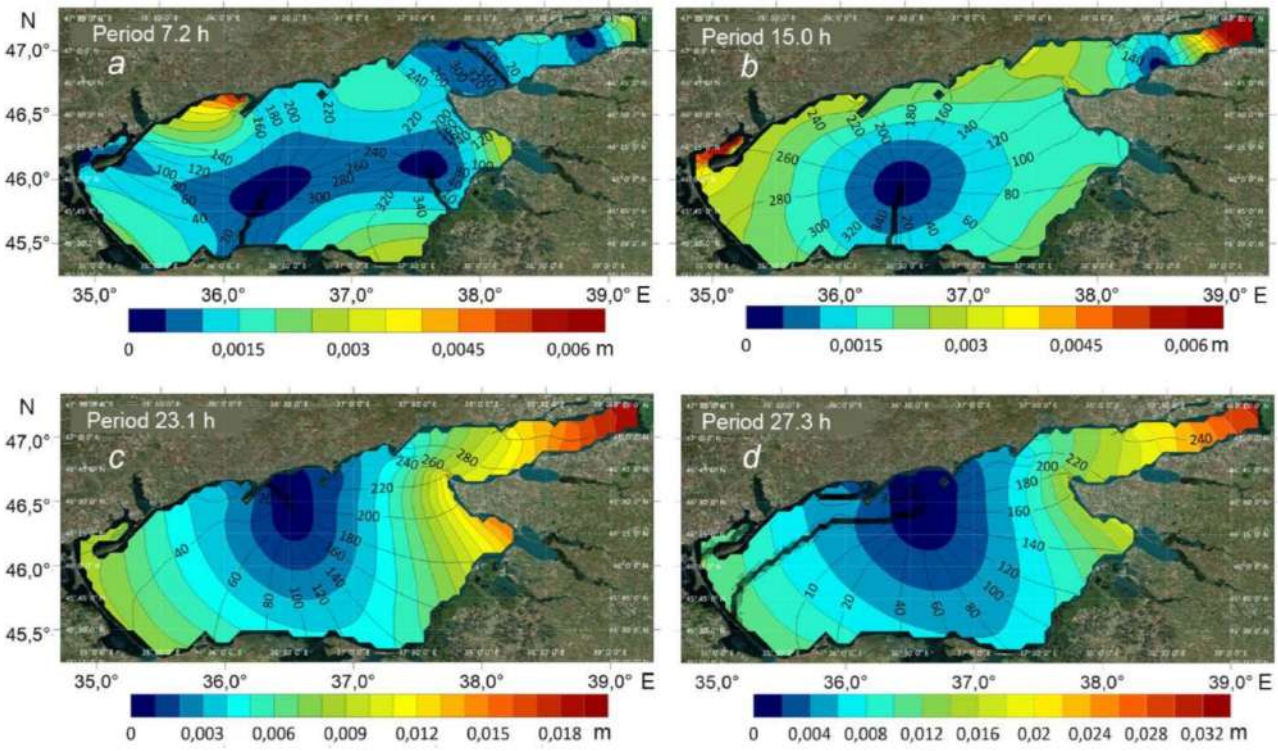

Figure 4.3.2 – Maps of amplitudes (m) and phases in degrees (isolines) of free level fluctuations with periods of 7.2 h (*a*), 15.0 h (*b*), 23.7 (*c*) and 27.3 h (*d*) in the Sea of Azov

Natural level fluctuations with periods of 27.3 and 23.1 h have one amphidromic system, the centers of which are shifted to the northern coast relative to the central part of the Sea of Azov. The main antinodes of these oscillations are located in the east of the Taganrog Bay and in the Yasensky Bay, and the less pronounced ones are in the west of the sea. The rotation of the level maxima around the amphidromic center occurs counterclockwise, as in Kelvin waves in the Northern Hemisphere (Figure 4.3.2, *a*, *b*). These results differ significantly from the study of seiches oscillations performed

by Matishov and Ingebeikin [Matishov, Ingebeikin, 2009]. According to their work, for oscillations of 23.7 h, the only developed amphidromic system is located near the southeastern coast of the sea, and 2 antinodes are located in the south of the sea and at the top of the Taganrog Bay [Matishov, Ingebeikin, 2009]. Such discrepancies with our results may be due to the fact that [Matishov, Ingebeikin, 2009] used a more primitive model based on the numerical integration of a system of linearized equations of shallow water theory.

Natural oscillations with a period of 15 h have 2 amphidromic systems, one of which is basic, and the second is degenerate (Fig. 4.3.2, *c*). The main one is located almost in the center of the Sea of Azov, and the center of degenerate amphidromia is confined to the southern shore of the central part of the Taganrog Bay. The main antinodes are located in opposite parts of the sea: one in the east of the Taganrog Bay, and the second in the west of the sea in the Utlyuk estuary. The rotation of the antinodes around the amphidromic center is carried out counterclockwise (Fig. 4.3.2, *c*).

The next mode of natural oscillations with a period of 7.2 h has two connected amphidromic systems in the open part of the Sea of Azov (Figure 4.3.2, *d*). The eastern one has a cyclonic rotation, and the western one has an anticyclonic rotation. The largest amplitude of the 7-hour oscillations is located in the Obitochny Bay, and the smaller ones are at the Arabatskaya Strelka spit, in the Temryuksky, Yasensky and Taganrog Bays (Figure 4.3.2, *d*).

4.4. Conclusions to Chapter 4

The analysis of the simulation results of free fluctuations in the Sea of Azov level, which occur after the cessation of the action of steady wind, allowed us to establish physical patterns of spatial distribution of fluctuations in the level and currents and changes in the velocity of currents. As follows from the analysis of the data presented in Table 4.1.2, the maximum values of the free and forced oscillations in the coastal zone are comparable, while the amplitudes of free oscillations in the open part of the sea are 50 – 89% of their values in its coastal zone.

In the central part of the sea, the maximum velocity of currents (84.8 cm/s) with seiches fluctuations is 21% higher than the velocity of stationary currents caused by gale force winds (70.4 cm/s). Thus, the seiches vibrations significantly affect the change in the velocity of the currents.

It has been found that disturbances moving at a speed close to the speed of a free long wave cause the generation of level fluctuations with larger amplitudes than with the same wind and constant atmospheric pressure. Their highest values are achieved at the rate of movement of the boundary of the baric disturbances of 9.4 m/s, corresponding to a sea depth of 9 m.

Moving baric fields for a time equal to the half-period of the natural oscillations of the basin cause forced and then free oscillations with amplitudes differing by no more than 14% from those obtained at a constant atmospheric pressure and the same wind.

Atmospheric pressure disturbance plays an important, but not decisive role in the formation of the structure of currents and fluctuations in the Sea of Azov level. It is shown that opposite currents, depending only on the direction of the acting wind, can correspond to the same direction of movement of the boundary of baric disturbances over the sea area. An important role in the formation of currents and levels belongs to the processes caused by a long-term constant wind.

Chapter 5.
REPRODUCTION OF THE CIRCULATION OF THE WATERS OF THE SEA OF AZOV CAUSED BY VORTEX ATMOSPHERIC MOVEMENTS

One of the manifestations of global climate change in recent years is the increase in the number of dangerous natural hydrometeorological phenomena in the coastal zones of the oceans and seas. According to the data given in [Matishov, Matishov, 2013], from 1970 to the present, the number of intense hurricanes of the 4^{th} and 5^{th} categories has almost doubled. The consequences of dangerous and natural phenomena in the Sea of Azov are often catastrophic. Storms here are often accompanied by numerous tragedies – the death of ships, the destruction of coastal infrastructure. In some cases (1739, 1831, 1843, 1877, 1914, 1969 storm surges in the eastern part of the Sea of Azov led to numerous casualties among the population in the coastal areas of the Temryuk Bay [Dotsenko, Ivanov, 2010; Shnyukov, Mitin, Tsemko, 1994; Mikhailov, Magritsky, Ivanov, 2010]. The development of seasonal fluctuations in the Sea of Azov level is facilitated by the physical and geographical conditions of this basin: a fairly large sea area (39 thousand km2) with an insignificant average depth (~ 7 m), as well as significant storm activity - the average number of days with a storm wind at a speed of 15 m/s or more is 24-34 days per year [Shnyukov, Mitin, Tsemko, 1994; Atlas of the waves ... , 2012; Hydrometeorological ..., 1986]. A study of the repeatability of overburden and overburden in the areas of the Sea of Azov revealed that the east coast of the sea and the Taganrog Bay are most often subject to catastrophic overburden (48% of all cases) and overburden (60%), the amplitudes of overburden fluctuations in these areas reach 2.0-3.5 m. In Taganrog, where the runoff of the Don River has a significant impact, the amplitude of run-up oscillations is maximum and amounts to 6.87 m [Atlas of the waves ..., 2012; Numerical studies ..., 2017]. Forecasting the impact of the characteristic extreme Azov Sea phenomena ("Chernomorka", or "reverse bottom"), which cause floods in coastal areas and the Taganrog Bay, as well as causing the greatest values of run-up fluctuations in the level of the Sea of Azov, determines the necessary condition for the safe operation of marine facilities, including marine transport. Therefore, it is

of scientific and practical interest to study the influence of atmospheric vortex anomalies such as cyclones and anticyclones on the circulation of waters in this basin.

As follows from the analysis of meteorological information [Belov, 1978; Hydrometeorological ..., 1986; Climatic Atlas of the Sea of Azov, 2006], there is a frequent change of winds in various directions over the Sea of Azov for short periods of time. Therefore, in this chapter, the simulation of water circulation and the spread of impurities is carried out on the condition that cyclonic atmospheric disturbances may have directions and speeds of movement that do not coincide with the direction and speed of the constant wind, bringing the currents to a steady state. It is assumed that as it moves, the center of the cyclone crosses the Sea of Azov along a given trajectory and passes through its central part [Investigation ... , 2009].

5.1. Assessment of the influence of moving atmospheric disturbances on dynamic processes in the presence of background stationary currents

The determination of the influence of geometric and evolutionary parameters of atmospheric vortex formations (base radius, direction and velocity of movement of cyclones or anticyclones) on currents arising in the Sea of Azov is based on the analysis of modeling results using an idealized model of these phenomena (2.1.1.3) – (2.1.1.5). In a series of numerical experiments, the influence of various directions of movement of atmospheric vortex formations on the deviations of the level and velocity of currents in the Sea of Azov caused by them is investigated. Based on the analysis of data from long-term observations [Hydrometeorological ..., 1962; Patterns ..., 2006; Climatic Atlas of the Sea of Azov, 2006], we believe that an atmospheric formation with a pressure drop between the center and the periphery of 15 gPa, with a base radius of 100 km, moves at a speed of 5 m/s. Numerical experiments reproduce the cases of its movement to the southwest (SW), west (W) and northwest (NW). The indicated directions are 135º, 180º and 225º angles with the x-axis, respectively [Investigation ..., 2009]. The action of vortex atmospheric formations develops in the field of background stationary currents in the sea. Based on the analysis of the simulation results described in paragraph 2.1

and the results given below, it is known that this time is longer the higher the speed of the current wind. In this regard, in all numerical experiments, the beginning of the motion of the vortex atmospheric formation is assumed to be equal to the highest value of the time of formation of steady-state movements in the Sea of Azov (t_{st} = 48 h).

Figure 5.1.1 shows the driving wind fields at a height of 10 m above the Sea of Azov $\mathbf{W}(\mathbf{r}, t)$, calculated based on the expression (2.1.1.4), corresponding to various stages of movement of atmospheric formation to the west in the field of a constant easterly wind with a speed of 10 m/s. It can be seen that at the first stage (1 h after the start of the cyclone's movement $t = t_{st} + 1$ h), the cyclone enters the water area (Figure 5.1.1, *a*), then at $t = t_{st} + 8$ h (Figure 5.1.1, *b*) crosses the central part of the sea and at $t = t_{st} + 15$ h (Figure 5.1.1, *c*) leaves the sea area. At the same time, the highest value of the driving wind velocity modulus $|\mathbf{W}(\mathbf{r}, t)|$ at the periphery of the atmospheric vortex formation reaches 22 m/s.

Figure 5.1.2 shows the current fields on the sea surface generated by a cyclone moving west at the same time points. The stationary regime (Figure 5.1.2, a) is characterized by the prevailing direction of currents towards the current wind and the presence of one anticyclonic vortex in the center of the northern part of the basin. With the onset of the cyclone, the structure of steady-state currents changes (Figure 5.1.2, *b*). Their direction after 8 h (the cyclone crosses the central part of the sea) in some areas is opposite to the direction of movement of the cyclone, in others – perpendicular to it.

After 15 h (Figure 5.1.2, *c*), when the cyclone leaves the water area, the direction of currents in the direction of atmospheric disturbances prevails in the northern part of the sea and the Taganrog Bay, in the central part – at an angle of 90° to them.

The sea level fields for the specified cyclone parameters obtained as a result of modeling are shown in Figure 5.1.3 (at the same time points). From their analysis, it follows that in the steady–state regime (Figure 5.1.3, a), there is a decrease in the level along the western coast (overcurrentss) and an increase along the eastern coast (overcurrentss).

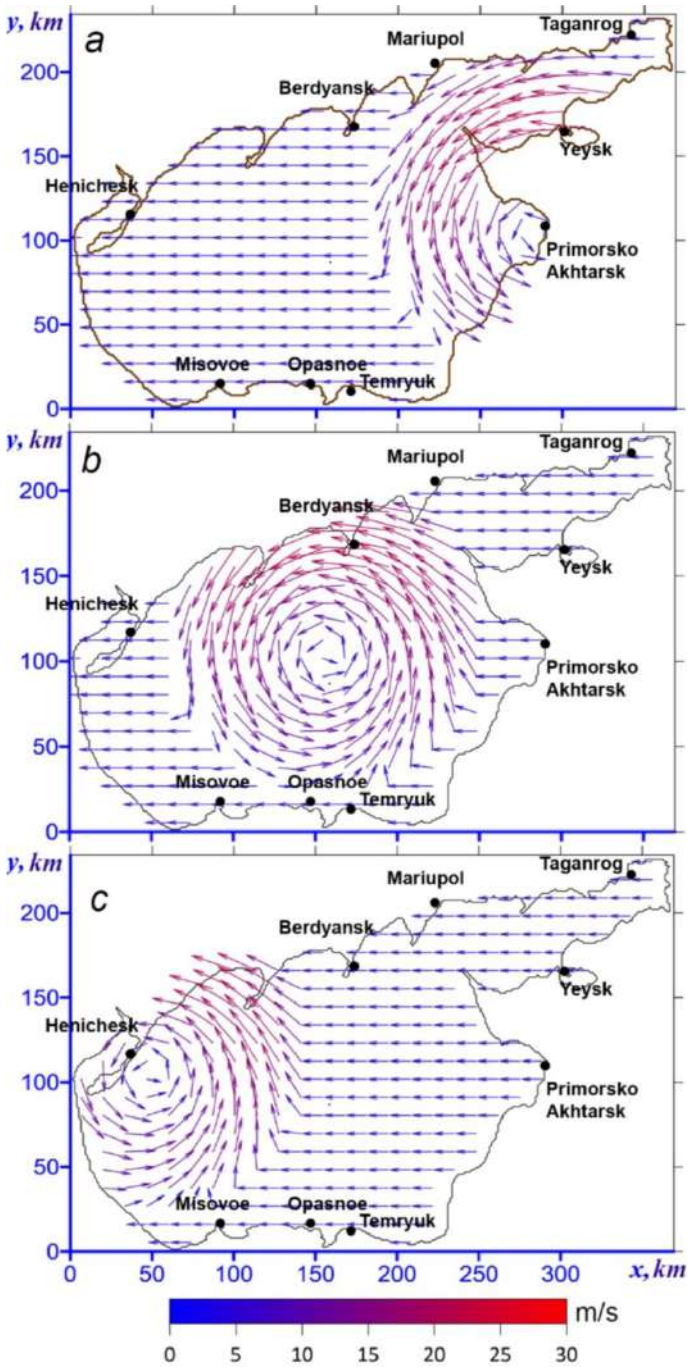

Figure 5.1.1 – Maps of the driving wind over the sea area when an atmospheric vortex formation of a velocity of 5 m/s moves westward in the field of a background constant easterly wind with a velocity of 10 m/s: the cyclone enters the water area $t = t_{st}$+1 h (*a*); the center of the cyclone crosses the central part of the sea $t = t_{st}$+8 h (*b*); the cyclone leaves the water area $t = t_{st}$+15 h (*c*)

The nodal line (dashed in the figure) crosses the central part of the sea, it is oriented perpendicular to the wind direction 8 h after the start of the cyclone (Figure 5.1.3, *b*),

the line of zero level deviations already has an elliptical shape and shifts from the center to the west. The major axis of this ellipse is oriented in the meridional direction, the minor axis is oriented in the zonal direction. The center of the ellipse approximately coincides with the nodal line of the steady-state regime dividing the sea into zones of overtaking and overtaking.

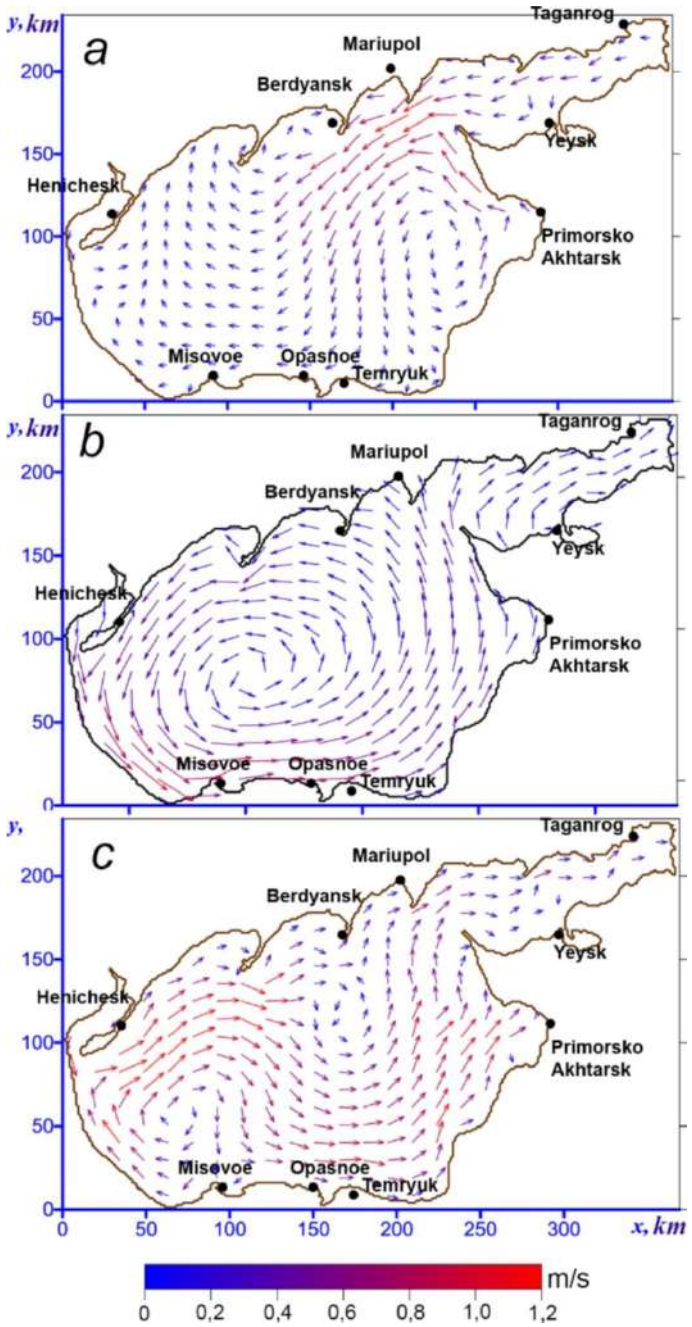

Figure 5.1.2 – Current velocity fields in the Sea of Azov at the same time points as in Figure 5.1.1

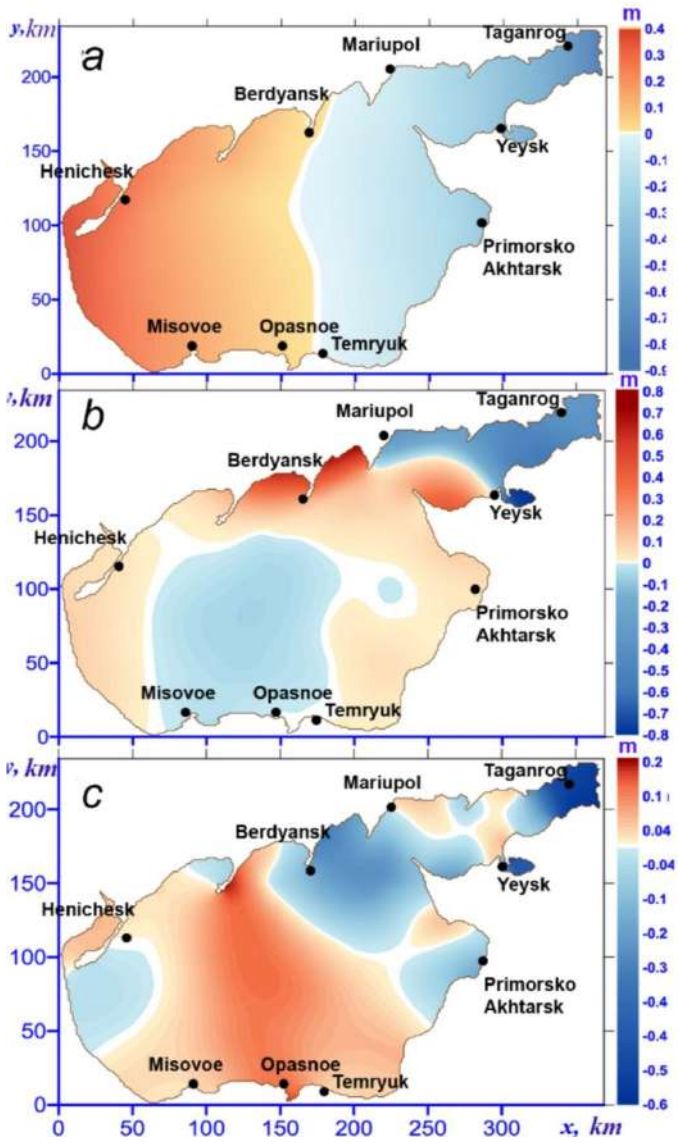

Figure 5.1.3 – Fields of the Sea of Azov level (m) at the same time points as in Figure 5.1.1.

With the distance to the east, the fluctuations gradually increase and reach the highest values near Mariupol. With further movement to the Taganrog Bay, areas of small level drops appear. To the west of the center of the ellipse (Figure 5.1.3, *b*), the level fluctuations do not exceed 3 cm. With the departure of the cyclone (Figure 5.1.3, *c*), one of the nodal lines passes through the central part of the sea, it is oriented in almost the same way as in the steady state. In the eastern part of the sea, there is a rise in the level again, in the western part – its decrease.

Table 5.1.1 shows the dependences of the velocity of steady currents in the Sea of Azov on the velocity of the stationary easterly wind causing them $|\mathbf{W}|_{st}^{l}$; l = 1, 2, 3. The maximum velocities of non-stationary currents arising in the sea after passing cyclones with a velocity of 5 m/s and a base radius of 100 km, depending on their direction, are also given here movements. From the analysis of the data presented in Table 5.1.1, it follows that, as expected, the highest velocities of steady-state currents occur in the near-surface layer of the sea (14; 34 and 62 cm/s) and depend on the speed of the constant wind generating them [Investigation ..., 2009].

Table 5.1.1 – The velocities of background stationary currents ($|\mathbf{U}|_{st}$, cm/s) caused by an easterly wind at speeds of 5, 10 and 15 m/s, and the maximum velocities of currents arising during the passage of cyclones at a speed of 15 m/s in various directions

z, m	$\mathbf{W}_{st}^{1}$	$\mathbf{W}_{st}^{1}+\mathbf{W}_c(\mathbf{r}, t)$			$\mathbf{W}_{st}^{2}$	$\mathbf{W}_{st}^{2}+\mathbf{W}_c(\mathbf{r}, t)$			$\mathbf{W}_{st}^{3}$	$\mathbf{W}_{st}^{3}+\mathbf{W}_c(\mathbf{r}, t)$		
		Cyclone direction				Cyclone direction				Cyclone direction		
		SW	W	NW		SW	W	NW		SW	W	NW
	$\|\mathbf{U}\|_{st}$	$\|\mathbf{U}\|_{max}$			$\|\mathbf{U}\|_{st}$	$\|\mathbf{U}\|_{max}$			$\|\mathbf{U}\|_{st}$	$\|\mathbf{U}\|_{max}$		
1	14	83	86	80	34	107	108	102	62	125	126	121
3	11	77	79	74	28	99	100	096	52	117	116	113
5	09	72	75	70	24	93	94	90	46	110	110	106
10	06	50	52	49	17	65	66	63	32	77	77	74

The action of the wind, the speed of which is several times higher (by 2 and 3 times) than the lowest of the studied speeds $\mathbf{U}|_{st}$ = 14 cm/s, causes currents in the sea, the speed of which is 1.8 and 4.4 times higher than this value. With the passage of cyclones over the sea, the current velocities on all horizons increase dramatically. The highest maximum velocities occur when atmospheric disturbances move to the west, the lowest – to the northwest (Table 5.1.1).

Based on the analysis of the data given in Table 5.1.1, we note their dependence on the speed of background steady-state movements in the sea. The maxima of the velocity of non-stationary currents in the field of background currents generated

by a stationary wind of higher velocity (10 and 15 m/s) exceed by 1.2 and 1.4 times the lowest value (86 cm/s) achieved with steady motion caused by a low-speed wind of 5 m/s (Table 4.1.1). The same characteristic ratio for the velocity of the currents, it can be traced on other horizons. Under the influence of atmospheric disturbances, the velocity of currents increases with depth, the greatest value is noted in the bottom layer [Investigation ..., 2009].

Based on the analysis of the data given in Table 5.1.1, the influence of the directions of movement of cyclones acting in the field of stationary currents on the maximum velocities of currents arising in the Sea of Azov has been determined. Cyclones moving westward lead to the formation of currents with higher velocity in the surface layers of the sea. In the bottom layer, the currents velocities generated by cyclones of different directions are almost the same. The lowest current velocities are formed in the sea when the cyclone passes to the northwest.

5.2. The influence of the parameters of vortex atmospheric formations on reproducible currents velocities and the magnitude of overburden fluctuations in sea level under various boundary conditions at the liquid boundary

Storm vortex atmospheric movements (cyclones and anticyclones) are observed over the Sea of Azov and its coast, which lead to catastrophic declines and level rises. They move over the Sea of Azov throughout the year, but most often in winter and spring. They most often come from the western regions of the Black Sea and the central regions of Europe (western cyclones), as well as from Asia Minor (southern) [Hydrometeorological ... , 1986; Ivanov, 2002; Scientific and applied … , 1990; Dyakov, Fomin, 2002]. Based on the analysis of materials from contact and satellite observations in the areas of the Black and Azov Seas [On the evolution ... , 1991; Patterns ..., 2006], the average characteristics of cyclones were obtained. The average velocities of translational movement of cyclones are 5-10 m/s, the average diameter of the area of atmospheric formations is 480-700 km, the pressure drop between the center and the periphery is 11 – 21 gPa [The influence of the Kerch ..., 2009].

A numerical study of the role of geometric characteristics of cyclonic formations in the formation of run-up oscillations and currents in the Sea of Azov was carried out for the southern (South) and western (West) directions of their movement. The indicated directions are 90° and 0° angles with the *x*-axis pointing east. The speed of the driving wind **W**(r, *t*) is given by the formula (2.1.1.4), in which the velocity of movement of cyclonic formations (**c**) is assumed to be 5 m/s, the maximum deviation (P_0) from the background pressure value P_0 is equal to 15 gPa. The geometry of the unsteady vortex formation is modified by setting the values of the radii of their bases of 100, 200 and 400 km (R_c^m, m = 1, 2, 3). It is assumed that as the center of the cyclone moves, it crosses the Sea of Azov along a given trajectory and passes through its central part.

The detailed analysis of the influence of background stationary currents on the maximum velocities of non-stationary currents arising in the Sea of Azov during the passage of cyclones, described in paragraph 5.1, allows us to study their direct impact on the marine environment in this experiment. The movement of the baric formation in the water area of the Sea of Azov begins from the moment of time ($t = t_0 = 0$), and the velocity of the stationary component of the wind speed in expression (2.1.1.3) is assumed to be zero ($\mathbf{W}_{st} = 0$).

The determination of the influence of another factor, water exchange with the Black Sea, on overburden phenomena and currents in the Sea of Azov, arising under the influence of these atmospheric disturbances, is based on a comparative analysis of the results of modeling performed under different boundary conditions in the strait. As one of the variants of boundary conditions, the condition of free passage of liquid (2.1.1) is chosen in those nodes of the computational grid that are located at the entrance to the Kerch Strait (the section runs along 45.25° E). In the second variant, a closed basin is considered, at the boundaries of which the condition of non-currents of liquid is fulfilled [Cherkesov, Ivanov, Khartiev, 1992; Blumberg, Mellor, 1987]. A variant of the calculation area with a simplified geometry is used – with a oundary at the entrance to the strait (Figure 1.2.2, on the right).

The values of run–offs and run-offs arising under the influence of cyclonic disturbances are analyzed at coastal stations of the Sea of Azov ($A_1 – A_9$) located near

large settlements (Figure 3.1.1, *a*). The study of vertically averaged current velocities in the strait is carried out at five points (P_1–P_5) evenly located on the liquid boundary (Figure 2.1.1, *b*) [The influence of the Kerch ..., 2009]. At each time step, the total currents rate of water passing through the Kerch Strait along a section perpendicular to the *y* axis is calculated. In this case, the volume of the currentsing liquid during the time $t_0 \le t \le t_{end}$ is determined by the expression (3.1.2). The moment of completion of the tend $t_{end} = t_c +$ 12 h simulation occurs 12 h after the passage of the cyclone between the extreme points of the Azov Sea (t_c).

Figure 5.2.1 shows the driving wind fields (at an altitude of 10 m), which correspond to three stages of movement of atmospheric formation from south to north at a speed of 5 m/s and a radius of the grounds are 100 km away.

The driving wind velocity fields determined on the basis of the formula (2.1.1.4) depend on the radius of the base of the vortex atmospheric formation (R_c). An analysis of the maxima of the driving wind velocity ($|\mathbf{W}(r, t)|_{max}$) caused by these disturbances moving at the same speed and pressure drop shows that its greatest value is generated by an atmospheric disturbance having a smaller base radius. Thus, at $R_c^1 = 100$ km, the maximum driving wind speed is 21.34 m/s; at $R_c^2 = 200$ km, the maximum is 19.5 m/s; at $R_c^3 = 400$ km, it is 16.5 m/s. The time during which the cyclone moves along the sea surface (trend) varies and depends on the size of the base radius: $t_c = 25$ h at R_c^1; $t_c = 36$ h at R_c^2; $t_c = 58$ h at R_c^3.

Thus, the passage of cyclones with large base sizes (by 2 and 4 times compared to the smallest radius of 100 km) leads to an increase in the time interval of their stay over the water area (t_c) by 1.4 and 2.3 times and to a decrease in the maximum speed of the driving wind ($|\mathbf{W}(r, t)|_{max}$) by 8.6% and 22.7%, respectively.

Figure 5.2.2 shows the fields of the Sea of Azov level generated by the passage of a southern cyclone with a velocity of 5 m/s and a base radius of 100 km, obtained as a result of modeling. Figures 5.2.2, *a* – *b* are given at time $t_1 = 1$; $t_2 = 8$; $t_3 = 25$ h, corresponding to the three stages of movement of atmospheric formation, Figure 5.2.2, *d* – 12 h after its departure from the water area.

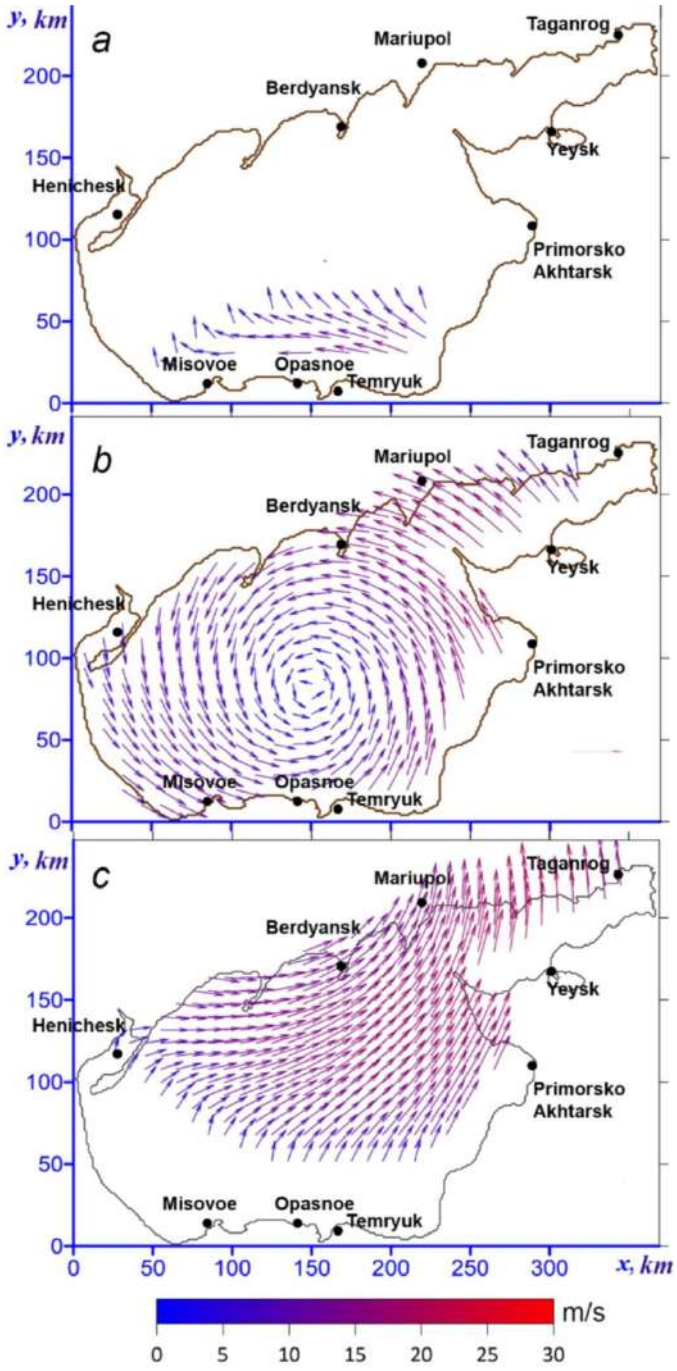

Figure 5.2.1 – Driving wind velocity fields over the Sea of Azov caused by the movement of the southern cyclone at a speed of 5 m/s: the cyclone enters the water area (*a*); the center of the cyclone crosses the central area of the sea (*b*); leaves the water area (*c*)

From the analysis of the above fields, it follows that after 1 hour from the beginning of the cyclone's movement (Figure 5.2.2, *a*), a level change occurs along the southern coast, symmetrical with respect to the entrance to the strait. At this time ($t = t_1$) there are

no disturbances near the northeastern and northwestern shores. The nodal line (dashed in the figure) crosses the central part of the sea and is oriented in the direction of movement of the cyclone. The second stage of displacement ($t = t_2$) is marked 8 h after the onset of the cyclone (Figure 5.2.2, *b*). The isolines of the level have an elliptical shape and are located in the central area of the water area. The conventional line dividing the sea into zones of overtaking and overtaking is shifted to the east and oriented along the course of the cyclone. Now there is an increase in the western part, and a decrease in the eastern part.

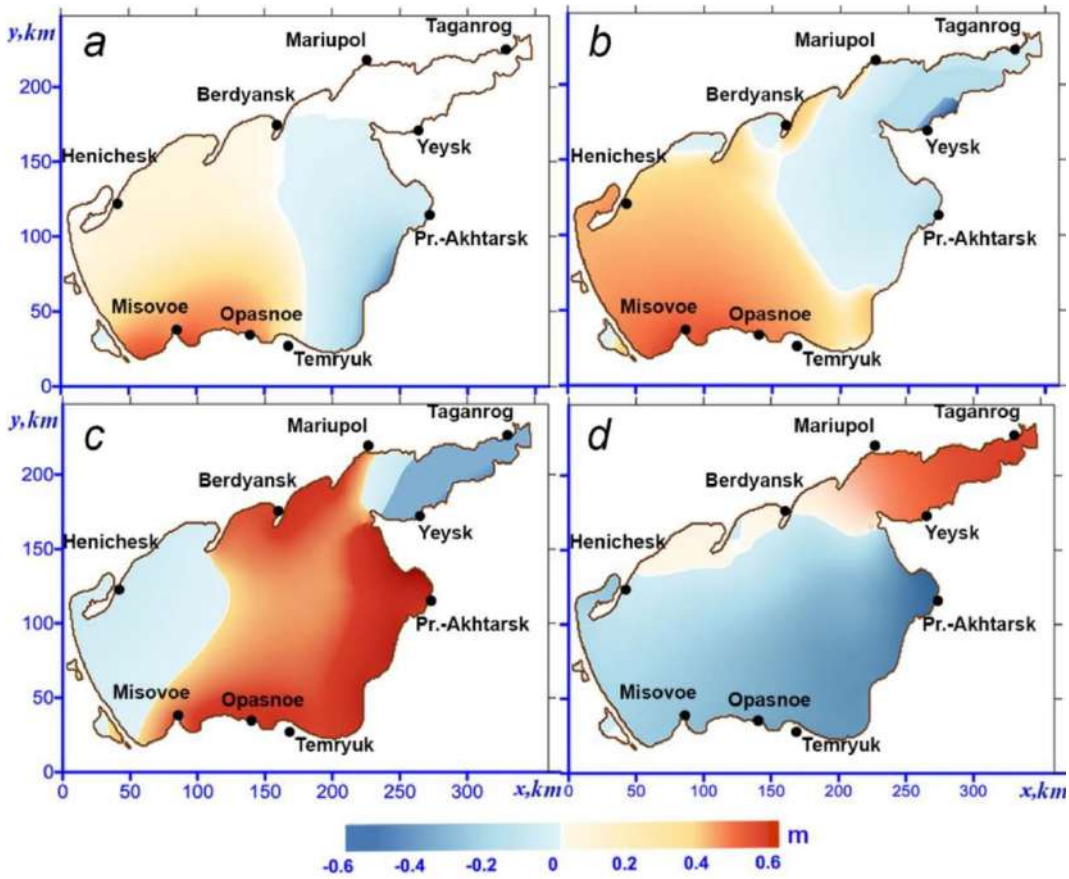

Figure 5.2.2 – The level of the Sea of Azov according to the simulation results during the passage of the southern cyclone at a speed of 5 m/s (base radius of 100 km): the cyclone enters the water area (*a*); the center of the cyclone crosses the central area of the sea (*b*); leaves the water area (*c*); 12 h after the cyclone leaves the water area (*d*)

With the departure of the cyclone (Figure 5.2.2, *c*), the level isolines cease to be closed, and the nodal line is still oriented along the course of the cyclone. In the Taganrog

Bay, in its western part, there is a thickening of the isolines of the level and its rise takes place, in the eastern part there is a decrease. From Figure 5.2.2, *d*, it can be seen that the nodal line is now oriented perpendicular to the trajectory of the cyclone, while the southern coast of the sea becomes a zone of run–off, the northern one becomes a zone of run-off. Table 5.2.1 shows the maximum values of the run–up and run-down and their corresponding time points at stations $A_1 - A_9$.

As follows from the analysis of the data given in Table 5.2.1, for various parameters of disturbing cyclonic formations and for all stations under consideration, the largest level deviations in absolute magnitude occur provided that water exchange through the strait is taken into account. From the analysis of the data on surges presented in the upper part of Table 5.2.1, it can be seen that the maximum surges take place at the Taganrog station.

Comparing the results obtained at this station for two variants of boundary conditions in the strait and for each of the disturbance bases of different sizes, we note that the maximum values of the surges at R_c^1 are 49 and 54 cm (taking into account and excluding water exchange through the strait); at R_c^2 – 93 and 97 cm; at R_c^3– 102 cm and 115 cm. Thus, the relative difference in the values of the wagons at the Taganrog station, calculated with and without taking into account the strait, does not exceed 12%. Minimum surges are noted in the village. Dangerous and correspondingly equal: at R_c^1 – 5 and 7 cm (including and excluding water exchange through the strait); at R_c^2 – 8 and 9 cm; at R_c^3 – 10 and 12 cm. The time to reach the highest level rises when taking into account the strait increases by no more than 7%. However, with a fourfold increase in the size of the cyclone, the time to reach peak surges does not exceed 40%.

The second (lower) part of Table 5.2.1 shows the maximum values of run-offs at the same stations. From this it can be seen that under the action of cyclones of various sizes, the greatest overcurrentss take place at the Yeysk station: at R_c^1 – 45 and 48 cm (taking into account and excluding water exchange through the strait); at R_c^2 – 48 and 53 cm; at R_c^3 – 39 and 44 cm.

Table 5.2.1 – Maximum surges and overcurrentss ($|\zeta|_{max}$, cm) with corresponding time points (t_{extr}, h) caused by southern cyclones with a speed of 5 m/s without and taking into account water exchange through the strait (*)

Stations	R_c^1 = 100 km		R_c^2 = 200 km		R_c^3 = 400 km	
	$\|\zeta\|_{max}$	t_{extr}	$\|\zeta\|_{max}$	t_{extr}	$\|\zeta\|_{max}$	t_{extr}
Surcharges						
Henichesk	10	24.6	12	11.0	12	15.8
	11*	25.1*	15*	21.1*	19*	16.3*
Berdyansk	8	19.6	11	20.5	10	39.8
	10*	20.0*	16*	21.2*	13*	41.1*
Mariupol	39	17.7	59	26.3	70	44.5
	46*	17.8*	68*	28.5*	79*	46.2*
Taganrog	49	22.6	93	29.4	102	45.3
	54*	23.6*	97*	31.4*	115*	46.7*
Yeysk	34	19.6	58	29.1	62	43.9
	48*	19.3*	64*	29.1*	70*	45.2*
Primorsko-Akhtarsk	35	13.2	57	22.2	32	36.2
	47*	14.1*	66*	22.3*	37*	38.6*
Temryuk	11	14.8	19	18.6	9	23.0
	8*	15.8*	10*	19.5*	15*	22.6*
Opasnoe	5	4.8	8	13.6	10	19.0
	7*	5.1*	9*	14.7*	12*	19.2*
Mysovoe	6	29.0	8	14.0	18	17.1
	10*	29.7*	12*	14.3*	19*	17.7*
Run-offs						
Henichesk	13	19.2	12	21.8	36	40.4
	22*	19.5*	18*	22.3*	43*	40.1*
Berdyansk	2	42.7	5	26.9	3	50.8
	3*	43.1*	8*	27.4*	4*	54.2*
Mariupol	12	30.3	15	15.3	22	20.5
	7*	31.4*	11*	15.5*	17*	21.3*
Taganrog	19	33.3	27	20.1	60	44.6
	21*	33.8*	47*	20.7*	63*	45.7*
Yeysk	45	12.6	48	15.5	39	20.6
	63*	45.7*	53*	16.8*	44*	20.9*
Primorsko-Akhtarsk	44	8.2	45	10.9	30	14.3
	46*	8.8*	52*	11.4*	34*	14.5*
Temryuk	9	20.5	12	28.3	26	46.1
	13*	21.1*	19*	29.6*	19*	47.1*
Opasnoe	8	19.7	12	27.4	27	43.2
	12*	20.6*	16*	27.2*	22*	44.2*
Mysovoe	10	17.6	10	23.0	31	40.1
	15*	18.4*	17*	23.6*	33*	41.9*

* The results of modeling performed taking into account water exchange through the Kerch Strait

The changes in the maximum values of landfills in the Yeysk area, taking into account and excluding water exchange through the strait, for R_c^1, R_c^2 and R_c^3, respectively, are 6, 15 and 11%.

The minimum run–offs are noted at Berdyansk station and are equal to: at R_c^1 – 2 and 3 cm (including and excluding water exchange through the strait); at R_c^2 – 5 and 8 cm; at R_c^3 – 3 and 4 cm. As for the landfills, with an increase in the radius of the base of the cyclone, the time to reach the maximum of the landfills decreases.

The results shown in Table 5.2.1 allow us to conclude that at the stations under consideration, with an increase in the size of the cyclone bases by a factor of two ($R_c^2 = 2\ R_c^1$), the increase in the maxima of run-off and run-up does not exceed 2.3 times. A fourfold increase in the size of the cyclone base ($R_c^3 = 4\ R_c^1$) leads to an increase in the highest values of run-off and run-up to 3 times. Accounting for water exchange through the strait leads to changes in extreme level deviations not exceeding 40%. The period of time during which the formation of extreme values of the level occurs decreases with an increase in the size of active cyclones.

Let's analyze the features of the spatial distribution of the velocity fields of currents in the surface layer of the sea, taking into account the water exchange through the strait. At the same time points ($t_1 = 1$; $t_2 = 8$; $t_3 = 24$ and $t_4 = 36$ h), Figure 5.2.3 shows the fields of the specified currents velocity generated by the action of a southern cyclone moving at a speed of 5 m/s, with a base radius of 100 km.

At time $t = t_1$ (Figure 5.2.3, *a*), the direction of the currents largely repeats the nature of the driving wind velocity fields (Figure 5.2.3, *a*). The structure and direction of the currents (Figure 5.2.3, *b*) change after 8 h. An anticyclonic vortex takes place in the central part of the basin; in the eastern and western regions of the sea, the currents are oriented perpendicular to the trajectory of the cyclone. After 24 h (Figure 5.2.3, c), when the cyclone leaves the water area, the western direction of currents prevails in most of the sea and the Taganrog Bay, while the anticyclonic structure remains in the central part 12 h after the cyclone leaves the water area, the current fields become more heterogeneous (Figure 5.2.3, *d*). In the western and central parts of the sea, several vortex

formations are noted, between which there is a band of currents directed towards the strait, in the eastern part the currents are oriented to the west.

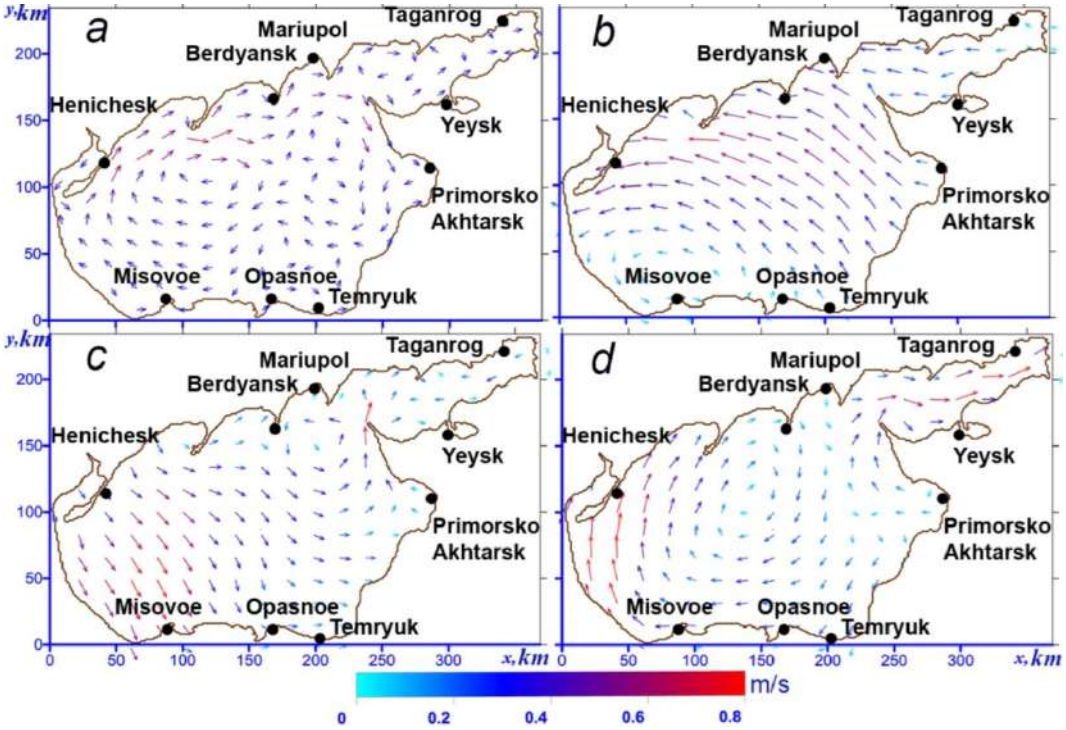

Figure 5.2.3 – Model velocity maps of surface currents in the Sea of Azov generated by a southern cyclone with a velocity of 5 m/s (base radius of 100 km) at the same time points as in Figure 5.2.2

Table 5.2.2 shows the maximum currents velocities calculated with and without the strait, generated by southern cyclones moving at a speed of 5 m/s, with base radii of 100, 200 and 400 km. The values of the maxima are presented at different depths of the sea. From the analysis of the above data, it follows that under the action of a cyclone with a radius of 200 km, taking into account water exchange through the strait, the current velocities at the considered horizons reach the highest values: 1.34 (in the surface layer), 1.23 (at a depth of 3 m), 1.16 (at $z = -5$ m), 0.82 m/s (in the bottom layer). It can be seen that taking into account the strait affects the values of the maximum currents velocities, which also depend on the size of the active cyclones. At the same time, the largest values of relative deviations of the currents velocity maxima for $U'_{\text{n}} = 0$ and $U_{\text{n}} = 0$ are: 23 (R_{c}^1), 18 (R_{c}^2) and 8% (R_{c}^3).

Table 5.2.2 – Maximum values of the current velocity (cm/s) caused by southern cyclones with a velocity of 5 m/s on various horizons of the Sea of Azov, excluding and taking into account water exchange through the Strait (*)

Horizon, m	R_c^1 = 100 km	R_c^2 = 200 km	R_c^3 = 400 km
0	89	110	104
	115*	134*	113*
3	82	102	91
	104*	123*	99*
5	75	97	81
	97*	116*	86*
10	55	70	68
	67*	82*	71*

Let us now consider the influence of various boundary conditions at the entrance to the Kerch Strait on the integral water exchange caused by the passage of southern cyclones. In numerical experiments, the values of the function $G(t)$ are calculated at each time step according to the formula (3.1.2). The time of completion of the simulation for the study of the volume of liquid currentsing through the cross-section of the strait was increased to 7 days (t_{end} = 168 h). From the analysis of the integral currents rates (m^3) of water through the strait, it follows that the largest currents rate of water through the strait occurs for a cyclone with the largest base size (400 km), –53.6 m^3, the smallest – 12.7 m^3 for a cyclone with a base of 100 km. The currents rate increases to a maximum from the initial moment of time until the moment when the center of the cyclone crosses the central part of the sea. After the cyclone leaves the sea, the currents rate decreases to zero and then takes on negative values caused by the outcurrents of water from the sea.

The results of calculations of the currents velocity at the points of the strait are presented in Table 5.2.3. The maximum values of the average depth velocity of currents generated by southern cyclones moving at a speed of 5 m/s are given here, depending on the magnitude of the radii of their bases with the corresponding time points. It follows from the above data that a decrease in the radius of the base of cyclones leads

* The results of modeling performed taking into account water exchange through the Kerch Strait

to an increase in the maximum velocity of currents in the strait. Note that the highest values of the maximum currents velocities are reached in the center of the strait (point P3) and are: 0.33 (R_c^1); 0.29 (R_c^2); 0.21 m/s (R_c^3). The lowest current velocity maxima occur at a point located near the western border of the strait (P_1): 0.23 (R_c^1); 0.19 (R_c^2); 0.14 m/s (R_c^3). It follows that at the same value of the radius of the base of cyclones, currents arise in the central part of the strait, the maximum speeds of which exceed 1.5 times the maximum speeds of currents at its border. With an increase in the size of the cyclone base by two and four times, the highest values of the current velocity in all the considered points of the strait decrease by 1.3 and 1.6 times, respectively. The time to reach the maximum speed values increases by three times with an increase in the size of cyclones.

Table 5.2.3 – The highest values of the vertically averaged ($|\bar{\mathbf{U}}|_{(z)}$, cm/s) velocity of currents generated by southern cyclones at a speed of 5 m/s with corresponding time points in the strait

Points in the Strait	R_c^1 = 100 km		R_c^2 = 200 km		R_c^3 = 400 km	
	$\|\bar{\mathbf{U}}\|_{(z)}$	t	$\|\bar{\mathbf{U}}\|_{(z)}$	t	$\|\bar{\mathbf{U}}\|_{(z)}$	t
P_1	23	11.1	19	17.6	14	34.5
P_2	27	11.2	23	17.8	17	34.6
P_3	33	11.2	29	17.8	21	34.6
P_4	32	11.3	29	17.9	22	34.8
P_5	31	11.3	28	17.9	21	34.8

In the next series of numerical experiments, we will evaluate the effect on the calculation results of changes in the trajectory of cyclones with the same basic parameters as in the previous experiment. The condition of free passage of liquid is chosen as the boundary condition at the liquid boundary (2.1.1). Since it was previously shown that the extreme characteristics of deviations in the level and velocity of currents arising in the Sea of Azov, when using this condition, are higher than when using the closed boundary condition.

We will simulate the storm situation for cyclones moving from west to east (H), taking into account water exchange through the strait. Table 5.2.4 shows the maximum

values of overcurrentss and overcurrentss caused by the action of western and southern cyclones moving at a speed of 5 m/s, obtained/observed at the coastal stations of the Sea of Azov for three values of the radius of their base. The relevant time points are given here.

Table 5.2.4 – Maximum ($|\zeta|_{max}$, cm) surges and overcurrentss at the coastal stations of the Sea of Azov caused by the movement of western (W) and southern (S) cyclones at a speed of 5 m/s, with corresponding time points (t_{extr}, h)

Stations	R_c^1 = 100 km				R_c^2 = 200 km				R_c^3 = 400 km			
	W		S		W		S		W		S	
	$\|\zeta\|_{max}$	t_{extr}	$\|\zeta\|_{max}$	t_{extr}	$\|\zeta\|_{max}$	t_{extr}	$\|\zeta\|_{max}$	t_{extr}	$\|\zeta\|_{max}$	t_{extr}	$\|\zeta\|_{max}$	t_{extr}
Surcharges												
Henichesk	9	25.7	11	25.1	12	21.8	15	21.1	17	17.1	19	16.3
Berdyansk	8	20.6	10	20.0	14	22.2	16	21.2	12	41.6	13	41.1
Taganrog	32	18.5	46	17.8	44	29.7	68	28.5	76	46.3	79	46.2
Mariupol	44	23.9	54	23.6	85	32.0	97	31.4	88	46.7	115	46.7
Yeysk	47	20.0	48	19.3	44	29.8	64	29.1	46	45.4	70	45.2
Primorsko-Akhtarsk	42	14.2	47	14.1	45	22.9	66	22.3	29	38.7	37	38.6
Temryuk	5	17.0	8	15.8	7	19.7	10	19.5	14	22.8	15	22.6
Opasnoe	7	6.4	7	5.1	7	14.9	9	14.7	11	19.3	12	19.2
Mysovoe	6	30.4	10	29.7	9	14.4	12	14.3	18	17.9	19	17.7
Run-offs												
Henichesk	17	20.3	22	19.5	16	22.5	18	22.3	37	40.3	43	40.1
Berdyansk	3	43.2	3	43.1	6	28.5	8	27.4	3	54.5	4	54.2
Taganrog	4	32.6	7	31.4	9	16.1	11	15.5	11	21.5	17	21.3
Mariupol	16	35.0	21	33.8	34	21.2	47	20.7	36	46.0	63	45.7
Yeysk	30	14.1	48	13.3	34	17.0	53	16.8	37	20.9	44	20.9
Primorsko-Akhtarsk	31	8.8	46	8.8	34	12.1	52	11.4	29	14.9	34	14.5
Temryuk	8	21.6	13	21.1	14	30.1	19	29.6	14	47.5	19	47.1
Opasnoe	8	20.7	12	20.6	12	27.3	16	27.2	16	44.7	22	44.2
Mysovoe	11	19.0	15	18.4	12	23.8	17	23.6	25	42.3	33	41.9

From the analysis of the presented data, it can be seen that southern cyclones (S) lead to the occurrence of large overcurrentss and overcurrentss at all points of the coast. The maximum deviations of the level values caused by cyclones of different directions do not exceed 40%. The time to reach the maximum of sea level rises and decreases under the influence of the western cyclone increases slightly (by less than 14%) compared with the southern cyclones.

As follows from the analysis of the results of modeling the storm situation caused by the passage of western cyclones, taking into account and without taking into account the strait, this direction of movement of atmospheric disturbances does not give a noticeable increase in the maxima of run-off and run-up compared with the action of southern cyclones. Thus, accounting for water exchange through the strait causes an increase of 40% in extreme run-offs and overcurrentss. With a 2-fold increase in the radius of the base of the southern cyclone, the maxima of run-offs and run-offs increase by no more than 2.3 times. A fourfold increase in the radius of the cyclone base leads to an increase in the highest values of run-offs and run-offs by no more than three times. The time during which the formation of extreme values of the level occurs decreases with an increase in the radius of the base of active atmospheric formations. In the central part of the strait, the maximum velocity of currents exceeds 1.5 times the velocity of currents near its lateral borders.

5.3. Numerical study of currents and run-up fluctuations of the Sea of Azov level during the period of extreme Azov winds

In the last decade, as a result of storm activity, catastrophic floods have been regularly observed in the Taganrog Bay and the Don Delta (April 12, 1997, March 1, 2005, September 30, 2010, March 23-24, 2013 and September 24, 2014) [The extreme flood ..., 2014; Numerical study ..., 2017]. The extreme Azov Sea phenomenon “Chernomorka”, or “reverse bottom” (in the terminology of local fishermen), occurs during strong storm cyclones moving from the north-east of the Black Sea. Prolonged action of winds from the south-south-east to the south-south-west with moderate or

hurricane speed leads to extreme overcurrentss and level rises, which are the cause of devastating floods on the Azov coast. These recent cases of flooding in the Taganrog Bay, as well as the storm situation in 1997, were characterized by the maximum values of sea level rise for the entire historical observation period (1882 – 2015). As follows from the observation data, the storm situation on March 23-24, 2013. it arose during the passage of a deep cyclone over the southern part of the European territory of Russia with a sharp increase in the south-westerly wind over the waters of the Sea of Azov. The passage of the cyclone was accompanied by storm surge and flooding of vast territories of the Don Delta and the eastern coast of the Sea of Azov [Matishov, Matishov, 2013; Modern ..., 2015; Matishov, Berdnikov, 2015]. An extremely dangerous phenomenon on September 24, 2014 was caused by a powerful cyclonic vortex formed in the Crimea region in a deep tropospheric hollow oriented from the Arctic to the south of Europe. The formation of the vortex was facilitated by a large thermodynamic instability of the atmosphere, which arose as a result of the collision of cold air coming from the north and from the middle troposphere, and warm moist air coming from the Black Sea. During the movement of the cyclone on the night of September 24, an intensification of the vortex occurred, which was accompanied by hurricane-force winds, intense precipitation and wind waves, as well as storm surge on the eastern coast of the Sea of Azov and in the Taganrog Bay.

The main approach to theoretical studies of extreme overcurrentss and overcurrentss, reproduction of water circulation in natural marine basins is the use of mathematical models. In paragraphs 3.1 and 3.2, conclusions are drawn about the influence of the parameters of model cyclones (direction, velocity, geometric characteristics) on the maximum velocity of the currents generated by them and extreme fluctuations in sea level. The results of research conducted using a two-layer mathematical model, as well as based on hydrometeorological observations at the coastal base of the Southern Scientific Center of the Russian Academy of Sciences, are known. They consider the case of abnormal flooding of the Don Delta from March 20 to March 26, 2013 [The extreme flood ... , 2014; Matishov, Berdnikov, 2015].

To understand the features of these recurring phenomena, a numerical analysis of the spatial and temporal variability of the dynamics of waters in the Sea of Azov during dangerous phenomena that demonstrated the destructive power of storm surges and led to catastrophic floods in the Taganrog Bay and the Don Delta (March 23–24, 2013 and September 24, 2014) was performed. In computational experiments reproducing these storm cyclones as atmospheric forcing, the fields of driving wind and atmospheric pressure obtained from the data of the SKIRON regional atmospheric model described in detail in paragraph 1.2.1. Based on the analysis of meteorological information from SKIRON data, conclusions were drawn about the nature of the wind regime over the waters of the Sea of Azov during these extreme events, and also during the month preceding them. The space-averaged wind speed during the development of extreme "bottoms" was determined by the formula

$$\left|\overline{\mathbf{W}}(t)\right| = \frac{1}{N}\sum_{k=1}^{N}\left|\mathbf{W}_{\mathrm{SKIRON}_k}(t)\right|, \qquad (5.3.1)$$

were N – the number of nodes of the calculated grid; $\left|\mathbf{W}_{\mathrm{SKIRON}_k}(t)\right| = \sqrt{W^2_{\mathrm{SKIRON}_X}(t)_k + W^2_{\mathrm{SKIRON}_Y}(t)_k}$ – the wind velocity module in its k^{th} node [Numerical study..., 2017]. The average wind speed (10.2 m/s) calculated in this way for the sea area is between its highest (2.7 m/s) and lowest (17.6 m/s) values in March 2013, and for September 2014 it is 13.6 m/s (between the lowest and highest values, respectively 2.5 and 24.7 m/s), which is 1.3 and 1.8 times higher than its average annual climatic value [Hydrometeorological ... , 1986].

Figure 5.3.1 shows graphs of the evolution of wind speed averaged over the sea area. It should be noted that in March 2013 (Figure 5.3.1, a) a comparable to the maximum, but short-term (within 3 h) increase in the average wind speed from 16 to 17.2 m/s (March 14, 2013) was not the cause of extreme fluctuations in sea level. The prolonged action of the wind with almost the same speed (from 16 to 17.6 m/s) for 12 h led to a dangerous phenomenon on March 23–24, 2013.

As follows from Figure 5.3.1, *b*, in general, moderate winds prevailed over the Sea of Azov throughout the month (September 2014). An increase in the average wind speed to 24.7 m/s occurred during the passage of the cyclone on September 24, 2014. In this case, the action of wind with a speed above 16 m/s for 22 h caused extreme overburden phenomena on the coast of the Sea of Azov. Thus, the action of a gale-force wind lasting less than 3 h does not lead to the occurrence of storm surges.

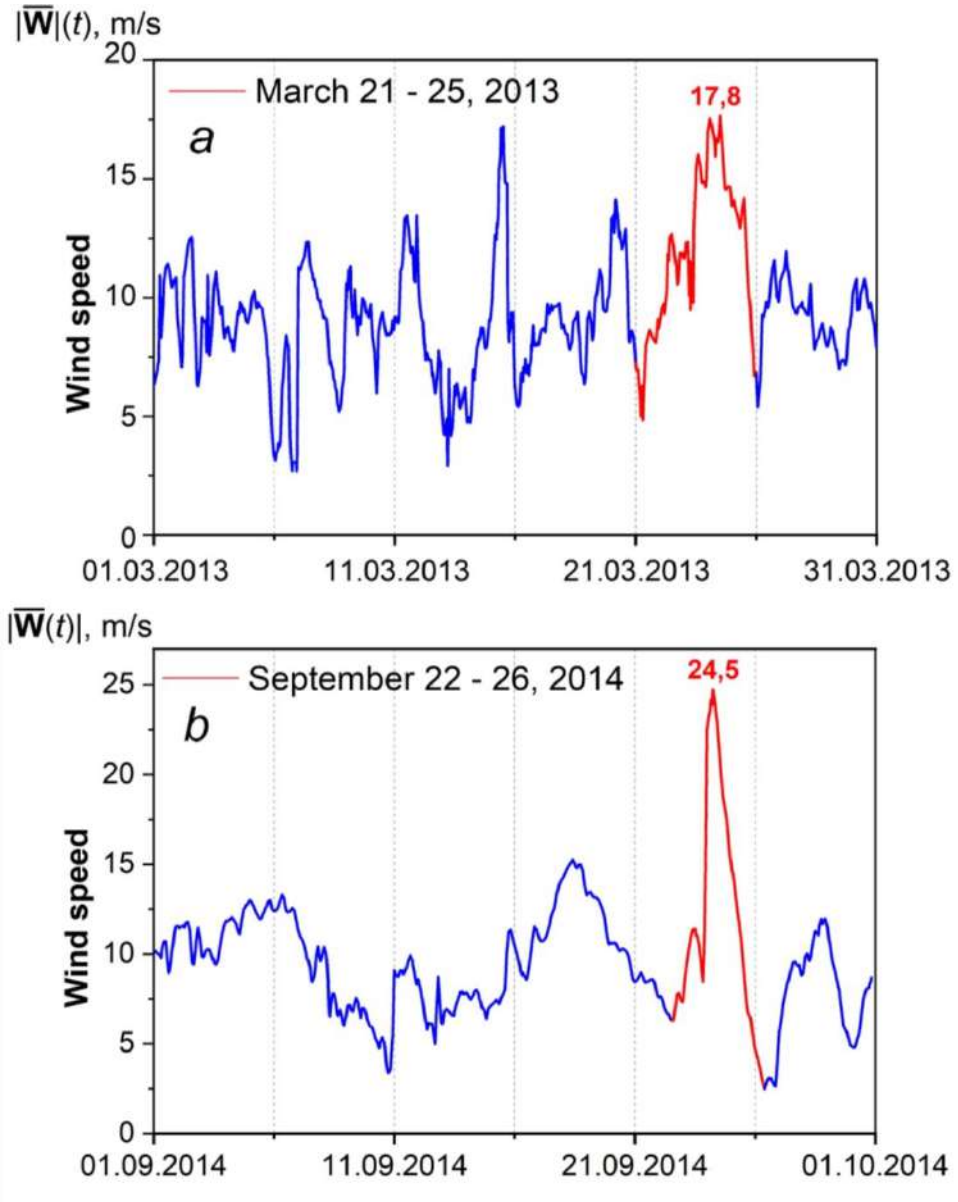

Figure 5.3.1 – Average wind speed in the Sea of Azov during stormy months: March 1, 31, 2013 (a); September 1, 30, 2014 (b). Vertical dotted lines are drawn with a discreteness of 5 days [Numerical study ..., 2017]

According to SB SOIN, at the Taganrog and Temryuk meteorological stations, the average wind speed on 23–24.03.2013 of the south-westerly direction was 9 – 13 m/s with maximum values of 21 – 22 m/s. At the Yeisk and Dolzhanskaya stations, the maximum wind speeds were 21 and 19 m/s, respectively, with average values of 9 – 10 m/s. On the western and southern coasts of the Sea of Azov (Genichesk, Mysovoye), the average wind speed of the western and north-western directions was 16 – 22 m/s with maximum values of 23 – 28 m/s.

It should be noted that the data from field observations are close to or exceed the calculated values of SKIRON. With an average wind speed of 11 – 15 m/s in the water area, its maximum values per Meteorological Stations (MS) in Taganrog, Dolzhanskaya and Temryuk reached 33 – 37 m/s. Such extreme wind speeds at these stations were recorded for the first time in the entire historical observation period. As a result of the hurricane-force wind on the coast of the Taganrog Bay, power lines were damaged, trees were broken, the roof of houses was damaged, power transmission poles were toppled, towers and a high-rise crane were toppled in the ports of Yeysk and Taganrog.

The spatial distribution of the driving wind fields over the Sea of Azov, obtained from the SKIRON model data during storm situations in March 2013 and September 2014, are shown in Figure 5.3.2. It is noticeable that in the situations under consideration, significant spatial heterogeneity of wind fields over the sea was observed both in speed and direction.

In the case of an extreme storm in 2013, according to SKIRON data (Figure 5.3.2, *a*), a wind increase of up to 10 m/s occurred at 12:00 on March 23, 2013 when the cyclone passed through the central part of the sea, while the wind changed its direction from northeast to southwest. The next maximum speed occurred in the middle of the day on March 24, 2013. Figure 5.3.2, *b* shows the movement of an extensive cyclonic formation from the north-east of the Black Sea with a high (up to 20 m/s) wind speed, the direction of which is heterogeneous in different parts of the Sea of Azov.

The maximum development of the storm occurred on the following day (March 24, 2013), during which the wind did not change direction and acted along the axis of the Taganrog Bay (south-southwest direction (Figure 5.3.2, *b*)), and the maximum wind

speed reached 25 m/s. Figures 5.3.2, *e*, *f* show the directions of the wind fields during the storm on September 24, 2014, according to the SKIRON reanalysis. During the day, as in the case of the 2013 storm, a steady south-southwesterly wind was observed (along the axis of the Taganrog Bay) speed up to 28 m/s. The obtained wind fields, according to SKIRON, generally agree well with the data of field observations at coastal meteorological stations and confirm the fact that the greatest increase in wind speed occurred over the waters of the Taganrog and Temryuk bays.

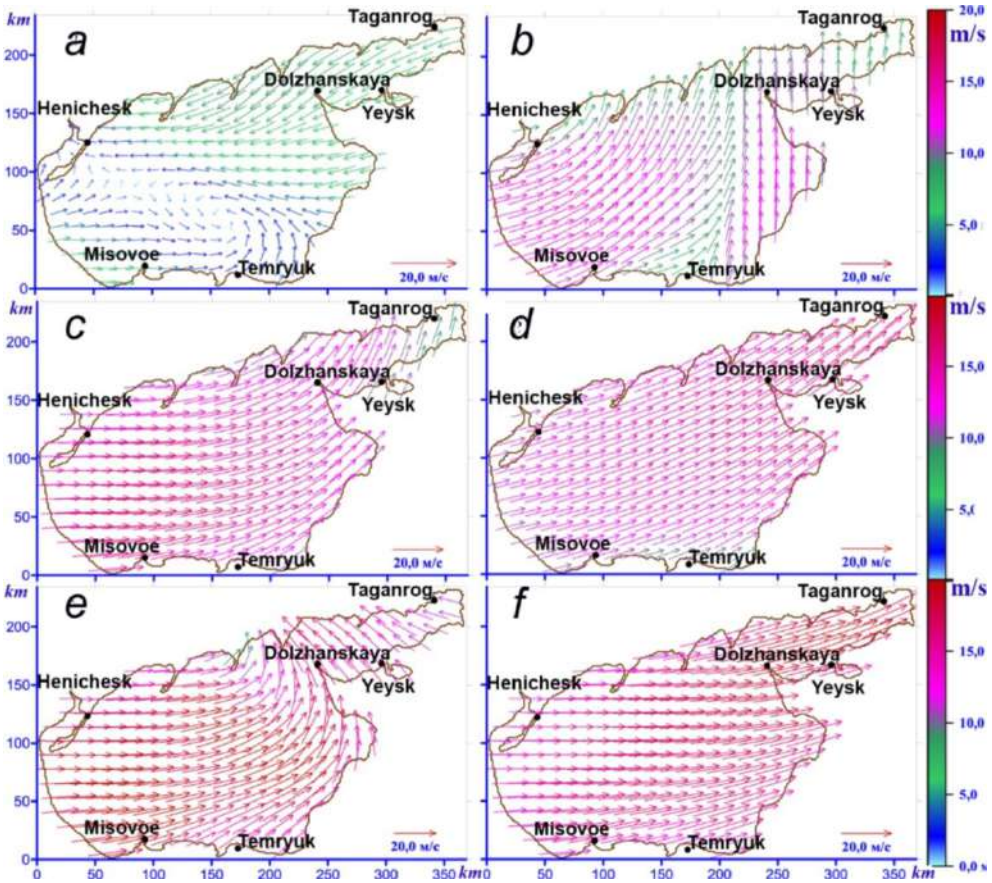

Figure 5.3.2 – Driving wind fields during a storm on March 23–24, 2013:
(*a*) – March 23, 12 h; (*b*) – March 23, 20 h; (*c*) – March 24, 12 h; (*d*) – March 24, 20 h;
during a storm on September 24, 2014; (*e*) – September 24, 12 h;
(*f*) – September 24, 20 h

A change in surface atmospheric pressure has been studied, a sharp drop in which, with the simultaneous impact of strong winds on the sea surface, leads to significant sea level rises. The time course of atmospheric pressure values averaged over the water area

of the Sea of Azov ($\overline{P(t)}$), calculated using the formula (3.2.1) during storm situations in 2013 and 2014, is shown in Figure 5.3.3. As follows from the analysis of the curves marked in red in Figure 5.3.3 (in the period from 20 to 25 the number of time intervals under consideration), storm situations were accompanied by a significant drop in atmospheric pressure. It can be seen that the atmospheric pressure in March 2013 varied from a minimum (995 gPa) to a maximum (1035 gPa). During September 2014, the atmospheric pressure drop was insignificant, but a sharp decrease in atmospheric pressure to 998 gPa is highlighted on the graph (Figure 5.3.3, *b*) during the passage of the cyclone on September 24, 2014.

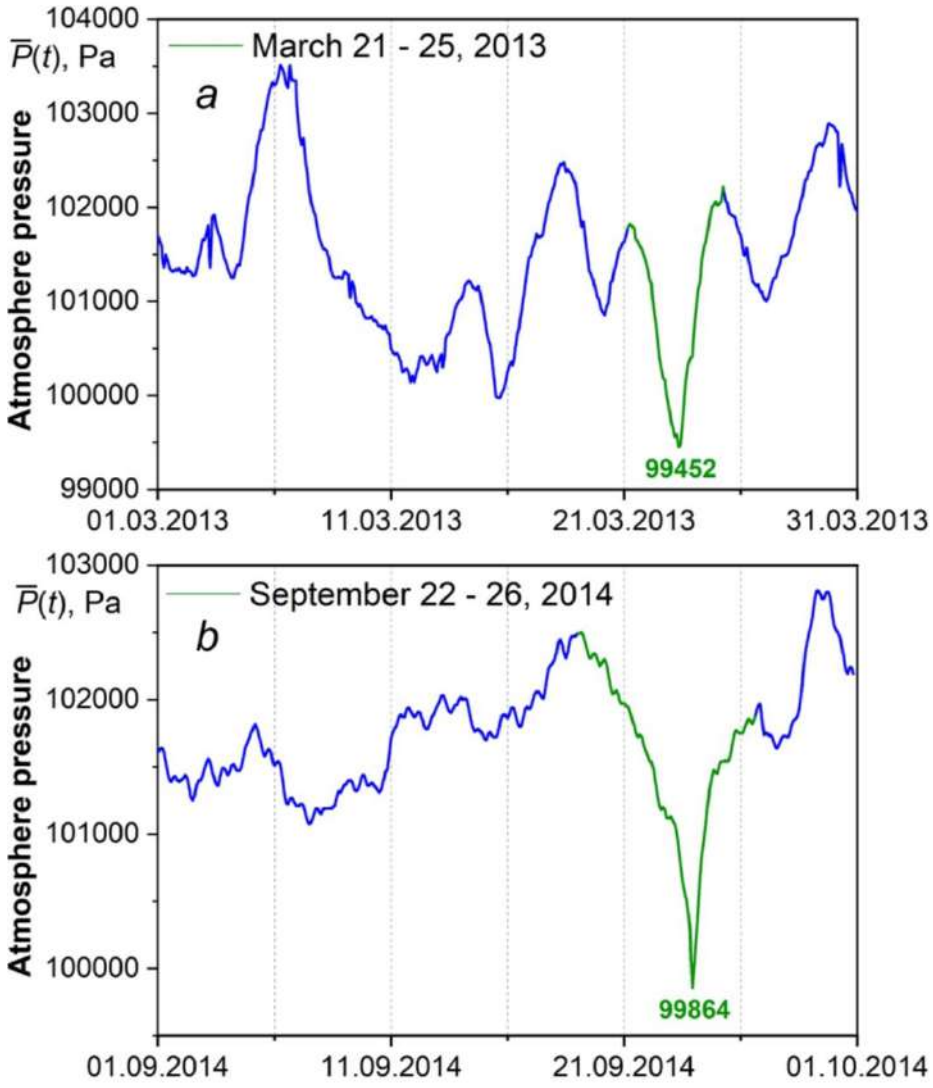

Figure 5.3.3 – Atmospheric pressure, according to the SKIRON model, averaged over the Sea of Azov in March 2013 (*a*) and September 2014 (*b*). Vertical dotted lines are drawn with a discreteness of 5 days

The description and study of the features of the circulation of the waters of the Sea of Azov under extreme Azov phenomena is based on the analysis of observational data and the results of three-dimensional hydrodynamic modeling (POM). Forecasting the consequences of recurring hurricane storms (March 23-24, 2013 and September 24, 2014) in the framework of numerical modeling is based on determining the extreme values of the current velocity and the magnitude of overburden phenomena occurring in the Sea of Azov due to critical atmospheric influences. A comparative analysis of the maximum values of the current velocity ($|\mathbf{U}|_{max}$) during the storms of March 2013 and September 2014 was performed based on the analysis of the data presented in Table 5.3.1.

Table 5.3.1 – Maximum values of the current velocity ($|\mathbf{U}|_{max}$, cm/s) on various horizons of the Sea of Azov, the time of their achievement and their corresponding coordinates (x_{max}, y_{max}, km) during periods of extreme storms

Date	Horizon, m	$\|\mathbf{U}\|_{max}$	x_{max}	y_{max}	Time, apm
March 1–31, 2013	1	2.12	230.23	42.85	March 24 17:00
	3	1.37	240.32	168.72	March 24 17:30
	5	1.33	150.37	41.511	March 24 23:00
	10	0.59	235.34	173.00	March 24 05:00
September 1–30, 2014	1	2.45	221.52	100.43	September 24 05:00
	3	1.57	220.18	100.43	September 24 17:00
	5	0.89	285.96	194.17	September 24 17:00
	10	0.44	89.951	14.73	September 24 19:00

The horizons and coordinates of the highest velocity values during the entire calculation period t ($0 \le t \le 744$ and $0 \le t \le 720$ h) are indicated here, as well as the time of the onset of the maxima. The analysis of the maximum currents velocities (Table 5.3.1) caused by the action of storm winds with a significant drop in atmospheric pressure showed that the values of $|\mathbf{U}|_{max}$ in the surface layer exceeded 2 m/s (2.12 m/s in March 2013 and 2.45 m/s in September 2014). Although the current velocities in the bottom

layer were somewhat lower (0.59 and 0.44 m/s), they reached values capable of causing intense lithodynamic processes in the coastal zone of the sea. Extremes of surface current velocities were observed in the Taganrog Bay and in the Dolzhansky Strait area. The maximum currents velocities in the bottom layer were observed near the Taganrog Bay and in the area of Genichesk. Figures 5.3.4 and 5.3.5 show the spatial distributions of the current velocity in the Sea of Azov at different horizons at time points corresponding to the extreme values of the surface current velocity given in Table 5.3.1.

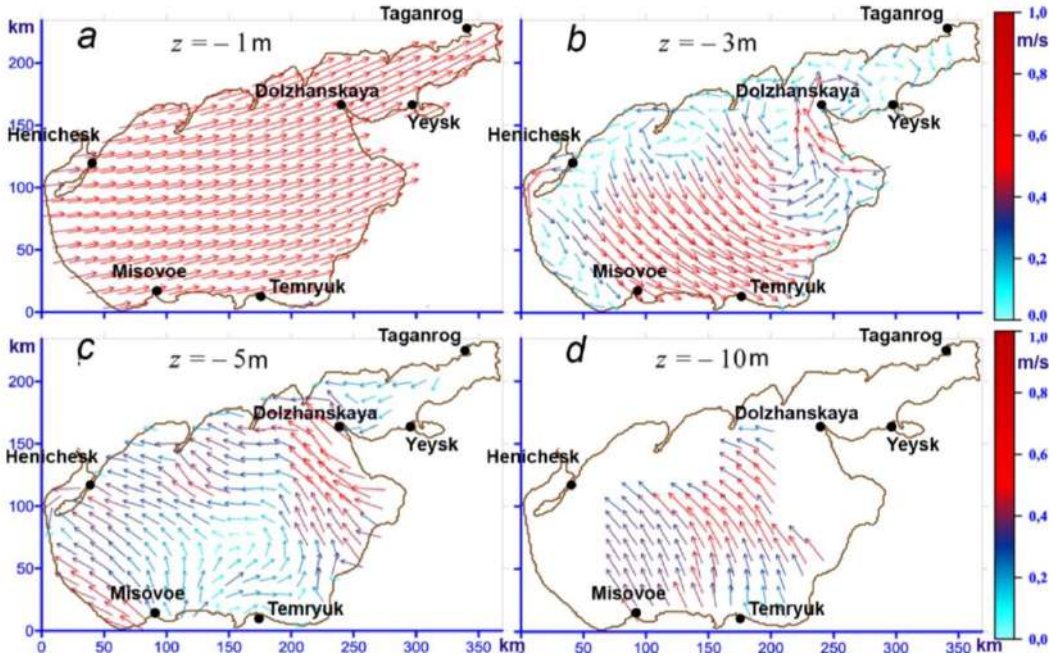

Figure 5.3.4 – Current fields during the storm on March 24, 2013 on the horizons: 1 m (*a*), 3 m (*b*), 5 m (*c*) and 8 m (*d*)

During the period of action of the storm steady southwesterly wind throughout the entire sea area (Figure 5.3.2, d), the direction of currents in the surface layer coincides with the direction of the wind (Figure 5.3.4, a). Starting from a depth of 3 m (Figure 5.3.4, *b*), the currents deviate by 90 degrees or more from the wind direction, eddies of different signs are traced at the entrance to the Taganrog Bay (in the Dolzhansky Strait). In the central part of the water area, a well-defined compensatory current is formed in a layer of 5 m, directed against the wind (Figure 5.3.4, c), at a depth of 8 m, currents

are observed that deviate by 135 degrees or more from the direction of currents in the surface layer of the sea and the direction of the acting wind (Figure 5.3.4, *d*). As follows from 5.3.4, *d*, the currents in the surface (1–3 m) and bottom layers (5–8 m) are directed oppositely. Currents similar in structure are observed during the development of the storm in September 2014 (Figure 5.3.5).

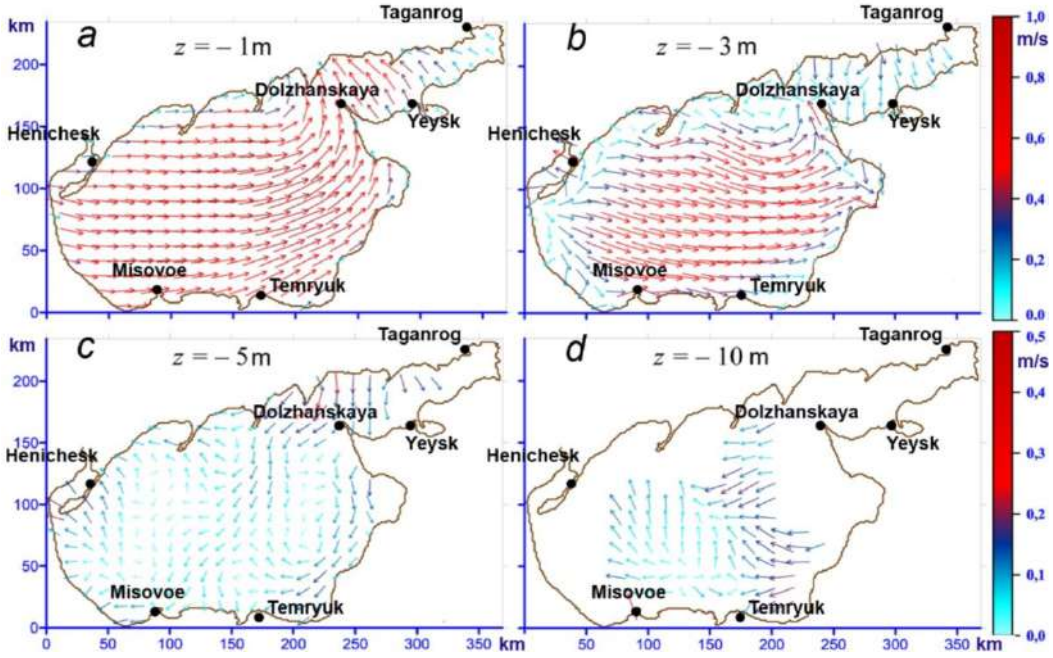

Figure 5.3.5 – Fields of currents during the storm on September 24, 2014 on the horizons: 1 m (*a*), 3 m (*b*), 5 m (*c*) and 8 m (*d*)

The numerical analysis of extreme run-up fluctuations in the Sea of Azov level was carried out in comparison with the observation data of Roshydromet and the Departments of the Ministry of Emergency Situations. According to these data, the flood of March 14, 2013 (the storm of March 23–24, 2013) covered the territory of the delta. The Don (an area of 538 km^2) and the eastern coast of the Taganrog Bay 21 settlements in the Azov, Neklinovsky and Myasnikovsky districts of the Rostov region fell into the flood zone, and the suburbs of Rostov-on-Don, Taganrog and Azov were flooded.

The total damage to the population and administrative facilities amounted to about 76 million rubles. The maximum increase in the level on March 24 reached the levels at MS Tagarog – 7.51 m, Ochakov Spit – 7.41 m, Azov – 7.40 m, Yeysk – 6.10 m and

Primorsko-Akhtarsk – 6.04 m. These settlements and areas of the coast of the Sea of Azov are shown in Figures 3.1 and 3.1.1. During overtaking, the excess of the maximum level over the average annual value for March was 3.40 m in Kagalnik, 2.84 m in Taganrog, 1.40 m in Yeysk and 1.30 m in Primorsko–Akhtarsk. In Genichesk, there was a run-off with a decrease in the level of 0.81 m. During the storm surge on September 24, 2014 in Taganrog, Yeysk and Azov, absolute highs of the level were recorded (7.96, 7.81 and 6.56 m, respectively) for the entire observation period.

The excess of the maximum level over the long–term average in September in Kagalnik reached 3.60 m, Taganrog – 3.35 m, Yeysk – 1.93 m and Primorsko-Akhtarsk – 1.85 m. According to the Ministry of Emergency Situations of Russia in the Krasnodar Territory, there were five settlements in the flood zone (Sadki, Morozovsky, Dolzhanskaya, Yasenskaya ferry, Yeysk). In the Rostov region, 26 settlements fell into the flood zone (Azov, Taganrog, Neklinovsky, Myasnikovsky and Azov districts), 3,091 houses were flooded, and the population was evacuated (971 people).

Table 5.3.2 shows the values of the largest run-up and run-off during the storms of 2013 and 2014, obtained from observations (taking into account long-term averages) and numerical calculations, depending on the wind speed and direction at coastal stations. Wind data are presented based on the results of observations by Roshydromet and the Departments of the Ministry of Emergency Situations. The values given with a minus sign correspond to overclocking.

From the data provided (Table 5.3.2) it can be seen that under the influence of wind with a speed from 17 to 32 m/s, the greatest deviations (1.81 and 1.36 m) in Taganrog occur in the South and South wind directions. According to the calculated data, the maximum slopes are observed in Genichesk and Mysov (0.99 and 0.49 m, respectively). It should be noted that, despite the high wind intensity according to SKIRON, the magnitude of the surges and overcurrentss caused by the storm on March 23–24, 2013 exceeded the extreme fluctuations in the level during the storm on September 24, 2014. This difference is explained by the longer duration of the storm wind (see Figure 5.3.1).

Table 5.3.2 – Dependences of extreme deviations of the Sea of Azov level (m) on the direction and speed of the current wind during the storms of 2013, 2014, according to the data of the coastal network of hydrometeorological stations and the results of modeling

Stations	March 23 – 24, 2013			
	Wind speed, m/s	Wind direction, (in deg. to the *x*-axis)	Sea level deviations	
			Observational data	Simulation results
Henichesk	28	NW, ЗNЗ (315, 292)	–0,94	–0,99
Berdyansk	19	SSW, W (200, 270)	0,39	0,28
Taganrog	19	W, WNW (270, 292)	0,95	0,82
Mariupol	22	WSW, SSW (200)	1,58	1,81
Yeysk	21	SSW, W (200, 270)	—	0,96
Pr.-Akhtarsk	17	W (270)	0,61	0,79
Temryuk	22	SSW, W (200, 270)	0,32	0,31
Opasnoe	20	W, WNW (270, 292)	–0,19	–0,27
Mysovoe	28	W, WNW (270, 292)	–0,61	–0,49
Stations	September 24, 2014			
	Wind speed, m/s	Wind direction, (in deg. to the *x*-axis)	Sea level deviations	
			Observational data	Результаты моделирования
Henichesk	25	SW, W (250, 270)	—	–0,87
Berdyansk	24	SW, W (250, 270)	—	–0,52
Taganrog	25	SSW, SW (225, 250)	—	0,88
Mariupol	32	SW (205, 225)	—	1,36
Yeysk	27	SW, WNW (225, 290)	1,12	1,06
Pr.-Akhtarsk	24	SSW, SW (225, 250)	1,20	1,11
Temryuk	30	SW, W (250, 270)	0,45	0,51
Opasnoe	28	SSW, W (200, 270)	—	–0,47
Mysovoe	25	SW (225, 250)	—	–0,53

From the analysis of the maps of sea level isolines, it follows that during the development of a storm (Figure 4.3.6, *a*), the area of lowering the level along the west coast repeats the geometry of the anticyclonic vortex of the wind field

(see Figure 5.3.2, *a*), has an elliptical shape and shifts from the center. The area of elevated values (up to 0.7 m) of the level is concentrated at the entrance to the Taganrog Bay (near the Dolzhansky Strait, the Long Spit). After 8 h from the beginning of the storm (Figure 4.3.6, *b*), the isoline of zero level amplitudes shifts from the center to the east. The overburden area is moving towards the Don Delta, and the areas of significant level decreases are shifting to the northwestern region of the sea (near Genichesk).

The subsequent development of the dangerous phenomenon and the peak of the storm in March 2013 (Figure 5.3.6, *c*, *d*) lead to the division of the water area by a line of zero amplitudes oriented in the meridional direction into areas of rising and falling levels in the western and eastern parts of the basin. It can be seen that the Taganrog Bay is subject to the strongest effects of overburden processes. Here, the maximum sea level deviations reach 4 m.

Figure 5.3.6, *e*, *f* shows the isolines of the Sea of Azov level during a storm in September 2014. It is noticeable (Figure 5.3.6, *e*) that complex fluctuations in the level are formed in the Taganrog Bay. Here, in a fairly shallow (the average depth of the bay is 9 m) semi-enclosed basin, fluctuations in the level with a nodal line passing through its center are recorded, different in sign. The greatest level rise takes place at the entrance to the estuary. Under the influence of a southwesterly wind with a speed of 25 m/s (Figure 5.3.6, *e*), sea level deviations acquire common features with maps of the storm level in 2013. (Figure 5.3.6, *d*) with the division of the water area into areas of elevation and depression (in the eastern and western parts of the sea).

In order to verify the simulation results, the values of the run-off and run-up obtained as a result of the simulation were compared with the data of field measurements for the same period, shown in the tables of hourly values of sea level altitude by the State Hydrometeorological service. For this purpose, data from observations of the level at coastal hydrometeorological stations and posts of the Sea of Azov and the Taganrog Bay in March 2013 and September 2014 were used. These observations are level measurements using recorders at MS Taganrog, Temryuk, Yeysk and Primorsko-Akhtarsk, as well as measurements with a 6-h footstock discreteness at other points along the coast of the Azov basin.

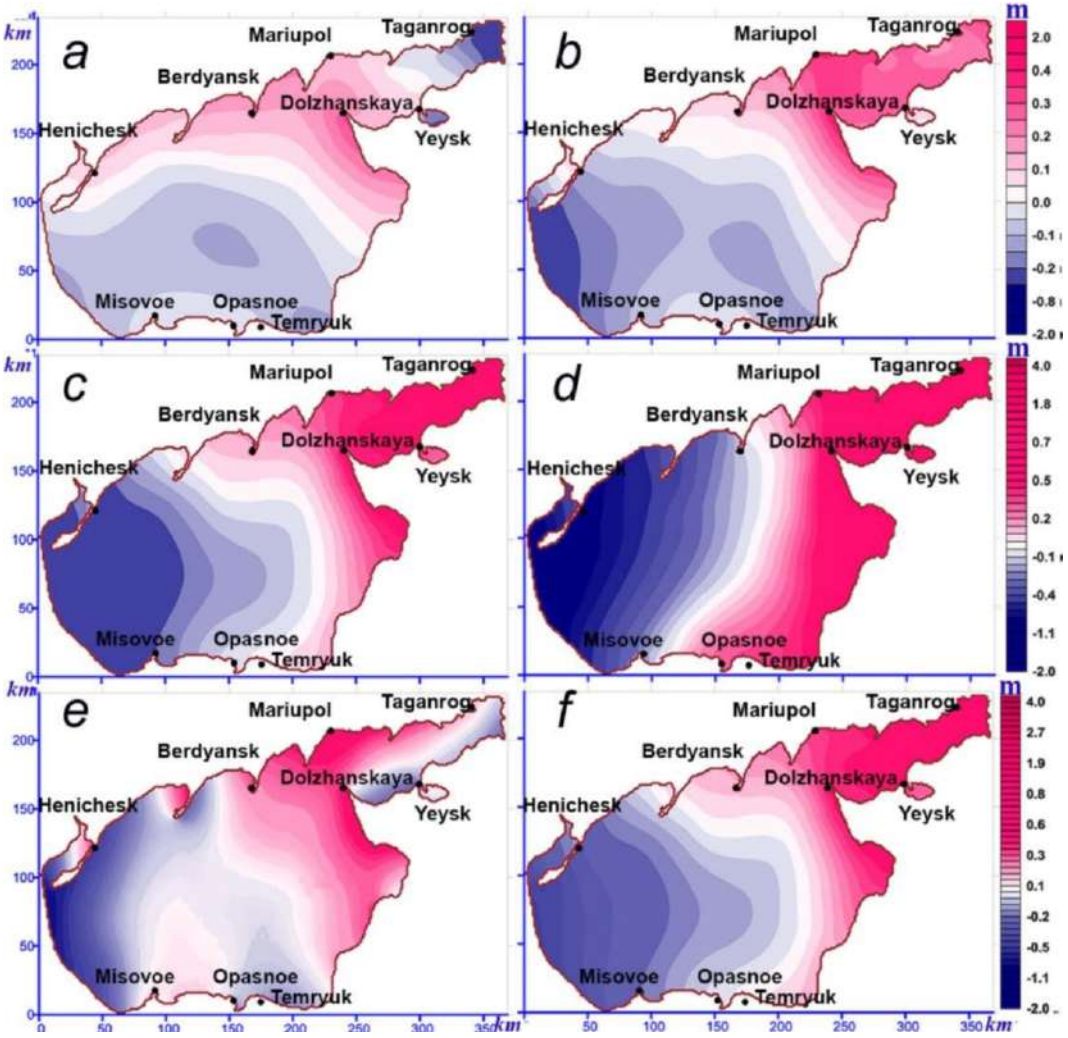

Figure 5.3.6 – Fields of the Sea of Azov level at the same time points as in Figure 5.3.2

Graphs of the sea level during March 2013 at the stations of Taganrog and Primorsko-Akhtarsk, obtained from observations and as a result of modeling, are shown in Figure 5.3.7. The analysis of the level charts indicates a relatively good correspondence of the fluctuation trends. Some differences, for example, in the values of the maxima of run-offs and run-offs, are explained by certain errors in measurements and calculations. Thus, in Taganrog (2013), the calculated maximum of overburden is 14% higher than according to observational data, and in Primorsko-Akhtarsk (2014), the maximum value of overburden is 8% less than the measured one.

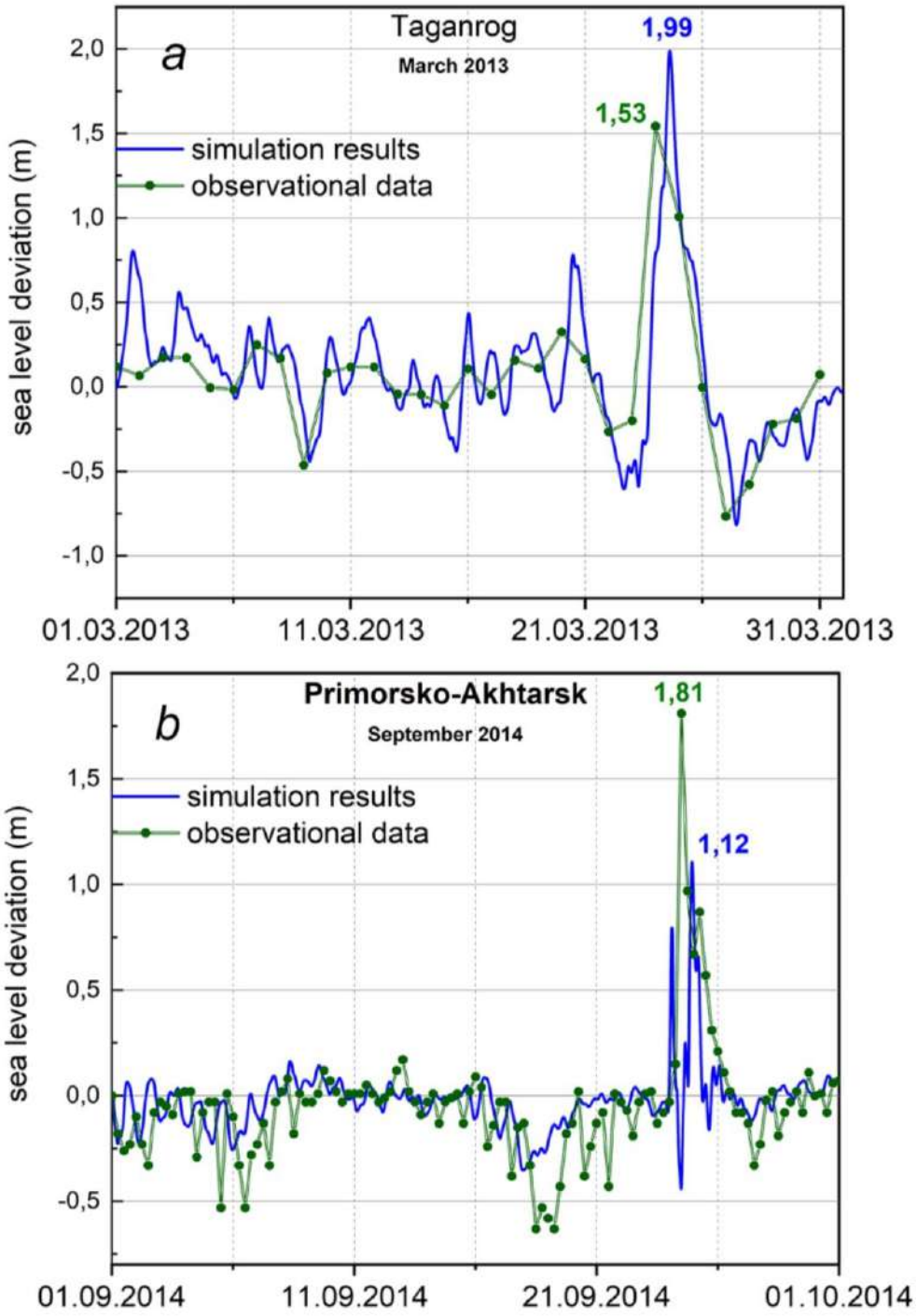

Figure 5.3.7 – Sea level deviations (m) according to direct measurements and simulation results: at the Taganrog station in March 2013 (*a*); at the Primorsko-Akhtarsk in September 2014 (*b*). Vertical dotted lines were drawn with a discreteness of 5 days [Numerical study..., 2017]

The simulation data showed that during the extreme storms of 2013 and 2014, the entire water area of the Sea of Azov, as a result of the action of the storm wind,

is conditionally divided by a line of zero amplitudes oriented in the meridional direction into separate areas of elevation and lowering in the western and eastern parts of the basin. The Taganrog Bay is most strongly affected by overburden processes during the action of extreme winds, where the maximum sea level deviations, according to numerical calculations, are 1.8–2.2 m. Extremes in the velocity of surface currents were observed in the Taganrog Bay and in the Dolzhansky Strait area. The maximum currents velocities in the bottom layer were observed near the Taganrog Bay and in the area of Genichesk [Numerical study ... , 2017]. This result is confirmed by comparing sea level measurements with calculation data using the POM hydrodynamic model for the forecast scenario November 1 - 30, 2007, described in detail in [Cherkesov, Shulga, Waves, Currents..., 2017, Ivanov, Cherkesov, Shulga, Computer..., 2011].

5.4. Forecasting the size of the area of flooding (drainage) in the coastal strip of the Sea of Azov with overburden winds

Level changes resulting from overburden phenomena and accompanied by shallowing of fairways during overburden, flooding of islands, shores, destruction of port facilities, occur, as a rule, in areas off the coast with gentle underwater slopes, as well as in bays and narrow straits (Lake Donuzlav, Taganrog, Finnish, Ob bays lip, etc.). The observed values of run-up fluctuations in the Sea of Azov level have significant amplitudes, which leads to the occurrence of dangerous and catastrophic phenomena on the coast. A reasonable representation and forecast of the consequences of extreme overburden events in its coastal zone is possible using three-dimensional modeling, in addition to a fairly complete database of instrumental observations of the Azov basin.

This approach, based on a numerical study of overburden processes and currents in the Azov basin, is applicable to assess the interaction of sea level fluctuations with the shore that occur when it rises (decreases). The most important consequences of extreme sea level rises include not only flooding of the coastal area with its waters, but also the activation of abrasive and accumulative processes on it. In addition, with an increase in its level, it becomes likely that salty sea waters will penetrate into some aquifers of

rocks used for the water supply of settlements. The use of modeling results contributes to the competent design of hydraulic engineering and civil structures, taking into account the forecasts obtained with its help. The study of such issues is also interesting from a theoretical point of view.

By analyzing the results of three-dimensional hydrodynamic modeling, it is possible to assess risks and damages caused by sea level changes that cause flooding (drainage) of large coastal areas with complex terrain. As a rule, in practical calculations it is required to determine only the size of the maximum flooding area (drainage). It is also of scientific and practical interest to study the maximum extent of flooding (drainage) territories depending on the parameters of atmospheric influences.

Figure 5.4.1 schematically shows the layouts of drainage and flooding areas in the coastal area of the sea. Here the x−axis is with an undisturbed sea surface; OO_1 is the sea level at the time of maximum run−up (in Figure 5.4.1, left) or OO_1 is the sea level at the time of maximum run−up (in Figure 5.4.1, right); α is the angle of inclination of the coastal slope; β is the angle of elevation of the coastal surface, which in this case is assumed to be flat. To find the dimensions of the dehumidification region BB_1~BO_1, we use the well–known geometry ratio $BO_1 = (OO_1^2 + OO_1^2 tg^{-2}\alpha)^{1/2}$, from which follows $BO_1 = OO_1 \sin^{-1}\alpha$.

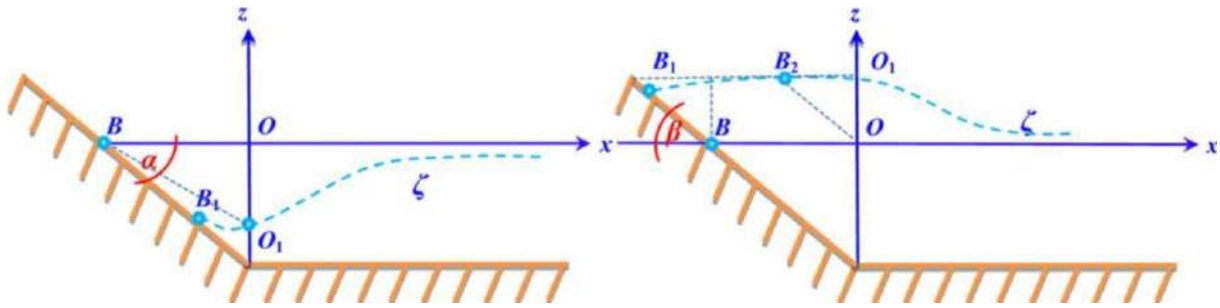

Figure 5.4.1 – Geometry of the bottom relief and a diagram of the drainage area (left) and flooding (right)

The distance from the coastline to the boundary of the possible drainage area (BB_1) in this area is determined by the known values of the maximum slope OO_1 and the angle of inclination of the coastal slope (α). Similarly, we write down the ratio that allows us to find the extent of the flooding area $BB_1 \sim OB_2$: for $BO_1 = (OO_1^2 + OO_1^2 tg^{-2}\beta)^{1/2}$ and $BO_2 = OO_1 \sin^{-1}\beta$.. Then, using the known value of the OO_1 surge and the angle of elevation of the coastal surface (β), we determine the distance of the boundary of the possible flooding area (BB_1) from the coastline in this area.

It should be noted that the values of the angles of inclination and elevation of the coast from 1° to 4° are characteristic for the Sea of Azov. By giving the specified values, we obtain a forecast of the size of the flooding and drainage areas depending on the direction and speed of the long-term quasi-homogeneous wind, the components of which are set based on the expression (2.1.1.1). The simulation is performed taking into account water exchange with the Black Sea using the condition of free passage of liquid through the strait (2.1.1). A variant of the calculation area is used, including the Sea of Azov and the Kerch Strait with a liquid boundary running along 45.25°N (the red line in Figure 1.2.2, on the left). The results of the simulation, the purpose of which was to predict the maximum value of seawater penetration on the coast or its retreat from the coastline, are shown in tables 5.4.1 – 5.4.8.

The data provided in these tables allowed us to establish the dependence of the maximum size of the flooding area (drainage) on the rise (lowering) of sea level caused by overburden winds of various directions, described in more detail in [Shulga, 2013]. Table 5.4.1 shows the linear dimensions of the boundary of the sea water indentation from the coastline in the western and eastern parts of the coast of the Sea of Azov caused by the action of the westerly wind at speeds of $|\mathbf{W}|_{st}^1 = 5$, $|\mathbf{W}|_{st}^2 = 10$, $|\mathbf{W}|_{st}^3 = 15$ and $|\mathbf{W}|_{st}^4 = 20$ m/s, depending on from the angle of inclination (elevation) of the coastal area.

Table 5.4.1 – Slopes and linear dimensions of the drainage area depending on the slope (α, °) of the coastal slope of the Sea of Azov with a west wind

Stations	Wind speed, m/s	Run-offs, m	The boundary of the drainage area, m			
			$\alpha_1 = 1°$	$\alpha_2 = 2°$	$\alpha_3 = 3°$	$\alpha_4 = 4°$
Henichesk	5	0.11	5.73	2.87	1.91	1.43
	10	0.39	22.35	11.17	7.45	5.59
	15	1.04	59.59	29.8	19.87	14.91
	20	2.10	120.33	60.17	40.13	30.1
Berdyansk	5	0.13	7.45	3.72	2.48	1.86
	10	0.34	19.48	9.74	6.5	4.87
	15	0.46	20.63	10.32	6.88	5.16
	20	0.68	38.96	19.48	12.99	9.75
Mysovoe	5	0.05	2.86	1.43	0.96	0.72
	10	0.22	12.61	6.3	4.2	3.15
	15	0.52	29.8	14.9	9.94	7.45
	20	0.96	55.01	27.51	18.34	13.76

It was previously shown (paragraph 3.1, Figure 3.1.2, a) that the prolonged action of the westerly wind causes a decrease in the level along the western coast of the Sea of Azov (overcurrentss), and a gradual increase in the level (surges) occurs near the eastern shore. As a result, wind action leads to the formation of areas of drainage (in the western part) and flooding (in the eastern part) on the corresponding sections of the coast of the Sea of Azov.

Table 5.4.2 shows the values of the maximum run-up and the size of the flooding areas in the areas of stations located along the eastern coast: Mariupol, Taganrog, Yeysk, Primorsko-Akhtarsk, Temryuk and Dangerous.

Table 5.4.2 – Surges and linear dimensions of the flooding area depending on the rise (β, °) of the coastal slope of the Sea of Azov with a west wind

Stations	Wind speed, m/s	Surcharges, m	The boundary of the flooding area, m			
			$\beta_1 = 1°$	$\beta_2 = 2°$	$\beta_3 = 3°$	$\beta_4 = 4°$
Mariupol	5	0.08	4.58	2.29	1.53	1.15
	10	0.29	16.62	8.31	5.54	4.16
	15	0.70	40.11	20.06	13.38	10.03
	20	1.28	73.34	36.68	24.46	18.35
Taganrog	5	0.17	9.74	4.87	3.25	2.44
	10	0.6	34.38	17.19	11.46	8.6
	15	1.42	81.36	40.69	27.13	20.36
	20	2.54	145.54	72.78	48.53	36.41
Yeysk	5	0.1	5.73	2.87	1.91	1.43
	10	0.38	21.77	10.89	7.26	5.45
	15	0.92	52.71	26.36	17.58	13.19
	20	1.7	97.41	48.71	32.48	24.37
Primorsko-Akhtarsk	5	0.09	5.16	2.58	1.72	1.29
	10	0.34	19.48	9.74	6.5	4.87
	15	0.91	52.14	26.07	17.39	13.05
	20	1.79	102.56	51.29	34.2	25.66
Temryuk	5	0.05	2.86	1.43	0.96	0.72
	10	0.21	12.03	6.02	4.01	3.01
	15	0.56	32.09	16.05	10.7	8.03
	20	1.09	62.46	31.23	20.83	15.63
Opasnoe	5	0.03	1.72	0.86	0.57	0.43
	10	0.12	6.88	3.44	2.29	1.72
	15	0.32	18.34	9.17	6.11	4.59
	20	0.6	34.38	17.19	11.46	8.6

Table 5.4.3 shows the maximum slopes and sizes of drainage areas at the coastal stations of Mariupol, Taganrog, Yeysk, Primorsko-Akhtarsk, Temryuk and Dangerous when the east wind, homogeneous in time and space, is selected as a disturbing factor.

Table 5.4.3 – Slopes and linear dimensions of the drainage area depending on the slope (α, °) of the coastal slope of the Sea of Azov with an east wind

Stations	Wind speed, m/s	Run-offs, m	The boundary of the drainage area, m			
			$\alpha_1 = 1°$	$\alpha_2 = 2°$	$\alpha_3 = 3°$	$\alpha_4 = 4°$
Mariupol	5	0.08	4.58	2.29	1.53	1.15
	10	0.18	10.31	5.16	3.44	2.58
	15	0.86	49.28	24.64	16.43	12.33
	20	1.35	77.35	38.68	25.79	19.35
Taganrog	5	0.16	9.17	4.58	3.06	2.29
	10	0.69	39.54	19.77	13.18	9.89
	15	1.73	99.13	49.57	33.06	24.8
	20	2.3	131.79	65.9	43.95	32.97
Yeysk	5	0.11	6.30	3.15	2.10	1.58
	10	0.49	28.08	14.04	9.36	7.02
	15	1.22	69.9	34.96	23.31	17.49
	20	1.54	88.24	44.13	29.43	22.08
Primorsko-Akhtarsk	5	0.13	7.45	3.72	2.48	1.86
	10	0.57	32.66	16.33	10.89	8.17
	15	1.42	81.36	40.69	27.13	20.36
	20	1.81	103.71	51.86	34.58	25.95
Temryuk	5	0.07	4.01	2.01	1.34	1.00
	10	0.3	17.19	8.6	5.73	4.3
	15	0.74	42.4	21.2	14.14	10.61
	20	1.24	71.05	35.53	23.69	17.78
Opasnoe	5	0.04	2.29	1.15	0.76	0.57
	10	0.22	12.61	6.30	4.20	3.15
	15	0.43	24.64	12.32	8.22	6.16
	20	0.64	36.67	18.34	12.23	9.17

Numerical experiments were carried out for the same values of the slope angles of coastal areas and the values of the elevation angles of coastal areas. Table 5.4.4 shows the values of the maximum run-up and the size of the flooding areas in the areas of the stations Genichesk, Berdyansk and Mysovoye caused by the action of the east wind at speeds of 5, 10, 15 and 20 m/s.

Table 5.4.4 – Surges and linear dimensions of the flooding area depending on the rise (β, °) of the coastal slope of the Sea of Azov with an easterly wind

Stations	Wind speed, m/s	Surcharges, m	The boundary of the flooding area, m			
			$\beta_1 = 1°$	$\beta_2 = 2°$	$\beta_3 = 3°$	$\beta_4 = 4°$
Henichesk	5	0.12	6.88	3.44	2.29	1.72
	10	0.53	30.37	15.19	10.13	7.6
	15	1.32	75.63	37.82	25.22	18.92
	20	1.87	107.15	53.58	35.73	26.81
Berdyansk	5	0.04	2.29	1.15	0.76	0.57
	10	0.18	10.31	5.16	3.44	2.58
	15	0.45	25.78	12.89	8.6	6.45
	20	0.52	29.8	14.9	9.94	7.45
Mysovoe	5	0.01	0.57	0.29	0.19	0.14
	10	0.05	2.86	1.43	0.96	0.72
	15	0.12	6.88	3.44	2.29	1.72
	20	0.18	8.96	5.48	3.99	2.50

Forecasting the size of the territory of possible drainage and flooding is feasible on the basis of a series of numerical experiments in which the south wind, homogeneous in time and space, is selected as a disturbing factor. This wind is directed from south to north and acts at a speed of $|\mathbf{W}|_{st}^{l}$; $l = 1, 2, \ldots, 4$. Numerical experiments were carried out for the same values of the slope angles of coastal areas and the values of the elevation angles of coastal areas. The south wind causes currents, the fields of which are a mirror image of the fields of currents arising from the north wind. The effect of this wind leads to the occurrence of overcurrentss at the stations of Genichesk, Berdyansk, Mariupol,

Taganrog and Yeysk. At the same time, overburden processes take place at the stations Primorsko-Akhtarsk, Temryuk, Dangerous and Mysovoye. Table 5.4.5 shows the values of the drainage areas in the areas of these stations, depending on the wind speed, the angle of inclination of the coastal area and the magnitude of the maximum run-off.

Table 5.4.5 – Slopes and linear dimensions of the drainage area depending on the slope (α, °) of the coastal slope of the Sea of Azov with a south wind

Stations	Wind speed, m/s	Run-offs, m	The boundary of the drainage area, m			
			$\alpha_1 = 1°$	$\alpha_2 = 2°$	$\alpha_3 = 3°$	$\alpha_4 = 4°$
Henichesk	5	0.01	0.57	0.29	0.19	0.14
	10	0.03	1.72	0.86	0.57	0.43
	15	0.08	4.58	2.29	1.53	1.15
	20	0.25	14.32	7.16	4.78	3.58
Berdyansk	5	0.06	3.44	1.72	1.15	0.86
	10	0.24	13.75	6.88	4.59	3.44
	15	0.63	36.1	18.05	12.04	9.03
	20	0.91	52.14	26.07	17.39	13.05
Mariupol	5	0.11	6.3	3.15	2.1	1.58
	10	0.41	23.49	11.75	7.83	5.88
	15	0.92	52.71	26.36	17.58	13.19
	20	1.14	65.32	32.67	21.78	16.34
Taganrog	5	0.21	12.03	6.02	4.01	3.01
	10	0.76	43.55	21.78	14.52	10.9
	15	1.67	95.69	47.85	31.91	23.94
	20	2.06	118.04	59.03	39.36	29.53
Yeysk	5	0.05	2.86	1.43	0.96	0.72
	10	0.18	10.31	5.16	3.44	2.58
	15	0.4	22.92	11.46	7.64	5.73

Table 5.4.6 shows the size of the flooding sites in the areas of Primorsko-Akhtarsk, Temryuk, Dangerous and Mysovoye stations caused by the action of south wind speeds of 5, 10, 15 and 20 m/s. Analysis of the extent of the territories of possible drainage and flooding caused by a uniform wind blowing in a meridional direction from north to south for the same values of the slope angles of coastal areas. The effect of this wind leads to the occurrence of overcurrentss at the stations Primorsko-Akhtarsk, Temryuk, Dangerous, Mysovoye and overcurrentss at the stations Genichesk, Berdyansk, Mariupol, Taganrog and Yeysk.

Table 5.4.6 – Surges and linear dimensions of the flooding area depending on the rise (β, °) of the coastal slope of the Sea of Azov with a south wind

Stations	Wind speed, m/s	Surcharges, m	The boundary of the flooding area, m			
			$\beta_1 = 1°$	$\beta_2 = 2°$	$\beta_3 = 3°$	$\beta_4 = 4°$
Primorsko-Akhtarsk	5	0.03	1.72	0.86	0.57	0.43
	10	0.12	6.88	3.44	2.29	1.72
	15	0.33	18.91	9.46	6.31	4.73
	20	0.5	28.65	14.33	9.55	7.17
Temryuk	5	0.06	3.44	1.72	1.15	0.86
	10	0.28	16.04	8.02	5.35	4.01
	15	0.72	41.26	20.63	13.76	10.32
	20	1.1	63.03	31.52	21.02	15.77
Opasnoe	5	0.07	4.01	2.01	1.34	4.01
	10	0.25	14.32	7.16	4.78	14.32
	15	0.66	37.82	18.91	12.61	37.82
	20	0.83	47.56	23.78	15.86	47.56
Mysovoe	5	0.06	3.44	1.72	1.15	0.86
	10	0.27	15.47	7.74	5.16	3.87
	15	0.66	37.82	18.91	12.61	9.46
	20	0.87	49.85	24.93	16.62	12.47

Tables 5.4.7 and 5.4.8 show the dependences of the maxima of run-off and run-up on the sea coast, as well as the linear dimensions of the boundary of penetration (indentation) of sea waters from the coastline in the western and eastern parts of the coast of the Sea of Azov caused by the action of the north wind, the studied velocities.

Table 5.4.7 – Slopes and linear dimensions of the drainage area depending on the slope (α, °) of the coastal slope of the Sea of Azov with a north wind

Stations	Wind speed, m/s	Run-offs, m	The boundary of the drainage area, m			
			$\alpha_1 = 1°$	$\alpha_2 = 2°$	$\alpha_3 = 3°$	$\alpha_4 = 4°$
Primorsko-Akhtarsk	5	0.01	0.57	0.29	0.19	0.14
	10	0.03	1.72	0.86	0.57	0.43
	15	0.08	4.58	2.29	1.53	1.15
	20	0.25	14.32	7.16	4.78	3.58
Temryuk	5	0.06	3.44	1.72	1.15	0.86
	10	0.24	13.75	6.88	4.59	3.44
	15	0.63	36.1	18.05	12.04	9.03
	20	0.91	52.14	26.07	17.39	13.05
Opasnoe	5	0.11	6.3	3.15	2.1	1.58
	10	0.41	23.49	11.75	7.83	5.88
	15	0.92	52.71	26.36	17.58	13.19
	20	1.14	65.32	32.67	21.78	16.34
Mysovoe	5	0.21	12.03	6.02	4.01	3.01
	10	0.76	43.55	21.78	14.52	10.9
	15	1.67	95.69	47.85	31.91	23.94
	20	2.06	118.04	59.03	39.36	29.53

With a northerly wind, two cycles of opposite signs are generated in the central part of the sea. The larger one (cyclonic) is adjacent to the western shore and contains a small vortex formation. A smaller but more powerful (anticyclonic) one is located in the eastern

part of the sea. In paragraph 3.1. in Figure 3.1.2, the location of the areas of rise and fall of the Sea of Azov caused by the north wind is demonstrated.

Table 5.4.8 – Surges and linear dimensions of the flooding area depending on the rise (β, °) of the coastal slope of the Sea of Azov with a north wind

Stations	Wind speed, m/s	Surcharges, m	The boundary of the flooding area, m			
			$\beta_1 = 1°$	$\beta_2 = 2°$	$\beta_3 = 3°$	$\beta_4 = 4°$
Henichesk	5	0.01	0.57	0.29	0.19	0.14
	10	0.04	2.29	1.15	0.76	0.57
	15	0.09	5.16	2.58	1.72	1.29
	20	0.28	16.04	8.02	5.35	4.01
Berdyansk	5	0.05	2.86	1.43	0.96	0.72
	10	0.23	13.18	6.59	4.39	3.3
	15	0.58	33.23	16.62	11.08	8.31
	20	0.77	44.12	22.06	14.71	11.04
Mariupol	5	0.08	4.58	2.29	1.53	1.15
	10	0.35	20.05	10.03	6.69	5.02
	15	0.88	50.42	25.22	16.81	12.62
	20	1.02	58.44	29.23	19.49	14.62
Taganrog	5	0.12	6.88	3.44	2.29	1.72
	10	0.51	29.22	14.61	9.74	7.31
	15	1.28	73.34	36.68	24.46	18.35
	20	1.75	100.27	50.14	33.44	25.09
Yeysk	5	0.02	1.15	0.57	0.38	0.29
	10	0.07	4.01	2.01	1.34	1
	15	0.17	9.74	4.87	3.25	2.44
	20	0.41	23.49	11.75	7.83	5.88

Analyzing the results presented in Tables 4.4.1–4.4.8, we find that the Taganrog Bay is most affected by overburden processes, the maximum sea level deviations occur

here with winds of various directions. Which in turn leads to the greatest flooding or drainage of the coastal areas adjacent to this bay.

Figure 5.4.2 shows the location of the area of possible flooding caused by a uniform wind acting in a zonal direction from east to west at a speed of 20 m/s for the most gentle slope ($\alpha_1 = 1°$).

Figure 5.4.2 – Areas of possible flooding of the Azov Sea coast

The areas of possible flooding in the Taganrog region caused by a uniform wind acting in a zonal direction from west to east at a speed of 20 m/s, depending on the angle of elevation of the coast, and draining under the influence of an easterly wind of the same speed, depending on the angle of inclination of the bottom area are shown in Figure 5.4.3, *a*.

Figure 5.4.3, b shows the areas of possible flooding and drainage in the area of Genichesk, generated by a uniform wind acting in a zonal direction from east to west at a speed of 20 m/s, depending on the angle of elevation of the coastal area: line 1 – at $\beta_1 = 1°$, line 2 – at $\beta_2 = 2°$, line 3 – at $\beta_3 = 3°$, as well as from the angle of inclination of the bottom area: line 1 – at $\alpha_1 = 1°$, line 2 – at $\alpha_2 = 2°$, line 3 – at $\alpha_3 = 3°$.

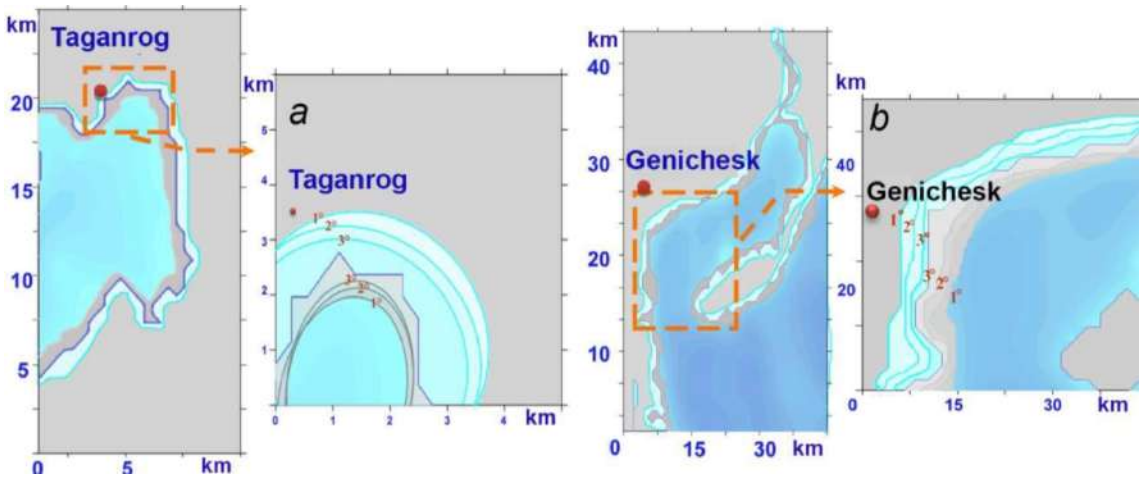

Figure 5.4.3 – Areas of possible flooding (drainage) in the Taganrog (*a*) and Genichesk (*b*) regions caused by a uniform westerly (easterly) wind at a speed of 20 m/s, depending on the angle of inclination of the coastal slope

5.5. Determining the size of drainage and flooding areas on the coast of the Sea of Azov, depending on the intensity of atmospheric fields

The reason for the flooding of the coastal zone or the drainage of the bottom that occurs on the seashore is the response of the aquatic environment to a powerful atmospheric effect that can cause extreme values of current velocity and sea level deviations. The consequence of the interaction of cyclones with the corresponding segments of anticyclones is a significant increase in the baric gradient of atmospheric pressure in the area separating them, as well as an increase in zonal wind (western and eastern points), creating a wind surge of water on the corresponding sections of the coast. Hurricane-force gale-force winds are observed over the Sea of Azov and its coast, capable of tearing roofs off houses, overturning small buildings, and uprooting trees. During one of the hurricanes in 1914, the level of the Sea of Azov and estuaries in the Temryuk area rose 3 m above the ordinary (from the average long-term level). The vast expanses of the Azov lowland between Temryuk and Achuyevskaya spit were flooded [Hydrometeorological ... , 1986; Hydrometeorological ..., 2009]. Gale-force winds from the north-east and east directions, on the contrary, cause a strong run-off of water along

the eastern coast of the sea and a surge of water into the Sivash. For example, in the Yeysk area, there were cases when the bottom of the sea was exposed tens of meters from the shore, and in 1946 a case of sea retreat by 1.5 km was recorded. In the Taganrog area, the water sometimes moved away from the shore by more than 5 km [Chernyakova, 1965].

Based on the analysis procedure described in clause 5.4, we will compare the size of the territories of possible drainage and flooding caused by constant wind (with non-stationary atmospheric effects of the SKIRON model), as well as as a result of the combined action of non-stationary disturbances and background stationary currents. Knowing the maximum amount of overburden and the angle of inclination (elevation) of the relief of the coastal zone (α), we determine the size of the maximum possible area of drainage (flooding) caused by the action of wind in various coastal areas.

Table 5.5.1 shows the dimensions of the areas of flooding (upper part of the table) and drainage (lower part) caused by the action of stationary and predictive winds in the coastal areas of the Sea of Azov. From the analysis of the above data, it follows that under the influence of the $\mathbf{W}_{st}^{2} + \mathbf{W}_{SKIRON}$ wind, the Primorsko-Akhtarsk area is exposed to the greatest flooding (21.8 m). At the same time, the length of the drainage area in the Genichesk area (16.2 m) exceeds the values obtained for other coastal territories. Comparing the values of the flooding and drainage areas for different angles of inclination of the coastal zone, we note that with an increase in these angles, the sizes of the flooding and drainage areas decrease.

So, if $\alpha = 3°$ the greatest flooding occurs at $\mathbf{W}_{st}^{1,2}$ in Mariupol (4 and 11.9 m), at $\mathbf{W}_{SKIRON}$ – in Primorsko-Akhtarsk (15.4 m), at $\mathbf{W}_{st}^{1,2} + \mathbf{W}_{SKIRON}$ – in Yeysk (19.5 m) and in Primorsko-Akhtarsk (10.9 m), respectively. If $\alpha = 1.5°$ the greatest flooding occurs at $\mathbf{W}_{st}^{1,2}$ in Mariupol (7.9 and 23.8 m), at $\mathbf{W}_{SKIRON}$ – in Primorsko-Akhtarsk (30.7 m), at $\mathbf{W}_{st}^{1,2} + \mathbf{W}_{SKIRON}$ — in Yeysk (39 m) and in Primorsko-Akhtarsk (21.8 m), respectively. At $\mathbf{W}_{SKIRON}$ and $\mathbf{W}_{st}^{1,2} + \mathbf{W}_{SKIRON}$, the greatest dehumidification for all values of angles is observed in Genichesk. So, for $\alpha = 1.5°$, the sizes of these areas are 29.2; 33.2 and 16.2 m, respectively [Cherkesov, Shulga, Impact Study ..., 2017].

Table 5.5.1 – Linear dimensions of flooding and drainage areas (m) in the areas of coastal settlements of the Sea of Azov

Stations	W_{st}^1		W_{st}^2		W_{SKIRON}		$W_{st}^1+W_{SKIRON}$		$W_{st}^2+W_{SKIRON}$	
	α=3°	α=1.5°	α=3°	α=1.5°	α=3°	α=1.5°	α=3°	α=1.5°	α=3°	α=1.5°
Henichesk	—	—	—	—	6.2	12.3	11.9	23.8	4.9	9.7
Berdyansk	1.9	3.7	7.1	14.2	3.2	6.5	8.5	16.9	1.7	3.5
Taganrog	4.0	7.9	11.9	23.8	8.9	17.7	15.4	30.7	5.6	11.2
Mariupol	2.6	5.3	10.0	19.9	12.1	24.1	17.1	34.2	9.7	19.3
Yeysk	1.5	3.1	8.3	16.5	14.5	29.0	19.5	39.0	7.3	14.6
Pr.-Akhtarsk	1.9	3.9	5.1	10.3	15.4	30.7	17.4	34.8	10.9	21.8
Temryuk	—	—	—	—	5.7	11.3	9.5	19.1	4.7	9.4
Opasnoe	—	—	—	—	3.1	6.2	6.5	13.0	1.8	3.6
Mysovoe	2.3	4.7	9.9	19.8	3.7	7.5	6.5	13.1	2.3	4.6
Henichesk	0.8	1.5	3.4	6.7	14.6	29.2	16.6	33.2	8.1	16.2
Berdyansk	—	—	—	—	5.9	11.8	11.9	23.7	3.3	6.6
Taganrog	—	—	—	—	5.0	9.9	7.6	15.2	3.5	7.0
Mariupol	—	—	—	—	8.1	16.2	13.9	27.8	5.5	11.1
Yeysk	—	—	—	—	7.9	15.7	8.7	17.3	3.6	7.2
Pr.-Akhtarsk	—	—	—	—	4.5	9.1	6.8	13.6	2.7	5.4
Temryuk	0.6	1.3	2.1	4.2	2.1	4.3	6.3	12.6	1.7	3.3
Opasnoe	1.9	3.7	7.1	14.2	3.9	7.8	5.8	11.5	2.0	4.0
Mysovoe	—	—	—	—	7.5	15.1	12.2	24.4	4.3	8.5

We use the above procedure for estimating the linear dimensions of the areas of drainage and flooding of the Azov Sea coast during the period of extreme Azov winds observed on March 23–24, 2013 and September 24, 2014. Table 5.5.2 shows the extreme values of run-up and run-down for coastal stations of the Sea of Azov, calculated from the wind and atmospheric pressure fields of the SKIRON model. Here are the sizes of the flooding (drainage) sites in the areas of these stations, depending on the angle of inclination of the coastal area and the magnitude of the sea level deviation.

Table 5.5.2 – Extreme surges and overcurrentss (ζ_{extr}) the Sea of Azov, linear dimensions of areas of flooding (drainage) in areas of coastal settlements caused by extreme storms

Stations	March 1–31, 2013				September 1–30, 2014			
	ζ_{extr}, m	The size of the flooding (drainage*[1]), m			ζ_{extr}, m	The size of the flooding (drainage*), m		
		α = 0,5°	α = 1°	α = 3°		α = 0,5°	α = 1°	α = 3°
Henichesk	1.07*	122.6*	61.3*	20.4*	1.03	118.0	59.0	19.7
Berdyansk	1.23	140.9	70.5	23.5	1.57	179.9	90.0	30.0
Taganrog	0.73	83.7	41.8	13.9	–1.08	123.8*	61.9*	20.6*
Mariupol	2.14	245.2	122.6	40.9	2.94	336.9	168.5	56.2
Yeysk	1.68	192.5	96.3	32.1	1.11	127.2	63.6	21.2
Pr.-Akhtarsk	1.08	123.8	61.9	20.6	–0.58	66.5*	33.2*	11.1*
Temryuk	0.56	64.2	32.1	10.7	1.34	153.6	76.8	25.6
Opasnoe	1.35	154.7	77.4	25.8	0.42	48.1	24.1	8.0
Mysovoe	1.23*	140.9*	70.5*	23.5*	0.76	87.1	43.5	14.5

From the analysis of the data presented in Table 5.5.2, it follows that the greatest surges during storm situations occurred in Taganrog (2.14 and 2.94 m). As a result, extensive flood areas appeared in this area, extending into the land 360 m from the water's edge and occupying up to 517.9 km^2 of the coastal area according to observations. According to the calculated data, the maximum slopes were observed in Genichesk and Mysovoe (1.07 and 1.23 m). They caused the greatest outcurrents of water at 122 and 140 m from the edge and drainage of coastal areas to 60.1 and 79.5 km^2.

It should be noted that despite the high intensity of the wind (according to the SKIRON model), the values of the run-up and run-off caused by the storm on March 23-24, 2013 exceeded the extreme fluctuations in the level during the "Chernomorka" on September 24, 2014. This difference is apparently explained by the longer duration of the storm wind, see Figure 5.3.1. The results of numerical modeling of extreme Azov

*The values given correspond to overclocking and dehumidification

phenomena confirmed the observed features of these storms off the coast of the Sea of Azov (maximum values of run-off and run-up, current velocities, the extent of the flooding area).

5.6. Conclusions to Chapter 5

The maximum velocities of surface currents caused by the passage of the same cyclone to the west (86, 108, 126 cm/s), the higher the velocity of the background stationary currents existing in the sea. The velocity maxima of non-stationary currents in the field of background currents generated by a stationary wind of higher velocity (10 and 15 m/s) exceed by 1.2 and 1.4 times the lowest value (86 cm/s) achieved with steady motion caused by a low-speed wind (5 m/s). Under the influence of atmospheric disturbances, the velocity of currents increases with depth, the greatest value is noted in the bottom layer. In the near-surface layer of the sea, the current velocities reach 1.25, 1.26 and 1.21 m/s (for southwestern, western and northwestern directions) in the field of stationary currents generated by a constant wind of the highest speed (15 m/s). The direction of movement of the cyclone does not have such a significant effect on reaching the maximum velocity of non-stationary currents. These velocities differ little in the selected directions of movement of cyclones, the difference between the highest and lowest velocity values is 4.1%.

The forecast of flooding (dehumidification) of coastal areas resulting from stable overhanging winds, as well as depending on the intensity of the forecast wind, has been made. The results of numerical modeling of extreme Azov Sea phenomena on March 23-24, 2013 and September 24-25, 2014 confirmed the observed features of these storms off the coast of the Sea of Azov (maximum values of run-off and run-up, current velocities, the extent of the flooding area). Good comparison results indicate the correctness of the numerical modeling strategy, including the choice of a method for calculating the size of the area of possible catastrophic floods (drainages).

The repeatability of overcurrentss and overcurrentss in the regions of the Sea of Azov was studied, which showed that the eastern coast of the sea and the Taganrog

Bay are most often prone to catastrophic overcurrentss (48 of all cases) and overcurrentss (60%). The amplitudes of run-up level fluctuations in these areas of the Sea of Azov often reach 2.0 – 3.5 m. In Taganrog, the amplitude of the run-up oscillations is maximum and is 687 cm.

The atmospheric fields of the SKIRON model, which generally agree well with the data of field observations at coastal meteorological stations, confirmed the fact that the greatest increase in wind speed during the storms of March 2013 and September 2014 occurred over the waters of the Taganrog and Temryuk bays. Numerical analysis of the maximum currents velocities caused by the action of storm winds during the extreme Azov Sea phenomena showed that in the surface layer the maximum currents velocities exceeded 2 m/s (2.12 m/s in March 2013 and 2.45 m/s in September 2014). Although the current velocities in the bottom layer were somewhat lower (0.59 and 0.44 m/s), they reached values capable of causing intense lithodynamic processes in the coastal zone of the sea.

Extremes of surface current velocities were observed in the Taganrog Bay and in the Dolzhansky Strait area. The maximum currents velocities in the bottom layer were observed near the Taganrog Bay and in the area of Genichesk. The Taganrog Bay is most strongly affected by overburden processes. Here, the maximum sea level deviations reach 3 – 4 m.

Chapter 6.
NUMERICAL FORECAST OF THE EVOLUTION OF POLLUTANTS IN THE SEA OF AZOV

The water area of the Sea of Azov and the coastal zones represent a single territorial region that requires the organization of rational nature management and environmental safety. Special attention is paid to the environmental problems of the Sea of Azov due to the ongoing significant anthropogenic impact. The scale of pollution is becoming threatening to the ecosystem and leads to extremely negative consequences [Matishov, Matishov, 2013]. As a rule, large industrial centers are located in coastal areas. Thus, enterprises of ferrous and non-ferrous metallurgy operate on the coast of the Sea of Azov [Ecosystem ... , 2007; Bufetova M.V., 2015]. The main sources of its pollution include water transport and dredging operations that ensure the normal operation of ships in shallow waters. The influence of water transport on the ecosystem of the Sea of Azov is quite great: about 7000 ships pass through the navigable channels dug through shallow waters here every year [Modern ... , 2015].

According to the information on the state of marine and coastal ecosystems obtained during marine expeditions to the NIS “Professor Panov” and “Deneb” of the UNC RAS [Marine Expeditionary Research ... , 2015], an assessment of the water quality of the Sea of Azov was carried out and environmental risk zones were identified. The position of these areas is confirmed by published data from other sources [Krukier, 1991; Matishov, Engebeikin, Savitsky, 2013; Matishov, Matishov, 2013; Drozdov, 2010; Integrated Satellite Monitoring ..., 2011]. According to the results of ecological mapping of the Taganrog Bay water area, it was revealed that a significant part of the ecosystem of the bay is in a disturbed state and has the highest degree of risk when exposed to natural processes and economic activities.

Due to the fact that direct experiments with natural ecosystems are difficult, mathematical modeling is one of the most promising methods for predicting dynamic processes and their impact on the spread of pollution in marine basins. Mathematical modeling makes it possible to carry out the necessary calculations in areas with arbitrary

bottom relief and complex outlines of the coastline. The analysis of the results of these calculations is the basis for forecasts of possible scenarios for the spread of pollution caused by the action of wind and currents, as well as the transformation of the pollution area under the action of buoyancy forces and turbulent diffusion. The simulation results, which make it possible to determine the trajectories of the pollution area and its size, can be used to eliminate the consequences of emergency incidents on land and at sea arising from the intensification of industrial and agricultural activities in the Azov-Black Sea region [Numerical study ... , 2016].

6.1. Reproduction of scenarios for the spread of pollution in various areas of the Sea of Azov with gusts of unsteady wind

Forecasting the environmental impact of accidental pollution discharges into the Sea of Azov was carried out using proprietary software blocks that complement the hydrodynamic POM model. A necessary part of numerical forecasting is meteorological data on regional atmospheric conditions, the location of the discharge source and detailed information about it (setting the depth and shape of the line covering the initial area of pollution), as well as a high-resolution bathymetric map of the Azov Sea basin.

We investigate the effect of sudden gusts of unsteady wind arising in the field of a homogeneous stationary wind on the evolution of pollution areas in various parts of the Sea of Azov. It was previously shown that during the prolonged action of a quasi-stationary wind, steady currents arise in the sea, the speed of which depends on the speed of the acting wind (Chapter 3). The time-variable wind $\mathbf{W}(\mathbf{r}, t)$ (2.1.1.2) begins to affect the sea surface in the field of background stationary wind. The beginning of variable wind gusts is counted from the time of establishment of stationary currents caused by the background constant wind $t = t_{st}$, and its direction is 45° with the direction of this wind $\mathbf{W}_{st}$ (2.1.1.1). From the beginning of the action of the unsteady wind, its speed increases linearly and after 3 h reaches its highest value ($|\mathbf{W}|_{var}$ = 10 m/s), then for 3 h the speed does not change and the next 3 h decreases linearly to zero.

The aim of the numerical experiments, in a formulation with a simple meteorological interpretation, was to substantiate the dependence of the characteristics of the pollution area on the velocity of the background stationary wind $\mathbf{W}_{st}$ and the presence of a non-stationary component $\mathbf{W}_{var}$. Reproduction of the processes of transport and diffusion of pollutants in the Sea of Azov using a three-dimensional hydrodynamic model POM was performed in the field of background steady-state currents generated in various experiments by wind speeds of $|\mathbf{W}|_{st}^1 = 5$, $|\mathbf{W}|_{st}^2 = 10$ and $|\mathbf{W}|_{st}^3 = 15$ m/s.

The areas of the pollution emission centers were selected based on an assessment of the state of the ecosystem of the Sea of Azov [Matishov, Ingebeykin, Savitsky, 2013; Matishov, Matishov, 2013; Modern ..., 2015; Drozdov, 2010; Integrated satellite monitoring ..., 2011]. Each of these areas is characterized by a maximum sea depth (h_{max}). These are shown in Figure 6.1.1: B_1 in the area of East-Kazantip gas field ($h_{max} = 10$ m); B_2 over the deep part of the sea ($h_{max} = 12$ m); B_3 in the Taganrog Bay ($h_{max} = 8$ m) [Study of the influence of ..., 2010].

The release of pollutants occurs on a free surface at time $t_{0p} = t_{st}$, which also corresponds to the beginning of the action of the unsteady wind, the contour of the initial contamination area is limited by a straight circular cylinder with a radius of 9 km. A quantitative assessment of the change over time in the area of the area covered by pollution is determined on individual horizons of the Sea of Azov. The most practically significant conclusions about the change in the size of the area of the area covered by pollution include the results of a study of its evolution in the surface layer $z = z_1$ (z_1 is the depth of the upper calculated σ–layer), in the area of half the depth of the basin $z = -H/2 = h_1$ and in the bottom layer $z = -H + z_b = h_2$ (z_b – is the first point of the grid closest to the bottom).

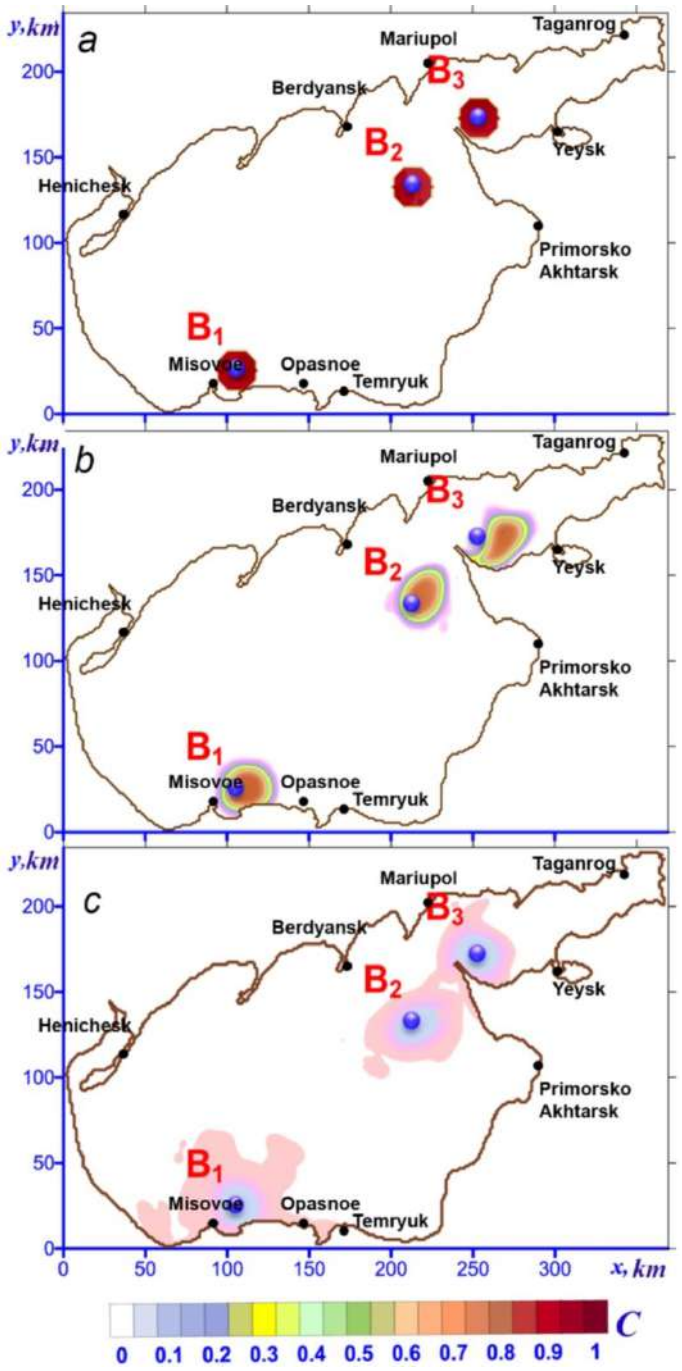

Figure 6.1.1 – Transformation of pollution areas at various points in time: in stationary mode $t = t_0$ (a); at $t = t_0 + 15$ h (*b*); at $t = t_0 + 30$ h (*c*).

We present the largest, according to the conclusions set out in [Modeling ... , 2008; Investigation ... , 2010], parameters of the penetration of emergency emissions in the presence of only stationary currents caused by a wind speed of 15 m/s. At the point of entry of pollutants, the velocities of stationary currents on the sea surface are 62 cm/s and their vectors are directed towards the active wind, where impurity transfer is observed.

These areas are increasingly stretching in a westerly direction over time. The impurity is lowered to the horizon z = h_1 after 2 h, into the bottom layer after 9 h. At these depths, the concentration areas have a shape elongated in a westerly direction.

Table 6.1.1 shows the coefficient of maximum coverage of the pollution area with the corresponding time (t_{max}, h) and the time of total dispersion (t_d, h) of the impurity at different depths of the sea for different velocities of stationary currents in the presence of non-stationary wind. Based on the analysis of the data given in Table 6.1.1 and Figure 6.1.1, we will draw conclusions about the influence of the velocity of stationary currents and variable wind on the transformation of pollution in area B_1, where gas fields are being developed. The sea depth in this area is 10 m.

Table 6.1.1 – Parameters (K_{max}, t_{max}, h; t_d, h) of the impurity evolution at different horizons of the Sea of Azov under the combined action of constant and variable winds

Horizont	Pollution parameters K_{max}, t_{max}, t_d	$\mathbf{W}_{st}^1 + \mathbf{W}_{var}$			$\mathbf{W}_{st}^2 + \mathbf{W}_{var}$			$\mathbf{W}_{st}^3 + \mathbf{W}_{var}$		
		B_1	B_2	B_3	B_1	B_2	B_3	B_1	B_2	B_3
$z = z_1$	K_{max}	1.22	1.21	1.14	1.23	1.22	1.15	1.25	1.22	1.16
	t_{max}	10	10	14	10	10	14	11	11	14
	t_d	84	74	60	84	74	60	87	74	60
$z = h_1$	K_{max}	1.24	1.23	1.22	1.24	1.24	1.22	1.27	1.25	1.22
	t_{max}	32	28	10	32	28	10	34	29	15
	t_d	100	84	6	101	86	67	104	89	70
$z = h_2$	K_{max}	1.31	1.32	1.24	1.31	1.32	1.24	1.33	1.33	1.24
	t_{max}	28	28	16	28	28	16	35	30	16
	t_d	108	90	76	108	90	78	110	92	79

As can be seen from Table 6.1.1, for area B_1, the maximum area of pollution occurs at the maximum value of the stationary wind speed ($\mathbf{W}_{st}^3$). In this area of the Sea of Azov, where the center of impurity intake is located, stationary currents are directed towards the active wind, into which impurities are transferred (Figure 6.1.1, *b*). 12 h after

the termination of the non-stationary wind, a decrease in the area of pollution and a decrease in the concentration of impurities is observed (Figure 6.1.1, *c*). So, on the free surface, the value $K_{max} = 1.25$ is reached 11 h after the release of the impurity (Table 6.1.1). At the same time, its total scattering time is 87 h [Investigation of the influence …, 2010].

The contamination penetrates to a depth of $z = h_1$ 2 h after its release to the surface. Further, the contamination area increases and becomes maximum at t_d = 34 h ($K_{max} = 1.27$, Table 6.1.1). The complete dispersion of pollution at this depth in the central part of the sea occurs 104 h after the start of its release. In the bottom layer ($z = h_2$), the highest coefficient (1.33) of coverage of the contamination area was noted at t_{max} = 35 h, and after 110 h from the moment of release of the impurity, its concentration becomes equal to C_d.

In the area of the B_2 release (x_0 = 180 km, y_0 = 120 km), under the action of an unsteady wind, the transfer of the pollution area (Figure 6.1.1, *b*) is also due to the direction of currents. After the cessation of the action of the variable wind, the spot shifts in the westerly direction, opposite to the direction of the wind (Figure 6.1.1, *c*). From the analysis of the data given in Table 6.1.1, it can be seen that at Wst3 the maximum area occupied by contamination on the surface is 1.22 (t_{max} = 11 h), at a depth of $z = h_1$ – 1.25 (t_{max} = 29 h), in the bottom layer – 1.33 (t_{max} = 33 h). The dispersion of the impurity occurs 92 h after its appearance in the sea.

The depth of the Sea of Azov in the area of pollution release, the center of which is located at point B_3 (x_0 = 260 km, y_0 = 170 km), is the smallest (8 m) among the depths in the considered areas of impurity intake. As follows from the analysis of modeling data, currents arise in the Taganrog Bay with steady motion, the highest speeds of which reach 86 cm/s. Figure 6.1.1, *b* corresponds to 15 h after the beginning of the action of the unsteady wind, when the most intense currents take place. It can be seen that areas with a concentration of 0.025 or more on the free surface increase and become elongated along the wind. At the same time, the area of pollution is moving to the east.

According to the data given in Table 6.1.1, the Kmax values for this point are the lowest compared to the others: on the surface K_{max} = 1.16 (14 h), at a depth of $z = h_1$ K_{max} = 1.22 (15 h), in the bottom layer K_{max} = 1.25 (16 h). Complete scattering occurs after 79 h from the moment of emission. The area of pollution distribution depends on the wind speed, as a result of which the currents reach a steady state. As the $\mathbf{W}_{st}$ value increases, the currents velocities in steady-state mode become higher, and therefore the area of the contamination area and the time of its complete dispersion increase.

Based on the analysis of the data given in Table 6.1.1, in the area of the Vostochno-Kazantipskoye gas field, the dispersion of impurities of the same volume takes longer than in the central part of the sea and the Taganrog Bay. The maximum area of contamination is also noted here. The lowest values of the dispersion time and the area covered by pollution occur for the source located in the Taganrog Bay.

6.2. Modeling of pollution propagation scenarios in the field of vortex atmospheric disturbances

Let's estimate the influence of time and space variables of atmospheric disturbances on the size of the region and the time of complete dispersion of pollutants entering the Sea of Azov. Pollutants spread on the surface and in the deep layers of the sea under the influence of turbulent diffusion, and are also transported by wind currents excited by a wind system consisting of constant $\mathbf{W}_{st}$ (2.1.1.1) and variable wind caused by the passage of a vortex atmospheric disturbance. In this case, the driving wind field is heterogeneous in time and space, and its velocity is a function of coordinates and time $\mathbf{W}(\mathbf{r}, t)$ (2.1.1.4).

Here are the results obtained in the study of the evolution of pollution, the center of which is located in the area of the Vostochno-Kazantipskoye gas field (point B_1 in Figure 6.1.1). An emergency release occurs in the surface layer of the sea, at the moment of the beginning of the action of a cyclonic disturbance arising in the field of steady motion ($t = t_{st}$), the contour of the initial contamination area is limited

by a straight circular cylinder with a radius of 9 km [Investigation of the influence …, 2009].

Let us establish the degree of influence of an atmospheric formation with a radius of 100 km, moving at a speed of 5 m/s to the west (W), on non-stationary currents generated by it in the field of background steady currents caused by wind with the lowest of the considered speeds ($|\mathbf{W}_{st}^{1}|$ = 5 m/s). The velocities of steady-state currents in the area of emergency discharge are: 14 cm/s in the surface layer; 9 cm/s at $z = h_1$; 6 cm/s at the bottom (Table 5.1.1). During the passage of a cyclone, these velocities increase and reach maximum values: 86 cm/s at $z = 0$ (after 15 h), 75 cm/s at $z = h_1$ (after 18 h); 52 cm/s at $z = h_2$ (after 20 h). The process of moving atmospheric formation entails a change in the direction of the velocity fields of the driving wind and, as a result, the direction of the currents generated by it. At the point of entry of pollutants, the velocities of stationary currents on the sea surface are 62 cm/s and are directed towards the active wind, where impurity transfer is observed (Figure 6.2.1). These areas are increasingly stretching in a westerly direction over time. The impurity is lowered to the horizon $z = h_1$ after 2 h, into the bottom layer after 9 h. At these depths, the concentration areas have a shape elongated in a westerly direction [Investigation of the influence .... 2009].

We investigate the influence of the direction of movement (SW, W, NW) of atmospheric formations with a radius of 100 km and a speed of 5 m/s on the evolution of the pollution area with the same parameters that were considered earlier in the steady-state regime. For cyclones of various directions, the penetration time of the impurity to a depth of $z = h_1$ lasts much longer than in the steady-state mode, and is 15 h after its release to the surface (Figure 6.2.2). Also, the lowering of pollutants into the bottom layer becomes longer (up to 20 h). Thus, the vertical propagation of an impurity under the action of a cyclone slows down in comparison with the stationary case by 7.5 times at ($z = h_1$) and by 2.2 times at $z = h_2$.

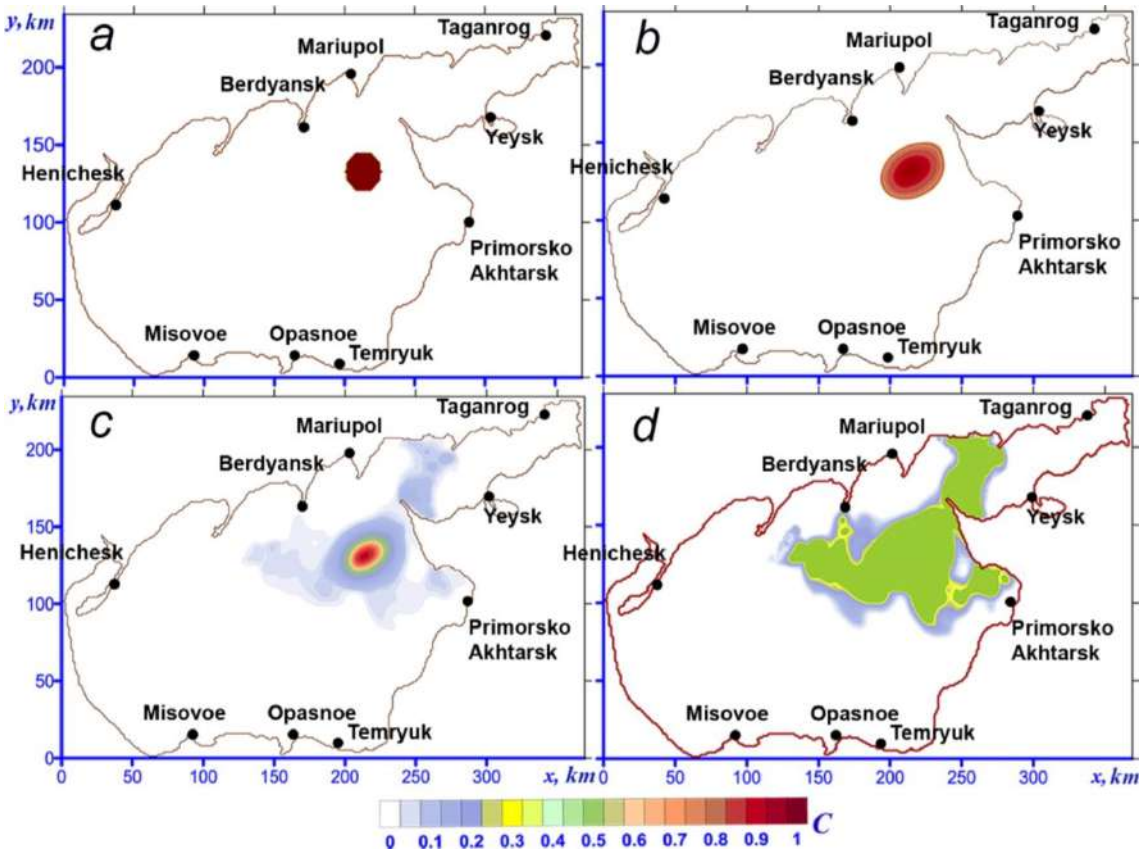

Figure 6.2.1 – Transformation of the pollution area into a background stationary wind field with a speed of 15 m/s: (*a*) – the cyclone enters the water area ($t = t_{st}$ +1 h); (*b*) – the center of the cyclone crosses the central part of the sea ($t = t_{st}$ + 8 h); (*c*) – the cyclone leaves the water area ($t = t_{st}$ + 15 h); (*d*) – 30 h after the cyclone leaves ($t = t_{st}$ + 45 h)

During the movement of the atmospheric formation, the direction of the driving wind and the direction of the currents generated by it change. As a result, the pollution areas move westward for the first 2 h (in the direction of stationary currents) (Figure 6.2.2, *a*), and then (after 10 h) break up into several small fragments (Figures 6.2.2, *b* and *c*). These fragments are transported from the center of the ejection in various directions over considerable distances and after 30 h reach the northern coast of the Sea of Azov in the area of Berdyansk and Mariupol (Figure 6.2.2, *d*). Over time, areas of pollutants are transferred to the west. Complete scattering occurs after 149 h, which exceeds 2.7 times the scattering time of the same contamination area in steady state.

Table 6.2.1 shows the coefficient of maximum coverage of the area of the pollution area, the time of its achievement (t_{max}, h) and the time of complete dispersion of the impurity (t_d, h) at various depths of the sea in steady state and in the presence of cyclones moving at a speed of 5 m/s in the directions south-west (SW), west (W) and the North-West (NW) [Investigation of the influence .... 2009].

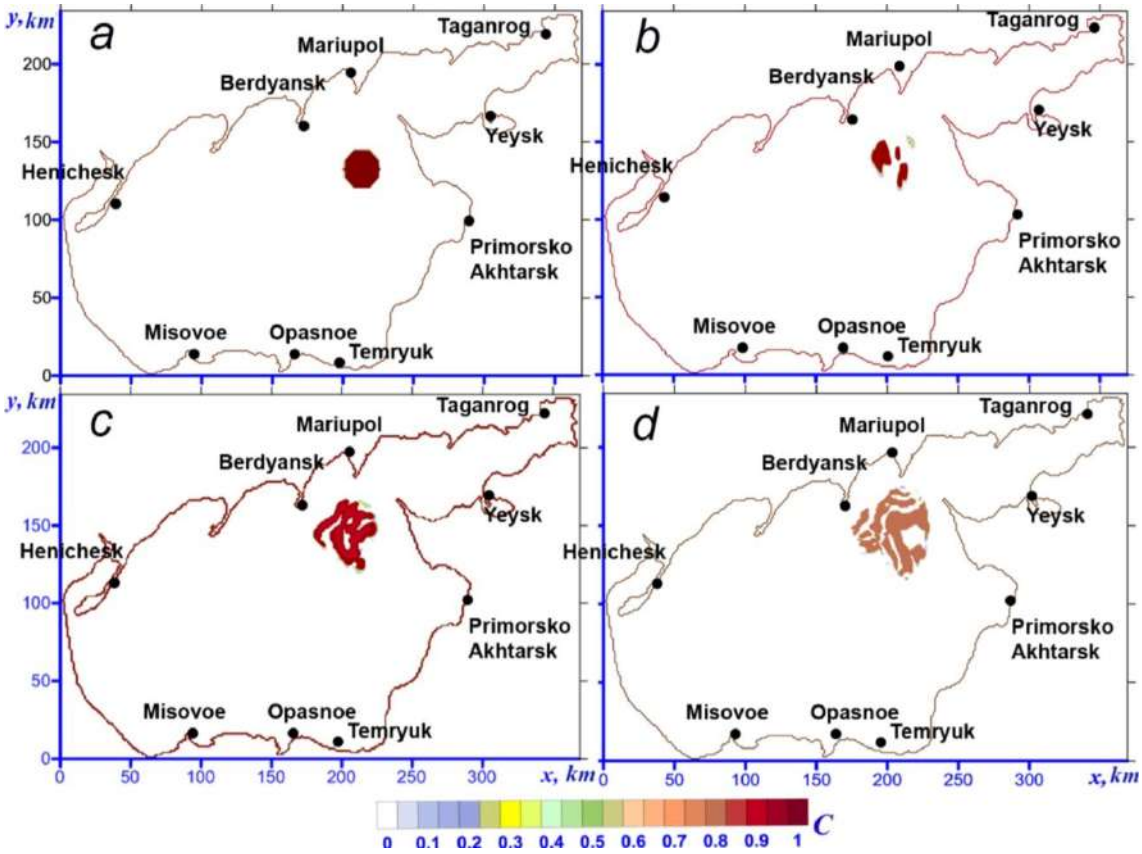

Figure 6.2.2 – Transformation of the pollution area when the cyclone moves westward at a speed of 5 m/s: (*a*), (*b*), (*c*) are given at the same time points as in Figure 6.2.1; (*d*) – 30 h after the cyclone leaves ($t = t_{st} + 45$ h)

From the analysis of the data given in Table 6.2.1, it follows that the passage of cyclones has a significant effect on the parameters of the impurity propagation. Among the considered directions of movement of atmospheric disturbances, the western direction corresponds to the highest parameters of penetration and time of complete dispersion of pollution areas. Comparing the K_{max} values for this direction of the cyclone with those

obtained in calculations in the presence of only stationary currents, we note their more than eightfold increase at various horizons.

The area of contamination distribution depends on the wind speed, which brings the currents to a steady state, and on the direction of movement of the cyclone. It can be seen that at high values of constant wind velocity ($\mathbf{W}_{st}$), steady currents with correspondingly high speeds arise in the Sea of Azov (Table 5.1.1). This, in turn, entails an increase in the penetration boundary and the time of complete dispersion of pollution (Table 6.2.1). For example, the longest total scattering time, based on the above data, is 1.2 times longer at $\mathbf{W}_{st}^3$ (176 h) than at $\mathbf{W}_{st}^1$ (151 h). In the considered field of steady-state currents, the maximum area occupied by pollution is 1.22 on the surface (t_{max} = 3 h); 1.23 at a depth of $z = h_1$ (t_{max} = 10 h); 1.22 in the bottom layer (t_{max} = 15 h). Complete scattering takes place 53 h after the moment of emission, while the direction of transformation of the impurity does not change significantly over time.

Table 6.2.1 – Parameters of impurity evolution at different depths under the action of stationary currents and cyclones moving in three directions

Horizont	K_{max}, t_{max}, t_d	$\mathbf{W}_{st}^1$	$\mathbf{W}_{st}^3 + \mathbf{W}_c(\mathbf{r}, t)$			$\mathbf{W}_{st}^2$	$\mathbf{W}_{st}^2 + \mathbf{W}_c(\mathbf{r}, t)$			$\mathbf{W}_{st}^3$	$\mathbf{W}_{st}^3 + \mathbf{W}_c(\mathbf{r}, t)$		
			Cyclone direction				Cyclone direction				Cyclone direction a		
			SW	W	NW		SW	W	NW		SW	W	NW
$z = z_1$	K_{max}	1.14	7.52	7.75	7.24	1.19	8.63	8.69	8.66	1.22	8.91	9.15	8.78
	t_{max}	4	140	142	141	3	150	156	150	3	162	165	162
	t_d	18	149	150	149	17	162	167	162	17	170	175	170
$z = h_1$	K_{max}	1.17	7.65	7.98	7.39	1.18	8.56	8.61	8.59	1.23	9.08	9.16	8.93
	t_{max}	13	140	143	141	10	151	157	151	10	162	166	162
	t_d	35	150	151	150	34	163	168	163	33	170	176	170
$z = h_2$	K_{max}	1.12	7.29	7.67	7.00	1.17	8.48	8.54	8.52	1.22	8.87	9.09	8.72
	t_{max}	23	140	143	141	21	151	157	151	15	163	166	162
	t_d	57	150	151	151	55	163	168	163	53	170	176	170

Thus, the vertical propagation of an impurity under the action of a cyclone in the presence of stationary currents slows down compared to the case of only a stationary

currents. The movement of the cyclone in the field of a stationary currents leads to a significant increase in the area of contamination distribution compared to the case of a stationary currents only.

We investigate the influence of the spatially heterogeneous distribution of the initial impurity concentration, decreasing with distance from the center of the contamination area, on the process of its evolution. The analysis is performed based on a comparison of the main pollution parameters (scattering time and maximum values of the area and volume of the pollution area) obtained as a result of numerical modeling with various initial concentration settings: constant C_1^0, and variable C_2^0, set by the ratios (2.2.2.1) and (2.2.2.2). The pollution release site is located in the open part of the sea in a deep-water area, the center of which is indicated by point B_1 (Figure 6.2.3, *a*). Figure 6.2.3, b shows the change over time in the pollution area of a variable initial concentration (C_{max} = 1) under the action of a cyclone with a radius of 100 km moving at a speed of 5 m/s to the west, while the center of the cyclone passes through the central region of the sea.

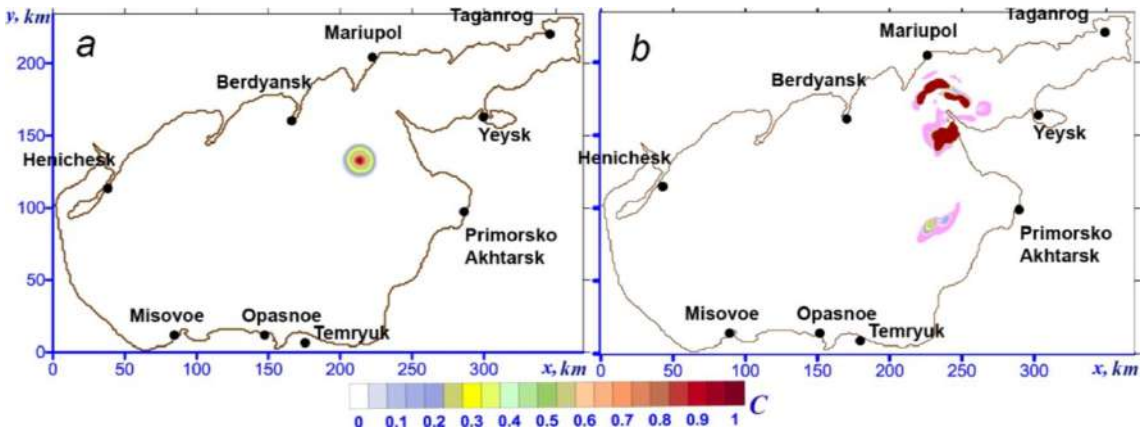

Figure 6.2.3 – Transformation of the pollution area when the cyclone moves westward at a speed of 5 m/s: (*a*) – the cyclone enters the sea ($t = t_{st}$ +1 h); (*b*) – 30 h after the cyclone leaves ($t = t_{st}$ + 45 h)

Under the influence of atmospheric disturbance, the pollution area initially moves to the west (in the direction of the cyclone), and then splits into several small areas that are transferred from the center of the emission in different directions (Figure 6.2.3, *b*).

Complete scattering occurs after 135 h, which is less than the scattering time of the same pollution area of constant initial concentration. Table 6.2.2 shows the values of C_{max} and T_{max}, the time of their achievement (t_{max}, h), as well as the time of complete dispersion of the impurity (t_d, h) at various horizons when moving a cyclone with a radius of 100 km to the west at a speed of 5 m/s, depending on the initial distribution of the impurity concentration [Cherkesov, Shulga, Study of the transformation ..., 2016].

Table 6.2.2 – Pollution parameters in the presence of a cyclone moving westward at a speed of 5 m/s, depending on the distribution of the initial impurity concentration

Horizont	Pollution parameters	C_1^0	C_2^0		
			$C_{2max} = 1$	$C_{2max} = 2$	$C_{2max} = 3$
$z = z_1$	K_{max}	2.7	1.9	2.2	2.6
	t_{max}	42	35	39	41
	t_d	149	110	122	140
$z = h_1$	K_{max}	1.8	1.3	1.5	1.8
	t_{max}	51	43	48	51
	t_d	152	131	139	140
$z = h_2$	K_{max}	1.1	0.7	0.9	1.1
	t_{max}	56	47	52	56
	t_d	155	135	141	155
$-H \le z \le z_1$	N_{max}	7.3	3.5	5.0	6.8
	t_{max}	55	35	42	45
	t_d	155	135	141	155

From the analysis of the data presented in Table 6.2.2, it follows that the values of the parameters of the impurity propagation of a constant initial concentration (C_1^0) exceed the values of the corresponding parameters obtained for a linear decreasing from the center of the initial distribution of its concentration (C_2^0). Note that in both cases $C_{max} = 1$. At the same time, the K_{max} value on the sea surface ($z = z_1$) and on the horizon $z = h_1$ for C_1^0 exceeds the K_{max} value for C_2^0 by 1.4 times; on the horizon of $z = h_2$, the K_{max} value is 1.6 times greater. Comparing the N_{max} values for these initial

concentration distributions, we obtain a more than twofold decrease for the linear initial impurity concentration [Cherkesov, Shulga, 2012].

Taking into account the simulation results shown in Table 6.2.2, we estimate the effect of the gradient of the initial linear impurity concentration on the size of its penetration area and the time of complete dispersion of the passive impurity in the presence of a cyclone. The study of the transport and distribution of impurities is performed for values of $C_{max} = 1$, $C_{max} = 2$ and $C_{max} = 3$. It is obtained that with the increase in C_{max} attitude largest area of contamination to its original value (Kmax) and increases at $z = z_1$ is 1.9 ($C_{max} = 1$), 2,2 ($C_{max} = 2$) and 2.6 ($C_{max} = 3$); at a depth $z = h_1$ – 1.3; 1.5 and 1.8; in the bottom layer ($z = h_2$) – 0.7; 0.9 and 1.1 respectively. From the analysis of these data, it follows that at the horizons under consideration, a twofold and threefold increase in the initial impurity concentration leads to an increase in the maximum area of the contamination area by 1.3 and 1.6 times, respectively.

The total dispersion time of the td impurity depends on the maximum of the initial concentration and becomes greater the higher the C_{max} value. In this case, td is equal to 135 h ($C_{max} = 1$), 141 h ($C_{max} = 2$), 155 h ($C_{max} = 3$) and increases by 4 and 15%, respectively, relative to $C_{max} = 1$. The simulation results presented in Table 6.2.2 indicate that the vertical spread of the impurity slows down with an increase in the maximum value of its initial concentration. In this case, the largest volume of the N_{max} contamination area at $C_{max} = 2$ and $C_{max} = 3$ is 1.4 and 1.9 times greater, respectively, than for $C_{max} = 1$.

Thus, a comparison of the contamination parameters calculated with different initial concentration settings showed that the inhomogeneous initial distribution of the impurity field leads to a decrease in the volume of the contamination area compared with the case of a constant initial concentration. The dependences of the change in the area of the contamination area at different horizons on the change in the gradient of the initial impurity concentration are obtained.

Let's compare the parameters of the impurity evolution in the central part of the Sea of Azov for different initial concentrations in the absence of wind (on calm water). Table 6.2.3 shows the values of K_{max}, N_{max}, the time of their achievement t_{max}

and the time of complete dispersion of the t_d impurity at various sea horizons, depending on the initial distribution of its concentration without taking into account the action of the cyclone.

From the analysis of the data given in Tables 6.2.2 and 6.2.3, it follows that in both calculation variants, in the presence of a cyclone and in quiet water, with an increase in the gradient of the initial concentration, there is an increase in the areas of contamination. As can be seen, for the same values of the initial concentration, in the absence of wind, the pollution parameters (K_{max}, N_{max}, t_d) increase by no more than 3 times compared with the case of a cyclone.

Table 6.2.3 – Pollution parameters in the absence of a cyclone, depending on the distribution of the initial impurity concentration

Horizon	Pollution parameters	C_1^0	C_2^0		
			$C_{2max} = 1$	$C_{2max} = 2$	$C_{2max} = 3$
$z = z_1$	K_{max}	8.8	3.6	4.1	8.7
	t_{max}	74	65	47	97
	t_d	168	199	345	343
$z = h_1$	K_{max}	2.0	2.3	3.0	5.9
	t_{max}	85	88	51	94
	t_d	254	157	363	168
$z = h_2$	K_{max}	4.3	1.5	1.1	2.6
	t_{max}	128	104	88	61
	t_d	224	377	377	279
$-H \le z \le z_1$	N_{max}	25.5	8.9	8.4	21.5
	t_{max}	118	39	86	63
	t_d	311	265	341	288

The study of the transport and propagation of impurities of constant and variable initial concentrations with equal maxima showed that in the first case, there are large scattering times and the size of the contamination penetration area. A twofold

and threefold increase in the gradient of the initial impurity concentration leads to an increase in the maximum area of the contamination penetration area by 1.3 and 1.6 times, respectively, during the passage of the cyclone over the Sea of Azov. The dispersion of the impurity in the presence of a cyclone and in still water slows down with an increase in the gradient of the initial concentration [Cherkesov, Shulga, 2012].

6.3. Investigation of the processes of pollution propagation and transformation in the Sea of Azov using data from the atmospheric model SKIRON

In the previous subsections, conclusions were drawn about the influence of model wind fields on the parameters characterizing the spread of pollution in the Sea of Azov. Two types of wind influences leading to the emergence of stationary and non–stationary currents in the sea are considered - quasi-stationary wind and non-stationary wind, which is the result of the superposition of the specified constant wind and the model of the non-stationary component. Setting the wind and atmospheric pressure components using data from the SKIRON regional atmospheric reanalysis is more approximate to real wind conditions. In this case, the vector of the driving wind velocity $\mathbf{W}(\mathbf{r}, t)$ and the atmospheric pressure value $P(\mathbf{r}, t)$ in each node of the computational grid of the model region are given in the form (2.1.1.4) and (2.1.1.3). At the moment of establishing the motion of the liquid ($t = t_{st}$), the stationary wind $\mathbf{W}_{st}$ is joined by the inhomogeneous in space and time wind $\mathbf{W}_{SKIRON}$. Then (at $t > t_{st}$) the $\mathbf{W}_{st}$ action supports stationary motion, and the $\mathbf{W}_{SKIRON}$ adds a non−stationary component to it. The start time of the $\mathbf{W}_{SKIRON}$ wind is the moment when the movement of liquid in the sea is established (t_{st1} = 37 h, $|\mathbf{W}|_{st}^1$ = 5 m/s; t_{st2} = 42 h, $|\mathbf{W}|_{st}^2$ = 10 m/s). The results of solving this problem are compared with the data of modeling performed when considering the action of constant wind or only atmospheric fields of the SKIRON model [Ivanov, Cherkesov, Shulga, 2012; Ivanov, Cherkesov, Shulga, 2014].

The atmospheric model data for the period from September 8 to September 18, 2007 were used in numerical experiments. The results obtained for the first three days are not analyzed and are used to set data on initial current velocities and sea level at 0 h

on September 11, 2007, the completion time of the simulation is t_{end} = 192 h. Figure 6.3.1 shows graphs of the average speed of the $\mathbf{W}_{SKIRON}$ predictive wind and its trend over 192 h. The average wind speed at each time is calculated using the formula (5.3.1). The approximation of the modulus of the average wind speed by a polynomial of the 9th degree is carried out using the least squares method and gives a trend in the behavior of the speed (Figure 6.3.1, dashed line) [Shulga, 2013]. In more detail, the maximum speeds of the predictive wind are given in [Cherkesov, Shulga, 2016].

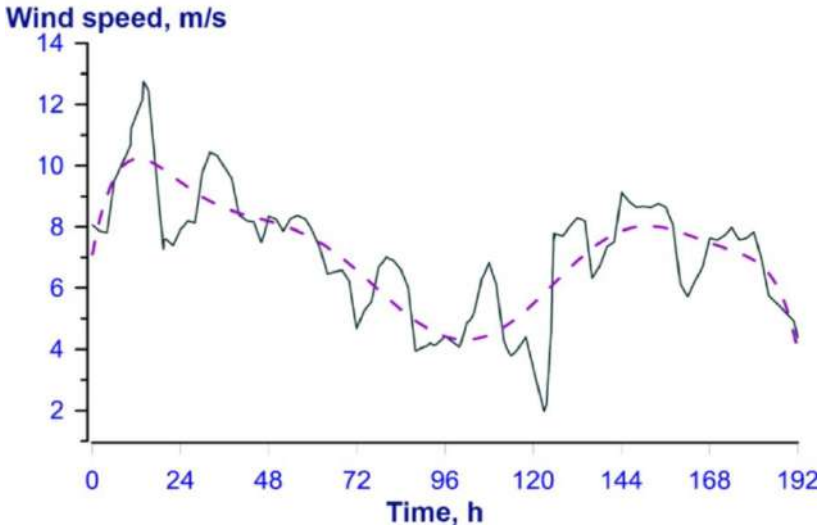

Figure 6.3.1 – Average wind speed over the Sea of Azov during the calculation period (solid line) and its trend (dashed)

Figure 6.3.1 shows that during the first two days the wind increased to 9 m/s, during the next three days the speed monotonously decreased to 5 m/s. Then, for another three days, its sharp decrease to 2 m/s was noted, after which it no longer exceeded 3 m/s (calm over the sea). Average (by time) The driving wind speed was 5.5 m/s. The maximum average speed was 12.7 m/s and took place on September 15, the minimum was 1.6 m/s on September 17. On average, during September, the driving wind speed was 5.5 m/s. During the specified period (192 h), the highest, average and lowest values of the maximum speed were 12.7; 6.7 and 1.6 m/s, respectively.

As follows from Figure 6.3.1 (solid line), the average velocity field is not uniform. During short periods of 1–2 days, the speed increases and decreases, therefore, the wind

direction changes. Deviations of the wind velocity vector from the direction of the x axis (the x axis is directed to the east at an angle of 50 degrees to the parallel) were analyzed in degrees. From the analysis of the prevailing wind directions, it follows that during the specified period, the prevailing directions were northeast and northwest, while the passage of several cyclones was also noted. We emphasize that the results of long-term observations of atmospheric disturbances in the area of the Sea of Azov are in satisfactory agreement with the atmospheric fields of the SKIRON model used in these calculations.

For comparison, Table 6.3.1 shows the maximum values of the velocity of stationary currents caused by constant wind ($\mathbf{W}_{st}^{1,2}$), the maximum values of the velocity of currents generated by the driving wind ($\mu_1 W_{SKIRON}$; μ_1 = ½; 1; 2) and their superposition ($\mathbf{W}_{st}^{1,2} + \mu_1 \mathbf{W}_{SKIRON}$). The horizons and coordinates of the highest velocity values, as well as the time of their achievement, are also indicated here [Ivanov, Cherkesov, Shulga, 2011]. From the analysis of these data, it follows that in the presence of stationary currents, the maximum velocities of non-stationary currents ($|\mathbf{U}|_{max}$) increase in comparison with their values under the action of only a predictive wind.

Comparing the maxima of currents velocities at different horizons, it follows that the values of $|\mathbf{U}|_{max}$ at $\mathbf{W}_{st}^{1} + \mathbf{W}_{SKIRON}$ increase by 38 (horizon 1 m); 43 (3 m); 39 (5 m) and 20% (10 m) compared with the case of $\mathbf{W}_{SKIRON}$ and by 78 (1 m); 81 (3 m); 80 (5 m) and 74% (10 m) compared to the action of only $\mathbf{W}_{st}^{1}$. When the constant wind speed is doubled, the combined action of $\mathbf{W}_{st}^{2} + \mathbf{W}_{SKIRON}$ leads to an increase in $|\mathbf{U}|_{max}$ by 50 (1; 3 m); 47 (5 m) and 30% (10 m) compared with the action of $\mathbf{W}_{SKIRON}$ and by 63 (1 m); 64 (3 m); 62 (5 m) and 57% (10 m) compared to the case of $\mathbf{W}_{st}^{2}$. At the same time, the maximum velocities of stationary currents caused by the action of constant wind at speeds of 5 m/s ($\mathbf{W}_{st}^{1}$) and 10 m/s ($\mathbf{W}_{st}^{2}$) increase at the same horizons by 52; 53; 50 and 47%, respectively. It follows that doubling the intensity of the stationary wind in combination with the same non-stationary wind leads to an increase in the maximum velocities of non-stationary currents by 64% and stationary currents by 53%.

Table 6.3.1 – Maximum values of the current velocity at various depths of the Sea of Azov, the time of their achievement and their corresponding coordinates

Wind speed	Horizon, m	$\|\mathbf{U}\|_{max}$, m/s	x_{max}, km	y_{max}, km	t_{max}, h, min
$\mathbf{W}_{st}^{1}$	1	0.16	236.29	174.08	8.00
	3	0.13	236.39	173.44	8.02
	5	0.12	237.01	173.31	8.22
	10	0.09	235.34	173.00	9.44
$\mathbf{W}_{st}^{2}$	1	0.34	235.38	172.19	8.35
	3	0.28	235.97	172.86	8.55
	5	0.24	237.07	171.50	8.26
	10	0.17	235.99	171.16	9.34
$½\mathbf{W}_{SKIRON}$	1	0.35	198.78	188.36	131.48
	3	0.28	242.27	184.59	132.00
	5	0.25	259.84	194.38	135.18
	10	0.24	228.97	174.97	140.00
$\mathbf{W}_{SKIRON}$	1	0.45	206.25	189.27	128.00
	3	0.39	241.76	188.88	130.00
	5	0.37	263.30	199.05	137.00
	10	0.28	238.20	175.76	145.00
$2\mathbf{W}_{SKIRON}$	1	0.58	206.69	190.59	132.36
	3	0.54	236.96	184.66	134.06
	5	0.52	263.53	193.96	136.24
	10	0.41	238.66	174.55	142.36
$\mathbf{W}_{st}^{1} + ½\mathbf{W}_{SKIRON}$	1	0.61	201.47	109.47	128.00
	3	0.59	224.43	183.70	130.00
	5	0.54	225.04	161.18	137.00
	10	0.35	174.63	166.87	145.00
$\mathbf{W}_{st}^{1} + \mathbf{W}_{SKIRON}$	1	0.73	201.48	106.15	128.00
	3	0.69	224.73	176.44	130.00
	5	0.61	225.31	156.78	137.00
	10	0.35	174.86	160.92	145.00
$\mathbf{W}_{st}^{1} + 2\mathbf{W}_{SKIRON}$	1	1.57	208.72	111.75	128.00
	3	1.39	229.55	183.06	130.00
	5	1.24	229.67	161.92	137.00
	10	1.02	175.72	168.25	145.00

Окончание таблицы 6.3.1

Wind speed	Horizon, m	$\|\mathbf{U}\|_{max}$, m/s	x_{max}, km	y_{max}, km	t_{max}, h, min
$\mathbf{W}_{st}^2 + ½\mathbf{W}_{SKIRON}$	1	0.57	166.19	176.81	152.00
	3	0.45	204.45	162.96	154.00
	5	0.43	258.30	194.36	157.00
	10	0.40	210.08	147.40	162.00
$\mathbf{W}_{st}^2 + \mathbf{W}_{SKIRON}$	1	0.91	159.09	175.58	152.00
	3	0.78	199.38	159.67	154.00
	5	0.70	258.19	188.40	157.00
	10	0.40	209.66	146.44	162.00
$\mathbf{W}_{st}^2 + 2\mathbf{W}_{SKIRON}$	1	1.32	161.14	176.58	152.00
	3	1.12	202.31	166.34	154.00
	5	0.77	259.62	194.33	157.00
	10	0.66	214.06	147.13	162.00

Table 6.3.2 shows the maximum values of ζ_{max} rises and $|\zeta|_{max}$ decreases in the open part of the Sea of Azov caused by the action of stationary wind ($\mathbf{W}_{st}^{1,2}$), the prognostic wind ($\mu_1\mathbf{W}_{SKIRON}$; μ_1 = ½; 1; 2) and their combined action. The time of reaching and the corresponding coordinates of the sea level extremes are also presented here. The analysis of these data indicates that with an increase in the speed of the current wind, the maximum deviations of the free surface increase.

Thus, doubling the velocity of only the stationary wind $\mathbf{W}_{st}^2$ leads to an increase in the values of ζ_{max} and $|\zeta|_{max}$ by 2 and 1.7 times compared with the action of $\mathbf{W}_{st}^1$. When the intensity of the wind fields obtained from the atmospheric model ($\mathbf{W}_{SKIRON}$) changes, the values of ζ_{max} and $|\zeta|_{max}$ increase by 1.3; 3 and 1.4; 3.3 times, respectively, compared with the effect of $½\mathbf{W}_{SKIRON}$. The combined effect of the superposition of the considered $\mathbf{W}_{st}^{1,2} + \mu_1\mathbf{W}_{SKIRON}$ winds also leads to an increase in the values of extreme deviations. So, at $\mathbf{W}_{st}^2 + ½\mathbf{W}_{SKIRON}$ ζ_{max} is 1.3 and $|\zeta|_{max}$ is 1.8 times more than at $\mathbf{W}_{st}^1 + ½\mathbf{W}_{SKIRON}$; with $\mathbf{W}_{st}^2 + \mathbf{W}_{SKIRON}$, ζ_{max} is 1.3 and $|\zeta|_{max}$ is twice as much as with $\mathbf{W}_{st}^1 + \mathbf{W}_{SKIRON}$; with $\mathbf{W}_{st}^2 + 2\mathbf{W}_{SKIRON}$, ζ_{max} is 1.2 and $|\zeta|_{max}$ is 2.1 times more than with $\mathbf{W}_{st}^1 + 2\mathbf{W}_{SKIRON}$. Thus, the action of a stationary wind of the same direction, but at a higher speed (10 m/s) causes an increase in the maximum deviations of the ζ_{max} and $|\zeta|_{max}$ levels: at $½\mathbf{W}_{SKIRON}$

– by 48 and 65%; at $\mathbf{W}_{SKIRON}$ – by 40 and 57%; at $2\mathbf{W}_{SKIRON}$ – by 37 and 54%, respectively.

Table 6.3.2 – Maximum values of rises (ζ_{max}) and decreases ($|\zeta|_{max}$) of the level caused by constant wind ($\mathbf{W}_{st}^{1, 2}$), wind ($\mu_I\mathbf{W}_{SKIRON}$; μ_I = ½; 1; 2) and their superposition ($\mathbf{W}_{st}^{1, 2} + \mu_I\mathbf{W}_{SKIRON}$) in the open part of the Sea of Azov with the corresponding coordinates

Wind speed	ζ_{max}, sm	x_{max}, km	y_{max}, km	t_{max}, h.min	$\|\zeta\|_{max}$, sm	x_{min}, km	y_{min}, km	t_{min}, h.min
$\mathbf{W}_{st}^{1}$	20	367	220	17.10	10	4	95	13.23
$\mathbf{W}_{st}^{2}$	69	368	218	18.46	39	4	107	13.47
½$\mathbf{W}_{SKIRON}$	32	283	96	168.14	17	24	127	190.55
$\mathbf{W}_{SKIRON}$	43	279	90	168.15	25	20	123	190.55
$2\mathbf{W}_{SKIRON}$	97	285	92	168.15	56	20	123	190.55
$\mathbf{W}_{st}^{1}$+½$\mathbf{W}_{SKIRON}$	46	299	105	171.11	27	30	128	191.30
$\mathbf{W}_{st}^{1}$+$\mathbf{W}_{SKIRON}$	55	296	100	171.11	28	22	124	191.30
$\mathbf{W}_{st}^{1}$+$2\mathbf{W}_{SKIRON}$	121	303	100	171.11	59	29	131	191.30
$\mathbf{W}_{st}^{2}$+½$\mathbf{W}_{SKIRON}$	62	295	102	172.20	49	23	124	192.45
$\mathbf{W}_{st}^{2}$+$\mathbf{W}_{SKIRON}$	72	290	101	172.20	58	21	124	192.45
$\mathbf{W}_{st}^{2}$+$2\mathbf{W}_{SKIRON}$	154	292	104	172.20	123	24	131	192.45

The fields of surface currents of the Sea of Azov, caused by the specified wind system, obtained as a result of modeling, are shown in Figure 6.3.2. During the initial period of the constant westerly wind at a maximum speed of 10 m/s, the direction of the currents coincides with the direction of the wind throughout the sea area. Starting from the moment the movement of the liquid in the northern part of the sea is established, there

is a decrease in the velocity of currents and a change in its direction to the opposite, two systems of cycles arise, which are oriented in the zonal direction (Figure 6.3.2, *a*).

With the onset of the action of the fields of the $\mathbf{W}_{SKIRON}$ wind variable in time and space, the water circulation is disrupted and the currents become chaotic, corresponding to an inhomogeneous acting wind (Figure 6.3.2, *b*). At the time of the passage of the cyclone at a wind speed of 11.6 m/s, the circulation of the waters of the Sea of Azov is characterized by the presence of three cycles (Figure 6.3.2, *c*): anticyclonic (in the north parts of the sea) and two cyclonic ones (near the southern coast). At the next moment in time (Figure 5.3.2, *d*), the pattern of currents changes: in the central part of the sea, an anticyclonic movement takes place, capturing the entire water area, with the exception of currents formed in the Taganrog Bay [Ivanov, Cherkesov, Shulga, 2014].

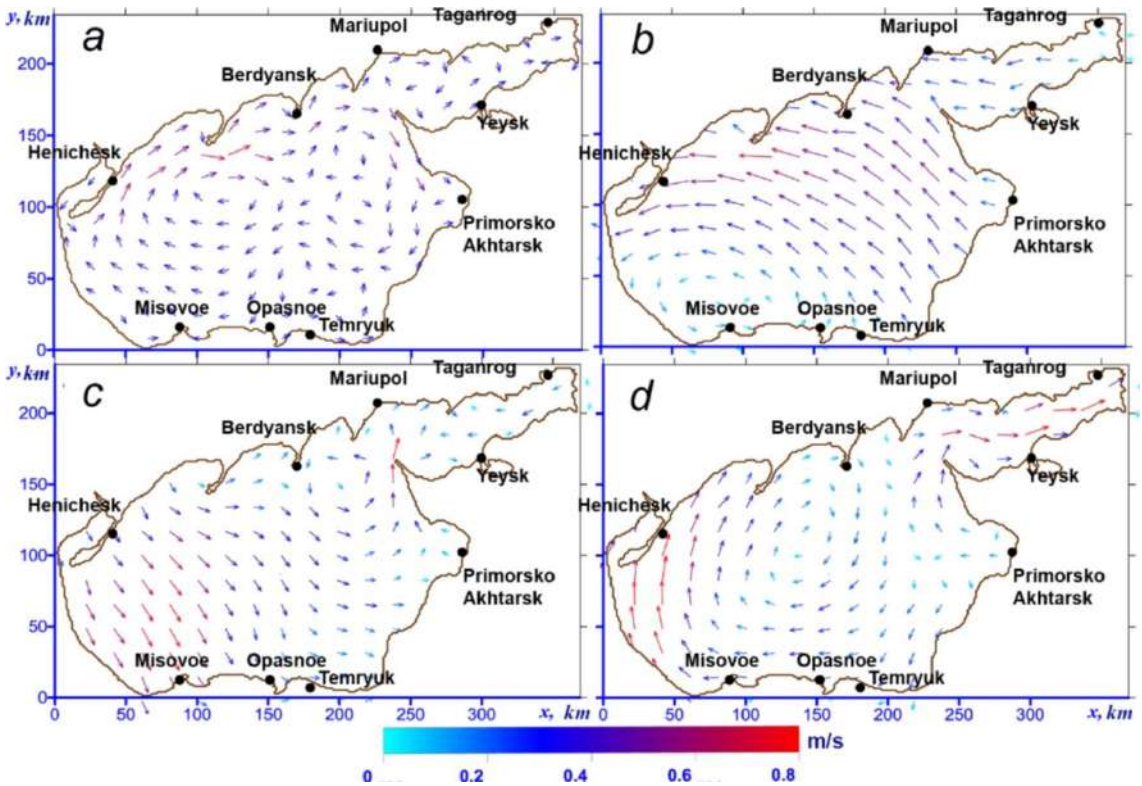

Figure 6.3.2 – Velocity fields of the surface currents of the Sea of Azov: (*a*) – steady currents ($t = t_{st}$); (*b*) – the beginning of the action of the predictive wind ($t = t_{st}$ +24 h); (*c*) – the moment of time ($t = t_{st}$ +120 h); (*d*) – the end of the action forecast wind ($t = t_{st}$ +170 h)

The comparison of the maximum level deviations obtained as a result of modeling at the coastal stations of the Sea of Azov was performed according to the data presented in Table 6.3.3. In the upper part of the table, the values of the surges are given, in the lower part, the surges that occur in the Sea of Azov under the action of both constant and variable winds.

Table 6.3.3 – Maximum surges and overcurrentss (cm) at coastal stations of the Sea of Azov caused by constant wind ($\mathbf{W}_{st}^{1,2}$), wind ($\mu_1 \mathbf{W}_{SKIRON}$; $\mu_1 = ½; 1; 2$) and their superposition ($\mathbf{W}_{st}^{1,2} + \mu_1 \mathbf{W}_{SKIRON}$) [Ivanov, Cherkesov, Shulga, 2012]

Stations	$\mathbf{W}^1_{st}$	$\mathbf{W}^2_{st}$	$\gamma_1 W_{SKIRON}$			$\mathbf{W}^1_{st} + \gamma_1 W_{SKIRON}$			$\mathbf{W}^2_{st} + \gamma_1 W_{SKIRON}$		
			$\mu_1 = ½$	$\mu_2 = 1$	$\mu_3 = 2$	$\mu_1 = ½$	$\mu_2 = 1$	$\mu_3 = 2$	$\mu_1 = ½$	$\mu_2 = 1$	$\mu_3 = 2$
Surcharges											
Henichesk	–	–	20.0	25.4	31.4	29.4	32.2	51.5	39.4	62.3	66.7
Berdyansk	–	–	4.9	9.6	10.9	7.0	16.9	16.9	10.2	44.3	51.7
Taganrog	9.8	37.3	18.5	29.3	39.9	28.0	46.4	65.4	35.5	80.4	85.1
Mariupol	20.7	62.4	40.6	50.6	79.6	57.1	63.1	128.2	81.2	89.5	159.1
Yeysk	13.8	52.2	19.1	38.1	59.9	30.0	76.0	93.7	38.5	102.2	123.1
Primorsko-Akhtarsk	8.1	43.2	40.6	57.1	89.3	61.7	80.4	129.2	85.2	91.1	189.5
Temryuk	10.2	26.9	20.2	24.5	28.6	28.4	29.7	43.3	40.8	49.9	60.9
Mysovoe	–	–	5.5	9.4	14.5	7.9	16.1	23.6	10.8	34.0	40.6
Opasnoe	7.5	13.9	7.5	12.1	17.0	12.1	19.6	25.0	15.2	34.2	34.9
Run-offs											
Henichesk	12.2	51.7	22.3	42.5	62.2	35.5	76.5	92.5	45.4	87.0	128.0
Berdyansk	4.0	17.6	9.7	17.3	27.1	15.1	30.9	38.0	20.5	62.1	77.0
Taganrog	–	–	12.7	18.2	27.2	18.7	26.0	43.7	24.6	39.7	51.9
Mariupol	–	–	21.2	29.0	37.2	35.0	42.4	60.8	40.3	72.9	74.0
Yeysk	–	–	8.7	18.9	21.5	12.3	41.1	34.5	17.6	45.3	47.4
Primorsko-Akhtarsk	–	–	8.4	14.1	16.1	12.2	23.8	26.2	16.3	35.5	44.4
Temryuk	–	–	6.8	8.7	13.3	10.2	11.2	18.9	13.0	33.0	36.0
Mysovoe	3.3	11.1	5.5	10.6	15.2	8.5	20.5	22.7	11.2	34.2	38.7
Opasnoe	–	–	12.6	22.3	30.0	20.0	39.4	42.8	24.7	63.9	67.3

From the analysis of the presented data, it follows that the greatest surges occur under the combined action of stationary and doubled predictive winds ($\mathbf{W}_{st}^2 + 2\,\mathbf{W}_{SKIRON}$)

and occur at the stations Primorsko-Akhtarsk (189.5 cm), Taganrog (159.1 cm) and Yeysk (123.1 cm). It can be seen (Table 6.3.3) that the maximum surge (189.5 cm) in the case of the considered wind system is 4.38 times greater than in stationary mode (43.2 cm). With the combined action of alternating and constant winds, the maximum slopes become larger than in steady-state mode. For all the considered types of wind, the maximum bends take place in Genichesk: 51.7 cm ($\mathbf{W}_{st}^2$); 45.4 cm ($\mathbf{W}_{st}^2 + ½\mathbf{W}_{SKIRON}$); 87.0 cm ($\mathbf{W}_{st}^2 + \mathbf{W}_{SKIRON}$); 128.0 cm ($\mathbf{W}_{st}^2 + 2\mathbf{W}_{SKIRON}$).

The work [Study of stationary currents ..., 2017] provides a detailed analysis of the extent of the territories of possible drainage/flooding that occur under the influence of only constant wind, only predictive fields, and also as a result of the combined action of non-stationary disturbances and background stationary currents. Knowing the maximum amount of overburden and the angle of inclination (elevation) of the relief of the coastal zone (α), the size of the maximum possible drainage area (flooding) caused by the action of wind in various coastal areas is determined.

The values of run-off and run-up, calculated as a result of modeling using wind obtained from the SKIRON/Eta predictive model, were compared with full-scale measurements for the same period, shown in the tables of hourly values of sea level heights by the State Meteorological Service. The analysis confirms a fairly good coincidence of the values of the amplitudes of the level fluctuations obtained by numerical calculations and natural data. So, in Genichesk, the calculated maximum of overburden is 16% less than according to observational data, and in Mariupol, the maximum model value of overburden is 12% less than the measured one.

Currents arising in the Sea of Azov under the influence of various wind fields have an impact on the transformation and spread of pollution in its surface and deep layers. The aim of the next series of numerical experiments is to assess the influence of the wind fields under consideration and the currents arising from this on the propagation of passive impurities entering the central region of the Sea of Azov. The initial position of the center of the impurity release area is located at point B_2 – above the deepest part of the sea (h_{max} = 12 m). The contamination area at the time of the emergency release is limited by a straight circular cylinder with a radius R_p = 9 km and a height equal to the thickness

of the surface layer of the sea. The evolution of an impurity with an inhomogeneous distribution of the initial concentration, decreasing with distance from the center of the contamination area, where the maximum concentration value ($C_{max} = 1$) is set, is studied.

The time of pollution release ($t = t_{0p}$) varies in experiments and is set according to the type of active wind. So, for a stationary wind $\mathbf{W}_{st}^{1,2}$, this time corresponds to the moment when the fluid movement is established ($t = t_{0p} = t_{st}$): 37 and 43 h, respectively. In calculations performed using only the fields of the SKIRON/Eta model, the moment of emission time occurs at 0 h on September 11, 2007 ($t = t_{0p} = 72$ h). With the combined action of stationary and predictive winds ($\mathbf{W}_{st}^{1,2} + \mu_l \mathbf{W}_{SKIRON}$), this time is determined by summing two intervals: necessary for the establishment of liquid in the sea and 3 days from the beginning of the action of the wind $\mathbf{W}_{SKIRON}$: $t_{0p} = t_{st} + 72$ h. When analyzing the propagation and scattering time of an impurity, for convenience, we assume that in all cases the emission time is zero ($t_{0p} = 0$).

Figure 6.3.3 shows the results of calculating the turbulent diffusion evolution of the surface pollution region. As can be seen, the pollution area moves westward for the first two h in accordance with the direction of stationary currents (Figure 6.3.3, *a*), and then after 10 h it splits into several small fragments (Figure 6.3.3, *b*, *c*). Parts of the area are transferred from the center of the emission in various directions over considerable distances [Ivanov, Shulga, 2018] and after 30 h they reach the northern coast of the Sea of Azov in the area of Berdyansk and Mariupol (Figure 6.3.3, *d*). Over time, areas of pollutants are transferred to the west. Complete scattering occurs after 149 h, which is 2.7 times longer than the scattering time of the same contamination area in steady state.

The analysis of the results of numerical calculations indicates that the area of distribution of the pollution area in the surface and deep layers of the Sea of Azov depends on the wind speed acting over the water area. With increasing wind intensity, the currents velocities become higher (see Table 6.3.1) and, as a result, the areas of impurity propagation and the time of its complete dispersion increase. In this regard, the largest area of pollution occurs at the maximum value of the current wind speed ($\mathbf{W}_{st}^{2} + 2\mathbf{W}_{SKIRON}$).

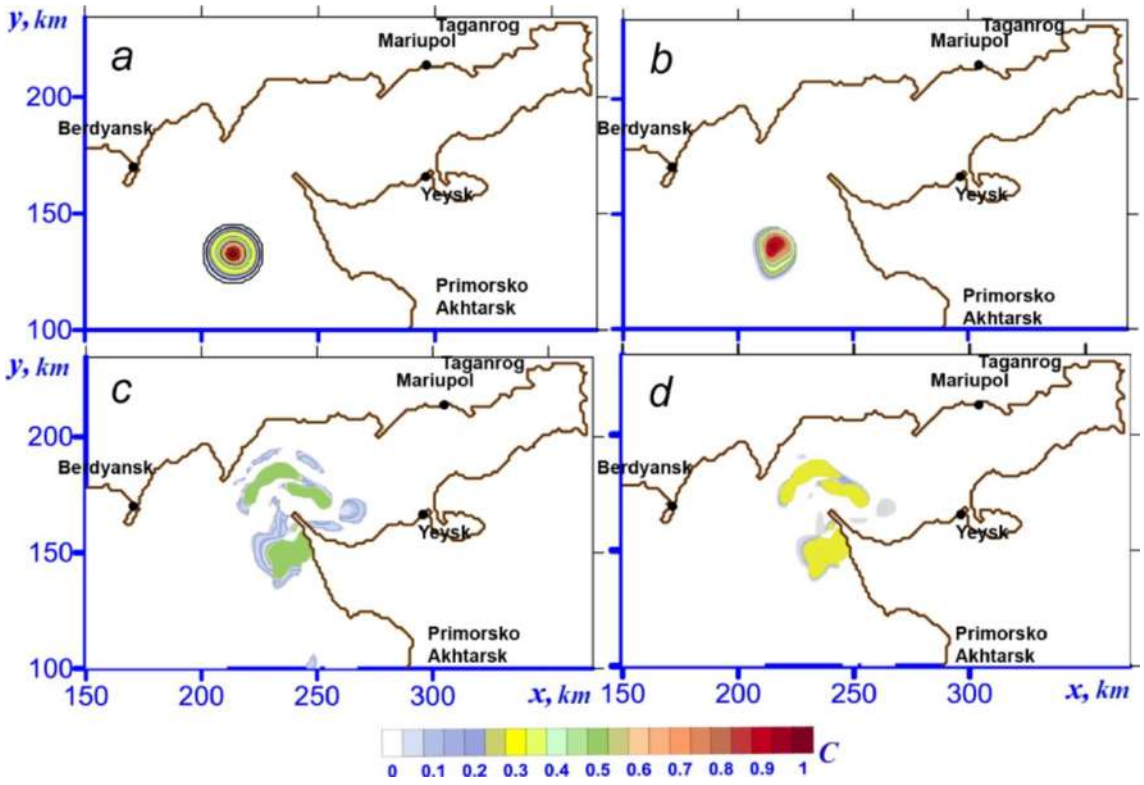

Figure 6.3.3 – Transformation of the pollution area in the Sea of Azov caused by the action of the predictive wind in the presence of stationary currents at the same time points as in Figure 6.3.2

In this case, the largest ratio of the area of the contamination area to the area of the initial contamination area (K_{max} =1.32) is achieved on the free surface 40 h after the release of the impurity, and the total scattering time is 87 h. The maximum value of the ratio of these areas (1.35) at a depth of 5 m is reached 42 h after the release of the impurity, and its complete dispersion after 110 h. In the bottom layer at a depth of 12 m, the maximum value of the ratio of these areas (1.38) is reached 59 h after the release of the impurity, and after 115 h its concentration in the entire sea area does not exceed 2.5% of the initial value [Ivanov, Cherkesov, Shulga, 2014, Shulga, 2013].

The effect of unsteady wind leads to a slowdown in the vertical spread of pollution, as well as to an increase in the area of the pollution impact zone and the time for complete purification of seawater compared with the case of exposure to quasi-stationary wind [Ivanov, Shulga, 2018; Shul'ga, Khartiev, Ioshpa, 2018].

6.4. Reproduction of the evolution of an optically active passive suspension in the Sea of Azov based on the assimilation of MODIS-Aqua/Terra scanner data

Satellite systems with high spatial resolution and daily data availability for any observation area make it possible to monitor the state and pollution of the marine environment. However, in the situation of a catastrophic fuel oil spill in the Kerch Strait that occurred on November 11, 2007 (accident of the tanker Volgoneft-139) during a powerful storm, the first satellite images were obtained five days after the disaster, on November 16, 2007 [Complex satellite monitoring ..., 2011, Shulga, 2017]. Cloudy weather was the reason for the lack of optical range data. Incomplete operational information significantly complicates the identification of pollution areas and the forecasting of their spread. In this regard, the joint analysis of satellite optical images and the results of numerical modeling seems to be the most effective, since it provides more complete information about the transfer directions, sizes and concentrations of contamination areas in the absence of images that are not distinguishable on optics. The simulation results make it possible to compare calculations with the operational situation identified by satellite images and lead to reasonable conclusions when making a forecast of the consequences of the spread of pollution.

The study of the evolution of pollution in the Sea of Azov was carried out using the developed new software codes that complement the hydrodynamic POM model. When integrating the transfer-diffusion equations, the author's procedures were used, which make it possible to set the values of the optically active suspension obtained from regular satellite observations in the model as initial data on the content of the contaminating substances. For this purpose, observations for 2013-2014 from MODIS-Aqua/Terra satellites were used http://oceancolor.gsfc.nasa.gov [(MODIS) Aqua, 2022; (MODIS) Terra, 2018].

The main objective of the study is to check whether it is possible to restore information about the content of passive impurities in the surface layer of the Sea of Azov by filling in data gaps caused by common problems of remote measurements

(for example, cloud cover) with the results of assimilation modeling. To do this, it was necessary: 1) to evaluate the quality of model calculations performed by various methods of assimilation of fragmentary series of remote ocean chromaticity measurements (OceanColor) into a continuous four-dimensional field of the POM model; 2) to show the advantages of using the results of hydrodynamic modeling when satellite images are unavailable, for example, to build spatial maps of the impurity distribution, to forecast transport and diffusion of bio-optical tracers in the sea area during extreme events. The possibility of assimilation of data on the impurity content into the hydrodynamic model has been little studied in comparison with the most widely reported methods of assimilation of data on temperature, free sea surface level, and ice concentration in the scientific literature.

Due to the expansion of satellite measurements of the marine environment in near-real-time modes, numerical models are the main tools for assessing the impact of regional and global stress factors on marine ecosystems. The existing classification of numerical models (minimal, intermediate and complex models) is based on the leading principle for model development – their realism and process detail. [How models can support ... , 2015] shows that minimal and intermediate models can be used to assess the response of the marine environment to extreme natural impacts and, therefore, contribute to understanding environmental consequences. Such models allow us to evaluate the effects of various potentially dangerous atmospheric influences. Although minimal models lack multidimensionality, complex ecosystem models are difficult to interpret because they require a lot of effort to decipher the many interactions and feedback loops. Initial testing of the method of assimilation of satellite data into a numerical model using a minimal type model will reveal its capabilities, as well as reduce excessive computing costs.

The stages of our numerical experiments to study the evolution of a passive impurity in the Sea of Azov are shown in Figure 6.4.1. The assimilation scheme is presented in more detail in [Shulga, Suslin, 2020]. These include: preprocessing satellite data to prepare information for assimilation in the model, calculating the suspension content from the model and performing the assimilation procedure.

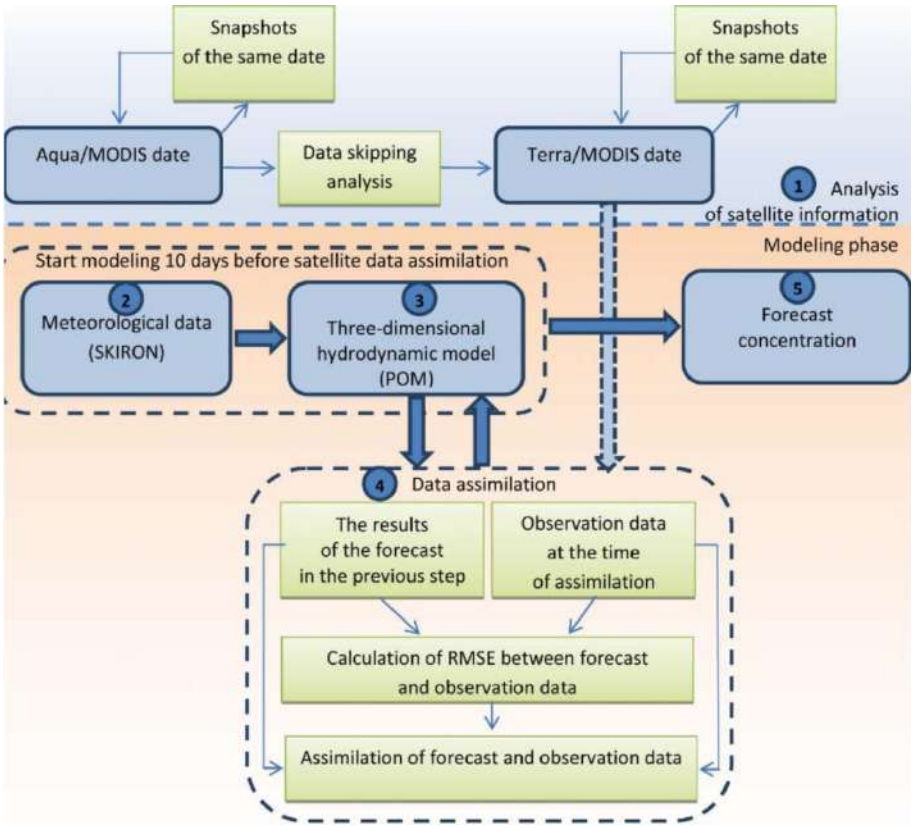

Figure 6.4.1 – Schematic representation of the algorithm for sharing remote sensing and hydrodynamic modeling data [Shulga, Suslin, 2018]

At the first stage, a preliminary analysis of satellite image data with kilometer spatial resolution is performed. At this stage, satellite observation data are being rejected according to certain criteria proposed in [Assessment ..., 2002]. Then, from the data set obtained in this way, the most informative images are selected, as free as possible from clouds and the presence of omissions.

All satellite images are organized into groups consisting of consecutive images with the shortest time interval between adjacent images. The selected periods correspond to good weather conditions over the Sea of Azov at cloud-free times. Thus, six time groups were selected, consisting of the most contrasting satellite images with a discreteness of 1–2 days, which were used in test calculations to assess changes in the distribution of the studied parameters *index*34 and $b_{bp}(555)$. Of these, three groups are of the greatest interest for analysis – data with daily discreteness. In the other three guppas, the interval between images is 2 days.

For each time group of satellite data, the distribution of the *index*34 and $b_{bp}(555)$ parameters defining the field of neutral buoyancy suspension in the near-surface layer of the Sea of Azov was simulated. The initial distribution of these parameters in the model is assimilated according to the satellite distribution data at the time coinciding with the first image in the group. The simulation was carried out with real atmospheric effects obtained from the data of the SKIRON regional model for the period 2013 – 2014, corresponding to a group of satellite images of the selected time period. Numerical experiments were carried out according to two schemes. *Scheme* I – single assimilation of *index*34 and $b_{bp}(555)$ parameters in the sea area only at the initial moment of time; *Scheme* II – sequential, regular assimilation of available satellite data every 24 or 48 h.

At the next stage, the solution of the problem of estimating the concentration of a passive impurity is based on a sequential recursive algorithm based on the theory of optimal Kalman filtration [Kalman, 1960; Klimova, 2003; Ghil, Malanotte-Rizzoli, 1991]. In the course of solving this problem, at time $t = t_k$, a vector of a priori estimation $\mathbf{x}_k^m$ is compiled based on the integration of the transport and diffusion equations. This vector is a short-term model forecast of the studied parameter from the previous step of assimilation. Its dimension is equal to the number of points in the model space ($n = n_\lambda n_\phi$, were $n_\lambda = 176$ and $n_\phi = 276$ are the number of grid nodes in longitude and latitude). The satellite observation data constitute the observation vector $\mathbf{y}_k^0$, the dimension of which (m) varies according to the available observational data and is generally not equal to n. The optimal estimate of the $\mathbf{x}_k^*$ concentration based on observational data and the model is found using the Kalman filter algorithm based on the forecast – correction system. The scheme of the algorithm is presented in detail in [Shulga, 2017; Shul'ga Evolution … , 2017].

Let us assume that at time tk–1 a forecast has been obtained for the distribution of the concentration of the parameter under study in the surface layer of the sea $\mathbf{x}_{k-1}^*$, and it is necessary to evaluate it at the next point in time t_k. In order to preview $\mathbf{x}_k^f$ in t_k, memory, we rely on $\mathbf{x}_{k-1}^*$. Next we obtain measurements $\mathbf{y}^0{}_k$ and adjusting the moment t_k, into the estimate, based on the forecast and measurements, we find the final a posteriori estimate of the state vector $\mathbf{x}_k^*$.

Components of the a priori function vector $\mathbf{x}^f = (x_1^f, x_2^f, \ldots, x_n^f)$ are transmitted according to the found values of the analysis vector $\mathbf{x}^* = (x_1^*, x_2^*, \ldots, x_n^*)$:

$$\mathbf{x}_k^f = A(\mathbf{x}_{k-1}^*) + \boldsymbol{\xi}_k \ (k = 1, \ldots, n), \tag{6.4.1}$$

were k –assimilation step; A – the model operator; $\mathbf{x}_{k-1}^*$ − the vector of analyzed values at a time t_{k-1} (the estimate that was obtained at the $(k-1)^{\text{th}}$ time step); $\boldsymbol{\xi}_k$ – a random vector of model errors. Satellite observation data form a vector $\mathbf{y}^0 = (y^0_1, y^0_2, \ldots, y^0_m)$:

$$\mathbf{y}_k^0 = B_k \bar{\mathbf{y}}^0_k + \boldsymbol{\varepsilon}_k \ (k = 1, \ldots, m). \tag{6.4.2}$$

Here B_k – the matrix of projections of the model space into the observation space of dimension $(m \times n)$; $\bar{\mathbf{y}}^0_k$ – m-dimensional vector of observations at a time t_k; $\boldsymbol{\varepsilon}_k^0$ – a random m-dimensional vector of observation errors. System noise (6.4.1) and measurement noise (6.4.2) are Gaussian random processes with zero mathematical expectation. Optimal concentration assessment $\mathbf{x}_k^*$ According to the observations and the model, it is found from the condition of the minimum trace of the matrix of covariances of estimation errors based on the Kalman filter algorithm [Kalman, 1960; Klimova , 2003; Ghil, Malanotte-Rizzoli, 1991]:

$$\mathbf{x}_k^* = \mathbf{x}_k^f + K_k(\mathbf{y}_k^0 - B_k\mathbf{x}_k^f), \tag{6.4.3}$$

$$K_k = P_k^f B_k^{\mathrm{T}}(B_k P_{k-1}^* B_k^{\mathrm{T}} + R_k)^{-1}, \tag{6.4.4}$$

$$P_k^f = A_{k-1} P_{k-1}^* A_{k-1}^{\mathrm{T}} + Q_{k-1}. \tag{6.4.5}$$

Here $\mathbf{x}_k^f$ – concentration forecast based on the model; K_k – unknown weight matrix (*Kalman gain*); P_k^f − prediction error covariance matrix; R_k и Q_k − covariance matrices of observational errors and models.

The first step of the Kalman filter algorithm consists of a forecast with the calculation of a preliminary concentration estimate using the formula (6.4.1) and the calculation of the forecast error covariance matrix (6.4.5). Next, the weight matrix

is calculated using the formula (6.4.4) K_k. At the next step of the analysis, the desired estimate is determined using the formula (6.4.3) based on the data (6.4.2) and the matrix of covariance of the analysis errors. If observations are not available, we assume that the analysis error covariance matrix is equal to the forecast error covariance matrix, and the analysis estimate coincides with the model forecast.

In this paper, a simplified model is used to calculate the covariance matrices of forecast errors [Klimova, 2003]. In numerical experiments, during the assimilation of satellite data, the standard error between the forecast and observation data is calculated. Then, in the area of the sea in which there is no data, the forecast data from the previous time step is assimilated, taking into account the calculated error. In the area of the sea where satellite information is present in the images, the interpolation of the observation data of the corresponding time step is performed. The error covariance matrix of the Q_k model was set to zero [Shulga, Suslin, Stanichnaya, 2017].

For each time group of satellite and model data, a statistical analysis was performed based on determining the spatial correlation of the values of the *index*34 and $b_{bp}(555)$ parameters. The sets of values of the specified parameters are heterogeneous. Satellite data is heterogeneously distributed over space and time. The modeling data obtained on the basis of the integration of the transport and diffusion equations have a constant discreteness (interval 3 min) [Shulga, 2017].

To analyze the results, 6 groups of the most informative images were selected, for which time series analysis of remote measurements was performed in the following periods:

1. April 26 – May 2, 2013 (interval between images 24-48 h).
2. March 21 – 26, 2013 (interval between images 24 h).
3. August 6 – 10, 2014 (interval between images 24 h).
4. June 23 – 29, 2013 (interval between images 48 h).
5. July 17 – 23, 2014 (the interval between images is 48 h).
6. November 3 –7, 2014 (the interval between images is 48 h).

All satellite data were preprocessed in such a way that, if there were a pair of images with an interval of 30 min of the same current date, they were concatenated into one image, including both of these images. For example, the initial image of the 4th group was obtained from two consecutive images at 9:35 and 11:50 on June 23, 2013 [Shulga, Suslin, Stanichnaya, 2017].

Let's compare the original time series in satellite data groups in order to assess the spread of bioptic indices over time in the waters of the Sea of Azov relative to their initial distribution. For each of the groups under consideration, the coefficient of mutual correlation (r) of the *index*34 and $b_{bp}(555)$ parameters between the observational data and the simulation results at the nodes where data from the two series under consideration are available was determined. The coefficient of mutual correlation of the distribution of biotic indices in the surface layer of the sea is found using the well-known formula

$$r = \frac{\sum_{i=1}^{k}(\mathbf{X} - \overline{\mathbf{X}})(\mathbf{Y} - \overline{\mathbf{Y}})}{\sqrt{\sum_{i=1}^{k}(\mathbf{X} - \overline{\mathbf{X}})^2 \sum_{i=1}^{k}(\mathbf{Y} - \overline{\mathbf{Y}})^2}}. \qquad (6.4.6)$$

The coefficient calculation procedure is performed for the *index*34 and $b_{bp}(555)$ parameters in each of the 6 time groups in those nodes (k) where data from the two series under consideration are available. The table shows the correlation r between the initial $\mathbf{X} = \mathbf{y}^0_{\text{first}}$ and the final $\mathbf{Y} = \mathbf{y}^0_{\text{end}}$ distribution of impurities in the surface layer of the sea according to the available images in groups. The values of this coefficient, varying from one to zero, determine the degree of consistency of the data.

Table 6.4.1 shows the highest ($r_{\max}$) and lowest ($r_{\min}$) values of the cross-correlation coefficients and indicates the time interval corresponding to the strongest or weakest correlation relative to the selected initial parameter in each group. Time series analysis shows that a weak correlation is primarily noted for cases where there is a large difference in the dimensions of n and m with a low-dimensional subspace of observational data. Detailed information on the values of the correlation coefficient is presented in [Shulga, 2017].

Table 6.4.1 – Estimates of the correlation coefficient in 6 groups of satellite images [Shulga, Suslin, 2018]

Group	Parameter	r_{max}	Time interval, h	r_{min}	Time interval, h
1	*index*34	0.83	120	0.63	25
	$b_{bp}(555)$	0.89	240	0.81	288
2	*index*34	0.91	72	0.21	96
	$b_{bp}(555)$	0.94	48	0.50	96
3	*index*34	0.77	72	0.48	24
	$b_{bp}(555)$	0.83	48	0.64	72
4	*index*34	0.86	96	0.14	120
	$b_{bp}(555)$	0.80	24	0.50	48
5	*index*34	0.61	24	0.19	264
	$b_{bp}(555)$	0.86	24	0.44	360
6	*index*34	0.84	48	0.32	96
	$b_{bp}(555)$	0.83	48	0.69	96

The propagation of the *index*34 and $b_{bp}(555)$ parameters was simulated using satellite images of the surface of the Sea of Azov for the same six time groups. Figure 6.4.2 shows the model and satellite distributions of the *index*34 parameter related to the first group of images on April 26 – May 2, 2013. Satellite images are presented in the left column, and in the right – the distributions of the index34 parameter corresponding to each satellite image, as well as the velocity of surface currents (Figure 6.4.2, *b*, *e*, *k*) according to the hydrodynamic model for a close moment in time (the time difference does not exceed 2 h).

Here, the areas shown in white correspond to either clouds or gradient zones that were cut out during data processing. The date and local time are indicated for the model distributions, and the name of the primary MODIS file is given in the satellite data. The color scales in which satellite and model data are presented correspond to each other. Figure 6.4.2, a show the satellite distribution of the index34 parameter adopted in the

experiment as the initial one on April 26, 2013, 10:35 a.m. This initial distribution is assimilated in the model at the time corresponding to the satellite image.

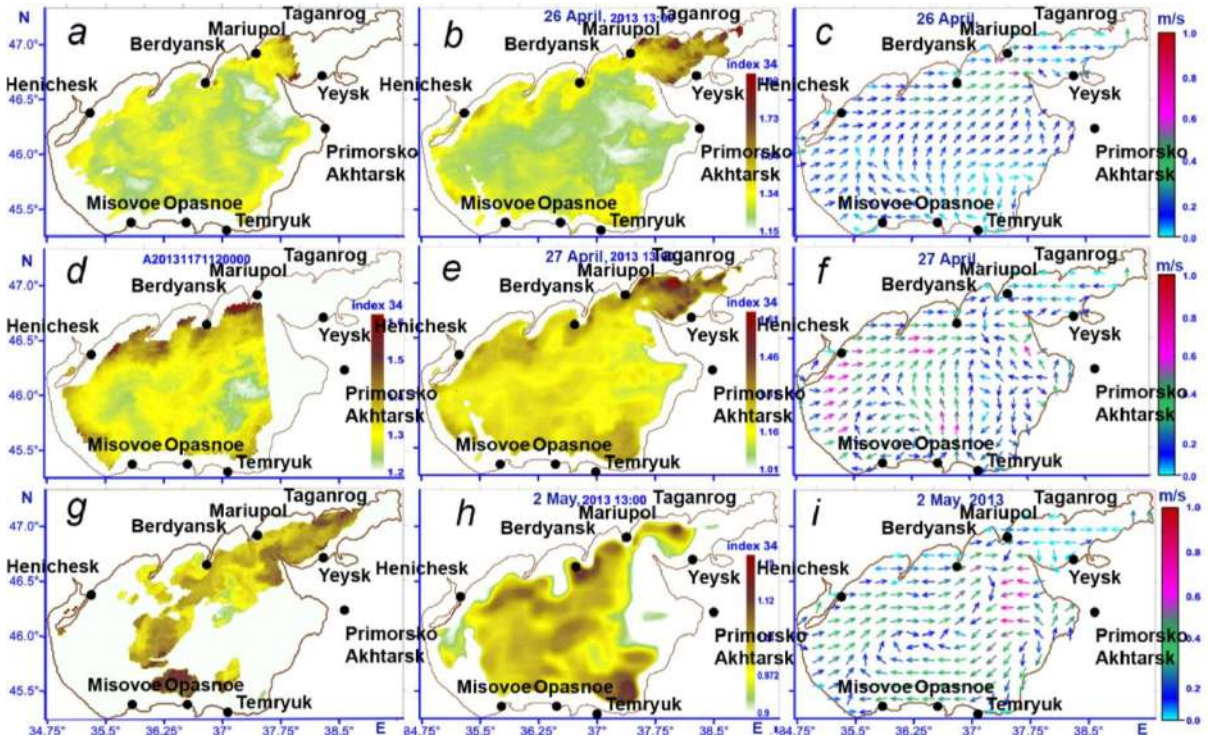

Figure 6.4.2 – Data from satellite observations (first column) and numerical modeling (second column) of the *index*34 parameter in the surface layer of the Sea of Azov. The velocities of surface currents are shown in the third column

Previously, from the start of the model on 04/20/2013, the fields of currents in the sea (Figure 6.4.2, *c*) were generated by the active wind of the SKIRON model. Here (Figure 6.4.2, *a*, *b*), areas with a high concentration of the *index*34 parameter are clearly traced, which extend from the base of the Taganrog Bay towards the open sea. The analysis of wind speed showed that approximately two days before the time under consideration (from 04/24/2013, 00:00), a north-easterly wind developed, the speed of which reached 10-12 m/s. This wind is the most favorable for the transfer of impurities from the Taganrog Bay. The described hydrodynamic scenario is confirmed by model distributions of the surface velocity of currents: the northeast wind is accompanied by currents directed in the same direction as the wind (Figure 6.4.2, *c*). These fields are presented in more detail in [Shulga, Suslin, 2017].

A series of numerical experiments was conducted to evaluate the capabilities of the assimilation algorithm and determine its effectiveness while reducing the interval between data assimilation. The results of the simulation performed using the sequential data assimilation procedure are compared with the results obtained with a single (initial) assimilation. Experiments in groups are performed using the specified algorithm at times when informative satellite images are available. To solve the problem of assimilation of the observational data of the *index*34 and b_{bp}(555) parameters, an algorithm based on the Kalman filter was used, with the calculation of the covariance matrix of forecast errors according to the formula (6.4.5).

The statistics of errors in forecasting the distribution of impurities in the surface layer of the sea is determined by the value of the coefficient of mutual correlation (r) using the formula (6.4.6). The estimation is performed at the same time (corresponding to the final image in the group) between the results of assimilation modeling ($\mathbf{X} = \mathbf{x}^*_{end}$) and satellite data ($\mathbf{Y} = \mathbf{y}^0_{end}$). The analysis of the results of the model forecast is carried out for two assimilation schemes: a single assimilation of the initial satellite image in the group (*Scheme* I); consistent (regular) assimilation of all available series of observations in the interval between the initial and final images (*Scheme* II) [Shulga, Suslin, Stanichnaya, 2017].

The correlation curves illustrating the accuracy of the predicted concentrations of the bio-optical index *index*34 relative to the observed ones are shown in Figure 6.4.3. The nature of the course of the curves reflecting a similar dependence for the parameter b_{bp}(555) is preserved. The analysis of errors in the model forecast performed using a single assimilation of observations is shown in Figure 6.4.3, on the left, and with sequential assimilation – in Figure 6.4.3, on the right [Shulga, 2017; Shul'ga, 2017].

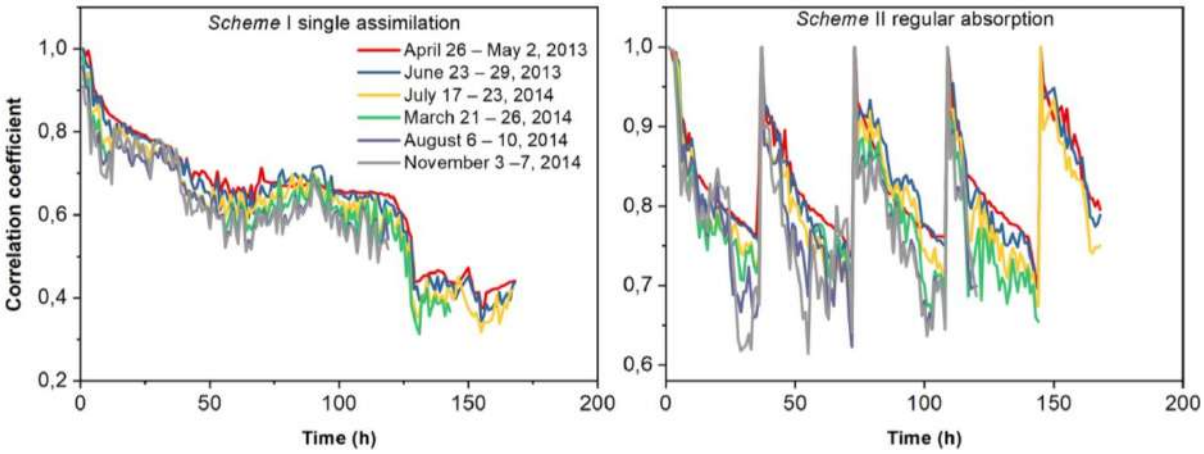

Figure 6.4.1 – Time series of correlation coefficients between satellite and modeled *index*34 values using the assimilation procedures of *Scheme* I (left) and *Scheme* II (right)

Based on the calculated values of *r* and the data given in Table 6.4.1, it can be concluded that the sequential assimilation method (*Scheme* II) is more accurate. Lower correlation values (< 0.5) of forecast and observation data were found for groups with long time intervals and using a single assimilation procedure. Table 6.4.1 shows that the correlation coefficient has a slightly larger error compared to the prediction error performed using sequential assimilation. This is due to the fact that the spatial coverage of the Sea of Azov with MODIS data is subject to significant variations primarily due to clouds and glare, while the results of assimilation modeling make it possible to restore information about the content of suspension in the surface layer of the Sea of Azov.

Figures 6.4.4 and 6.4.5 for comparison show the spatial distribution of the suspension in the surface layer of the Sea of Azov according to the MODIS color scanner and based on numerical modeling using two data assimilation schemes (*Schemes* I and II) developed for this study.

As can be seen from the satellite maps of the transfer of matter, the images are missing in the part of the Azov Sea; where they were under constant cloud cover during this period (such areas are marked in white). The graphs shown in the central and right columns (Figures 6.4.4 and 6.4.5) will allow us to evaluate the improvement of the image

of the spatial distribution of the suspension concentration in the surface layer, based on modeling with the two assimilation schemes discussed above.

	NASA OceanColor data	The modeling results of 3-D POM	
		Scheme I	*Scheme* II
10.01.2013 28.04.2013 19.05.2014 27.11.2014	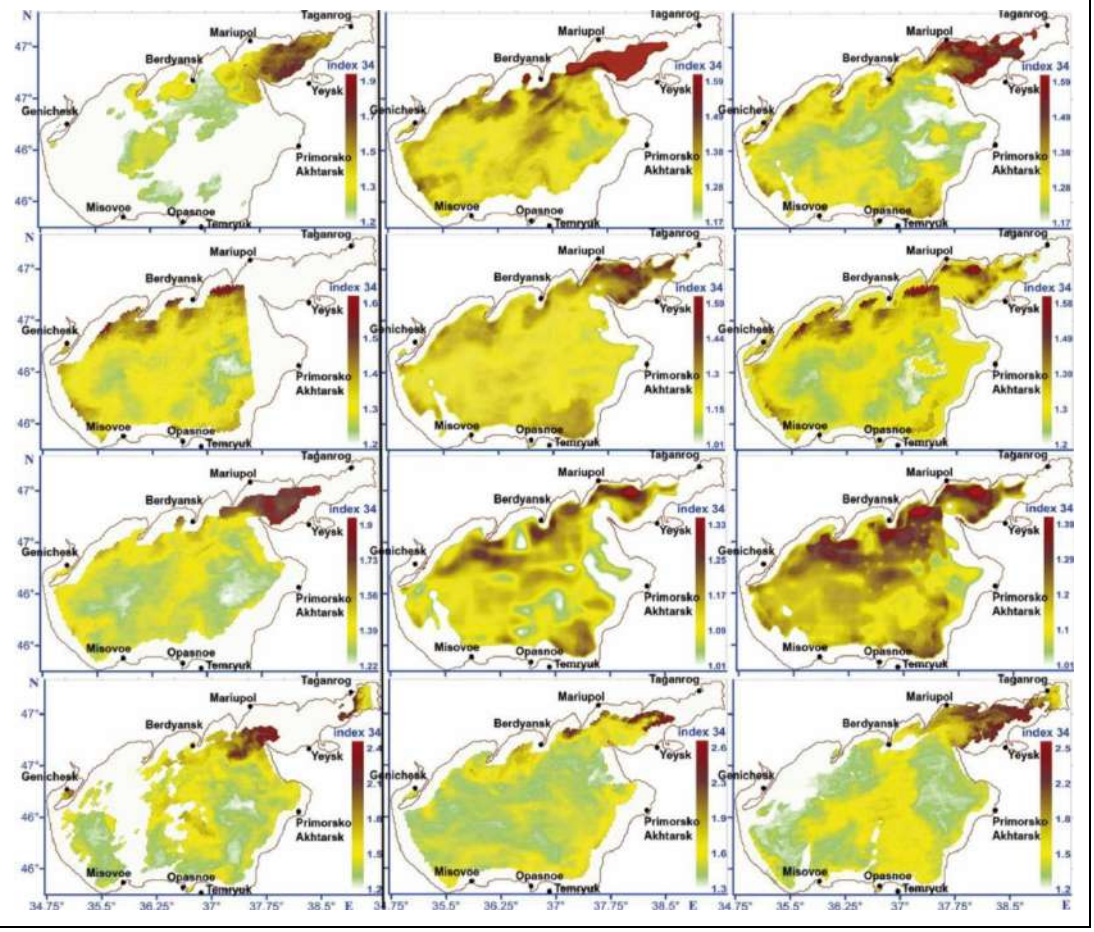		

Figure 6.4.4 – *index*34 spatial distribution maps: MODIS data (left) and based on simulation results using *Scheme* I (center) and *Scheme* II (right)

The right column in Figures 6.4.4 and 6.4.5 demonstrates that the scheme of regular assimilation of observational data makes numerical modeling a more accurate tool for filling gaps due to the unavailability of satellite images and cloud cover [Studies of particulate ... , 2018].

It is easy to see that the highest concentration of suspended matter in the surface layers is observed in Taganrog Bay and Berdyansk, which is closest to the shore.

Apparently, very turbid water is caused by the abrasion of the bottom and shore caused by currents and the transfer of turbid waters from the Don. As expected, the zones with the lowest concentrations of suspended matter are found in the central part of the Sea of Azov, where the concentration of suspended matter drops sharply by an order of magnitude or more. In this area, the currents rate of water into the sea slows down, and the main amount of suspended particles sinks to the bottom (Figures 6.4.4 and 6.4.5).

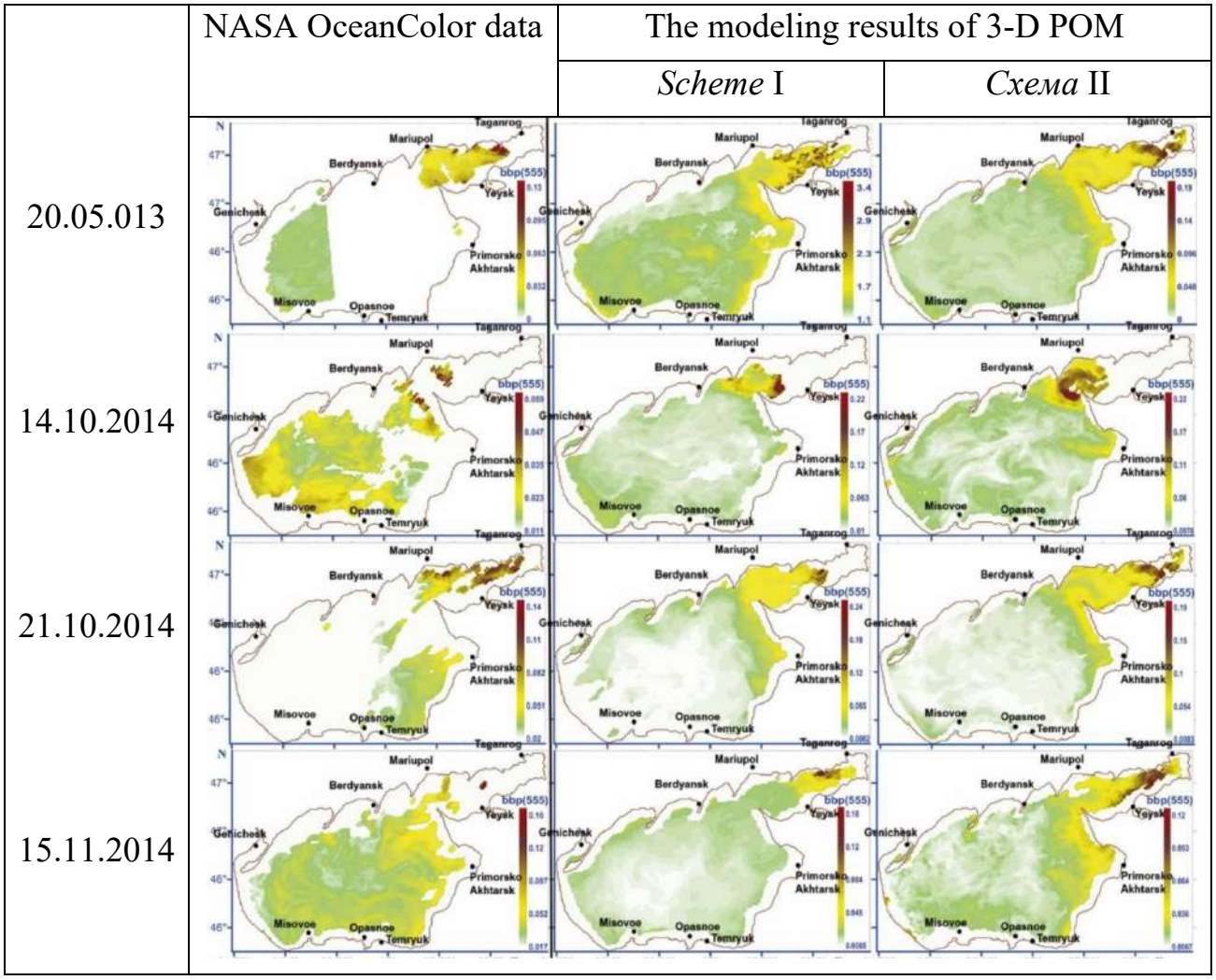

Figure 6.4.5 –Spatial Distribution Maps $b_{bp}(555)$: MODIS data (left) and simulation results using *Scheme* I (center) and *Scheme* II (right)

The analysis of the correlation value between the observational and modeling data carried out for these two experiments indicates that the assessment of the concentration field of the *index*34 and $b_{bp}(555)$ parameters with subsequent assimilation leads

to a significant decrease in the standard error and an increase in the correlation coefficient. A consistent pattern of assimilation of observational data improves the prediction of the distribution of suspended solids according to the model, even with unstable satellite images [Shulga, Suslin, Stanichnaya, 2017; Studies … 2018].

Thus, one of the methods to assimilate more information into the model is to supplement the already available data with information received from other satellites. MODIS-Aqua satellite images used in hydrodynamic modeling are supplemented with MODIS-Terra satellite data in case of partial or complete absence of images. The procedure for supplementing incomplete MODIS-Aqua data with images from the MODIS-Terra satellite corresponds to combining the images shown in Figure 2.1.2.2.

Let us demonstrate (Figure 6.4.6) how the occupancy of observational data (N) on the distribution of, for example, the index34 parameter changes during 2013, 2014 when merging data from MODIS-Aqua/Terra satellites in comparison with information received from each of the satellites. Another modification of the assimilation algorithm is the assignment to the model of information about the distribution of suspended matter not only in the surface layer of the sea, but also in depth. For this purpose, the standard satellite product $K_d(490)$ was used – the attenuation coefficient of scattered light at a wavelength of 490 nm.

For comparison, Figure 6.4.7 shows histograms of observation occupancy based on combined data obtained from MODIS-Aqua/Terra satellites on the distribution of the index34 parameter in the surface and deep layers of the Sea of Azov for 2013, 2014. Figures 6.4.6 and 6.4.7 illustrate that the proposed additional methods of obtaining information will allow for the assimilation of a much larger volume of observational data, allowing for a better assessment of suspended matter in the Sea of Azov.

The evolution of the suspension in the Sea of Azov is determined by the results of modeling performed under the condition that its initial distribution on the sea surface corresponds to a two-dimensional field of satellite data, and the depth distribution is determined by the corresponding thickness of sigma levels set by the value of the coefficient $K_d(490)$. Figure 6.4.8 shows maps of the vertical distribution of the *index*34 parameter at the time of data assimilation ($t = t_{0p}$) and with an integration interval of 1 day.

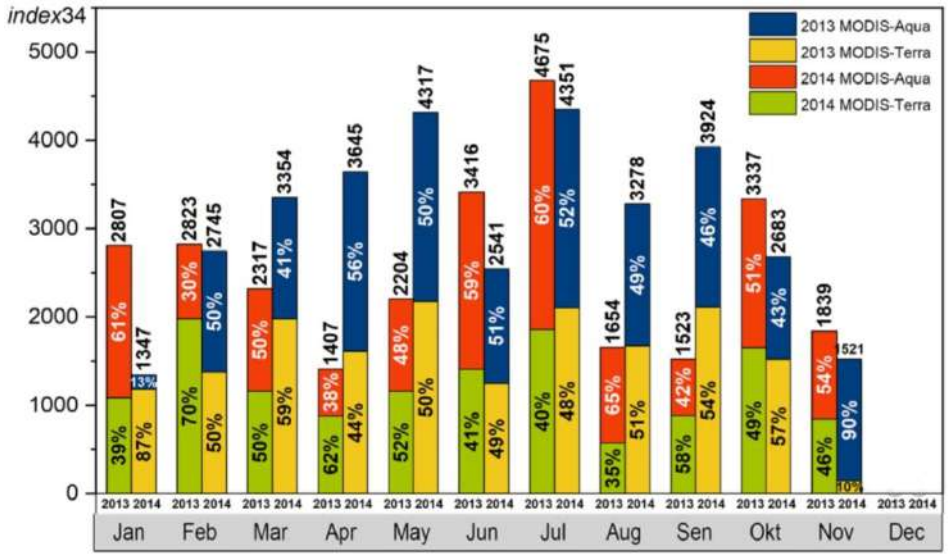

Figure 6.4.6 – Histograms of occupancy with MODIS-*Aqua/Terra* observational data from each of the satellites and when merging data on the *index*34 content on the surface layer of the Sea of Azov in 2013 and 2014

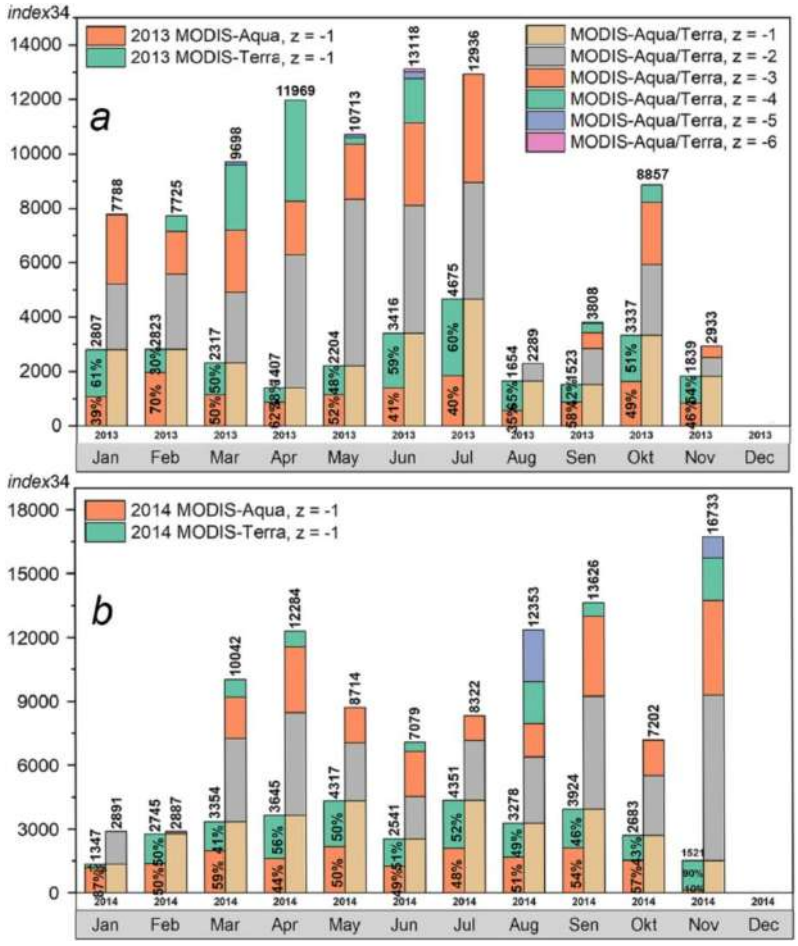

Figure 6.4.7 – Histograms of occupancy with MODIS-*Aqua/Terra* data on the content of *index*34 in the surface layer of the Sea of Azov and at a depth of 2–6 m: *a* – 2013; *b* – 2014

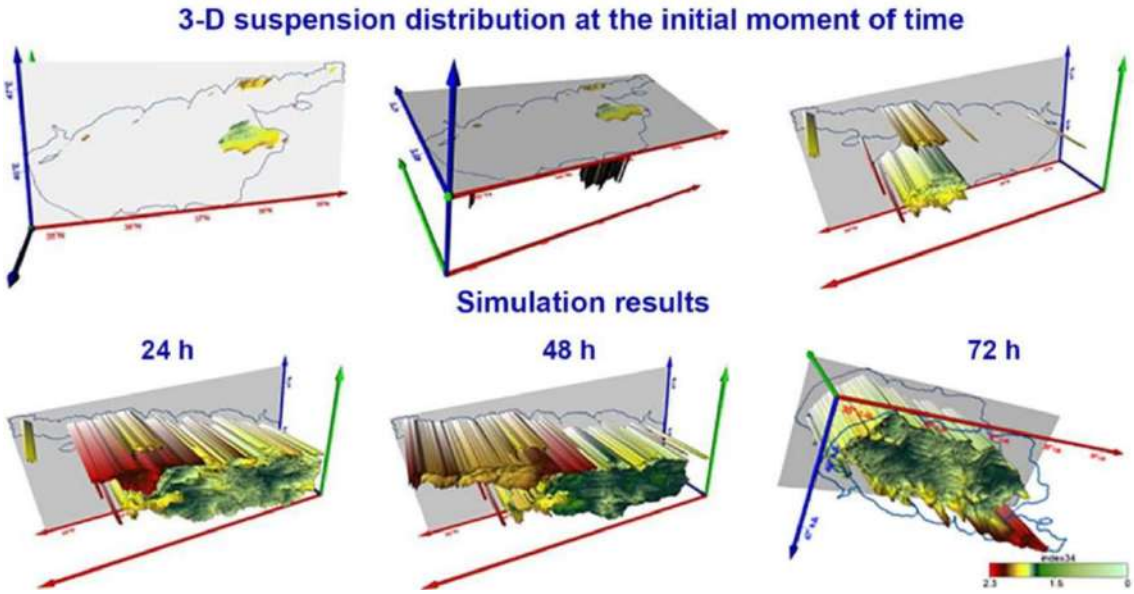

Figure 6.4.8 – Distribution of the *index*34 parameter in the surface and deep layers of the Sea of Azov at the time of assimilation of satellite images and simulation results over the next 3 days

The analysis of the simulation results makes it possible to estimate the total content of suspended matter in the Sea of Azov for the period 2013 – 2014 according to the data of the bioptic indices *index*34 and $b_{bp}(555)$. Figure 6.4.9 shows the distribution of these data: in the rows of histograms on the right are generalized satellite data (MODIS–Aqua/Terra), on the left are the simulation results.

It can be seen that, based on the results of assimilation modeling, it is possible to restore information about the suspension content in the Sea of Azov by filling in data gaps caused by common problems of remote measurements. It has been shown that a consistent pattern of assimilation of observational data improves the prediction of the distribution of suspended solids according to the model even with unstable satellite images [Shulga, Suslin, 2018].

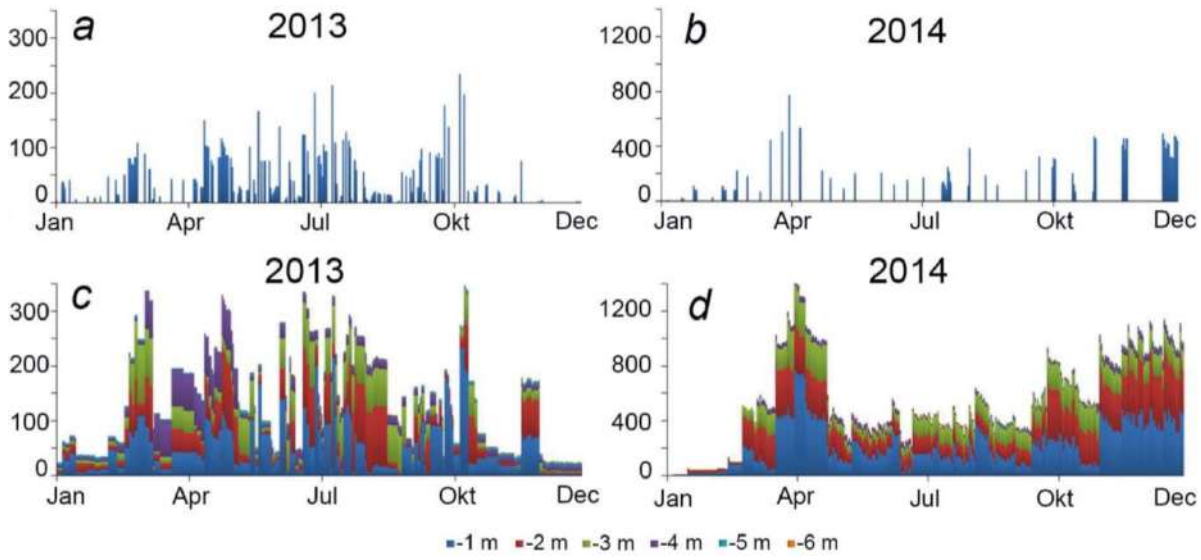

Figure 6.4.9 – Distribution of the $b_{bp}(555)$ parameter in the Sea of Azov for 2013-2014: (a) and (b) – combined MODIS-Aqua/Terra data; (c) and (e) – simulation results

The total content of suspended matter in the Sea of Azov according to $b_{bp}(555)$ for 2013 – 2014. According to modeling and observations, it is shown in Figure 6.4.10 and in percentage terms in Figure 6.4.11. Based on modeling data that most fully reflect the content of suspended matter in seawater, it can be concluded that the highest concentrations of suspended matter throughout the region in the period under review. Comparing the total values of the $b_{bp}(555)$, we note that its highest values are observed from May to June, the lowest in March and December.

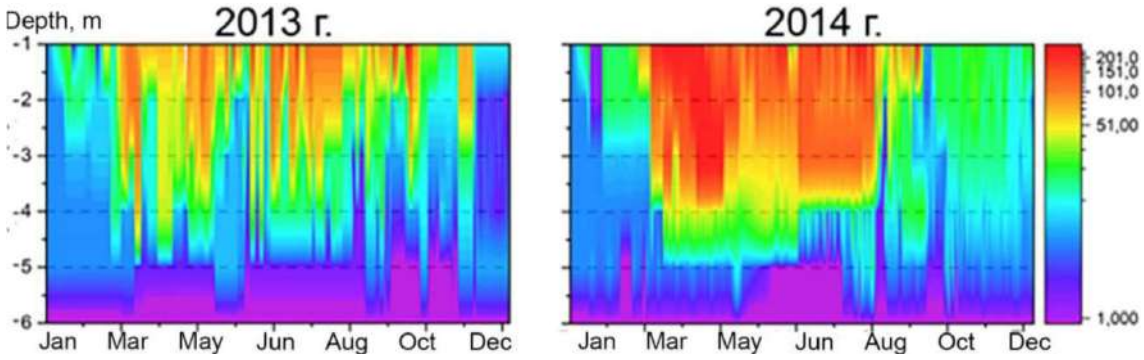

Figure 6.4.10 – Total suspension content in the Sea of Azov according to $b_{bp}(555)$: left – 2013, right – 2014

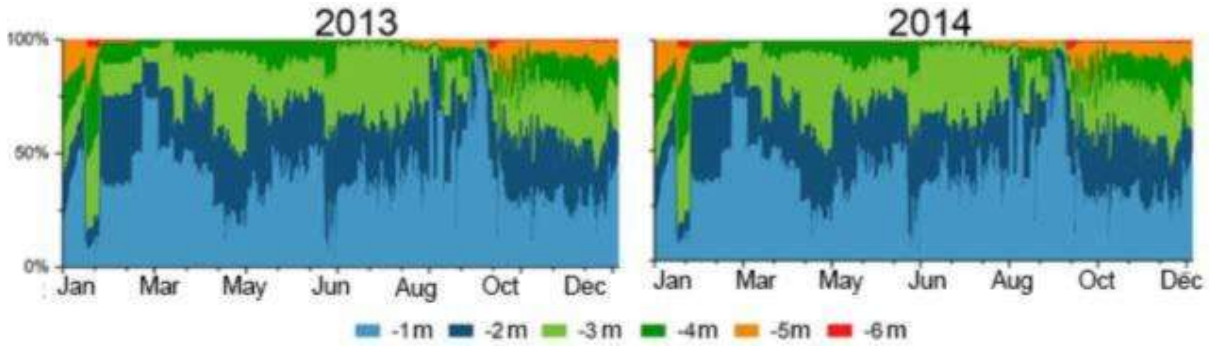

Figure 6.4.11 – Total suspension content in the Sea of Azov according to $b_{bp}(555)$ as a percentage: left – 2013, right – 2014

6.5. Conclusions to Chapter 6

The presented results of mathematical modeling of the spread of pollution in the Sea of Azov make it possible to analyze the characteristic features of changes in its concentration on any selected horizon. Conclusions on the nature of the evolution of pollutants in the Sea of Azov were obtained using the results of hydrodynamic modeling (POM), supplemented by a block for calculating the transport and diffusion of passive impurities. A comparison of the scattering time, as well as the maximum volume of impurity penetration (with constant and variable initial distributions of its concentration) in the presence of a cyclone and gusts of unsteady wind is performed.

It was found that an increase in the maximum wind speed (from 5 to 20 m/s) leads to an increase in the volume of the pollution area due to an increase in the coefficient of turbulent exchange. The transformation of the pollution areas is due to the magnitude and direction of wind currents, the time of lowering the impurity to the horizon equal to half the depth of the sea does not exceed 4 h, into the bottom layer does not exceed 16 h. The total scattering time of the impurity increases with depth. In the field of background stationary currents with maximum velocity values of 14, 34, 62 and 107 cm/s, the total scattering time of the impurity is 54, 55, 58 and 61 h, respectively, under the action of wind gusts of 60, 65, 63 and 71 h, respectively. The movement of a cyclone with a base radius of 100 km at a speed of 5 m/s in the south-west, west and north-west

directions leads to an increase in the time of complete dispersion of the impurity by 107, 113 and 107 h compared with the case of the absence of a cyclone, in the presence of a stationary currents with a maximum speed of 62 cm/s.

The joint analysis of the results of numerical modeling and satellite data provides the most complete information about the directions of transport, sizes and concentrations of pollution areas at the moments of absence of images. A new method of assimilation modeling is proposed, which makes it possible to use the simulation results to restore satellite information losses (primarily due to clouds) when monitoring the content of passive impurities in the surface and deep layers of the Sea of Azov.

Chapter 7.
A METHOD FOR RESTORING DATA ON THE SALINITY OF THE SEA OF AZOV BASED ON NATURAL AND SATELLITE DATA

The Sea of Azov, the shallowest sea in the world, is connected to the Black Sea through the rather narrow Kerch Strait, which causes significant variability in the main hydrometeorological parameters associated with seasonal river currents, salt water intake from the Black Sea and Lake Sivash, weather conditions and anthropogenic pollution [Wolanksi, Elliott, 2015; Climate Change ..., 2021]. River runoff and anthropogenic activities have a great impact on salinity in coastal areas, which makes it more difficult to assess using optical scanner data than in the open sea. [Fournier, Lee, Gierach, 2016]. The high cost and irregularity of field data have led to the search for alternative ways to obtain information about temperature and salinity, including from remote sensing data. However, the gaps caused by the common problems of remote sensing significantly limit the scope and effectiveness of these observations. Alternatively, three-dimensional hydrodynamic models provide full spatial coverage data with a resolution of ~ 1 km, similar to the spatial resolution of remote sensing data in the visible region (~1 km). In addition, the simulated data have a higher time resolution (3 min), which better corresponds to the time resolution of remote sensing observations (~ 1 day). [Shulga and Suslin, 2018, The operational method ... , 2019].

Among the finished products for the study of marine surface salinity (SSS) in real time, data from L-band radiometers on satellites are used: Soil Moisture and Ocean Salinity (SMOS, https://earth.esa.int/web/guest/missions/esa-operational-eo-missions/smos) – a unique MIRAS radiometric interferometer with a resolution of 36×36 km since 2009; Aquarius/SAC-D (https://podaac.jpl.nasa.gov/Aquarius) with a resolution of 110×110 km since 2011; Soil Moisture Active Passive (SMAP, https://smap.jpl.nasa.gov /) with a resolution of ~ 45×45 km since 2015. For shallow, slightly saline waters, there is a possibility of significant SSS errors during remote observations, and the small size of the Sea of Azov requires higher satellite data resolution than provided by Aquarius/SAC-D. Although the natural way to obtain data

on the salinity of the sea surface from a satellite is to use L-band radiometers (SMOS [SMOS ... , 2010], SMAP [The Soil Moisture ... , 2010], Aquarius), with a resolution of at least 25 km, land, sea and radio frequency interference pollution [SMOS instrument ... , 2016] to prevent obtaining valid L-band salinity values in this region. Due to this, unlike sea surface temperature (SST), obtaining up–to-date information about salinity in the Sea of Azov from remote sensing data is possible only indirectly, for example, using the method proposed in the article - by establishing empirical links with available OceanColor satellite data https://oceancolor.gsfc.nasa.gov/ [(MODIS) Aqua, 2022; (MODIS) Terra, 2018].

Today, data from optical satellites making daily overflights and high-resolution images are widely used for near-real-time salinity studies. In [Khorram, 1982], which is one of the first papers devoted to the results of using optical satellite images to estimate SSS based on the multiple linear relationship between MSS Landsat and SSS. The reconstruction of the SSS is based on its significant correlation with the Colour Dissolved Organic Matter (CDOM) defined for the oceans [Pan-Arctic optical ... , 2017] and seas, for example, the Clyde Sea [Optical Properties ... , 2000], the Kara Sea [Glukhovets, Goldin, 2018]. This method directly links the SSS to the CDOM calculated on the basis of the satellite product, the reflection coefficient of remote sensing. (R_{rs}) [Retrieval ... , 2019], or indirectly based on the association of SSS with regional bio-optical parameters [Glukhovets, Goldin 2018]. Indeed, there are some successes in the search for L-band data in the Black Sea [Monitoring ... , 2023], but there is no data consistent with observations in the Sea of Azov yet [Shukalo, Shulga, Suslin, 2023].

This section is devoted to the analysis of the results of the proposed method for restoring surface salinity in the Sea of Azov, which will: (1) establish general empirical regression relationships between regional bio-optical parameters based on MODIS images and *in situ* climatological data, (2) provide a flexible approach to a variety of data sets, (3) confirmed by comparing the reconstruction salinity values with long-term average climatic trends based on *in situ* data.

A flexible approach is provided by choosing one of two methods for restoring salinity, depending on the availability of statistically significant data sets. The first one

is used if the available *in situ* data sets and bio-optical parameters have sufficient sample sizes in individual years. In this case, it is sufficient to obtain a regression for each such year, and a general equation (*average regression*) by directly averaging the regression coefficients. In the second approach, cumulatuve regression equations are established between general aggregates combining *in situ* data and bio-optical parameters for the entire observation period. This approach was used in [Communication Research ..., 2020; Shulga, Suslin, Shukalo, 2020]. The terms "*average regression*" and "*cumulatuve regression*" are discussed in detail in subsection 7.4.

7.1. Construction of climate data sets on temperature and salinity of the Sea of Azov based on oceanographic databases

Long-term trends and seasonal variability of temperature and salinity were calculated using field measurements from the oceanographic database of the Federal Research Center “Southern Scientific Center of the Russian Academy of Sciences” in 1913–2018 (http://atlas.ssc-ras.ru/azs/azs-invent.html), www.seadatanet.org/ and www.nodc.noaa.gov/OC5/WOD/pr_wod.html. Analysis of observational data confirmed the high variability of the distribution of temperature and salinity in the sea (Table 7.1.1). Such high spatial variability was one of the reasons for identifying three subregions to describe.

Another reason for their isolation was the peculiarity of the geomorphological structure of the Sea of Azov, namely the high heterogeneity of its relief in the areas of braids, overcurrentss, estuaries and bays compared with deeper areas of the central part of the sea [Hydrometeorological ..., 1962; Hydrometeorological ..., 1986; Hydrometeorology ..., 1991; Black Sea and Sea of Azov, 2003]. For this purpose, the research area is divided into subdistricts (Figure 7.1.1, *b*): the shallowest part is the Taganrog Bay (AZ1: 37.7–39.3° E; 46.7–47.3° N) with depths of no more than 4 m; the central part of the sea (AZ2) with a maximum depth of ~ 14 m; and the deep–water part with depths up to 200 m, including the Kerch Strait and the adjacent part of the Black Sea (AZ3: 35.3-37.6 ° E; 45-45.5° N). Moreover, this division of the waters of the Sea

of Azov into subregions is due to the fact that that the bio-optical model used here is configured properly only for the central part of the sea (for a detailed description of the model, see section 7.3) [Regional ..., 2020].

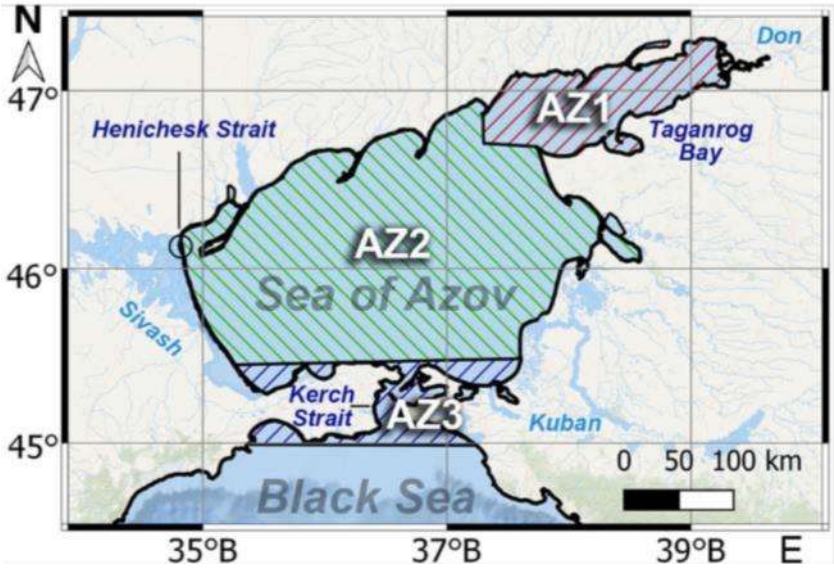

Figure 7.1.1 – The basin of the Sea of Azov, indicated on the map in a black rectangle (*a*). Map of the Sea of Azov. Green, blue and red shading indicate the subregions: AZ1 – Taganrog Bay, maximum depths no more than 4 m; AZ2 – the central part of the Sea of Azov, maximum depth ~ 14 m; AZ3 – Kerch Strait and adjacent parts of the Azov and Black Seas, depths up to 200 m (*b*).

In addition, it is necessary to divide the subregions of the Sea of Azov vertically into surface, middle and deep-water layers in order to establish a correlation between natural salinity and remote sensing data at the first optical depth (0.2 m). The same is true for the correct verification of the results of the reconstruction of salinity in the surface layer. The threshold for *in situ* data to be taken into account in the regression is a depth of 0 – 2 m. The remaining dimensions are filtered out. This separation is also motivated by the need to use datasets of long-term average values of field data in the next stages of work. It determines the need for a separate analysis of the thermohaline structure of the sea in the selected areas, taking into account the depth differentiation. The ranges of temperature and salinity changes, maximum and minimum values according to observations for 1913 – 2018, presented in Table 7.1.1, confirm the validity of such a separation.

The data analyzed *in situ*, averaged by month at all stations for the entire observation period (1913 – 2018), are presented in Figure 7.1.2 as cumulative graphs of temperature and salinity for each subregion. The curves of average salinity values show noticeable differences for the deep-water (AZ3) and shallow-water areas (AZ1, AZ2) of the studied area. Salinity in the Taganrog Bay in the surface and middle layers of the sea (AZ1) does not exceed 7 % (October), its minimum values occur in March (0.9%). In the central part of the Sea of Azov (AZ2), salinity varies in a narrow range of 9 – 13 %, its highest values are observed in March and October (Table 7.1.1). The highest salinity values for the studied area are observed in the area of the Kerch Strait (AZ3). In the middle layer of the sea, its values reach 17.9 %, exceeding three times the salinity in the Taganrog Bay [Research ... , 2020].

Table 7.1.1 – Range of changes in salinity (S, %) and temperature (T, °C) for the areas of the Sea of Azov according to field observations in 1913 – 2018

Subregion	**Depth (m)**	**Salinity (%)**			**Temperature (°C)**		
		S_{min}	S_{max}	$S_{avg} \pm \sigma$	T_{min}	T_{max}	$T_{avg} \pm \sigma$
AZ1	0–2	1.0	6.4	4.26±1.37	0.1	24.1	11.58±9.45
	2–4	1.9	7.0	4.87±1.28	1.1	23.7	12.80±9.08
AZ2	0–2	9.9	11.8	10.89±0.53	0.4	24.2	12.21±9.23
	2–6	10.0	12.4	11.08±0.61	1.1	24.7	11.92±8.81
	6-14	10.9	12.1	11.62±0.38	0.9	23.9	11.53±9.08
AZ3	0–2	12.4	15.9	13.63±1.11	3.6	23.9	12.85±8.09
	2–10	11.4	17.9	12.95±1.71	3.2	23.7	12.51±8.00
	> 10	10.8	14.0	12.52±0.94	1.1	23.8	13.08±8.13

Compared with changes in salinity, the seasonal nature of temperature changes is almost the same for different layers of the sea and subregions of the studied area (Figure 7.1.2). The maximum temperature of the Sea of Azov is observed in August and is 24.7 °C, the deviation of maximum temperature values between subregions and layers

does not exceed 1 °C. The minimum sea temperature observed in January in the AZ1 sub-region (0.1 °C) is 3.5 °C less than the minimum observed in the AZ3 sub-region due to water exchange with the Black Sea. A detailed quantitative analysis of the average monthly data averaged over the entire observation period is presented in Table 7.1.1. Here, the maximum, minimum and average values for temperature and salinity are given at various layers of the sea for each studied sub-region, taking into account their standard deviations (σ) [Research ... , 2020].

The nature of the interannual temperature variability is confirmed by thermal maps of normalized salinity and temperature anomalies shown in Figure 7.1.2.

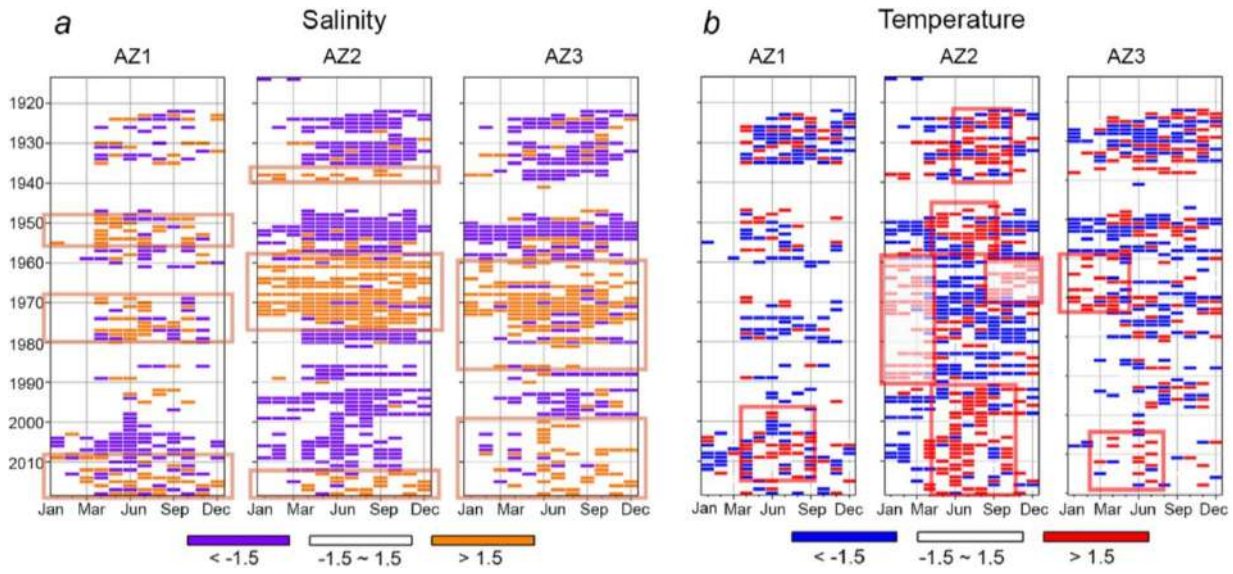

Figure 7.1.2 – Thermal maps of normalized anomalies of salinity (*a*) and temperature (*b*) in the subregions of the Sea of Azov. Periods of positive normalized anomalies, defined as strong and very strong, are marked with orange and red rectangles.

Normalized anomalies were calculated as the standard normalized equivalent: $Ai = (X_i - X_{mean})/\sigma$, were X_i is the value of a variable (for example, salinity, temperature), Xmean is the monthly average, σ is the standard deviation for the same month. Further, anomalies are classified as follows: < 0.5 – minor, 0.5 – 1 – weak, 1 – 1.5 – moderate, 1.5–2 – strong, > 2 – very strong. Linear trends of normalized anomalies of temperature and salinity of the Sea of Azov for 1913-2018 are given for each subregion and layer [Shukalo, Shulga, 2021]. These dimensionless normalized anomalies allow for joint

analysis of various types of data (for example, temperature and salinity). They allow you to identify trends rather than similarities/differences in the amplitude of data sets. Such a comparison of the structure of temperature and salinity anomalies observed in the formation can be carried out using heat maps, as shown in Figure 7.1.2. Here, periods of positive normalized anomalies, defined as strong and very strong, are marked with orange and red rectangles.

Since salinity is not directly dependent on the atmosphere, salinity anomalies can be very stable for several years. On the contrary, temperature anomalies are often compensated by heat exchange between air and sea [Bull. ... , 2021]. In Figure 7.1.2, periods of desalination and salinization lasting several years are clearly distinguished for each of the subregions of the Sea of Azov (Table 7.1.2). The boundaries of the periods (for example, salinity in orange rectangles) for AZ2 and AZ3 are shifted relative to each other and, compared with AZ1, practically do not coincide, except for general salinity trends in the modern period 2000 – 2018.

Table 7.1.2 – Periods of salinization and desalination of the Azov sub-regions according to field observations in 1913 – 2018

Subregion	**Periods (years)**	
	Salinization	Desalination
AZ1	1948–1956; 1969–1980; 2008–2018	1922–1934; 1996–2002
AZ2	1937–1940; 1959–1986; 2012–2018	1913–1935; 1947–1958; 1987–2002
AZ3	1960–1987; 2000–2018	1922–1939; 1948–1959; 1986–1999

As can be seen from Figure 7.1.2, seasonal differences in salinity anomalies are not pronounced, unlike sea temperature anomalies. Seasonal fluctuations in sea temperature (warming in red rectangles) with slight interannual variability are clearly visible. In spring and summer (April – August 1946 – 1957 and 1993 – 2018), negative temperature anomalies are replaced by positive ones in autumn and winter (in red rectangles). The reverse process, demonstrating the change of positive temperature anomalies in autumn-winter to negative anomalies in spring-summer, can be observed in the periods

1958 – 1992 in January – April and 1959 – 1969 in September – December. These results are recorded in the registered electronic database "Thermohaline electronic Atlas of the Sea of Azov" [Shulga, Shukalo, 2023].

7.2. Building a dataset of bio-optical parameters and combining it with *in situ* data

At the second stage, the data covering the last period of remote sensing of ocean color MODIS Aqua/Terra (R2018) in 2000-2018 were analyzed, systematized and rejected according to the criteria proposed in [Assessment …, 2002]. These data were processed to implement quality control and combine all satellite data. The stage included combining the prepared MODIS data with field measurements based on compliance with the following criteria: (1) salinity was measured at a depth of no more than 2 m; (2) the dates of satellite images and field observations coincided; (3) for the same dates of remote sensing and field data, the deviation of their coordinates did not exceed 0.01°: $\sqrt{(lat_{in\ situ} - lat_{\mathrm{MODIS}})^2 + (long_{in\ situ} - long_{\mathrm{MODIS}})^2} < 0.01°$. The ocean color data set processed in this way was further transformed into spatio-temporal maps of bio-optical parameters calculated using regional algorithms proposed in [Regional ..., 2020; Spectral ..., 2022].

The source of information for obtaining the values of bio-optical parameters are operational satellite products of remote sensing of Ocean Color. Each set of satellite data with a spatial resolution of 1 km was converted by linear spatial interpolation into spatial maps of five bio-optical parameters on a regular grid of the Sea of Azov with a resolution of 0.01° (0.77 km) in longitude and 0.01° (1.11 km). km) latitude (451×220 knots).

7.3. Regional bio-optical algorithm for remote assessment of the *IOP*s of the Sea of Azov

It is well known that the standard satellite algorithm [Ocean color ... , 1988; SeaWiFS ... , 2000] incorrectly determines the concentration of chlorophyll in coastal areas and inland seas, for example, in the Black Sea [Assessment …, 2002; Application ... , 2004; Suslin, Churilova, Sosik, 2008]. In this case, the Sea of Azov is no exception.

According to the classification given in Table 6.2.1, the Sea of Azov better corresponds to the category of "Inland seas, estuaries, lakes". Therefore, to obtain our own optical properties (*IOP*s), we use an algorithm close to that described in [Gitelson, 1992; Dall'Olmo, Gitelson, 2005; A simple semi-analytical ... , 2008; A bio-optical algorithm ... , 2009]. The similarity of our algorithm with that described in [Dall'Olmo, Gitelson, 2005; A simple semi-analytical ... , 2008; A bio-optical algorithm ... , 2009] is that we used spectral bands in the long-wavelength region of the spectrum to obtain *IOP*s. The difference is that we have obtained a complete set of *IOP*s, and not only in terms of chlorophyll concentration, so a regional algorithm was developed for the central part (AZ2) of the Sea of Azov [Regional ..., 2020; Spectral ..., 2022]. This article discusses the results of applying a salinity estimation algorithm that uses predicted *IOP*s parameters as input data [Regional ..., 2020]. The main source of information about the *IOP*s of the upper water layer is the spectrum of the reflection coefficient of remote sensing (R_{rs} – "normalized" reflective radiance (nL_w), which is associated with the reflectivity of remote sensing through $R_{rs}=nL_w/F_o$, were F_o is the solar radiation of the upper atmosphere), which is the product of atmospheric correction of measurements of the spectrum of ascending radiation of the "reservoir" system – a cloudless atmosphere."

The classification given in Table 7.3.1 reflects the relationship of the spectral range with the maximum variability of the Rrs spectrum with the trophic status of reservoirs in the chlorophyll concentration scale. The maximum variability of the R_{rs} spectral range shifts from blue to red during the transition from low biological productivity to high (see Table 7.2.1).

This is a consequence of the following: (1) for oligotrophic water, there is an unambiguous relationship between the concentrations of optically active substances and, as a result, one R_{rs} ratio in two bands located in the blue-green region of the spectrum. It is sufficient to determine the concentration of chlorophyll; (2) for mesotrophic waters, absorption requires at least two R_{rs} ratios from the green-yellow visible region, i.e. at least three bands, to separate the absorption associated with algae (phytoplankton) and non-algae (phytoplankton) and non-algae (phytoplankton). the sum of colored components of dissolved organic matter and inorganic suspension) of independently varying optically

active components of seawater; (3) for eutrophic waters of the red region of the spectrum, the main factors are particle scattering and absorption by phytoplankton.

Table 7.3.1 – Classification of trophic water levels depending on the wavelength range of the maximum variability of the spectrum R_{rs}.

Region	**Maximum variability of R_{rs} spectrum, nm**	**Range of chlorophyll a concentration, mg·m^{-3}**	**Reference**
Offshore ocean water	400 – 500	0,01 – 1,0	[SeaWiFS ... , 2000]
Coastal areas, inland seas	500 – 600	0,1 – 10	[Assessment …, 2002; Gitelson, 1992]
Inland seas, estuaries, lakes	600 – 700	1,0 – 100	[Dall'Olmo, Gitelson, 2005; A simple semi-analytical ... , 2008; A bio-optical algorithm ... , 2009]

The essence of our approach was as follows: (1) the use of regional connections between the measured values of light absorption and the combination obtained from satellite products (R_{rs} spectrum from the wavelength range 600-700 nm, namely: central bands at 645, 667 and 678 nm); (2) correction taking into account scattering by suspensions in the long-wave part of the spectrum and possible atmospheric correction errors, which were minimized by using the difference between bands for close wavelengths. On the other hand, the difference $R_{rs}(667) - R_{rs}(678)$ was proportional to the difference $a_{ph}(667) - a_{ph}(678)$, and the difference $R_{rs}(645) - R_{rs}(667)$ t o the backscattering coefficient of light by particles, which is up to a multiplier equal to the backscattering coefficient of light by particles for the difference $R_{rs}(667) - R_{rs}(678)$. The essence of the approach is that $R_{rs}(678)$ is, in the first approximation, a function of $a_{ph}(678)$ and $b_{bp}(678)$. The other two bands $R_{rs}(645) - R_{rs}(667)$ are functions of $b_{bp}(678)$ and $b_{bp}(678)$ respectively. In the modern version of the regional algorithm, we ignore

the solar-induced fluorescence signal. We have studied the following bio-optical parameters, which are markers of living and inanimate organic matter in seawater.

The light absorption coefficient of phytoplankton at 678 nm is calculated according to the equation obtained on the basis of empirical data [Spectral ..., 2022]:

$$a_{\mathrm{ph}}(678) = -0.312\frac{R_{\mathrm{rs}}(667)-R_{\mathrm{rs}}(678)}{R_{\mathrm{rs}}(645)-R_{\mathrm{rs}}(667)} - 0.3, \text{ м}^{-1} \quad (7.3.1)$$

were $R_{\mathrm{rs}}(645)$, $R_{\mathrm{rs}}(667)$ and $R_{\mathrm{rs}}(678)$ are the remote sensing reflectances at 645, 667 and 678 nm, respectively. The range of applicability of expression (1) is determined by the range of variability of *in situ* measurements of $a_{ph}(678)$ from 0.014 to 0.3 m^{-1}, which approximately corresponds to the interval to the interval of *TChl* from 1 to 30 $mg \cdot m^{-3}$.

The sum of concentrations of chlorophyll a and pheophytin *TChl* ($mg \cdot m^{-3}$) is a function of $a_{ph}(678)$ (m^{-1}) obtained from *in situ* measurements [Spectral ..., 2022]:

$$TChl = a_{\mathrm{ph}}(678)\left(50\left[1 + cos\left(\frac{2\pi}{365}sday\right)\right] + 90\right), \quad (7.3.2)$$

where *sday* is the sequent day in year.

The coefficient of light absorption by coloured detrital matter:

$$a_{\mathrm{CDM}}(438) = a_{\mathrm{COM}}(438) - a_{\mathrm{ph}}(438), \quad (7.3.3)$$

where $a_{COM}(438) = a_{tot}(438) - a_w(438)$ (*COM* stands for Coloured Organic Matter), which is easy to obtain from the desired inherent optical properties (*IOP*s) characteristics

at 438 nm, a_{tot} and a_w (coefficients of light absorption by sea water and pure sea water, respectively).

The light absorption coefficient by all optically active components of the medium:

$$a_{\text{tot}}(438) = a_{\text{CDM}}(438) + a_{\text{w}}(438) + a_{\text{ph}}(438). \quad (7.3.4)$$

The particle backscattering coefficient:

$$b_{\text{bp}}(438) = b_{\text{b}}(438) - b_{\text{bw}}(438), \quad (7.3.5)$$

where $b_b(438)$ and $b_{bw}(438)$ are the backscattering coefficients by sea water and pure sea water, respectively.

7.4. Regression models for salinity reconstruction

In the third stage, we determined the regression relationships between the measured salinity values and regional satellite products. These equations were derived for the central part of the Sea of Azov (AZ2) in the spring-summer period in the upper layer of the sea. Ideally, we would like to obtain a general equation that establishes the relationship between field and remote measurement data. In fact, we have to face serious practical problems, such as the small sample size in individual years or seasons, determined by the number of pairs meeting the criteria described in paragraph 7.2. For autumn and winter, the number of synchronous pairs of bio-optical and *in situ* salinity data turned out to be insufficient, so we limited our study to two seasons. This has also led to the use of conceptually different approaches to obtain regression equations:

Average regression is a method based on obtaining the resulting regression by directly averaging the coefficients of statistically significant regressions obtained for each selected year, provided that the pairs of on–site and remote sensing measurement data are representative.

Cumulative regression is a method based on obtaining the resulting regression between the general data sets for the entire observation period 2000 – 2018.

The present study is devoted to comparing the results of salinity reconstruction obtained using the above methods. The choice between these methods, which depends on the availability of representative datasets of on-site measurements and remote sensing, provides flexibility in their use. Another purpose of the study is to identify a regional bio–optical parameter, the use of which shows a high correlation between the reconstructed salinity values and *in situ* data.

At the final stage of the work, the results of the reconstruction of surface salinity were compared with natural data for the central part of the Sea of Azov (AZ2). An integral statistical evaluation of the differences between the reconstruction and initial values for the spring and summer seasons was performed. Two *in situ* observation periods were selected in order to estimate the average values of the reconstruction salinity in time and beyond the calibration/study period. The choice of a short-term period (calibration period 2000 – 2018) is due to the limitation associated with the availability of MODIS-Aqua/Terra satellite data. The period 1990 – 2018 covering the calibration period was chosen to justify that beyond the calibration period, the average values of reconstruction salinity are within 95% confidence intervals of the long-term trend in situ. This will allow the proposed method to be used for retrospective reconstruction of salinity in the protosatellite epoch (in the absence of MODIS data).

Average regression.

Regression dependences linking these parameters with *in situ* data were obtained for each of the considered bio-optical parameters for the AZ2 region in spring and summer. Regression dependencies for spring and summer with confidence limits with a 95% probability were obtained using the OriginLab application, a software for plotting and data analysis (*www.originlab.com*). This study does not consider autumn and winter,

since the amount of available data for these seasons does not allow for a statistically significant correlation analysis. In the future, we plan to conduct research for the autumn and winter seasons.

The correlation coefficients of linear regressions between regional bio–optical products and *in situ* data in 2004, 2005, 2007, 2009, 2018 are shown in Figure 7.4.1. Here is the total value of sample volumes (N_1 for spring, N_2 for spring). summer) and regression statistics (R_1 for spring, R_2 for summer). Detailed graphs of regression dependencies for each bio-optical parameter are given in [Shulga, Suslin, Shukalo, 2022].

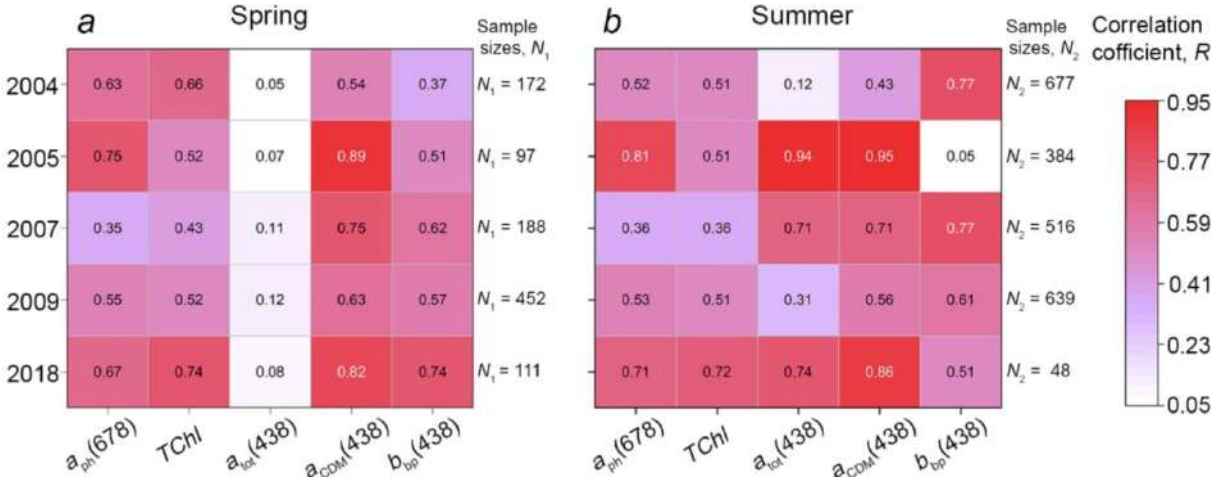

Figure 7.4.1 – Correlation coefficients of linear mean regressions between regional bio–optical products (7.3.1) – (7.3.5) and *in situ* data in spring (*a*) and summer (*b*).

As can be seen in Figure 7.4.1, in a number of the cases considered, there is a weak linear correlation between the measured salinity and regional satellite products (for example, $R = 0.05$ for $b_{bp}(438)$ in 2005). Such cases are excluded when compiling generalized empirical equations for regressions with correlation coefficients not exceeding 0.5. Bio-optical parameters with a coefficient of correlations of less than or equal to 0.5, for which more than half of the dataset was excluded, are not used for the average regression approach. In these cases, a more complex nonlinear relationship was established between the optical parameters and the observed salinity. This relationship is described by a polynomial above the second degree.

The *average regression* equations have the form:

$$y = (a_{\text{aver}} \pm \sigma_1)x + (b_{\text{aver}} \pm \sigma_2), \qquad (7.4.1)$$

were $x - x$ is salinity (‰); y is the value of the regional bio-optical products; a_{aver} and b_{aver} are the mean values of the regression coefficients; σ_1 and σ_2 are their corresponding RMS. As a result of the average regression dependence for each bio–optical parameter calculated using formulas (7.3.1) – (7.3.5), two families of lines of the form (7.4.1) corresponding to spring and summer were obtained, as shown in the upper part of Table 7.4.1. Also, in the lower part of Table 7.4.1, a variant of generalized linear regression equations compiled from cumulative sets is presented data.

Table 7.4.1 – Linear regression equations [Shulga, Suslin, Shukalo, 2022]

Biooptical parameter	**Spring**	**Summer**
	Average regressions	
$a_{ph}(678)$, m^{-1}	$y = (0.038 \pm 0.008)x + (-0.334 \pm 0.132)$	$y = (0.041 \pm 0.024)x + (-0.355 \pm 0.250)$
TChl, mg m^3	$y=(2.442 \pm 0.110)x + (-20.940 \pm 2.594)$	$y=(1.894 \pm 1.008)x + (-16.500 \pm 11.004)$
$a_{tot}(438)$, m^{-1}	non linear relations	$y = (-0.192 \pm 0.078)x + (3.654 \pm 0.515)$
$a_{CDM}(438)$, m^{-1}	$y = (-0.287 \pm 0.303)x + (4.710 \pm 3.816)$	$y = (-0.261 \pm 0.071)x + (4.217 \pm 0.548)$
$b_{bp}(438)$, m^{-1}	$y = (-0.082 \pm 0.029)x + (1.006 \pm 0.334)$	$y = (-0.043 \pm 0.029)x + (0.561 \pm 0.296)$
	Cumulative regressions	
$a_{ph}(678)$, m^{-1}	$y = 0.015x - 0.09$, $R_1 = 0.50$	$y = 0.017x - 0.072$, $R_2 = 0.56$
TChl, mg m^3	$y = 0.765x - 2.865$, $R_1 = 0.34$	$y = 0.820x - 4.134$, $R_2 = 0.61$
$a_{tot}(438)$, m^{-1}	non linear relations	$y = -0.173x + 3.516$, $R_2 = 0.70$
$a_{CDM}(438)$, m^{-1}	$y = -0.070x + 1.993$, $R_1 = 0.68$	$y = -0.214x + 3.690$, $R_2 = 0.77$
$b_{bp}(438)$, m^{-1}	$y = -0.035x + 0.509$, $R_1 = 0.43$	$y = -0.022x + 0.332$, $R_2 = 0.53$

Cumulative regression.

Another way to restore salinity is to construct cumulative regression equations between aggregated *in situ* and MODIS datasets. In this case, a general linear regression relationship is established for two datasets of the AZ2 region prepared in accordance with the above criteria. Here (Table 7.4.1) we present regression statistics (R_1 for spring,

R_2 for summer) for cumulative regression with corresponding sample sizes N_1 = 10240 for spring, N_2 = 18362 for summer; The sample sizes for the selected years of the average regression are also shown in Figure 7.4.2.

Maps illustrating the spatial distribution of *in situ* and MODIS data pairs and sample sizes used for *cumulative regression* in the spring and summer of 2000 – 2018 are shown in Figure 7.4.2. Note that when mapping using the OriginLab application for closely spaced *in situ* and MODIS pairs, these points overlap, forming clusters with minimal difference in the center clusters.

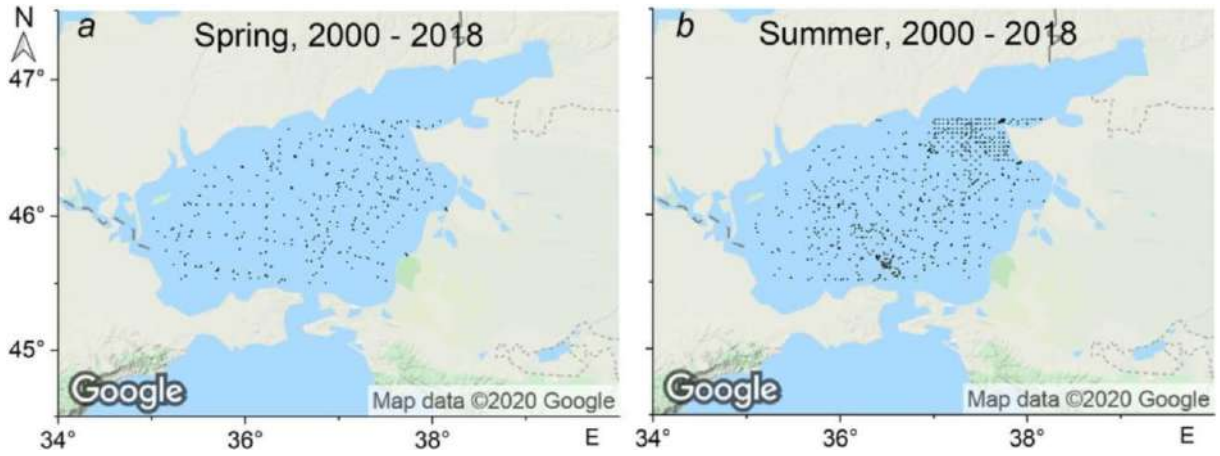

Figure 7.4.2 – Spatial maps of the distribution of *in situ* and MODIS data pairs over the water area of the AZ2 subregion in spring (*a*) and summer (*b*) 2000 – 2018

Comparison of the two approaches in the compilation of regressions. Let's analyze the overlap of forecast areas and generalized regression lines obtained on the basis of two approaches. Figure 7.4.3 shows graphs and bands of regression forecasts for spring and summer to compare the two approaches and prove the validity of using salinity recovery models separately for spring and summer.

Graphs constructed using cumulative regressions (solid lines) with corresponding 95% confidence intervals and 95% forecast areas in spring and summer are shown in Figure 7.4.3, which also shows the values of correlation coefficients and sample sizes. For comparison, we also present here the average regression graphs (dotted lines) based on the equations of the upper part of Table 7.4.1.

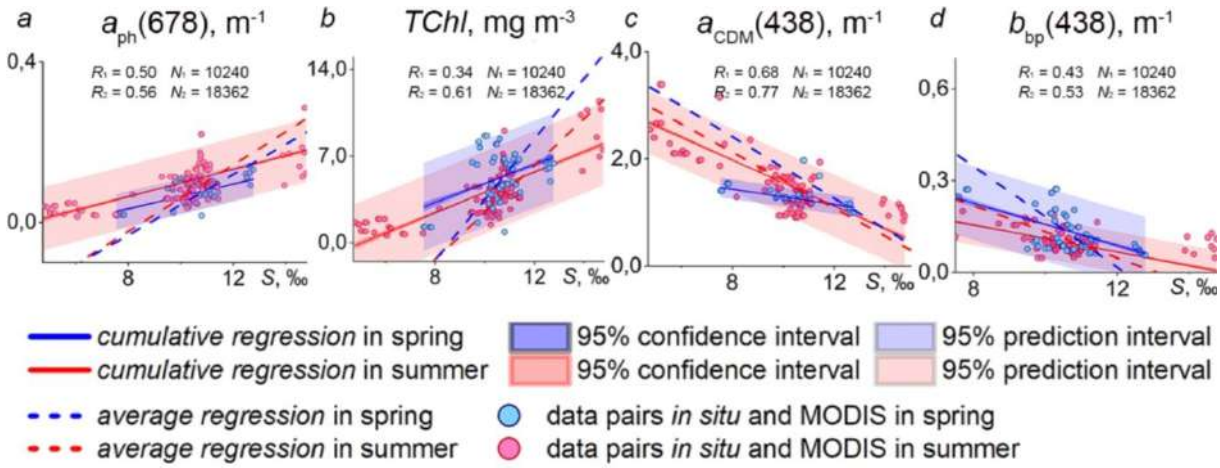

Figure 7.4.3 – Graphs of seasonal regressions (Table 7.4.1) between regional bio-optical parameters and *in situ* salinity values with corresponding 95% confidence intervals, 95% forecast intervals, correlation coefficients and sample size

As can be seen from Figure 7.4.3 for $a_{ph}(678)$, *TChl* and $a_{CDM}(438)$, the 95% forecast band for summer regressions based on cumulative regressions includes all regression lines for spring based on the same principle, and both spring-summer regression lines are based on average regressions. The best correspondence of the regression graphs obtained using the two approaches was found for the $a_{CDM}(438)$.

The largest difference between the spring and summer forecast areas can be seen in $b_{bp}(438)$ (Figure 7.4.3 *d*). Here, the difference between the forecast areas of the summer and spring regressions obtained from the combined sets is ~80% of the summer one. However, the forecasting area of the summer regression completely covers the 95% confidence interval of the spring regression. Thus, in general, one general equation can be used to restore salinity, constructed either from average regressions or cumulative regressions.

7.5. Comparison of the results of reconstruction of surface salinity using various bio-optical parameters in regression models

Let's compare the quality of salinity recovery over space using the *average regression* models shown in the upper part of Table 7.5.1 for various bio-optical parameters. Figure 7.5.1, as an example for the situations of 06/23/2009 and 06/24/2009, shows the spatial fields of reconstruction salinity according to the bio-optical parameters $a_{ph}(678)$ и *TChl*, $a_{CDM}(438)$ and $b_{bp}(438)$. It can be seen that the salinity field of the Sea of Azov does not change significantly during the day, but there is an influx of fresh water from the Taganrog Bay and a decrease in salinity along the eastern coast of the sea.

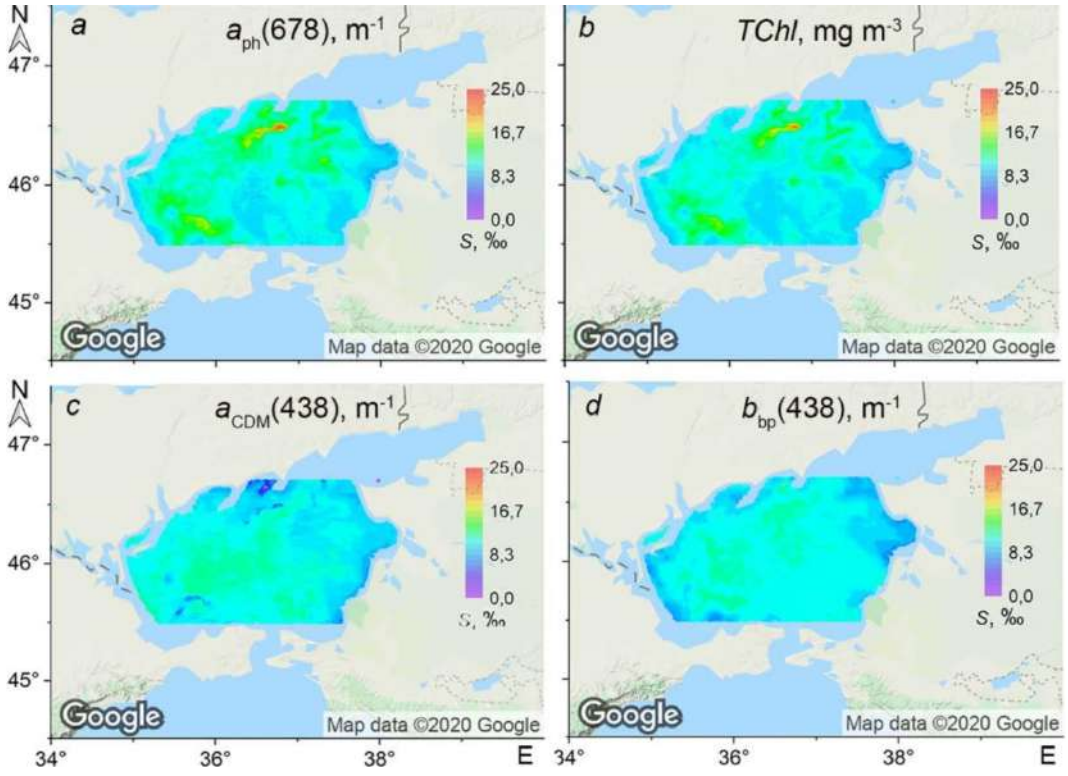

Figure 7.5.1 – Results of reconstruction of the salinity field according to $a_{ph}(678)$ (*a*) and *TChl* (*b*), $a_{CDM}(438)$ (*c*) and $b_{bp}(438)$ (*d*) for AZ2.

The maps of Figure 7.5.1 show that the local maxima of surface salinity ~24% in the northern part of the Sea of Azov (in the two upper panels of Figure 7.5.1), reconstructed according to the bio-optical parameters $a_{ph}(678)$ and *TChl* during

phytoplankton currentsering, significantly exceeded the observed salinity values (Table 7.1.1). These maps demonstrate one of the many cases when the spatial distribution of salinity, reconstructed according to the parameters $a_{ph}(678)$ and *TChl*, does not correspond to the observed climatic distribution. That is why the $a_{ph}(678)$ and *TChl* parameters were not used in the reconstruction models, although the average salinity values recovered from various parameters are in good agreement with each other (Figures 7.5.2 and 7.5.3).

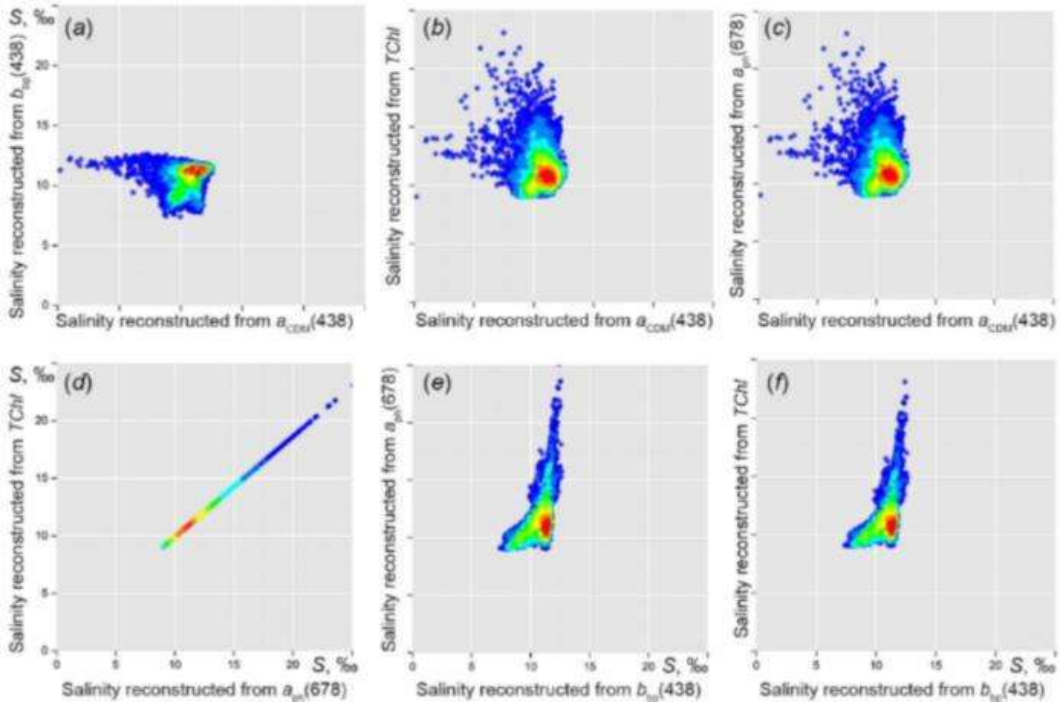

Figure 7.5.2 – Comparison of the results of salinity reconstruction by bio-optical parameters $a_{ph}(678)$, *TChl* (*b*), $a_{CDM}(438)$, $b_{bp}(438)$ 06/23/2009 for AZ2. The colors indicate an increase in data scattering density from blue to red [Shulga, Suslin, 2022]

A comparison of the reconstructed salinity values for the same date according to the considered bio-optical parameters was carried out based on the results of cluster analysis presented in Figure 7.5.2. There is a linear relationship between $a_{ph}(678)$ and *TChl* [Regional ..., 2020], therefore, the variation of the reconstruction salinity values obtained from these parameters tends to zero. As can be seen from Figure 7.5.2, the corresponding relationships between $a_{ph}(678)$ and $a_{CDM}(438)$ and *TChl* and $a_{CDM}(438)$ are identical. Similar variations are observed with the ratio parameters

$a_{ph}(678)$ vs. $b_{bp}(438)$ and *TChl* vs. $b_{bp}(438)$. It should be noted that the salinity values recovered for each bio–optical parameter correlate well in the range of average values of 10-12%. This is also clearly seen from Figure 7.5.3, the salinity values recovered from various bio-optical parameters ($a_{ph}(678)$, *TChl* (*b*), $a_{CDM}(438)$, $b_{bp}(438)$) agree well in the range of average salinity values. Here, the average salinity value of 10 – 12 % determines the center of the ellipse, and the standard deviations determine the boundaries of the rectangle into which the ellipse is inscribed.

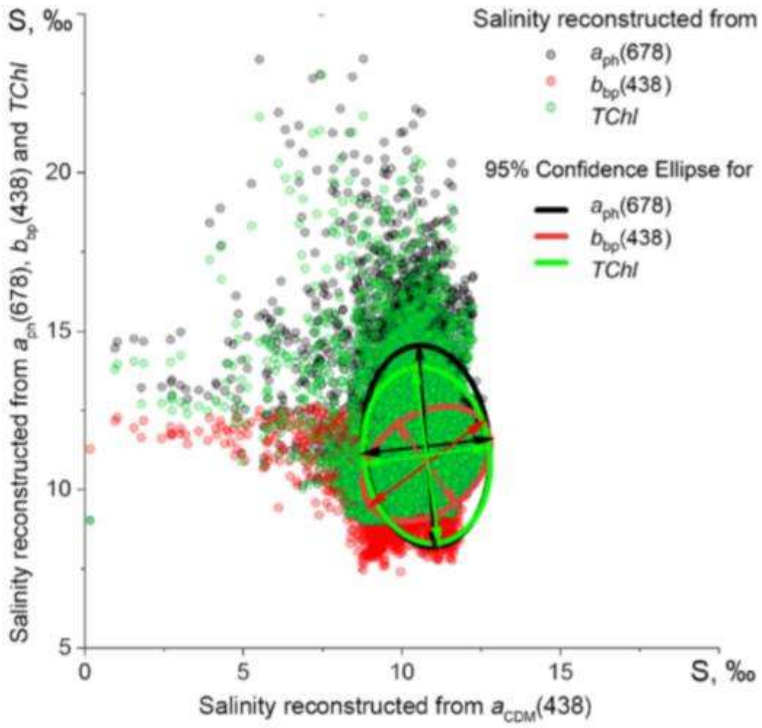

Figure 7.5.3 – Ellipses of 95% confidence probability obtained for salinity reconstruction by bio-optical parameters $a_{ph}(678)$, *TChl* (*b*), $a_{CDM}(438)$, $b_{bp}(438)$ on 06/23/2009 for AZ2

7.6. Comparison of the results of reconstruction of surface salinity in the Sea of Azov for the period 2000-2018 with *in situ* climatic trends for 1913 – 2018

Figure 7.6.1 shows maps of the average monthly values of reconstruction salinity for the spring and summer seasons in the central part of the Sea of Azov (AZ2) in 2000-

2018 to illustrate the results of the proposed method of restoring surface salinity using $a_{CDM}(438)$. These maps show that over the period under study, the average monthly SSS values ranged from 2 to 16%. The tails of high SSS values are directed towards the central part of the Sea of Azov south of the more desalinated waters of the Taganrog Bay. Areas with relatively high salinity values (more than 12 %) are located in the southwestern part of the sea, connected by a narrow bay to Lake Sivash with a salinity of up to 50%. In addition, the SSS gradient extends towards the southern part of the sea to the Kerch Strait with a salinity of up to 18%. In the summer of 2000-2018, saltier waters form a heterogeneous structure and are a reaction to external factors such as wind and runoff of the Don and Kuban rivers [Hydrology and Hydrochemistry … , 1991; Hydrometeorological …, 2009]. In spring, the salinity distribution is more uniform with lower values compared to summer, with the exception of May 2014. In general, this spatial distribution of SSS is in good agreement with the observed one [Hydrometeorological ... , 1962; Hydrometeorological ..., 1986; Hydrometeorology ..., 1991].

Table 7.6.1 shows the range of monthly average SSS values (March – August), reconstruction according to $a_{CDM}(438)$ data in 2000-2018 for AZ2. These statistics are compared with the climatological variability shown in Table 7.1.1 (S_{min} = 9.9; S_{max} = 11.8; $S_{avg} \pm \sigma = 10.89 \pm 0.53$) for the AZ2 sub-region. We note a good coincidence of the averages ($SSS_{avg} \pm \sigma$) and maximum (SSS_{max}) values of model and climatic salinity for individual months and for the whole six months. The largest difference is observed in the minimum values (SSS_{min}).

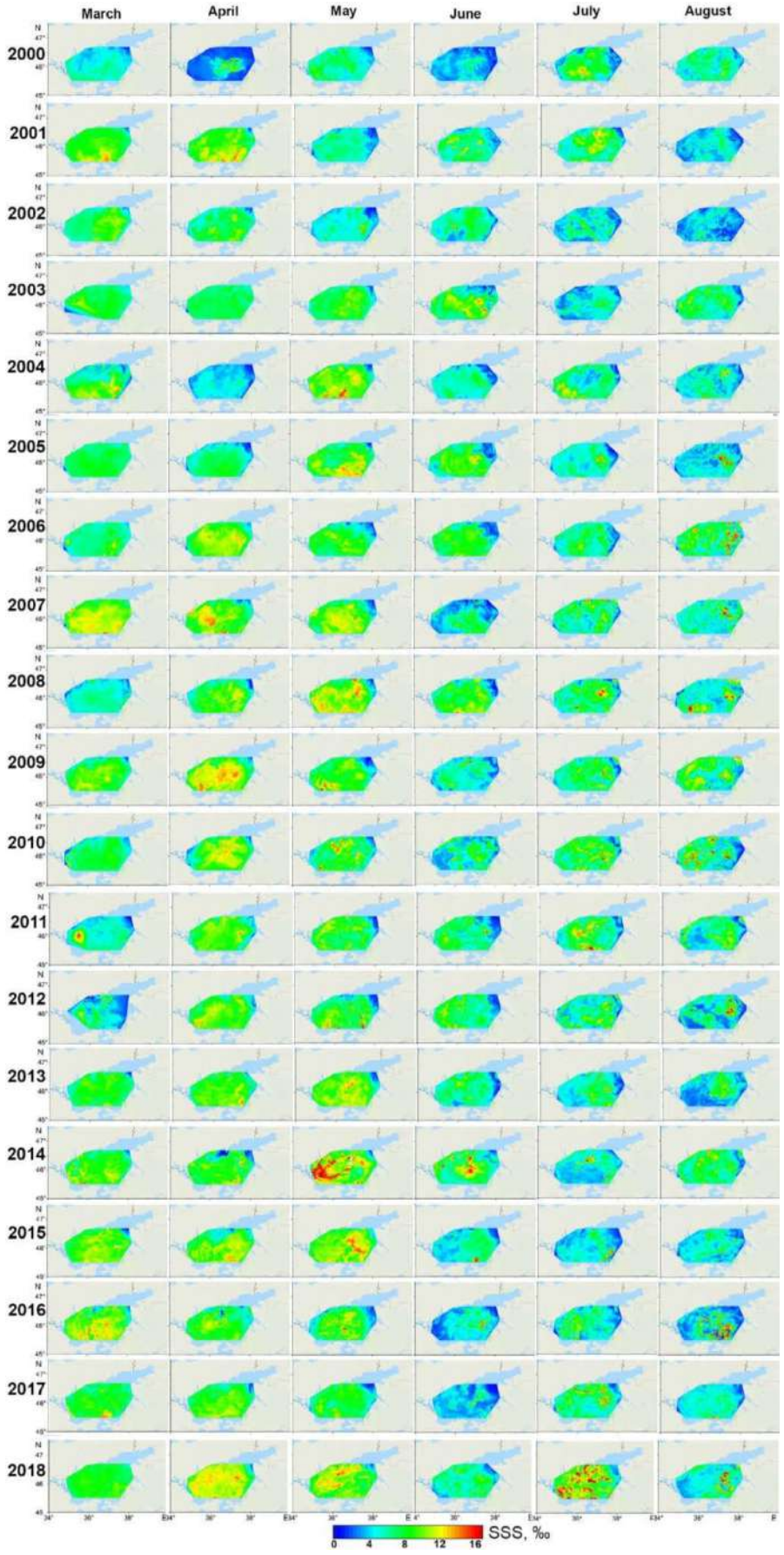

Figure 7.6.1 – Maps of average monthly SSS values (March – August), reconstructed according to $a_{CDM}(438)$ data for 2000-2018 [Shulga, Suslin, 2023]

Table 7.6.1 – Range of multiannual monthly average SSS (Marth – August) reconstructed from $a_{CDM}(438)$ in 2000 – 2018 for AZ2.

SSS (‰)	**Marth**	**April**	**May**	**June**	**July**	**August**	**Marth–August**
SSS_{min}	0.5	0.5	5.5	0.5	0.3	0.3	0.3
SSS_{max}	11.5	12.3	13.9	10.9	8.9	10.0	13.9
$SSS_{avg} \pm \sigma$	9.89±1.23	10.77±1.01	11.13±0.49	9.28±1.16	6.93±1.21	7.49±1.16	9.36±1.17

The results were analyzed on the basis of an integral comparison of the average long-term values of reconstruction salinity and field data in the surface layer of the sea. For this analysis, two observation periods were selected from the *in situ* dataset for 1913-2018:

a short-term period (2000 – 2018) limited by the availability of 2000 sensing data, and a long-term period (1990 – 2018) accepted due to the availability of data without omissions for each year of observations. During these periods, *in situ* datasets were created on average annual values of surface salinity in the AZ2 sub-region for the summer and spring seasons. *In situ* data for 2000-2018 were used to restore salinity for regional MODIS products based on equations (Table 7.5.1). Thus, the obtained long-term average values of reconstruction salinity are statistically compared with the average long-term trends *in situ* salinity for 2000-2018, and also compared with the long-term linear trend *in situ* for 1990 – 2018. The analysis allows us to conclude that the average values of the reconstruction and observed salinity differ and that the proposed method can be used in the future for retrospective reconstruction of salinity.

Figure 7.6.2 shows graphs of average salinity reconstructed from regional MODIS products for spring and summer, as well as historical salinity trends for 18- and 32-year periods of *in situ* observations with 95% confidence intervals. For comparison, Figure 7.6.2 shows the average regression graphs reconstructed from the bio-optical parameters $a_{ph}(678)$, *TChl* (*b*), $a_{CDM}(438)$ and $b_{bp}(438)$ using average regression (solid lines) and cumulative regression (dotted lines) [Shulga, Suslin, Shukalo, 2022].

Figure 7.6.2 also shows graphs based on weighted averages of recovered salinity. A reasonable best estimate is to find the weighted average of all time series

of reconstruction salinity. So, the optimal average salinity for each year (W_k, here k is the number of years for which regressions are built) was found by summing the weighted average salinity values for each biooptical parameter and dividing these values by N (where N is the number of biooptical parameters). The weighted average estimate of the salinity of W_k is described as follows:

$$W_k = \sum_{i=1}^{N} \mathrm{SSS}_i^k w_i^k / \sum_{i=1}^{N} w_i^k. \qquad (7.6.1)$$

Here, S_i^k is the value of salinity reconstructed from the corresponding bio-optical parameter for the k-th year; $w_i^k = S_i^k / \frac{1}{N}\sum_{i=1}^{N} s_i^k$ is a weighting factor determined for the i^{th} biooptical parameter for each k^{th} year.

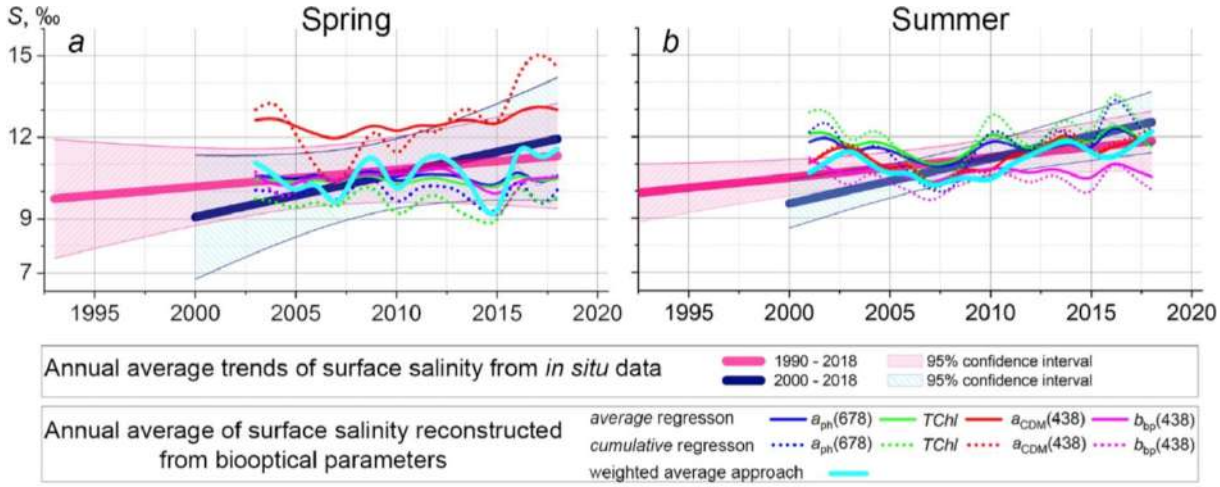

Figure 7.6.1 – Spring (*a*) and summer (*b*) surface salinity annual average trends in 1990–2018 (pink line) and 2000–2018 (deep blue line) with the corresponding 95% confidence intervals. Time series of annual average SSS reconstructed from biooptical parameters: $a_{ph}(678)$, *TChl*, $a_{CDM}(438)$, and $b_{bp}(438)$. The solid lines show the results of reconstruction by *average regressions*, the dotted lines show the results of reconstruction by *cumulative regressions*. The cyan line shows the graph of weighted average approach (7) of salinity reconstructed

Figure 7.6.2 shows that the observed salinity of the sea surface shows an average annual trend with a positive slope. In spring, it is 0.07 for 1990-2018 and 0.16

for 2000–2018. (Figure 7.6.2, *a*), in summer – 0.09 for 1990–2018 and 0.18 for 2000–2018. (Figure 7.6.2, *b*). It can be seen that the spring-summer trends of the modern period 2000 – 2018 have a steeper gradient than the same seasonal trends of the period 1990 – 2018. Trend analysis shows that in the modern period we can observe a fairly stable salinization associated, among other things, with a decrease in river runoff due to the intake of river water for industrial and domestic purposes. It can be seen that in 2000 – 2018, 95% confidence intervals of modern salinity trends almost completely covered the deviation of the average values of the reconstructed salinity from all bio-optical parameters.

The only exceptions are the results obtained by $a_{CDM}(438)$ in spring and $b_{bp}(438)$ in summer. In these cases, the charts go beyond or are present in the confidence area of only one of the trends. However, in the summer seasons of 2000-2005, the best result of salinity reconstruction was obtained by $b_{bp}(438)$, and the average salinity, reconstruction by other parameters $a_{ph}(678)$, *TChl* and $a_{CDM}(438)$, is outside the confidence intervals. both trends. Also in 2005 – 2018. The best result of the salinity reconstruction was obtained according to $a_{CDM}(438)$, the average salinity graph practically coincides with the recent trend of 2000 – 2018. Thus, no satellite regional bio-optical parameter has shown superiority in terms of accuracy of salinity reconstruction. In this regard, in order to reconstruct the salinity closest to the average long-term trends, a comprehensive analysis of the results obtained for various biooptical parameters is necessary.

Comparing the results of salinity reconstruction using various approaches to the compilation of generalized regression equations, we note that the graphs of average salinity reconstruction by averaging regression coefficients are more often present in 95% confidence intervals compared with the graphs of average salinity reconstruction from aggregate data. Thus, to restore salinity in spring, it is advisable to use the formula: $y = (–0{,}287 \pm 0{,}303)x + (4{,}710 \pm 3{,}816)$, and in summer: $y = (–0{,}261 \pm 0{,}071)x + (4{,}217 \pm 0{,}548)$. These formulas are obtained for the AZ2 region.

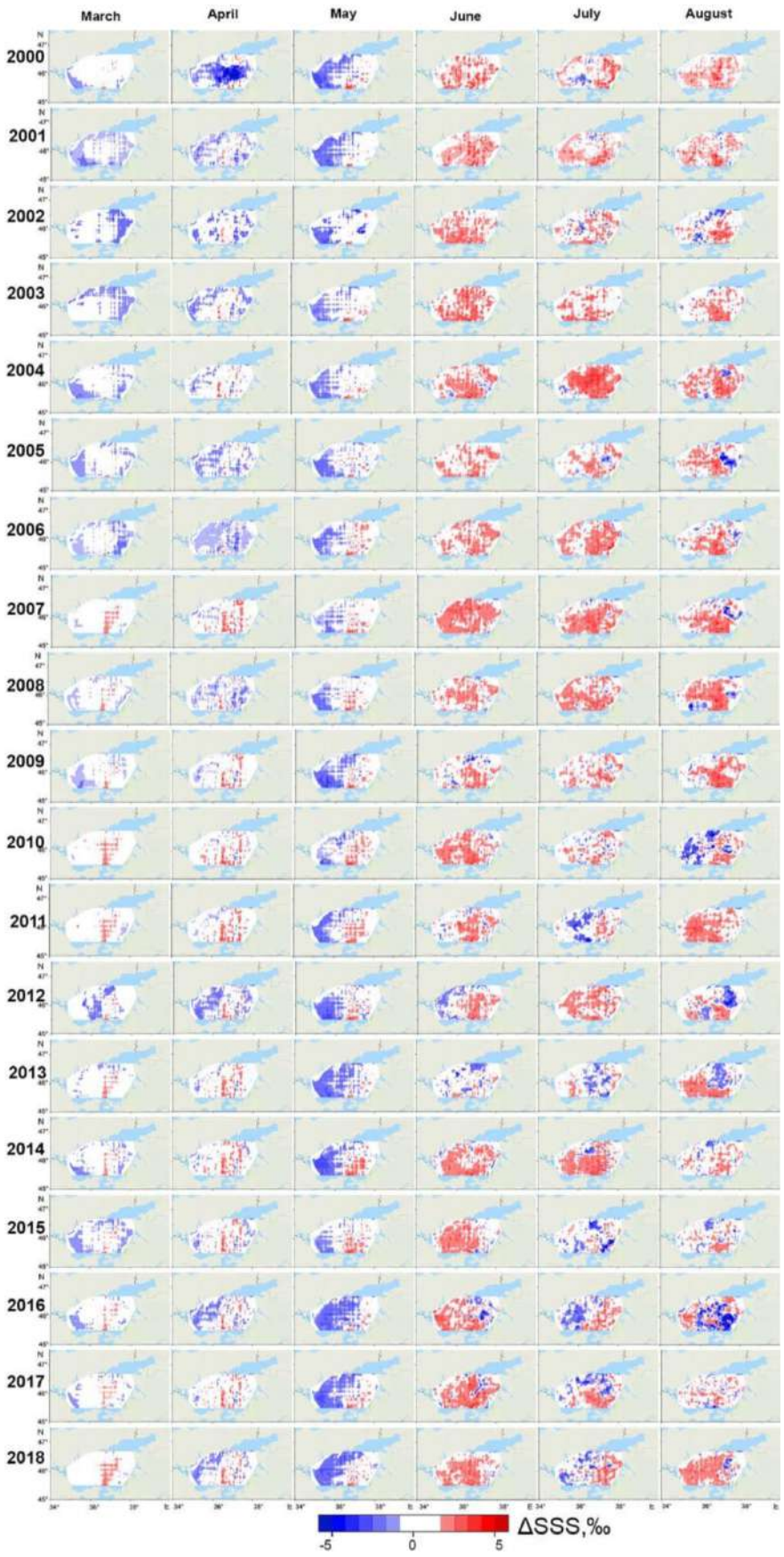

Figure 7.6.3 – Maps of monthly average deviations ΔSSS (%) (March-August) reconstruction salinity from $a_{CDM}(438)$ (2000 – 2018) relative to the average monthly climatological values *in situ* (1913 – 2018) [Shulga, Suslin, 2023]

In the other two regions, their use is not recommended, since the empirical coefficients of the regional bio-optical algorithm have been adapted to the data of the central part of the Sea of Azov.

We also compared the results of SSS reconstruction from $a_{CDM}(438)$ with climatological salinity fields *in situ* (1913 – 2018) in Figure 7.6.3. For this analysis, the set of monthly average SSS data *in situ* was linearly interpolated onto a regular grid. The Sea of Azov. Figure 7.6.3 shows the spatial distribution of differences between the SSS reconstructed using the regression model and the *in situ* data found in matching pairs, namely ΔSSS, ‰ ($SSS_{model} - SSS_{in\ situ}$), also spatially linked to the grid throughout the marine basin. As can be seen, in general, the range of deviations of the reconstruction SSS from the climatological data is within ± 3%.

Table 7.6.2 shows the range of average monthly long-term deviations of the reconstruction SSS (March – August) in relation to the natural climatological values in 2000 – 2018 for AZ2. These statistics are compared with the climatological variability shown in Table 7.1.1 ($\sigma = 0.53$) for the AZ2 sub-region. We note a good correspondence of the long-term average values of ΔSSS in spring with the climatological variability in this region, which is about 0.53 [Research ... , 2020]. In summer, the variability is somewhat greater than the climatic one, which can be judged by a longer period of climatological observations, including year-round data. Nevertheless, this is the subject of research in order to adjust the coefficients of summer regressions.

Table 7.6.2 – The range of long-term monthly average deviations ΔSSS (‰) of reconstruction salinity from $a_{CDM}(438)$ (2000 – 2018) in relation to the average monthly climatological values *in situ* (1913 – 2018) for the AZ2 subregion.

ΔSSS (‰)	**Marth**	**April**	**May**	**June**	**July**	**August**	**Marth–August**
$\mathbf{\Delta SSS_{min}}$	–3.7	–3.9	–3.5	–2.3	–1.9	–1.8	–3.9
$\mathbf{\Delta SSS_{max}}$	1.7	2.0	1.5	2.8	2.0	1.9	2.8
$\mathbf{\Delta\lvert SSS_{avg}\rvert \pm \sigma}$	0.51±0.25	0.86±0.61	0.94±0.54	1.12±0.66	1.33±0.41	1.24±0.42	1.11±0.61

In 2000–2018, the reconstructed sea waters were fresher than climatology data in the spring seasons, and in the summer seasons they were saltier than climatology data (Figure 7.6.3). The figure clearly shows that in May of the studied period, the sea area is divided into zones of desalination and salinization relative to climatology according to natural data. This is due to the structure of currents in the Sea of Azov, which is formed with stable meridional winds. It has the shape of a dipole, which is a union of a cyclone and an anticyclone, the centers of which are shifted to the western and eastern parts of the sea. In the period from 2010 to 2018, in the central part of the Sea of Azov, SSS desalination mainly occurred in spring and summer, with the exception of a few cases of light salinization in May. This is in good agreement with the course of normalized SSS anomalies *in situ* during this period (Figure 7.1.2). In addition, the analysis of the average monthly salinity deviations shown in Figure 7.6.3 shows the division of the research period 2000-2018 into separate years of salinization/desalination. For example, the period from 2010 to 2018 is highlighted, when desalination is observed in the central part of the Sea of Azov in spring and summer, with the exception of cases of minor salinization in May. This is in good agreement with the course of normalized anomalies of surface salinity according to natural data during this period [Dashkevich Kulygin, Berdnikov, 2017; Shul'ga, Shukalo, Suslin, 2020].

The performance of model runs is estimated by analyzing statistical differences between *in situ* (I_i) and model (M_i) monthly average salinity values determined by the values of standard errors:

$$\text{Mean error (ME)} = \overline{M_i - I_i}, \tag{7.6.2}$$

$$\text{Root Mean Square Error (RMSE)} = \sqrt{\overline{(M_i - I_i)^2}}, \tag{7.6.3}$$

$$\text{Mean Absolute Error (MAE)} = |\overline{M_i - I_i}|, \tag{7.6.4}$$

$$\text{Relative Error (RE)} = \overline{|M_i - I_i| / I_i}, \tag{7.6.5}$$

$$\text{Correlation Coefficient (Corr)} = (\overline{M_i \cdot I_i} - \bar{M} \cdot \bar{I}) / \sqrt{\overline{M_i^2} - \bar{M}^2} \cdot \sqrt{\overline{I_i^2} - \bar{I}^2}, \quad (7.6.6)$$

$$\text{Scatter Index (SI)} = \sqrt{\overline{[(M_i - \bar{M}) - (I_i - \bar{I})]^2}} / \bar{I}. \quad (7.6.7)$$

here i is the number of synchronized pairs of *in situ* data and reconstruction salinity values.

The result of comparing the average monthly values of reconstruction salinity according to the $a_{CDM}(438)$ obtained in runs Run A (*average regression*) and Run B (*cumulative regression*) with those observed in situ is shown in the graphs of error statistics (7.6.2) – (7.6.7) Figure 7.6.4. It can be seen that for Runs A and B from March to August in 1913 to 1918, there is a noticeable difference in statistical parameters between the spring and summer seasons.

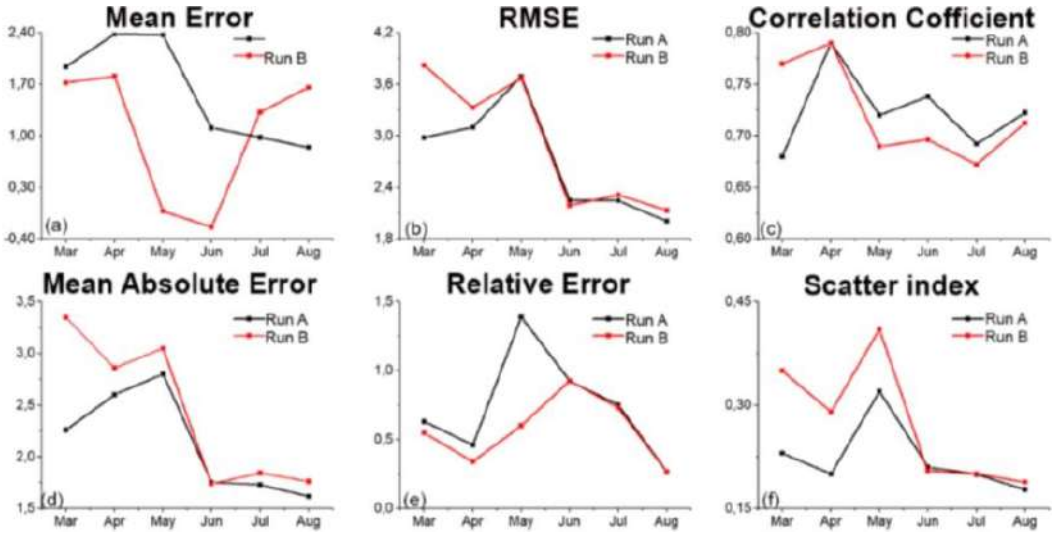

Figure 7.6.4 – Graphs of error statistics of the average monthly salinity values reconstruction according to $a_{CDM}(438)$ with respect to *in situ* from March to August 2000 – 2018 [Shulga, Suslin, 2023]

This is due to seasonal changes in the salinity of the sea surface and a large number of observations in the summer. For RunA, there is a trend of MAE, RMSE and RE with a maximum value in May and a minimum value in August. However, from April

to August, the correlation coefficient of Run A is better compared to Run B, and the spread index (SI) for Run B from May to June is higher compared to Run A. Thus, according to the main indicators, the results of salinity reconstruction by the average regression model agree with the data *in situ* better than when using cumulative regression.

The most effective bio-optical parameter was evaluated in terms of the best correlation of the reconstruction salinity values with *in situ* data. To achieve this goal, we are running both model regressions to restore salinity in terms of light absorption by phytoplankton $a_{ph}(678)$ and backscattering $b_{bp}(438)$ from March to August in 2000 –2018. Runs on $a_{ph}(678)$ using average regression are designated Run C, and cumulative regression is Run D. Similarly, $b_{bp}(438)$ are designated as Run E and Run F. Graphs of error statistics of all runs are shown in Figure 7.6.5, here for comparison are also statistics of Run A (black line) and Run B (red line), previously data in Figure 7.6.4. It can be seen that the correlation coefficient between the average monthly values of model and *in situ* salinity is much higher when using the $a_{CDM}(438)$ for compared with the results of using $a_{ph}(678)$ and $b_{bp}(438)$. The lines of other statistics also indicate the effectiveness of using the $a_{CDM}(438)$ in restoring salinity.

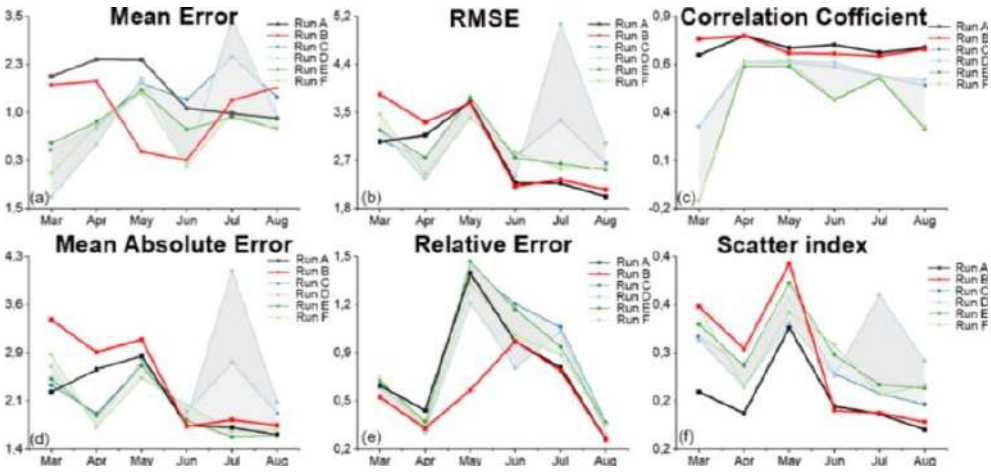

Figure 7.6.5 – Graphs of error statistics of the average monthly salinity values reconstruction by $a_{CDM}(438)$, $a_{ph}(678)$ and $b_{bp}(438)$relative to *in situ* from March to August 2000-2018 [Shulga, Suslin, 2023]

The obtained conclusion is confirmed by maps of the spatial distribution of deviations of the average monthly values of reconstruction salinity relative to the observed *in situ* ($\Delta SSS = SSS_{model} - SSS_{in\ situ}$, %) in the spring and summer seasons of 2000 − 2018, shown in Figure 7.6.3. As can be seen, in the spring seasons, the reconstruction salinity of marine waters was lower, and in the summer seasons – higher, than according to climatology data.

7.7. Conclusions to Chapter 7

Section 7 analyzes the climatic trends of the thermohaline structure of the Sea of Azov according to *in situ* observations for 1913–2018. The conclusions of the long-term average climatic values of temperature and salinity are drawn, climatic trends are constructed, periods of salinization/desalination of the sea are highlighted. This paper proposes a method for restoring the salinity of the Sea of Azov based on the use of generalized empirical (regression) equations linking field data with regional satellite products. Examples of spatial maps of the reconstructed salinity of the Sea of Azov are given. The result of the analysis of various approaches to obtaining generalized empirical (regression) equations showed the possibility of using a single general equation constructed by averaging regressions for the spring and summer seasons. The result of comparing the reconstruction values of average salinity showed good agreement with the observed salinity trends. It was found that the graphs of the average values of the reconstruction salinity are in 95% confidence intervals of long-term and short-term trends (1990–2018 and 2000–2018). It is noted that the graphs of average salinity reconstruction by averaging the regression coefficients practically do not exceed the specified 95% confidence intervals compared with the graphs of salinity reconstruction by cumulative regression. Our results showed that the average values of the reconstruction surface salinity in the central part of the Sea of Azov are reliable and consistent with the field data using average regression compared with the results obtained using cumulative regression. In addition, the salinity values recovered from $a_{CDM}(438)$ most realistically reflect its changes in the observed salinity range (1-18%). A comparison

of the results of the reconstruction of surface salinity according to $a_{CDM}(438)$ with climatological salinity fields *in situ* (1913–2018) showed their fairly good spatial agreement. In addition, the deviation of the reconstruction salinity fields relative to climatological ones is consistent with the structure of the stationary currents of the Sea of Azov. For a more accurate reconstruction of salinity close to the average long-term trends, a comprehensive analysis of the results obtained for various bio-optical parameters is necessary.

The proposed method of salinity reconstruction based on the use of climatic and satellite data makes it possible to further use only satellite images to assess the salinity of the water of the Sea of Azov. This mainly concerns those sections of the reservoir and the time when field research was not carried out in the Azov.

CONCLUSION

Let's formulate the main results obtained in the dissertation:

1. Within the framework of a three-dimensional hydrodynamic model, the physical patterns of the generation of surface and deep currents in a natural sea basin, and their influence on the surge processes and the evolution of passive impurities caused by the action of atmospheric disturbances obtained through their theoretical reproduction and using a regional forecast model, have been established. A modification of the three-dimensional hydrodynamic model POM has been carried out, which makes it possible to study the influence of various scenarios of regional meteorological phenomena to study the extreme characteristics of currents and the level of the Azov Sea that arise in the presence of stationary and non-stationary movements. The modified model was tested on a number of examples for which analytical solutions or direct measurement data are known.

2. The structure of surface currents caused by the action of a zonal wind uniform in space and time manifests itself in the form of an unstable alongshore current in the northern part of the Sea of Azov and the Taganrog Bay, representing anticyclonic gyres of a sub-basin scale, and a median basin anticyclonic current, shifted to the eastern part of the sea. The structure of surface currents with meridional winds has the form of a dipole, which is an association of a cyclone and an anticyclone. Between them there is a narrow strip of boundary current, oriented opposite to the acting wind. A feature of the established movements in the Sea of Azov is the existence of compensatory countercurrents in the lower layers. The formation time of countercurrents that arise under the influence of constant winds with different (from 5 to 15 m/s) speeds ranges from 10 to 12 hours. In the bottom layer of the sea, the currents are unidirectional, deviating by 135º from the direction of the acting wind. Under the influence of a quasi-stationary wind, the sea waters are divided into zones of increased and decreased levels, with an increase in the level observed on the windward shores and a decline on the leeward shores. The zero amplitude curve is oriented perpendicular to the direction of the acting wind and crosses the central part of the sea in the zonal and meridional directions. The Taganrog Bay, located in the northeastern part of the Sea of Azov, is subject to the strongest

influence of surge processes. A characteristic feature of the time course of the level at coastal stations under constant wind action is the achievement of its extreme values 15 hours after the onset of wind action. It has been shown that the action of winds at three times higher speeds (5 and 15 m/s) leads to an increase in maximum surges in the bay by 1.2 m and a 6-fold increase in the speeds of steady currents. Areas exposed to the danger of flooding/drainage due to surge winds have been identified - Mysovoe, Temryuk, Genichesk and Taganrog.

3. Seiche-like fluctuations that regularly occur in the Azov Sea basin play an important role in the formation of extreme currents and sea level amplitudes, leading to increased effects that occur during storm surges. The maximum values of the amplitudes of seiche-like oscillations in the coastal zone of the Sea of Azov and storm surges and surges are comparable, while the amplitudes of free oscillations in the open part of the sea are 50–89% of their values in its coastal zone. The hypothesis about the role of the resonance mechanism in the occurrence of extreme amplitudes of seiche oscillations has been numerically confirmed. It has been established that disturbances moving at a speed close to the speed of a free long wave cause the generation of level oscillations with larger amplitudes than with the same wind and constant atmospheric pressure. Their highest values are achieved at a speed of movement of the boundary of pressure disturbances of 9.4 m/s, corresponding to a sea depth of 9 m. Natural level fluctuations with periods of 27.3 and 23.1 hours each have one amphidromic system, the centers of which are shifted to the northern coast relative to the central one parts of the Azov Sea. The main antinodes of these oscillations are located in the east of the Taganrog Bay and in Yasensky Bay, and less pronounced ones are in the west of the sea. The rotation of the level maxima around the amphidromic center occurs counterclockwise.

4. Non-stationary atmospheric disturbances disrupt the nature of the background stationary circulation. The action of a vortex atmospheric formation disrupts the distribution pattern of stationary surges and surges, as well as areas of flooding/draining. It has been established that a cyclone moving westward causes currents with higher maximum speeds than cyclones of other directions. It has been shown that a cyclone with a multiple larger base (for example, a southern cyclone) leads to the appearance of surges

and surges with larger amplitudes. Thus, a cyclone with a base 2 times larger causes an increase in the values of surges and surges by 2.3 times, and one with a base 4 times larger causes an increase of 3 times. Also, an increase in the size of active atmospheric formations leads to a decrease in the time during which extreme level values are formed. Vortex atmospheric disturbances in zonal directions (for example, a western cyclone) do not lead to a noticeable change in the magnitude of surges compared to the action of cyclones moving in the meridional direction (for example, a southern cyclone)

5. The influence of sea water incurrents through the Kerch Strait on extreme level deviations and current speed in the Sea of Azov caused by the action of quasi-stationary wind fields was studied. It has been established that the southern wind, when taking into account water exchange through the strait, causes currents whose maximum speeds are 30% higher than the speeds of steady movements caused by the western and northern winds. Taking into account water exchange through the strait leads to significantly higher values of the speed of steady currents only at wind speeds of 10 and 15 m/s (increasing to 53% compared to the action of the wind of the same direction with a speed of 5 m/s). Conclusions were drawn about the danger of sea water entering through the Kerch Strait under the influence of moving anticyclones. The movement of anticyclones over Eastern Europe from northern points passing through the waters of the Sea of Azov can lead to an increase in the surface speed of the Azov Current to a maximum value of 0.54 m/s, and sea level to 52 cm.

6. The transformation of polluting substances is determined by the magnitude and direction of wind currents. The time for complete dispersion of the impurity increases with depth, and under the influence of higher wind speed. The penetration of substances entering the surface layer of the sea to a depth $z = -H/2$ occurs after 4 hours, into the bottom layer after 16 hours. The action of cyclonic formations leads to the fragmentation of the area containing substances into a number of fragments, their spread from the place of entry and, consequently, to an increase in the area of the volume of pollution compared to the case of the action of a quasi-stationary wind. The passage of cyclonic disturbances leads to a more than 7-fold increase in the size of the area occupied by the substance and

an 11-fold increase in the dissipation time compared to its propagation in the field of stationary currents.

7. Results of numerical modeling of extreme storms during extreme Azov events in 2013 and 2014. confirmed the observed maximum values of surges and surges, the extent of the flooding area. The largest surges occurred in Taganrog (2.14 and 2.94 m). As a consequence, extensive areas of flooding arose in this area, extending 360 m from the water's edge according to observational data and 336.9 m according to modeling data. The maximum surges, according to calculated data, were observed in Genichesk and Mysovoy (1.07 and 1.23 m).

8. New procedures for assimilation of bio-optical indices into a three-dimensional hydrodynamic model have been proposed, allowing the use of modeling results to restore losses of satellite information (primarily due to cloudiness) necessary for monitoring the content of substances in the Sea of Azov. The proposed procedures made it possible to obtain continuous information on the content of declared substances in the marine environment and to estimate their highest and total content in the surface and deep layers of the Sea of Azov for 2013–2014.

9. An analysis of climate trends in the thermohaline structure of the Sea of Azov was carried out based on in situ observation data for 1913–2018. Conclusions were drawn and long-term average climatic values of temperature and salinity were drawn, climatic trends were constructed, and periods of sea salinization/desalination were identified.

10. Seasonal regression coefficients were obtained for four bio-optical parameters to restore the salinity of the Azov Sea. The proposed method makes it possible to reduce the cost of assessing salinity by direct methods and fill gaps in the hydrochemical study of the sea. Systematized information on the temperature and salinity of sea water based on in situ observations was the basis for the creation of the “Thermohaline Electronic Atlas of the Azov Sea” database. The observational database is complemented by simulated salinity data obtained using the proposed seasonal regression models, as well as information on the main bio-optical indicators in the Sea of Azov for 2000–2019.

REFERENCE

1. Abuzyarov, Z. K. Sea agitation and its forecasting / Z. K. Abuzyarov. – L.: Hydrometeoizdat, 1981. – 166 p.
2. Averbukh, E. L. Dynamic regimes of pollution and contamination in the field of topographically trapped waves / E. L. Averbukh, D.Yu. Tyugin, A.A. Kurkin, Kurkina O.E. // Bulletin of the Moscow State Regional University. Series: Natural Sciences. – 2011. – no. 5. – P. 27–38.
3. Aksenov, A. A. Morphology and dynamics of the northern shore of the Sea of Azov / A. A. Aksenov // Proceedings of the GOIN. Moscow : Hydrometeoizdat, 1955. – iss. 29(41). – P. 107–143.
4. Altman, E. N. Features of horizontal turbulence in a shallow strait / E. N. Altman, B. L. Lagutin, D. M. Tolmazin // Collection of works of the Basin hydrometeorological Observatory of the Black and Azov Seas. – L. : Hydrometeoizdat, 1966. – iss. 4. – P. 75–87.
5. Altman, E. N. The structure of the currents of the Kerch Strait / E. N. Altman // Proceedings of GOIN. – L. : Hydrometeoizdat, 1975. – iss. 125. – P. 3-16.
6. Altman, E. N. On the issue of variability of water currents in the Kerch Strait according to field observations / E. N. Altman // Proceedings of GOIN. – M. : Hydrometeoizdat, 1976. – iss. 132. – P. 17-28.
7. Altman, E. N. Dynamics of waters of the Kerch Strait / E. N. Altman // Hydrometeorology and hydrochemistry of the seas of the USSR. Volume 4: The Black Sea. iss. 1: Hydrometeorological conditions. – L. : Hydrometeoizdat, 1991 – P. 291-328. – URL: http://www.geokniga.org/books/10858 (date of application: 10.01.2019).
8. Appel, P. Equilibrium figures of a rotating homogeneous liquid / P. Appel. – L.-M.: ONTI, 1936. – 375 p.
9. Atlas of the waves, currents and level of the Sea of Azov / [V. V. Fomin [etc.]; in edc. V. V. Fomin. – K. : Phoenix, 2012. – 240 p.
10. Atlas of the ice of the Black and Azov Seas [Maps] / Federal Service for Hydrometeorology and Environmental Monitoring (Roshydromet), Federal State Budgetary Institution "State. Oceanographic Institute named after N. N. Zubov", Sevastopol Department ; [comp.]: N. N. Dyakov [et al.]. – Sevastopol : State Universiy. Oceanographic Institute named after N. N. Zubov, 2015. – 1 atlas (219 p.).
11. Belov, V. P. The main features of the dynamics of the waters of the Sea of Azov and the Kerch Strait / V. P. Belov, Yu. G. Filippov // Trudy GOIN. – M. : Hydrometeoizdat, 1978. – iss. 139. – P. 11–20.
12. Belov, V. P. Dynamics and vertical structure of the currents of the Sea of Azov / V. P. Belov, Yu. G. Filippov // Trudy GOIN. – M. : Hydrometeoizdat, 1980. – iss. 159. – P. 127–134.
13. Bronfman, A.M. Some features of circulation on the estuarine coast of the Don during the run–off / A.M. Bronfman // Trudy GOIN. - M. : Hydrometeoizdat, 1964. – iss. 78.

14. Bukatov, A. E. Numerical modeling of the dynamics of the Sea of Azov during overburden phenomena / A. E. Bukatov, D. D. Zavyalov, T. A. Solomakha // Russian Metrology and hydrology. – 2006. – no. 6. – P. 69–75.
15. Bufetova, M. V. Pollution of the waters of the Sea of Azov by heavy metals / M. V. Bufetova // South of Russia: ecology, development. – 2015. – Vol. 10, no. 3. – P. 112–120. – https://doi.org/10.18470/1992-1098-2015-3-112-120.
16. Bykov, F. L. Objective analysis of the three-dimensional structure of atmospheric fronts / F. L. Bykov, V. A. Gordin // Izv. RAS. Physics of the atmosphere and ocean. – 2012. –Vol. 48, no. 2. – P. 172–188.
17. The influence of the Kerch Strait on overburden phenomena and currents in the Sea of Azov caused by cyclonic disturbances / V. A. Ivanov, V. V. Fomin, L. V. Cherkesov, T. Ya. Shulga // Marine Hydrophysical Journal. – 2009. – no. 4. – P. 3–18.
18. Intrasecual fluctuations of the Azov Sea climate (according to thermohaline data for 120 years) / G. G. Matishov [et al.] // Reports of the Academy of Sciences. 2008. Vol. 422, No. 1. pp. 106-109.
19. Wolzinger, N. E. The main oceanological problems of shallow water theory / N. E. Volzinger, R. V. Pyaskovsky. – L. : Hydrometeoizdat, 1968. – 300 p.
20. Volzinger, N. E. Long waves in shallow water / N. E. Volzinger. – L. : Hydrometeoizdat, 1985. – 160 p.
21. Volzinger, N. E. Long–wave dynamics of the coastal zone / N.E. Volzinger, K.A. Klevanny, E.N. Pelinovsky - L. : Hydrometeoizdat, 1989. – 271 p.
22. Wrangel, F.F. On physical research in the Black and Azov Seas / F. F. Wrangel. – St. Pb : B. I., 1875 – Marine collection no. 12. – P. 9-29.
23. Geology of the USSSR: Kerch. Strait. F. Shnyukov [etc.]; Rev. red. D. Well. Makarenko. - K. : Science. Dumka, 1981. – 158 p.
24. German, V. H. Spectral analysis of fluctuations in the level of the Azov, Black and Caspian seas in the frequency range from one cycle in a few h to one cycle in a few days / V. H. German// Proceedings of the GOIN. – M. : Hydrometeoizdat, 1970. – iss. 103. – P. 52–73.
25. German, V. H. Investigation and calculation of probabilistic characteristics of extreme sea levels / V. H. German; Edited by B. H. Glukhovsky. // Trudy GOIN. – M. : Hydrometeoizdat, 1971. – iss. 107. – 148 p.
26. Hydrodynamics of the coastal zone and estuaries / Translated from the English by A. V. Nekrasova. – L. : Hydrometeoizdat, 1970. – 392 p.
27. Hydrology of the delta and the mouth of the Kuban coast / [D. V. Magritsky et al.] ; edited by V. N. Mikhailov, D. V. Magritsky, A. A. Ivanov. – M. : GEOS, 2010. –728 p.
28. Hydrometeorological conditions of the shelf zone of the seas of the USSR. Vol. III: The Sea of Azov. – L. : Hydrometeoizdat, 1986. – P. 218.
29. Hydrometeorological conditions of the seas of Ukraine. Vol. 1: The Sea of Azov / Y. P. Ilyin [et al.]; Ministry of Emergency Situations and the National Academy of Sciences of Ukraine, Marine Department of the Ukrainian Research

Hydrometeorological Institute. – Sevastopol : EKOSI-Hydrophysics, 2009. – 400 p.
30. Hydrometeorological handbook of the Sea of Azov / Glav. upr. hydrometeorol. services under the Council of Ministers of the USSR. Upr. hydrometeorology. services of the Ukrainian SSR. Hydrometeorol. Observatory of the Black and Azov Seas ; Edited by A. A. Aksenov. – L. : Hydrometeoizdat, 1962. – P. 247.
31. Hydrometeorology and hydrochemistry of the seas of the USSR. Vol. V: Sea of Azov / [N. P. Goptarev et al.]; Edited by N. P. Goptarev and others – St.Pb. : Hydrometeoizdat, 1991. – 234 p. – (Project "Seas of the USSR").
32. Gill A. Dynamics of the atmosphere and ocean in 2 volumes /Gill A.; translated from English by V. E. Ryabinina, A. N. Filatov; edited by G. P. Kurbatkin. M. : Mir, 1986.
33. Goldstein, R.V., Mechanics of continuous media. Part 1. Fundamentals and classical models of liquids / R.V. Goldstein, V.A. Gorodtsov. – M.: Nauka. Fizmatlit, 2000. – 255 p.
34. Grigorkina, R. G. The impact of typhoons on the ocean / R. G. Grigorkina, V. R. Fuchs. – L. : Hydrometeoizdat, 1986. – 242 p.
35. Grishin, G. A. On the evolution of southern cyclones entering the Black Sea and the territory of Ukraine, according to satellite and ground-based observations / G. A. Grishin [et al.] // Exploration of the Earth from space. – 1991. – no. 3. – P. 89-94.
36. Gulev, S. K. Synoptic interaction of the ocean and the atmosphere in the middle latitudes / S. K. Gulev, A.V. Kolchenko, S. S. Lappo. – St. Petersburg : Hydrometeoizdat, 1994. – 320 p.
37. Research on the state of fishing in Russia. – St. Petersburg : published by the Ministry of State Property, 1860-1876 (in the Printing House of V. Bezobrazov and company), 1871. – Vol. 8: Description of fishing in the Black and Azov Seas / compiled by the head of the Expedition [for the study of fisheries in the Azov and Black Seas], inspector of agriculture N. Y. Danilevsky. – 316 p.
38. Datsyuk, V. N. Modeling of extreme flooding in the Don Delta on multiprocessor computing systems / V. N. Datsyuk [et al.] // Bulletin of the South Ural State University. Series: Computational Mathematics and Computer Science. – 2014. – Vol. 3, iss. 1. – P. 80-88.
39. Dashkevich, L. V. Mathematical modeling of the temperature regime and thermal balance of the Sea of Azov / L. V. Dashkevich, S. V. Berdnikov // Ecological Bulletin of the scientific centers of the Black Sea Economic Cooperation. – 2008. – no. 4. – P. 5-18.
40. Demyshev, S. G. Numerical simulation of the seasonal variability of hydrophysical fields in the Black Sea / S. G. Demyshev, V. V. Knysh, G. K. Korotaev // Physical Oceanography. – 2002. – no. 3. – P. 12-27.
41. Demyshev, S. G. Aanalysis of effects of constant wind on the velocity of currents and seiche oscillations in the Azov Sea level / S. G. Demyshev, L. V. Cherkesov, T. Ya. Shul'ga // Russian Meteorology and Hydrology. – 2017. – Vol. 42, no. 6. – P. 388–393. – DOI:10.3103/S1068373917060048.

42. Didenkulova, I. I. Run-up of solitary waves on slopes with different profiles / I. I. Didenkulova, A. A. Kurkin, E. N. Pelinovsky // Izvestiya, Atmospheric and Oceanic Physics. – 2007. – vol. 43, no. 3. –P. 419–425.
43. Dotsenko, S. F. Natural disasters of the Azov-Black Sea region / S. F. Dotsenko, V. A. Ivanov. – Sevastopol : EKOSI Hydrophysics, 2010. – 174 p.
44. Drozdov, V. V. Features of the long–term dynamics of the ecosystem of the Sea of Azov under the influence of climatic and anthropogenic factors / V. V. Drozdov // Scientific notes of RGGMU. – 2010. – no. 15. – P. 155–176.
45. Dubinin, M. Sources of meteorological data on the territory of the Russian Federation by stations [Electronic resource] / M. Dubinin, I. Pospelov. – 03 12 2018 – URL: http://gis-lab.info/qa/meteo-station-sources.html (date of application: 05.01.2019).
46. Dyakov, N. N. Synoptic conditions for the occurrence of abnormal fluctuations in the level of the Sea of Azov / N. N. Dyakov, V. V. Fomin // Sciences. prati UkrNDGMI. – 2002. – iss. 250. – 10 p. – URL: http://uhmi.org.ua/pub/np/250/28_Djakov.pdf (date of application: 09.01.2019).
47. Eremeev, V. N. Modeling long waves in the Sea of Azov due to cyclone passages / V. N. Eremeev [et al.] // Oceanology. – 2000. – Vol. 40, No. 5. – pp. 658-665.
48. Efimov, V. V. Numerical modeling of the effect of land–sea temperature contrasts on atmospheric circulation in the Black Sea region / V. V. Efimov, A. E. Anisimov // Physical Oceanography. – 2011. – no. 4. – P. 3–12.
49. Patterns of ecosystem processes in the Sea of Azov / G. G. Matishov [et al.]. – M. : Nauka, 2006. 304 p.
50. Zalesny, V. B. Numerical model of the hydrodynamics of the Black Sea and the Sea of Azov with variational initialization of temperature and salinity / V. B. Zalesny, A.V. Gusev, S. N. Moshonkin // Izvestiya, Atmospheric and Oceanic Physics. – 2013. – Vol. 49, no. 6. – P. 699-716. – DOI:10.7868/S000235151306014X.
51. Zakharchuk, E. A. On the spatiotemporal structure and mechanisms of the Neva River flood formation / E. A. Zakharchuk, N. A. Tikhonova // Russian Meteorology and Hydrology. – 2011. – no. 8. – P. 54–64.
52. Zakharchuk, E. A. Spatial structure and propagation of the Neva flood waves / E. A. Zakharchuk, V. N. Sukhachev, N. A. Tikhonova // Russian Meteorology and Hydrology. – 2020. – №4. – P. 42–53.
53. Ivanov, V. A. Monitoring of the ecosystem of the shelf zone on the example of the Black Sea (Strategy and tactics of the implementation of the program for the study of the ecosystem of the Black Sea) / V. A. Ivanov. – Sevastopol : Edition of the Black Sea Fleet of Moscow State University, 2002. – 151 p.
54. Ivanov, V. A. The influence of cyclones on changes in the level surface of the Azov and Black Seas / V. A. Ivanov, A.V. Konovalov, L. V. Cherkesov // Meteorology and hydrology. – 2003. – no. 4. – P. 73-80.
55. Ivanov, V. A. Investigation of the influence of wind action upon the currents and propagation of impurities in the Azov Sea / V. A. Ivanov, V. V. Fomin, L. V.

Cherkesov, T. Ya. Shulga // Physical Oceanography. – 2010. – Vol. 20, no. 3. – P. 170–183. – DOI:10.1007/s11110-010-9076-0.

56. Ivanov, V. A. Analysis of the influence of water exchange through the Kerch Strait on the surge processes and currents in the Azov Sea / V. A. Ivanov, L. V. Cherkesov, T. Ya. Shulga // Physical Oceanography. – 2010. – Vol. 20, no. 4. – P. 239–250. – DOI:10.1007/s11110-010-9081-3.
57. Ivanov, V. A. Extreme deviations of the sea level and the velocities of currents induced by constant winds in the Azov Sea / V. A. Ivanov, L. V. Cherkesov, T. Ya. Shul'ga // Physical Oceanography. – 2011. – Vol. 21, no. 2. – P. 98–105. – DOI:10.1007/s11110-011-9107-5.
58. Ivanov, V. A. Computer simulation of dynamic processes in the Sea of Azov / V. A. Ivanov, L. V. Cherkesov, T. Ya. Shul'ga // Ecological Safety of Coastal and Shelf Zones of Sea. – 2011. – no. 25-2. – P. 294–304.
59. Ivanov, V. A. Atlas of overburden processes, waves and currents caused by atmospheric disturbances in the Sea of Azov / V. A. Ivanov, L. V. Cherkesov, T. Ya. Shul'ga. – Sevastopol: MHI NANU, 2012. – 96 p.
60. Ivanov, V. A. Investigation of effects of spatially and temporally variable wind on currents, surges, and admixture spread in the Sea of Azov / V. A. Ivanov, L. V. Cherkesov, T. Ya. Shul'ga // Russian Meteorology and Hydrology. – 2012. – Vol. 37, no. 8. – P. 553–559. –DOI:10.3103/S1068373912080079.
61. Ivanov, V. A. Dynamic processes and their influence on the transformation of the passive admixture in the sea of Azov / V. A. Ivanov, L. V. Cherkesov, T. Ya. Shul'ga // Oceanology. – 2014. – Vol. 54, no. 4. – P. 426–434. – DOI:10.1134/S0001437014030023.
62. Ivanov, V. A. Numerical analysis of currents, surge phenomena, and evolution of pollutants caused by the action of unsteady wind in the Sea of Azov / V. A. Ivanov, L. V. Cherkesov, T. Ya. Shul'ga // Ecological Safety of Coastal and Shelf Zones of Sea. – 2014. – no. 28. – P. 375–386.
63. Ivanov, V. A. The study of the spatial structure of free oscillations in the Sea of Azov by mathematical modeling / V. A. Ivanov, L. V. Cherkesov, T. Ya. Shul'ga // Ecological Safety of Coastal and Shelf Zones of Sea. – 2014. – no. 28. – P. 453–461.
64. Ivanov, V. A. Numerical analysis of the impact of dynamic processes on the evolution of pollution in the Sea of Azov / V. A. Ivanov, L. V. Cherkesov, T. Ya. Shulga // Marine Hydrophysical Journal. – 2014. – no. 4. – P. 3–13.
65. Ivanov, V. A. Studies of free fluctuations of the Sea of Azov level arising after the termination of prolonged wind effect / V. A. Ivanov, L. V. Cherkesov, T. Ya. Shul'ga // Physical Oceanography. – 2015. – no. 2. – P. 15–25. – DOI:10.22449/1573-160X-2015-2-14-23
66. Ivanov, V. A. Investigation of the influence of stationary currents on the dynamic processes and evolution of impurities in the Sea of Azov caused by the action of wind/ V. A. Ivanov, L. V. Cherkesov, T. Ya. Shul'ga // Marine Hydrophysical Journal. – 2013. – no. 3. – P. 13–24.

67. Ivanov, V. A. Impact of atmospheric front parameters on free and forced oscillations of level and current in the Sea of Azov / V. A. Ivanov, T. Ya. Shul'ga // Journal of Applied Mechanics and Technical Physics. – 2018. – Vol. 59, no. 5. – P. 912–921. – DOI:10.1134/S002189441805019X
68. Ivanov, V. A. Numerical analysis of surge phenomena, currents, and pollution transport in the Sea of Azov / V. A. Ivanov, T. Ya. Shul'ga // Doklady Earth Sciences. – 2018. – Vol. 479, part 2. – P. 543–546. – DOI:10.1134/S1028334X18040256.
69. Ivanov, V. A. The influence of atmospheric fronts on free and forced oscillations of the water level in the Sea of Azov / V. A. Ivanov, T. Ya. Shul'ga // Doklady Earth Sciences. – 2019. – Vol. 486, no. 2. – P. 737–740.
70. Ingebeikin, Yu. I. Features of the formation of short–term floods and extreme currents in the Sea of Azov / Yu. I. Ingebeikin // Proceedings of the State Oceanographic Institute. - M. : GOIN, 2011. – iss. 213. – P. 91-102.
71. Ingebeikin, Yu. I. The Marine program of the YUNTS RAS and some scientific results of expeditionary research (subinertial processes on the northeastern shelf of the Black Sea) / Yu. I. Ingebeikin, D. G. Matishov // Environmental safety of coastal and shelf zones and integrated use of shelf resources. – Sevastopol : EKOSI-Hydrophysics, 2012. – vol. 26, iss. 2. – P. 380-392.
72. Investigation of the influence of cyclonic disturbances on the dynamic processes and the evolution of impurities in the Sea of Azov in the presence of stationary currents / V.A. Ivanov, V.V. Fomin, L.V. Cherkesov, T.Ya. Shulga // Physical Oceanography. – 2009. – no. 2. – P. 12–25.
73. Kamenkovich, V. M. Fundamentals of ocean dynamics. L., 1973.
74. Karakash, A. Method of predicting short-term level changes in the inland seas of the USSR (Caspian, Black, Azov) / A. Karakash // Russian Meteorology and hydrology. – 1939. – no. 3. – P. 78–82.
75. Klimova, E. G. Numerical experiments on the assimilation of meteorological data using a suboptimal Kalman filter / E. G. Klimova // Meteorology and hydrology. - 2003. – no. 10. – P. 54–67.
76. Knipovich, N. M. The work of the Azov scientific and fishing expedition in 1922-1924 (preliminary report) / N. M. Knipovich // Proc. of the Azov-Black Sea scientific and fishing expedition / Edited by N. M. Knipovich. – Kerch, 1926. – iss. 1. – P. 4–51.
77. Knipovich, N. M. Hydrological Handbook of the Seas of the USSR / N. M. Knipovich, G. R. Bregman // Main Directorate of the Hydrometeorological Service of the USSR under the Council of People's Commissars of the USSR. State Hydrological Institute Leningrad, 1937. – M.: Hydrometeorological Publishing House, vol. 3, iss. 2. – P. 229-463.
78. Knipovich, N. M. Hydrology of seas and brackish waters : (As applied to the fishing business) / N. M. Knipovich, Honorary member of the Academy of Sciences of the USSR; Russian Scientific Research Institute of Marine Fisheries and Oceanography. – M. ; L. : Food industry publishing house, 1938. – 514 p.

79. Kozhukhov, V. P. Mathematical foundations of navigation / V. P. Kozhukhov, A.M. Zhukhlin. – M. : Transport, 1987. – 208 p.
80. Complex satellite monitoring of the Russian Seas / O. Y. Lavrova [et al.]. Moscow : IKI RAS, 2011. – 470 p.
81. Konovalov, A.V. influence of the sea of azov and the kerch strait upon the storm surge oscillations in the Black Sea / A.V. Konovalov, Yu. V. Manyluk, L. V. Cherkesov // Physical Oceanography. – 2000. – no. 5. – P. 5-14.
82. Korotenko, K. A. Modeling of the circulation and transport of oil spills in the Black Sea / K. A. Korotenko, D. E. Dietrich, M. J. Bowman // Oceanology. – 2003. – vol. 43, no. 4. – P. 504-515.
83. Kochin, N. E., Theoretical hydromechanics, Part 1 (6th edition) / N. E. Kochin, I.A. Kibel, N.V. Rose. – M.: Fizmatlit, 1963. – 584 p.
84. Kochin, N. E. Theoretical hydromechanics, Part 2 (4th edition) / N. E. Kochin, I.A. Kibel, N.V. Rose. – M.: Fizmatlit, 1963. – 728 p.
85. Krukier, L. A. Mathematical modeling of the hydrodynamics of the Sea of Azov in the implementation of projects for the reconstruction of its ecosystem / L. A. Krukier // Mathematical modeling. – 1991. – Vol. 3, no. 9. – P. 3–20.
86. Krylov, Yu. M. Orbits of water particles in a progressive standing wave on the example of the White Sea / Yu. M. Krylov // Russian Meteorology and hydrology. – 1946. – no. 2. – P. 69-74.
87. Kulikov, E. A. Variability of the Baltic Sea level and floods in the Gulf of Finland / E. A. Kulikov, I. P. Medvedev // Oceanology. – 2013. – no 53(2). – P. 161–174.
88. Kulikov, E. A. Numerical modeling of anemobaric fluctuations of the Baltic Sea level / E. A. Kulikov, I. V. Fine, E. P. Medvedev // Russian Meteorology and Hydrology. – 2015. – № 2. – P. 41–52.
89. Kurkin, A. A. Nonlinear and nonstationary dynamics of long waves in the coastal zone: monograph / A. A. Kurkin. – N. Novgorod : NNSU Type, 2005. – 329 p.
90. Labzovsky, N. A. Non-periodic fluctuations of sea level / N. A. Labzovsky. – L. : Hydrometeoizdat, 1971. – 237 p.
91. Lamb, G. Hydrodynamics / G. Lamb. – M.-L.: State Publishing house of technical and theoretical literature, 1947. – 928 p.
92. Le Blon, P. Waves in the ocean / P. Le Blon, L. Maysek. – M.: Mir. – 1981. – Vol. 1. – 680 p.
93. The ice regime of the Sea of Azov and climate in the early 21st century / G. G. Matishov [et al.] // Doklady Earth Sciences. – 2014. – Vol. 457, no. 5. – P. 603. – DOI:10.7868/S0869565214230200.
94. The lot of the Azov Sea [Electronic resource]. – URL: http://parusa.narod.ru/bib/books/azov_loc (дата обращения: 11.01.2019).
95. Marchuk, A. G. Numerical modeling of tsunami waves rolling onto the shore of an arbitrary profile / A. G. Marchuk, P. S. Moshkalev // Bulletin of Novosibirsk State University. Series: Information Technology. – 2014. – Vol. 12, no. 2. – P. 55-63.
96. Marchuk, G. I. Mathematical modeling of ocean circulation / G. I. Marchuk, A. S. Sarkisyan. – M. : Nauka, 1988. – 301 p.

97. Masterskih, M. A. Methodological guide for making a forecast of the frontal boron / M. A. Masterskih; Edited by M. A. Sorochinsky. – L. : Hydrometeoizdat, 1980. – 35 p.
98. Matishov, G. G. Kerch Strait and the Don Delta: security of communications and population / G. G. Matishov // Bulletin of the Southern Scientific Center of the Russian Academy of Sciences. – 2015. Vol. 11, no. 1. – P. 6-15.
99. Matishov, G. G. The influence of seish on the formation of extreme levels and currents in the Sea of Azov / G. G. Matishov, D. G. Matishov, Yu. I. Ingebeikin // Bulletin of the Southern Scientific Center of the Russian Academy of Sciences. – 2008. – Vol. 4, no. 2. – P. 46–61.
100. Matishov, G. G. Conditions and consequences of ship accidents in the Kerch Strait during a storm on November 11, 2007 / G. G. Matishov, R. M. Savitsky, Yu. I. Ingebeikin // Bulletin of the Southern Scientific Center of the Russian Academy of Sciences. – 2008. – Vol. 4, no. 3. – P. 54–63.
101. Matishov, G. G. Numerical studies of seiche-like fluctuations of the Sea of Azov level / G. G. Matishov, Yu. I. Injebeikin // Oceanology. – 2009. – Vol. 49, no. 4. – P. 485-493.
102. Matishov, G. G. Modeling of ice formation in the Sea of Azov with account for the climatic trend in the early twenty-first century / G. G. Matishov, Yu. M. Gargopa, A. L. Chikin // Doklady Earth Sciences. – 2012. – Vol. 445, no. 5. – P. 590–593.
103. Matishov, G. G. Study of wind currents in the Kerch Strait applying mathematical modeling / G. G. Matishov, A. L. Chikin // Bulletin of the Southern Scientific Center of the Russian Academy of Sciences. – 2012. – Vol. 8, no. 2. – P. 27–32.
104. Matishov, G. G. An approach to modeling wind currents in Kerch Strait / G. G. Matishov, A. L. Chikin // Doklady Earth Sciences. – 2012. – Vol. 445, no. 3. – P. 342–345.
105. Matishov, G. G. The environmental and biotic impact of the oil spill in Kerch Strait in november 2007 / G. G. Matishov, Yu. I. Engebeikin, R. M. Savitsky // Water resources. – 2013. – Vol. 40, no. 3. – P. 259–273. – DOI:10.7868/S0321059613020041.
106. Matishov, G. G. Modern natural and social risks in the Azov-Black Sea region / G. G. Matishov, D. G. Matishov // Bulletin of the Russian Academy of Sciences. – 2013. – Vol. 83, no. 12. – P. 1059–1067. – DOI:10.7868/S0869587313100071.
107. Matishov, G. G. Extreme flooding of the Don Delta in the spring of 2013 / G. G. Matishov, S. V. Berdnikov // Izv. RAS. The series is geographical. – 2015. – no. 1. – P. 111–118. – DOI:10.15356/0373-2444-2015-1-111-118.
108. Matishov, G. G. Studies of particulate matter distribution by Aqua MODIS data and simulation results / G. G. Matishov, T. Y. Shul'ga, S. M. Khartiyev, A. R. Ioshpa // Doklady Earth Sciences. – 2018. – Vol. 481, no. 1. – P. 967–971. – DOI:10.1134/S1028334X18070267.

109. Medvedev, I. P. Numerical modeling of sea level oscillations in the Caspian Sea / I. P. Medvedev, E. A. Kulikov, I. V. Fine, A. E. Kulikov // Russian Meteorology and Hydrology. – 2019. – № 8. – P. 42–56.
110. Mikhailova, E. N. Modeling of the spread of passive impurities in Sevastopol bays / E. N. Mikhailova, N. B. Shapiro, S. A. Yushchenko // Physical Oceanography. – 1999. – no. 3. – P. 29–42.
111. Miropolsky, Yu. 3. Dynamics of internal gravitational waves in the ocean. – L., 1981. – 302 p.
112. Simulation of surge phenomena and transformation of the admixture field in the Sea of Azov in the presence of stationary currents / V. A. Ivanov [et al.] // Physical Oceanography. – 2008. – no. 4. – P. 52–68.
113. Monin, A. S. Classification of nonstationary processes in the ocean / A. S. Monin // Izv. of the USSR Academy of Sciences. Physics of the Earth. – 1972. – no. 7. – P. 26-30.
114. Monin, A. S. Physics of the ocean. Vol. 1: Hydrophysics of the ocean / A. S. Monin, V. M. Kamenkovich. – M. : Nauka, 1978. – 455 p.
115. Marine expeditionary research on scientific research vessels ”Deneb“ and ”Professor Panov" in 2013 / G. G. Matishov [et al.] // Oceanology. – 2015. – Vol. 55, no. 5. – P. 861–865. – DOI:10.7868/S0030157415050135.
116. Scientific and applied reference book on the climate of the USSR. Series 3: Long-term data. Parts 1– 6. Issue 10: Ukrainian SSR. Book 1. – L. : Hydrometeoizdat, 1990. – 604 p.
117. Nekrasov, A.V. Tidal waves in marginal seas / A.V. Nekrasov. – L. : Hydrometeoizdat, 1975. – 248 p.
118. Ovsienko, S. N. Calculation of overburden fluctuations of the Sea of Azov level / S. N. Ovsienko // Proceedings of the Hydrometeorological Center of the USSR. – L. : Hydrometeoizdat, 1972. – iss. 60. – P. 55–58.
119. Ovsienko, S. N. Calculation of the catastrophic surge off the southeastern coast of the Sea of Azov / S. N. Ovsienko // Proceedings of the Hydrometeorological Center of the USSR. – L. : Hydrometeoizdat, 1973. – iss. 127. – p. 33–36.
120. Oceanographic atlas of the Black and Azov Seas. – K. : Ukrmorkartografiya, 2009. – 356 p.
121. Features of water circulation in the vicinity of Zmeiny Island under the influence of winds of various directions / E. N. Mikhailova [et al.] // Physical Oceanography. – 1998. – no. 4. – P. 17–23.
122. Features of circulation in the Strait, taking into account the influence of the Azov and Black Seas / V. A. Ivanov, V. V. Fomin, L. V. Cherkesov, T. Ya. Shulga // Modeling of water dynamics in the Kerch Strait and pre-flood zones / edited by V. A. Ivanov. – Sevastopol : EKOSI-Hydrophysics, 2010. – P. 18.
123. Estimation of variability of optical properties of water in the Black Sea in the summer of 1998 according to the SeaWiFS satellite instrument / V. S. Suetin [et al.] // Physical Oceanography. – 2002. – no. 6. – P. 44–54.

124. Calculation of the transfer of petroleum products from discharge sources in the Taganrog Bay of the Sea of Azov / O. I. Oradovsky [et al.] // Russian Meteorology and Hydrology. – 1999. – no. 5. – P. 77–90.
125. Regime, diagnosis and forecast of wind waves in the oceans and seas / [Z. K. Abuzyarov et al.] ; Federal Service for Hydrometeorology and Environmental Monitoring (Roshydromet) ; edited by E. S. Nesterov. – M. : Hydrometeorological Scientific Research. The Center of the Russian Federation, 2013. – 292 p.
126. Polupanov, V. N. On modeling of suspension transfer and deposition using cellular automata / V. N. Polupanov, S. S. Zhugailo // Environmental control systems. – 2017. – no. 8(28). – C. 37–46.
127. Pukhtyar, L. D. Turbulent characteristics of the coastal zone of the sea / L. D. Pukhtyar, Y. S. Osipov // Trudy GOIN. – M. : Gidrometeoizdat, 1981. – iss. 158. – P. 35–41.
128. Reanalysis of the average daily values of atmospheric pressure in the period starting from 1.01.1948 [Electronic resource]. – ftp.cdc.noaa.gov/Datasets/ncep.reanalisis.dailyavgs/levelsea/.
129. Sirotov, K. M. Experience in calculating wind speed and wave height in the cold front zone / K. M. Sirotov, T. M. Sidelnikova // Proceedings o the Hydrometeorological Center of the USSR. – 1984. – iss. 263. – P. 72–34.
130. Scriptunov, N. A. Currents on the estuarine coast of the Don (Taganrog Bay) / N. A. Scriptunov // Trudy GOIN. – M. : Hydrometeoizdat, 1978. – iss. 139. – P. 43–57.
131. Modern dangerous exogenous processes in the coastal zone of the Sea of Azov / G. G. Matishov [et al.]. – Rostov-on-Don : Publishing House of the Southern Federal University, 2015. – 324 p.
132. Сретенский, Л. Н. Теория волновых движений жидкости (2-е издание) / Л. Н.Сретенский. – М. : Наука, 1977. – 816 с.
133. Sudolsky, R. V. Dynamic phenomena in reservoirs / A. S. Sudolsky. – L. : Hydrometeoizdat, 1991. – 261 p.
134. «Thermohaline electronic atlas of the Sea of Azov» : database [Electronic resource] / T. Ya. Shul'ga, D. M. Shukalo ; FSBIS FRC MHI. Electron. dan. Moscow, 2023. State registration number № 2023621161.
135. Timonov, V. V. On the kinematic analysis of tides / V. V. Timonov // Trudy GOIN. – M. : Hydrometeoizdat, 1959. –iss. 37. – P. 181–204.
136. Tolmazin, D. M. Problems of water dynamics in the north-western part of the Black Sea / D. M. Tolmazin, V. A. Schneidman, Zh. M. Artsikhovskaya – K. : Naukova Dumka, 1969. – 130 p. (in Russian).
137. Faschuk, D. Ya. Ecological problems of the Cimmerian Bosporus / D. Ya. Faschuk, S. N. Ovsienko, O. A. Petrenko // Black Sea Bulletin. – 2007. – no. 1. – P. 52–78.
138. Faschuk, D. Ya. Ecological and geographical consequences of the disaster of the tanker Volgoneft-139 in the Kerch Strait on November 11, 2007 / D. Ya. Faschuk // Proceedings of the Russian Academy of Sciences. The series is geographical. – 2009. – no. 1. – P. 105–117.

139. Filippov, Yu. G. On one method of calculating sea currents / Yu. G. Filippov // Proceedings of the GOIN. – M. : Hydrometeoizdat, 1970. – iss. 103. – P. 87–94.
140. Filippov, Yu. G. Investigation of some difference schemes for calculating the spread of impurities in the sea / Yu. G. Filippov // Proceedings of GOIN. – M. : Hydrometeoizdat, 1975. – iss. 126. – P. 49–73.
141. Fomin, V. V. Numerical model of circulation of waters of the Sea of Azov / V. V. Fomin // Scientific works of UkrNIGMI. – 2002. – iss. 249. – P. 246–255.
142. Fomin, V. V. Modeling drift currents in a shallow basin with allowance for variations in tangential stresses induced by wind waves / V. V. Fomin, L. V. Cherkesov // Izvestiya, Atmospheric and Oceanic Physics. – 2006. – Vol. 42, no. 3. – P. 393–402.
143. Cherkesov, L. V. Introduction to hydrodynamics and wave theory / L. V. Cherkesov, V. A. Ivanov, S. M. Khartiev. – St. Petersburg : Hydrometeoizdat, 1992. – 264 p.
144. Cherkesov, L. V. Investigation of the dependence of the impurity evolution on the initial distribution of its concentration and cyclone parameters / L. V. Cherkesov, T. Ya. Shul'ga // Physical Oceanography. – 2012. – no. 5. – P. 24–33.
145. Cherkesov, L. V. Investigation of the effect of the baric formation parameters on free and forced oscillations of the level and currents in the Sea of Azov/ L. V. Cherkesov, T. Ya. Shulga // Physical Oceanography. – 2016. – no. 4. – P. 12–24. – DOI:10.22449/1573-160X-2016-4-12-24.
146. Cherkesov, L. V. Simulation and early warning of natural and technogenic influences in coastal areas in the Sea of Azov / L. V. Cherkesov, T. Ya. Shul'ga // Russian Journal of Hydrometeorology and ecology. – 2016. – no. 45. – P. 100–112.
147. Cherkesov, L. V. Study of the transformation of pollution caused by cyclones passing over the Sea of Azov / L. V. Cherkesov, T. Ya. Shul'ga // Proceedings of the Karelian Scientific Center of RAS. – 2016. – no. 8. – P. 108–115.
148. Cherkesov, L. V. Numerical analysis of the effect of moving the pressure fields on the currents free and forced oscillations of level in the Azov Sea / L. V. Cherkesov, T. Ya. Shul'ga // Environmental Bulletin of the scientific centers of the Black Sea Economic Cooperation. – 2016. – no. 2. – P. 99–110.
149. Cherkesov, L. V. Waves, currents, overburden processes and pollution transformation in the Sea of Azov / L. V. Cherkesov, T. Ya. Shul'ga. – Sevastopol: MHI RAS, 2017. – 228 p.
150. Cherkesov, L. V. Numerical study of storm surge processes and currents of the Sea of Azov during a period of extreme winds / L. V. Cherkesov, T. Ya. Shul'ga, N. N. Dyakov, R. R. Stanichnaya // Physical Oceanography. – 2017. – Iss. 5. – P. 3–18. – DOI:10.22449/1573-160X-2017-5-3-18.
151. Cherkesov, L. V. Study of stationary currents for dynamic processes and admixtures of pollution in the sea of Azov / L. V. Cherkesov, T. Ya. Shul'ga // Bulletin of the South Ural State University. Series: Computational Mathematics and Software Engineering. – 2017. – vol. 6, no. 1. – P. 56–72. (in Russian). – DOI:10.14529/cmse170104.

152. Cherkesov, L. V. Numerical analysis of the influence of parameters of atmospheric fronts to the free and forced oscillations level and incurrentss into the Azov Sea / L. V. Cherkesov, T. Ya. Shul'ga // Proc. of N.N. Zubov State Oceanographic Institute. – M. : SOIN, 2017. – iss. 218. – P. 120–136.
153. Cherkesov, L. V. Numerical analysis of the effect of active wind speed and direction on circulation of Sea of Azov water with and without allowance for the water exchange through the Kerch Strait / L. V. Cherkesov, T. Ya. Shul'ga // Oceanology. – 2018. – Vol. 58, no. 1. – P. 19–27. – DOI:10.1134/S0001437018010022.
154. Chernyakova, A. P. Typical wind fields of the Black Sea / A. P. Chernyakova // Collection of works of the Basin hydrometeorological Observatory of the Black and Azov Seas. – L. : Hydrometeoizdat, 1965. – iss. 3. – P. 78–121.
155. Chikin, A. L. The three-dimensional problem of calculating the hydrodynamics of the Sea of Azov / A. L. Chikin // Mathematical modeling. – 2001. – Vol. 13, no. 2. – P. 86-92.
156. Chikin, A. L. Modeling of the pollutant transfer process in the Tsimlyansk reservoir / A. L. Chikin, I. N. Shabas, S. G. Sidiropulo // Water resources. – 2008. – Vol. 35, то. 1. – P. 53–59.
157. Chikin, A. L. A two-layer mathematical model of wind currents in reservoirs with large areas of shallow water / A. L. Chikin // Mathematical modeling. – 2009. – Vol. 21, no. 12. – P. 152–160.
158. Chikin, A. L. Mathematical model of wind currents in the Kerch Strait / A. L. Chikin // Bulletin of the Southern Scientific Center of the Russian Academy of Sciences. – 2009. – Vol. 5, no. 2. – P. 58-63.
159. Chikin, A. L. Calculation of wind currents in the Kerch Strait using a two-layer mathematical model / A. L. Chikin, P. A. Biryukov // Izvestia of Higher Educational Institutions. The North Caucasus region. Series: Technical Sciences. – 2010. – no. 5. – P. 12-16.
160. Shabas, I. N. The three-dimensional problem of impurity propagation / I. N. Shabas, A. L. Chikin // Mathematical modeling. – 2001. – Vol. 13, no. 3. – P. 85-89.
161. Shamin, R. V. Computational experiments in modeling surface waves in the ocean / R. V. Shamin. – M. : Nauka, 2008. – 132 p.
162. Sheremetevskaya, O. I. Overburden fluctuations of the Sea of Azov level, methods of their calculations and forecasts / O. I. Sheremetevskaya ; All-Union Scientific Research Institute of Hydrometeorology. Information is a global data center. – Obninsk : VNIIGMI MCD, 1977. – 39 p. – (Series "Oceanology").
163. Shnyukov, E. F. Catastrophes in the Black Sea / E. F. Shnyukov, L. I. Mitin, V. P. Tsemko ; National Academy of Sciences of Ukraine, Department of Marine Geology and Sedimentary Ore Formation, Central Research Institute. – K. : Manuscript, 1994. – 296 p.
164. Shpindler, I. B. Materials on the hydrology of the Black and Azov Seas, collected in the expeditions of 1890 and 1891 / I. B. Shpindler, F. F. Wrangel //

Appendix to the issue of XX notes on hydrography. – St. Pb : Type. Imp. Academy of Sciences, 1899. – 70 p.

165. Shukalo, D. M. Investigation of long-term variability of temperature and salinity of the Sea of Azov for the period 1913-2018 / D. M. Shukalo, T. Ya. Shulga // Ecology. Economy. Computer science. Series: System analysis and modeling of economic and ecological systems. – 2020. – T. 1, № 5. – C. 220–223.

166. Shul'ga, T. Ya. Influence of intensity of driving wind fields on dynamic processes and transformation of passive admixture in the presence of stationary currents in the Sea of Azov / T. Ya. Shul’ga // Physical Oceanography. – 2013. – no. 4. – P. 3–16.

167. Shul'ga, T. Ya. Numerical research of the pollution surface and deep-sea evolution in the Sea of Azov using satellite observation data / T. Ya. Shul'ga, V. V. Suslin, R. R. Stanichnaya // Physical Oceanography. – 2017. – Iss 6. – P. 36–46. – DOI:10.22449/1573-160X-2017-6-36-46.

168. Shul'ga, T. Ya. Evolution of the pollution in the Sea of Azov by satellite data and simulation results / T. Ya. Shul’ga // Vestnik Udmurtskogo Universiteta: Matematika, Mekhanika, Komp'yuternye Nauki. – 2017. – Vol. 27, iss. 3. – P. 450-459. – DOI: 10.20537/vm170312.

169. Shulga, T. Ya. Analysis of pollution propagation processes in the Sea of Azov using satellite data and modeling results / T. Ya. Shulga, V. V. Suslin // Proceedings of the IX All-Russian Conference "Modern problems of optics of natural waters" (ONW'2017), St. Petersburg, September 20–22, 2017 – St. Petersburg, 2017. – P. 156–160.

170. Shulga, T. Ya. Analysis of the results of numerical modeling and satellite observations of the evolution of pollution in the Sea of Azov for the period from 2013 to 2014 / T. Ya. Shulga // Ecology. Economy. Computer science. Series: System analysis and modeling of economic and ecological systems. – 2017. – Vol. 1, no.2. – P. 123–133.

171. Shul'ga, T. Ya. Investigation of the evolution of the suspended solids in the Sea of Azov based on the assimilation of satellite data in a hydrodynamic model / T. Ya. Shul’ga, V. V. Suslin // Fundamental and Applied Hydrophysics. – 2018. – Vol. 11, iss. 3. – P. 73–80. – DOI:10.7868/S2073667318030097.

172. Shul'ga, T. Ya. Research of the relations between the seasonal variability of salinity and bio-optical features in the Sea of Azov using the satellite data in the visible spectrum range / T. Ya. Shul’ga, V. V. Suslin, D. M. Shukalo, A. V. Ingerov // Fundamental and Applied Hydrophysics. – 2020. – Vol. 13, № 2. – C. 68–75. DOI:10.7868/S2073667320020082.

173. Shul'ga, T. Ya. Data recovery of the Sea of Azov salinity fields using regression analysis between in situ data and regional satellite products / T. Ya. Shul’ga, V. V. Suslin, D. M. Shukalo // Fundamental and Applied Hydrophysics. – 2022. – Vol. 15, no. 3. – C. 114–124. – DOI:10.59887/fpg/bkug-hzez-xx59.

174. Ecological mapping of the water area of the Sea of Azov and the coastal zone based on integrated ecosystem monitoring and modern information technologies / G. G. Matishov [et al.] // Nauka Kubani. – 2008. – Vol. 12, no. 3. – P. 57-63.

175. Ecosystem of the Sea of Azov: anthropogenic pollution / A. A. Klenkin, K. I. Gorchakova, L. F. Pavlenko, Z. A. Temerdashev. – Krasnodar : Prosveshchenie-Yug, 2007. – 324 p.
176. Extreme flooding of the Don Delta in the spring of 2013: chronology, conditions of formation and consequences [Article] / G. G. Matishov [et al.] // Bulletin of the Southern Scientific Center of the Russian Academy of Sciences. 2014. – Vol. 10, no. 1. – P. 17–24.
177. The extreme flood in the Don River delta, march 23-24, 2013, and determining factors / G. G. Matishov [et al.] // Doklady Earth Sciences. – 2014. – Vol. 455, no. 1. – P. 360– 363. – DOI:10.7868/S0869565214090229
178. Yakushev, E. V. The Azov Sea in the 28th voyage scientific and research vessel "Aquanaut" (July-August 2001) / E. V. Yakushev [et al.] // Oceanology. – 2003. – Vol. 43, no. 1. – P. 44–53.
179. Aiken, J. The SeaWiFS CZCS-Type Pigment Algorithm / James Aiken [et al.]. – Greenbelt, Maryland : Ed. NASA Goddard Space Flight Center, 1995. – NASA Technical Memorandum 104566, Vol. 29. – 34 p. – URL: https://oceancolor.gsfc.nasa.gov/docs/technical/seawifs_reports/prelaunch/PreLVol29.pdf (accessed: 05.01.2019). – (SeaWiFS Technical Report Series).
180. Application of SeaWiFS data for studying variability of bio-optical characteristics in the Barents, Black and Caspian Seas / O. V. Kopelevich [et al.] // Deep-Sea Research. Part II: Tropical Studies in Oceanography. – 2004. – Vol. 51, iss. 10–11. – P. 10P63-1091. –https://doi.org/10.1016/j.dsr2.2003.10.009
181. Bautista, E. G. Propagation of shallow water waves in an open parabolic channel using the WKB perturbation technique / E. G. Bautista [et al.] // Applied Ocean Research. – 2011. – Vol. 33, iss. 3. – P. 186-192. – https://doi.org/10.1016/j.apor.2011.03.002.
182. Bio-optical characteristics of the Russian seas from satellite ocaen color data of 1998-2010 / O. V. Kopelevich [et al.] // Proc. VI Int. Conf. Current problems in optics of natural waters. – St-Petersburg, 2011. – P. 181–182.
183. Black Sea and Sea of Azov. – Taunton : United Kingdom Hydrographic office, 2003. – 292 p. –URL: http://b-ok.xyz/ireader/3087211 (accessed: 05.01.2019).
184. Blumberg, A. F. A description of three dimensional coastal ocean circulation model / A. F. Blumberg, G. L. Mellor // Three-Dimensional Coast Ocean Models. / Ed. N. S. Heaps. – Washington DC : American Geophysical Union, 1987. – Vol. 4. – P. 1–16. –https://doi.org/10.1029/CO004p0001. – (Coastal and Estuarine Sciences).
185. Chang, H. K. Long wave reflection from submerged trapezoidal breakwaters / Hsien-Kuo Chang, Jin-Cheng Liou // Ocean Engineering. – 2007. – Vol. 34, iss. 1. – P. 185–191. –https://doi.org/10.1016/j.oceaneng.2005.11.017.
186. Churilova, T. Ya. Spectral Light Absorption Coefficient of Particles and Colored Dissolved Organic Matter in the Sea of Azov / Churilova, T. Ya., Efimova T.V., Moiseeva N.A., E. Yu. Skorokhod // Fundamental and Applied Hydrophysics. – 2022. – 15 (3). – P. 73–83. DOI:10.48612/fpg/ex1p-9vtp-phu8.

187. Climatic Atlas of the Sea of Azov / Matishov G. [et al.] ; G. Matishov, S. Levitus, Ed. – U.S. Govern, 2006. – (NOAA Atlas NESDIS 59).
188. Climatic Atlas of the Sea of Azov 2008. / Matishov G. [et al.] ; G. Matishov, S. Levitus, Ed. – U.S. Govern, 2008. – (NOAA Atlas NESDIS 65). 148 p., CD-ROM.
189. Courant, R. On the partial difference equations of mathematical physics / R. Courant, K. Friedrichs, H. Lewy // IBM Journal of Research and Development. – 1967. – Vol. 11, iss. 2. – P. 215–234. – DOI:10.1147/rd.112.0215.
190. Dall'Olmo, G. Effect of bio-optical parameter variability on the remote estimation of chlorophyll-a concentration in turbid productive waters: experimental results / G. Dall'Olmo, A. Gitelson // Applied Optics. – 2005. – 44 (3). – P. 412–422. – DOI: 10.1364/AO.44.000412.
191. Dashkevich, L.V. Many-year variations of the average salinity of the Sea of Azov / L.V. Dashkevich, V.V. Kulygin, S.V. Berdnikov // Water Resources. – 2017. –44(5). – P. 749–757. DOI:10.1134/S0097807817040042
192. Entekhabi, D. The Soil Moisture Active Passive (SMAP) Mission / D. Entekhabi, Njoku E. G., O'Neill P. E., Kellogg K. H., Crow W. T., Edelstein W. N., Entin J. K., Goodman S. D., Jackson T. J., Johnson J., Kimball J., Piepmeier J. R., Koster R. D., Martin N., McDonald K. C., Moghaddam M., Moran S., Reichle R., Shi J. C., Spencer M. W., Thurman S. W., Tsang L., J. Van Zyl. // Proceedings of the IEEE. – 2010. – 98(5). – P. 704–716. – DOI: 10.1109/JPROC.2010.2043918
193. Ezer, T. Developments in terrain–following ocean models: intercomparisons of numerical aspects / Tal Ezer, Hernan Arango, Alexander F. Shchepetkin // Ocean Modelling. – 2002. – Vol. 4, iss. 3–4. – P. 249–267. – DOI 10.1016/S1463-5003(02)00003-3.
194. Font, J. SMOS: The challenging sea surface salinity measurement from space / J. Font, Camps A., Borges A., Martin-Neira M., Boutin J., Reul N., Kerr Y., Hahne A., S. Mecklenburg // Proceedings of the IEEE. – 2010. – 98(5). – P 649–665. – DOI: 10.1109/JPROC.2009.2033096
195. Fournier, S. Seasonal and interannual variations of sea surface salinity associated with the Mississippi River plume observed by SMOS and Aquarius / S. Fournier, T. Lee, M. M. Gierach // Remote Sens. Environ. – 2016. – 180. – P. 431–439.
196. Ginzburg, A.I. Climate Change in the Hydrmeteorological Parameters of the Black and Azov Seas (1980–2020) / A.I. Ginzburg, A.G. Kostianoy, I.V. Serykha, S.A. Lebedev. // Oceanology. – 2021. – 61(6). – P. 900–912. – DOI:10.1134/S0001437021060060.
197. Gitelson, A. A. The peak near 700 nm on radiance spectra of algae and water: relationships of its magnitude and position with chlorophyll-a concentration / A. A. Gitelson // International Journal of Remote Sensing. – 1992. – 13 (17). – P. 3367–3373. – DOI: 10.1080/01431169208904125.
198. Gitelson, A.A. 2008. A simple semi-analytical model for remote estimation of chlorophyll-a in turbid waters: Validation / A. A. Gitelson, G. Dall'Olmo, W. Moses, D. C. Rundquist, T. Barrow, T. R. Fisher, D. Gurlin, J. Holz // Remote

Sensing of Environment. – 2008. – 112 (9). – P. 3582–3593. – DOI:10.1016/j.rse.2008.04.015.

199. Gitelson, A. A. A bio-optical algorithm for the remote estimation of the chloro-phyll-a concentration in case 2 waters / A. A. Gitelson, D. Gurlin, W. J. Moses, T. Barrow // Environmental Research Letters. – 2009. – 4 (045003). – P. 5. – DOI:10.1088/1748-9326/4/4/045003.

200. Ghil, M. Data Assimilation in Meteorology and Oceanography / Michael Ghil, Paola Malanotte-Rizzoli // Adv. Geophys. – 1991. – Vol. 33. – P. 141–266. – DOI:10.1016/S0065-2687(08)60442-2.

201. Glukhovets, D. I. Research of the relationship between salinity and yellow substance fluorescence in the Kara Sea / D. I. Glukhovets, Yu. A. Goldin // Fundamentalnaya i Prikladnaya Gidrofizika. – 2018. – 11 (3). – P. 34–39. – DOI:10.7868/S2073667318030048.

202. Goptarev, N. P. Hydrology and Hydrochemistry of the Seas. V the Azov Sea / N. P. Goptarev, A. I. Simonov B. M. Zatuchnaya D. E. Gershanovich. Gidrometeoizdat, St. Petersburg, 1991. – 236 p. (in Russian)

203. Grégoire, M. Monitoring Black Sea environmental changes from space: New products for altimetry, ocean colour and salinity. Potentialities and requirements for a dedicated in-situ observing system / M. Grégoire, Alvera-Azcaráte A., Buga L., Capet A., Constantin S., D'ortenzio F., Doxaran D., Faugeras Y., Garcia-Espriu A., Golumbeanu M., González-Haro C., González-Gambau V., Kasprzyk J-P., Ivanov E., Mason E., Mateescu R., Meulders C., Olmedo E., Pons L., Pujol M-I., Sarbu G, Turiel A., Vandenbulcke L., M-H. Rio // Frontiers in Marine Science. – 2023. – 9. – P. 998970. – DOI: 10.3389/fmars.2022.998970

204. Grant, W. D. Combined wave and current interaction with a rough bottom / William D. Grant, Ole Secher Madsen // J. Geophys. Res. – 1979. – Vol. 84, iss. C. 4. – P. 1797–1808. – DOI:10.1029/JC084iC04p01797.

205. Hsu, S. A. A Mechanism for the Increase of Wind Stress (Drag) Coefficient with Wind Speed over Water Surfaces: A Parametric Model / S. A. Hsu // J. Phys. Oceanogr. – 1986. – Vol. 16, no. 1. – P. 144–150. – DOI:10.1175/1520-0485(1986)016<0144:AMFTIO>2.0.CO;2.

206. Johnson, G. C. Global Oceans / G. C. Johnson, et al. // Bull. Amer. Meteor. Soc. – 2021. – 102. – P. 143–198. DOI:10.1175/BAMS-D-21-0083.1

207. Kalman, R. E. A New Approach to Linear Filtering and Prediction Problems / R. E. Kalman // Journal of Basic Engineering. – 1960. – Vol. 82, iss. 1. – P. 35–45. DOI:10.1115/1.3662552.

208. Khorram, S. 1982. Remote sensing of salinity in the San Francisco Bay Delta / S. Khorram // Remote Sens. Environ. – 1982. – 12. – P. 15–22. – DOI:10.1016/0034-4257(82)90004-9.

209. Kholoptsev, A.V. The Influence of Anticyclonic Movement Over the Sea of Azov on Variations of Maximum Instantaneous Current Speed in the Kerch Strait During 1948-2017 Ice Seasons / A. V.Kholoptsev, T. Ya. Shul'ga, O. Ye.Shchodro, S. A. Podporin // Physical and Mathematical Modeling of Earth

and Environment Processes (2018) / Springer Proceedings in Earth and Environmental Sciences. – 2019. – P. 1–14. – DOI:10.1007/978-3-030-11533-3_1

210. Konik, M. The operational method of filling information gaps in satel-lite imagery using numerical models / M. Konik, M. Kowalevski, K. Bradtke, M. Darecki // International Journal of Applied Earth Observation and Geoinformation. – 2019. – 75. – P. 66–82. – DOI:10.1016/j.jag.2018.09.002.

211. Kopelevich, O. V. Application of Sea-WiFS data for studying variability of bio-optical characteristics in the Barents, Black and Caspian Seas / O. V. Kopelevich, V. I. Burenkov, S. V. Ershova, S. V. Sheberstov, M. A. Evdoshenko // Deep Sea Research Part II Topical Studies in Oceanography. – 2004. – 51(10-11). – P. 1063–1091. – DOI:10.1016/S0967-0645(04)00101-8.

212. Large, W. G. Open ocean momentum fluxes in moderate to strong winds / W. G. Large, S. Pond // J. Phys. Oceanogr. – 1981. – Vol. 11. – P. 324–326. – DOI:10.1175/1520-0485(1981)011<0324:OOMFMI>2.0.CO;2.

213. Martín-Neira, M. SMOS instrument performance and calibration after six years in orbit / M. Martín-Neira, Oliva R., Corbella I., Torres F., Duffo N., Duran I., Kainulainen J., Closa A., Zurita A., Cabot F., Khazaal A., Anterrieau E., Barbosa J., Lopes G., Tenerelli J., Diez-Garcia R., Fauste J., Martin-Porqueras F., González- Gambau V., Turiel A., Delwart S., Crapolicchio R., M. Suess // Remote Sensing of Environment. 2016. – 180. – P. 19–39. – DOI:10.1016/j.rse.2016.02.036

214. Mathematical modeling of storm surge in three dimensional primitive equations / W. Wannawong [et al.] // International Journal of Computational and Mathematical Sciences. - 2011. – Vol. 5, no. 6. – P. 797–806. – DOI:10.5281/zenodo.1062708.

215. Matishov, G. G. Studies of Particulate Matter Distribution by *Aqua* Modis Data and Simulation Results / G. G. Matishov [et al.] // Doklady Earth Sciences. – 2018. – Vol. 481, iss. 1. – P. 967–971. – DOI:10.1134/S1028334X18070267.

216. Matsuoka, A. Pan-Arctic optical characteristics of colored dissolved organic matter: Tracing dissolved organic carbon in changing Arctic waters using satellite ocean color data / A. Matsuoka, E.S. Boss, M. Babin, L. Karp-Boss, M.A. Hafez, A. Chekalyuk, C.W. Proctor, P.J. Werdell, A. Bricaud // Remote Sensing of Environment. – 2017. – 200. – P. 89–101. – DOI:10.1016/J.RSE.2017.08.009.

217. Medina-Lopez, E. Machine Learning and the End of Atmospheric Corrections: A Comparison between High-Resolution Sea Surface Salinity in Coastal Areas from Top and Bottom of Atmosphere Sentinel-2 Imagery / E. Medina-Lopez // Remote Sensing. – 2020. – 12 (18). – P. 2924. – DOI:10.3390/rs12182924.

218. Mellor, G. L. Development of a turbulence closure model for geophysical fluid problems / G. L. Mellor, T. A. Yamada // Rev. Geophys. – 1982. – Vol. 20, iss. 4. – P. 851– 875. – http://dx.doi.org/10.1029/RG020i004p00851.

219. Mellor, G. L. A Hierarchy of Turbulence Closure Models for Planetary Boundary Layers / G. L. Mellor, T. A. Yamada // Journal of Atmospheric Sciences.

– 1974. – Vol. 31, no. 7. – P. 1791–1806. DOI:10.1175/1520-0469(1974)031<1791:AHOTCM>2.0.CO;2.

220. NASA Goddard Space Flight Center, Ocean Ecology Laboratory, Ocean Biology Processing Group. Moderate-resolution Imaging Spectroradiometer (MODIS) Aqua Ocean Color Data; 2022 Reprocessing. NASA OB.DAAC, Greenbelt, MD, USA. DOI:10.5067/AQUA/MODIS/L2/OC/2022.

221. NASA Goddard Space Flight Center, Ocean Ecology Laboratory, Ocean Biology Processing Group. Moderate-resolution Imaging Spectroradiometer (MODIS) Terra Ocean Color Data; 2018 Reprocessing. NASA OB.DAAC, Greenbelt, MD, USA. DOI: 10.5067/TERRA/MODIS/L2/OC/2018.

222. Oguz, T. Seasonal variability of wind and thermohaline-driven circulation in the Black Sea: Modeling studies / Temel Oguz, Paola Malanotte-Rizzoli // J. Geophys. Res. – 1996. – Vol. 101, iss. C7. – P. 16551–16569. – DOI:10.1029/96JC01093.

223. O'Reilly, J. E. Ocean color chlorophyll algorithms for SeaWiFS / J. E.O'Reilly, S. Maritorena, B. G. Mitchell, D. A. Siegel, K. L. Carder, S. A. Garver, M. Kahru, C. R. McClain // Journal of Geophysical Research. – 1988. – 103. – P. 24937–24953. – DOI:10.1029/98JC02160.

224. O'Reilly, J. E. SeaWiFS Postlaunch Calibration and Validation Analyses, Part 3 / J. E. O'Reilly, et al. // NASA Tech. Memo. 2000-206892, S.B. Hooker and E.R. Firestone, Eds., NASA Goddard Space Flight Center. – 2000. – 11. – P. 49.

225. Owers, D. G. Optical Properties of a Region of Freshwater Influence (The Clyde Sea) / D.G. Owers, G.E.L. Harker, P.S.D. Smith, P. Tett. // Estuarine Coastal and Shelf Science. – 2000. – 50 (5). – P. 717–726. – DOI:10.1006/ecss.1999.0600.

226. Penny, S.G. A hybrid global ocean data assimilation system at NCEP / S. G. Penn, W.D. Behringer, J.A. Carton, E. Kalnay // Monthly Weather Review. – 2015. – 143. – P. 4660–4677. – DOI:10.1175/MWR-D-14-00376.1.

227. Pietrzak, J. The use of TVD limiters for forward-in-time upstream-biased advection schemes in ocean modeling / J. Pietrzak // Mon. Weather Rev. – 1998. – Vol. 126, no. 3. – P. 812–830. – DOI:10.1175/1520-0493(1998)126<0812:TUOTLF>2.0.CO;2.

228. Schwab, D. Computerized Bathymetry and Shorelines of the Great Lakes / D. Schwab, D. Sellers. – Springfield, Va.: National Technical Information Service, 1980. – (NOAA Data Report ERL-GLERL-16).

229. Qing, S. Retrieval of sea surface salinity with MERIS and MODIS data in the Bohai Sea / Qing, S.; J. Zhang, T. Cui, Y. Bao // Remote Sensing of Environment. – 2013. – 136. – P. 117–125. – DOI:10.1016/j.rse.2013.04.016.

230. Rabinovich, A. B. Seiches and harbor oscillations. In: Handbook of Coastal and Ocean Engineering / Ed. Kim. Y.C. Chapter 9. World Scientific Publ., Singapore, 2009. P. 193–236.

231. Rajabi-Kiasari, S. An efficient model for the prediction of SMAP sea surface salinity using machine learning approaches in the Persian Gulf / S. Rajabi-Kiasari, M. Hasanlou // International Journal of Remote Sensing. – 2020. – 41(8). – P. 3221–3242. – DOI:10.1080/01431161.2019.1701212.

232. Shukalo, D.M. Long-term and seasonal anomalies of the Sea of the Azov thermohaline structure for 1913–2018 / D. M. Shukalo, T. Ya. Shul'ga // Journal of Physics Conference Series. – 2021. – 2057(1): 012133. – DOI:10.1088/1742-6596/2057/1/012133.
233. Shukalo, D.M. Analysis of the monthly average salinity of the surface layer of the Sea of Azov, obtained by remote sensing and in situ measurement methods / D. M. Shukalo, T. Ya. Shul'ga, V. V. Suslin // Proceedings Volume 12780, 29th International Symposium on Atmospheric and Ocean Optics: Atmospheric Physics. – 2023. – 127804A. – DOI: 10.1117/12.2690983
234. Shul'ga, T. Ya. Analysis of the distribution of pollution in the Sea of Azov by the results of numerical simulation and data of satellite observations / T. Ya. Shul'ga // Journal of Physics: Conf. Series. – 2017. – Vol. 899, Iss. 092013. – DOI:10.1088/1742-6596/899/9/092013
235. Shulga, T.Ya. Remote sensing and modeling of the evolution of suspended matter in the Sea of Azov / T. Ya. Shul'ga, V. V. Suslin // Proceedings of SPIE - The International Society for Optical Engineering. – 2018. – Vol. 10833, № 108334G. – DOI:10.1117/12.2504196
236. Shul'ga, T.Ya. Numerical Analysis and Prediction of the Consequences of Natural and Technological Impacts in Coastal Areas of the Azov Sea / T. Ya. Shul'ga, S. M. Khartiev, A. R. Ioshpa // Physical and Mathematical Modeling of Earth and Environment Processes, Springer Geology 2018, P. 317–326. – DOI:10.1007/978-3-319-77788-7_33
237. Shulga, T.Ya. Assimilation modeling and MODIS color scanner data to obtain continuous information about the thermohaline structure in the Sea of Azov / T. Ya. Shul'ga, V. V. Suslin // Proceedings of SPIE - The International Society for Optical Engineering. – 2020. – Vol. 11560, № 115603J. – DOI:10.1117/12.2574975
238. Shulga, T.Ya. Reconstruction of salinity data in the Sea of Azov from satellite measurements in the visible spectrum / T. Ya. Shul'ga, V. V. Suslin, D. M. Shukalo // Limnology and Freshwater Biology. – 2020. – № 4. – P. 942–943.– DOI:10.31951/2658-3518-2020-A-4-942
239. Shul’ga, T.Y. Numerical Analysis of the Velocities of Currents Forming in the Kerch Strait at the Motion of Domains of Higher Atmospheric Pressure / T. Ya. Shul'ga, A. E. Shchodro, A. V. Kholoptsev // Water Resources. – 2021. – Vol. 48(3). – P. 378–386. – DOI: 10.1134/S0097807821030131
240. Shulga, T.Ya. Results of salinity recovery in the Sea of Azov according to in situ data and regional biooptical parameters / T. Ya. Shul'ga, V. V. Suslin // Proc. SPIE 12341, 28th International Symposium on Atmospheric and Ocean Optics: Atmospheric Physics. – 2022. – Vol. 12341, № 1234149. – DOI: 10.1117/12.2643239
241. Shulga, T.Ya. The *in situ* and satellite data blended for reconstruction of the surface salinity of the Sea of Azov / T. Ya. Shul'ga, V. V. Suslin // International Journal of Remote Sensing. – 2023. – P. 1–25. – DOI:10.1080/01431161.2023.2255355

242. Shulga, T.Ya. Analysis of seasonal anomalies of recovered salinity in the Sea of Azov in 2000–2018 by climatology / T. Ya. Shul'ga, V. V. Suslin // Proceedings Volume 12780, 29th International Symposium on Atmospheric and Ocean Optics: Atmospheric Physics. – 2023. – 127803X. – DOI: 10.1117/12.2685162
243. Smagorinsky, J. General circulation experiments with primitive equations: I. The basic experiment / J. Smagorinsky // Mon. Weather Rev. – 1963. – Vol. 91, no. 3. – P. 99–164. – DOI:10.1175/1520-0493(1963)091<0099:GCEWTP>2.3.CO;2.
244. Stanev, E. V. Understanding Black Sea Dynamics: Overview of Recent Numerical Modeling / E. V. Stanev // Oceanography. – 2005. – Vol. 18, no. 2. – P. 56–75. –https://doi.org/10.5670/oceanog.2005.42.
245. Suetin, V. S. Assessment of the variability of the optical properties of water in the Black Sea in the summer of 1998 using SEAWIFS satellite equipment / V. S. Suetin, V.V. Suslin, S.N. Korolev, A.A. Kucheryavyj // Physical Oceanography. – 2002. – 12(6). – P. 331–340. – DOI:10.1023/A:1021729229168.
246. Suslin, V. A simple approach for modeling of downwelling irradiance in the Black Sea based on satellite data / V. Suslin [et al.] // Proc. of VI International Conference “Current problems in optics of natural waters” (ONW'2011). – Saint-Petersburg : Nauka. – 2011. – P. 199–203.
247. Suslin, V. V. The Seawifs Algorithm of Chlorophyll a in the Black Sea / V. V. Suslin, T. Y. Churilova, H. M. Sosik // Marine Ecological Journal. – 2008. – VII (2). – P. 24-42. (in Russian)
248. Suslin, V. A regional algorithm for separating light absorption by chlorophyll-a and coloured detrital matter in the Black Sea, using 480–560 nm bands from ocean colour scanners / V. Suslin, T. Churilova // International Journal of Remote Sensing. – 2016. – Vol. 37, iss. 18. – P. 4380–4400. – DOI:10.1080/01431161.2016.1211350.
249. Suslin, V. V. Regional bio-optical algorithm for remote estimation of the sea of Azov`s IOPS / V. V. Suslin, T. Ya. Churilova, T. V. Efimova, N. A. Moiseeva, E. Yu. Skorokhod, I. Stepochkin. // Proceedings of SPIE. – 2020. – V: 115600R. – DOI:10.1117/12.2574273.
250. Teng, M. H. Evolution of long water waves in variable channels / M. H. Teng, T. Y. Wu // Fluid Mech. – 1994. – Vol. 266. – P. 303–317. – DOI:10.1017/S0022112094001011.
251. The Regional Weather Forecasting System SKIRON and its capability for forecasting dust uptake and transport / G. Kallos [et al.] // Proceedings of the WMO conference on dust storms (1–6 Nov. 1997, Damascus). – Damascus, 1997. – P. 9.
252. Weijerman, M. How models can support ecosystem-based management of coral reefs / M. Weijerman [et al.] // Progress in Oceanography. – 2015. – Vol. 138, part B. – P. 559–570. – DOI:10.1016/j.pocean.2014.12.017.
253. Wolanksi, E. Estuarine Ecohydrology: An Introduction / E. Wolanksi, M. Elliott // Elsevier, 2015. – 168 p. – DOI:10.1016/C2013-0-13014-0.

254. Wu, J. Wind-stress coefficients over sea surface from breeze to hurricane / J. Wu // J. Geophys. Res. – 1987. – Vol. 87, iss. C12. – P. 9704–9706. – DOI:10.1029/JC087iC12p09704.
255. Yang, Zh. Variational inverse parameter estimation in a cohesive sediment transport model: An adjoint approach / Zhaoqing Yang, John M. Hamrick // Journal of Geophysical Research. – 2003. – Vol. 108, iss. C2. – Article no. 3055. – DOI:10.1029/2002JC001423.
256. Zakharchuk, E. A. Free low frequency waves in the Baltic Sea / E. A. Zakharchuk, N. A. Tikhonova, V. R. Fuks // Russ. Meteorol. Hydrol. – 2004. – Vol. 11. – P. 53–64.
257. Zakharchuk, E. A. Spatiotemporal structure of Baltic free sea level oscillations in barotropic and baroclinic conditions from hydrodynamic modelling / E. A. Zakharchuk, N. Tikhonova, E. Zakharova, A. V. Kouraev // Ocean Sci. – 2021. – Vol. 17. – P. 543–559. – DOI:10.5194/os-17-543-2021.